Experimental studies and numerical modelling of the combustion, performance, and emission characteristics of a diesel engine fuelled with biodiesel mixture and alcohol blends.

by

SHUMANI RAMUHAHELI

submitted in accordance with the requirements for the degree of

DOCTOR OF PHILOSOPHY

at the

UNIVERSITY OF SOUTH AFRICA

SUPERVISOR: PROF. C.C. ENWEREMADU

CO-SUPERVISOR: PROF V.R. VEEREDHI

JANUARY 2023

DECLARATION

I, RAMUHAHELI, S., declare that the thesis called "EXPERIMENTAL STUDIES AND NUMERICAL MODELLING OF THE COMBUSTION, PERFORMANCE, AND EMISSION CHARACTERISTICS OF A DIESEL ENGINE FUELLED WITH BIODIESEL MIXTURE AND ALCOHOL BLENDS" is my original work and I have not previously in its part submitted it to any university for a degree.

Ramuhaheli Shumani
University of South Africa
2023

Signature: 

ACKNOWLEDGEMENTS

First of all, I would like to thank the almighty God for providing me with the strength to complete my doctoral studies.

Likewise, my most sincere gratitude goes to my supervisor Prof. C.C. Enweremadu and co-supervisor Prof. V.R. Veeredhi for providing guidance and support for my doctoral degree programme. Without these individuals, this thesis would not have been possible.

I would also like to thank the Department of Mechanical Engineering for their support and Jezreel Eduscience cc for their technical support.

DEDICATION

I would like to dedicate this thesis:

To my late parents,

To my wife,

To my children,

To my brother,

And friends.

ABSTRACT

The increase in energy demand, air pollution, and the decrease of fossil fuels globally has led to the partial substitution of diesel fuel with biodiesel in diesel engines. Biodiesel is known to have some properties like high density and viscosity which makes it difficult to use in such engines. One of the methods used to decrease the density and viscosity and decrease engine emissions is to blend it with alcohol. Due to its renewable nature and oxygen component, ethanol has become a good additive to biodiesel. Most literature focus on the use of blends of single biodiesel. However, there exists a knowledge gap in the use of biodiesel mixture, its blends with alcohol, and engine performance, combustion, and emission characteristics of these mixtures. The biodiesel mixture was produced from waste vegetable oil and soybean oil. The fuel property test results showed that the biodiesel mixture-ethanol blends exhibited decreased viscosity and density compared to WVB100, SB100, and BM100. The heating value of BM100 was superior to the individual biodiesels and the BME blends. The engine and combustion parameters, and emissions of the individual biodiesels, BM100 and BME blends were tested in a single-cylinder diesel engine. The experimental results were compared with predicted results obtained from Diesel-RK software. The experimental results for performance and combustion parameters of biodiesel mixture were better compared to individual biodiesels and BME blends. In terms of emissions, CO, NO, HC, and smoke for the BME blends decreased compared to the individual biodiesels and BM100 at maximum speed. The simulation results for ICP and HRR of BM100 were higher than those of BME and individual biodiesels. BME attained a longer ignition compared to other fuels tested while the STP values of BME were lower compared to the other fuels. BM100 exhibited better engine performance parameters compared to individual biodiesels and biodiesel mixture-ethanol blends. At maximum speed, BM100 had the highest value of NO_x while BME had decreased NO, CO_2, PM, and smoke emissions. BME15 emits lower CO_2, NO, and smoke by 29.1%, 75.9%, and 35.7% compared to diesel. There were marginal differences between the experimental and simulation results.

Keywords: Alcohol blends, Biodiesel mixture, Combustion, Diesel engine, Diesel-RK, Emission characteristics, Engine performance, Ethanol, Experimental, Numerical.

TABLE OF CONTENTS

DECLARATION……...……i

ACKNOWLEDGEMENT……...ii

DEDICATION……iii

ABSTRACT……iv

TABLE OF CONTENTS……v

LIST OF FIGURES……x

LIST OF TABLES……xii

LIST OF ABBREVIATIONS AND SYMBOLS……xiii

PUBLICATIONS……xvii

CHAPTER ONE 1

1.0 Introduction 1

1.1 Background of the Study 1

1.2 Biodiesel Production 4

1.3 Properties of Fuels 5

1.4 Impacts of Ethanol on Diesel Engines and the Environment 5

1.5 Effects of Biodiesel on Engine Performance 6

1.6 Effects of Biodiesel on Engine Emissions 6

1.7 Setup of a Diesel-RK Software 6

1.8 Motivation for the Study 7

1.9 Problem Statement 8

1.10 Research Aim 9

1.11 Objectives of the Study 9

1.12 Justification for the Research 9

1.13 Scope of the Research 10

1.14 Organisation of the Thesis 10

1.15 Summary of Chapter One 12

CHAPTER TWO 13

2.0 Literature review 13

2.1 Introduction 13

2.2 Overview of the Global Status of Biodiesel Production 13

2.3 Production of Biodiesel 14

2.3.1 Transesterification 17

2.3.2 Micro-Emulsification.....18
2.3.3 Direct Application and Blending of Oils.....18
2.3.4 Pyrolysis.....19
2.4 Advantages of Using Biodiesel.....19
2.5 Disadvantages of Using Biodiesel (Mahmudul et al., 2017).....19
2.6 Classification of Biodiesel Production Feedstocks.....20
2.6.1 First-generation Feedstocks.....20
2.6.2 Second-generation Feedstocks.....20
2.6.3 Third-generation Feedstocks.....21
2.6.4 Fourth Generation Feedstocks.....21
2.7 Catalytic Biodiesel Production Methods.....22
2.7.1 Biodiesel Production Using Homogeneous Catalysts.....22
2.7.2 Biodiesel Production Using Heterogeneous Catalysts.....24
2.7.3 Biodiesel Production Using Enzymatic Catalysts.....26
2.8 Properties of Biodiesel.....28
2.8.1 Density.....30
2.8.2 Viscosity.....31
2.8.3 Cetane Number.....32
2.8.4 Heating Value.....32
2.8.5 Flash Point.....33
2.8.6. Cloud Point (CP).....33
2.8.7 Pour Point (PP).....34
2.8.8 Cold Filter Plugging Point (CFPP).....34
2.8.9 Acid Value (AV).....35
2.9 Fuel Blending Techniques.....35
2.10 Influences of Biodiesel-Diesel-Ethanol Blend on Performance, Combustion, and Emission Characteristics.....36
2.11 Influences of Biodiesel-Ethanol Blends on the Performance, Combustion, and Emission Characteristics.....41
2.12 Numerical Modelling on Performance, Combustion, and Emission Characteristics of Diesel Engine Powered by Biodiesel and Alcohol Fuel Blends.....45
2.12.1 Single-dimensional Model.....45
2.12.2 Single-dimensional Model Equations.....45
2.12.3 Multi-dimensional Model.....46

2.12.4 Multi-dimensional Model Equations 47
2.13 Summary of Chapter Two 50
CHAPTER THREE-METHODOLOGY 52
3.0 Experimental studies on performance, combustion, and emission characteristics of sample fuels on a diesel engine 52
3.1 Introduction 52
3.2 Materials 52
3.3 Titration Process and Biodiesel Production 55
3.3.1 Titration Process 55
3.3.2 Biodiesel Production 56
3.4 Blending of the Fuel Samples 57
3.5 Measurement of Fuel Properties 58
3.5.1 Operating Procedure for Densitometer Model DDM2910 for Density Meter Measurement 59
3.5.2 Operating Procedure for ASTM D93 Flash Point Measurement 59
3.5.3 Operating Procedure for IKA Oxygen Bomb Calorimeter Measurement 60
3.6 Experimental Setup of a Diesel Engine and Parameter Measurement Procedure 61
3.7 X-Tract Extreme Software 64
3.8 Measurement System for Combustion and Performance of Diesel Engine Parameters 65
3.8.1 In-Cylinder Pressure 65
3.8.2 Crank Angle (CA), Engine Speed (N), and Top dead Centre (TDC) Mark 66
3.8.3 Heat Release Rate 67
3.9 Engine Performance 68
3.9.1 Power and Torque 68
3.9.2 Fuel Mass Flow Rate 69
3.9.3 Brake Specific Fuel Consumption 69
3.9.4 Brake Thermal Efficiency 70
3.10 Emissions 70
3.10.1 Emission Characteristics Measurement 70
3.11 Uncertainty Analysis 71
3.12 Prediction of performance, combustion, and emission characteristics 72
3.12.1 Introduction 72
3.12.2 Physical Properties Used as Input Data 73

3.12.3 Diesel-RK Computer Simulation Model.....74
3.12.4 Methodology for Diesel-RK.....74
3.12.5 Heat Release Model.....77
3.12.6 Spray Tip Penetration Model.....81
3.12.7 NO_x Formation Modelling.....81
3.12.8 Soot and Particulate Matter Formation Model.....82
CHAPTER FOUR-RESULTS AND DISCUSSION.....84
4.1 Experimental Studies of Characterization, Performance, Combustion, and Exhaust Gas Emissions......84
4.1.1 Properties of the Fuel Samples.....84
4.1.2 Combustion Characteristics Under Full Load Conditions.....86
4.1.3 Performance Characteristics Under Full Load Conditions.....96
4.1.4 Effects of the Fuel Samples on the Engine Emission Characteristics.....104
4.2 Prediction of performance, combustion, and emission characteristics.....111
4.2.1 Combustion Parameters.....111
4.2.2 Engine Performance Analysis.....136
4.2.3 Emission Analysis.....143
4.3 Summary of Experimental and Prediction Studies.....149
CHAPTER FIVE.....153
5.0 Validation of numerical with experimental results.....153
5.1 Comparison of Numerical and Experimental Results.....153
5.1.1 Heat Release Rate.....154
5.1.2 In-Cylinder Pressure.....158
5.1.3 Brake Power.....162
5.1.4 Brake-Specific Fuel Consumption.....163
5.1.5 Brake Torque.....165
5.1.6 Brake Thermal Efficiency.....166
5.1.7 Brake Mean Effective Pressure.....167
5.1.8 CO_2 Emissions.....169
5.1.9 NO Emissions.....170
5.1.10 Bosch Smoke Number Emissions.....171
5.2 Summary of Chapter Five.....172
CHAPTER SIX.....173
6.0 General discussions and future perspective.....173

6.1 Introduction 173
6.2 General Discussion 173
6.3 Conclusions 178
6.4 Recommendations for Further Studies 179
APPENDICES 180
Appendix A: Combustion Simulation Curves 180
Appendix B: Performance Simulation Curves 185
Appendix C: Emissions Simulation Curves 186
Appendix D: Diesel-RK Software User Interface 187
References 192

LIST OF FIGURES

Figure 1.1: Shares of primary energy 2
Figure 1.2: Primary energy consumption by end-use sector 3
Figure 1.3: Primary energy consumption by fuel 3
Figure 1.4: Liquid fuel demands by sectors 4

Figure 2.1: Standard procedure of biodiesel production from vegetable oils 16
Figure 2.2: Transesterification reaction 18

Figure 3.1: Experimental Pignat® biodiesel plant 53
Figure 3.2: Principal schematic of biodiesel processer 53
Figure 3.3: Titration kit process 56
Figure 3.4: Biodiesel and glycerol separation 57
Figure 3.5: Biodiesel fuel blends preparation 58
Figure 3.6: DDM2910 density meter 59
Figure 3.7: Automatic flash point Pensky-Martens apparatus 60
Figure 3.8: IKA oxygen bomb calorimeter apparatus 61
Figure 3.9: Experimental YANMAR diesel engine facilities 62
Figure 3.10: Schematic diagram of a Yanmar diesel engine 63
Figure 3.11: AutoPSI pressor sensor 66
Figure 3.12: Rotary encoder 67
Figure 3.13: Screenshot of X-Tract extreme software 68
Figure 3.14: Promass 83 fuel meter apparatus and specifications 69
Figure 3.15: BOSCH BEA 060 Emission analyser 71
Figure 3.16: BOSCH BEA 070 Emission analyser 71
Figure 3.17: The different zones of diesel spray 78
Figure 3.18: The vaporization of spray evaluation of the engine 81

Figure 4.1: Variation of in-cylinder pressure with crank angle 90
Figure 4.2: Variation of heat release rate with crank angle 95
Figure 4.3: Variation of brake power with engine speed 97
Figure 4.4: Variation of brake specific fuel consumption with engine speed 98
Figure 4.5: Variation of brake torque with engine speed 100
Figure 4.6: Variation of brake thermal efficiency with engine speed 101
Figure 4.7: Variation of brake mean effective pressure with engine speed. 103
Figure 4.8: Variation of CO emission with engine speed 104
Figure 4.9: Variation of HC emissions with engine speed 106
Figure 4.10: Variation of NO emissions with engine speed 107
Figure 4.11: Variation of CO_2 emissions with engine speed 109
Figure 4.12: Variation of Bosch smoke number emission with engine speed. 110
Figure 4.13: Variation of in-cylinder pressure with the crank angle of simulated data 115
Figure 4.14: Variation of heat release rate with the crank angle of simulated data 120
Figure 4.15: Variation of in-cylinder temperature with the crank angle of simulated data 125
Figure 4.16: Variation of ignition delay period with an engine speed of simulated data 126
Figure 4.17: Variation of spray tip penetration with the crank angle of simulated data 131

Figure 4.18: Variation of the start of combustion with an engine speed of simulated data...132
Figure 4.19: Variation of combustion duration with engine speed of simulated data. 133
Figure 4.20: Variation of friction mean effective pressure with an engine speed of simulated data. 135
Figure 4.21: Variation of brake power with engine speed of simulated data. 136
Figure 4.22: Variation of brake-specific fuel consumption with engine speed of simulated data. 138
Figure 4.23: Variation of brake torque with engine speed of simulated data. 139
Figure 4.24: Variation of brake thermal efficiency with an engine speed of simulated data.141
Figure 4.25: Variation of brake mean effective pressure with an engine speed of simulated data. 142
Figure 4.26: Variation of CO_2 with engine speed of simulated data. 143
Figure 4.27: Variation of NO with engine speed of simulated data. 144
Figure 4.28: Variation of NOx with engine speed of simulated data. 145
Figure 4.29: Variation of particulate matter with an engine speed of simulated data. 147
Figure 4.30: Variation of Bosch smoke number with an engine speed of simulated data.....148

Figure 5.1: Comparison of the heat release rate of Diesel-RK prediction and experimental data. 157
Figure 5.2: Comparison of in-cylinder pressure of Diesel-RK prediction and experimental data. 161
Figure 5.3: Comparison of brake power of Diesel-RK prediction and experimental data. ...162
Figure 5.4: Comparison of brake-specific fuel consumption of Diesel-RK prediction and experimental data. 163
Figure 5.5: Comparison of brake torque of Diesel-RK prediction and experimental data. ...165
Figure 5.6: Comparison of brake thermal efficiency of Diesel-RK prediction and experimental data. 166
Figure 5.7: Comparison of brake mean effective pressure of Diesel-RK prediction and experimental data. 167
Figure 5.8: Comparison of CO_2 emissions of Diesel-RK prediction and experimental data.169
Figure 5.9: Comparison of NO emissions of Diesel-RK prediction and experimental data..170
Figure 5.10: Comparison of Bosch smoke number emissions of Diesel-RK prediction and experimental data. 171

LIST OF TABLES

Table 2.1: Classification of different feedstocks for biodiesel production 15
Table 2.2: Challenges of using vegetable oils on diesel engines 15
Table 2.3: Contrast of the biodiesel production techniques 17
Table 2.4: Biodiesel production with homogeneous catalysts 23
Table 2.5: Biodiesel production using heterogeneous catalysts. 25
Table 2.6: Biodiesel synthesis using enzymatic catalysts. 27
Table 2.7: Properties of diesel fuel and soybean methyl ester 28
Table 2.8: Properties of waste cooking oil methyl ester 29
Table 2.9: Properties of diesel (D100: 100% Diesel), biodiesel (B100: 100% Biodiesel), and ethanol fuel 29

Table 3.1: Technical Descriptions of Yanmar Diesel engine 61
Table 3.2: Parameters of the diesel engine 64
Table 3.3: Technical specifications of the pressor sensor 65
Table 3. 4: Specifications of the Promass fuel meter 69
Table 3.5: Uncertainties of the parameters 72
Table 3.6: Input boundary condition for simulation 75

Table 4.1: Fuel properties 84

LIST OF ABBREVIATIONS AND SYMBOLS

Abbreviations

ASTM	American Society for Testing Materials	(-)
AV	Acid value	(-)
aTDC	After top dead centre	(-)
BDE	Biodiesel-diesel-ethanol blend	(-)
BE	Biodiesel-ethanol blend	(-)
B100	100% Biodiesel	(-)
BEA	Bosch exhaust emission analyser	(-)
BM100	Biodiesel mixture	(-)
BME	Biodiesel mixture-ethanol blends	(-)
BME5	Biodiesel mixture-5%ethanol blends	(-)
BME10	Biodiesel mixture-10%ethanol blends	(-)
BME15	Biodiesel mixture-15%ethanol blends	(-)
BMEP	Brake mean effective pressure	(bar)
BSFC	Brake specific fuel consumption	(g/kWh)
BSN	Bosch smoke number	(%)
BP	Brake power	(kW)
BT	Brake torque	(Nm)
bTDC	Before top dead centre	(-)
BTE	Brake thermal efficiency	(%)
Bu	Butanol	(-)
CA	Crank angle	(degree)
CD	Combustion duration	(degree)
CFD	Computational fluid dynamics	(-)
CFPP	Cold filter plugging point	(ºC)
CI	Compression ignition	(-)
CO	Carbon monoxide	(ppm)
CO_2	Carbon dioxide	(%vol)
CP	Cloud point	(ºC)
CN	Cetane number	(-)
CR	Compression ratio	(-)

D100	Diesel fuel	(-)
DI	Direct injection	(-)
DRK	Diesel-RK	(-)
E20	20%Ethanol80%Diesel	(-)
EGR	Exhaust gas recirculation	(-)
EGT	Exhaust gas temperature	(K)
EN	European standards	(-)
FAAE	Fatty acid alkyl esters	(-)
FFA	Free Fatty Acids	(-)
FAME	Fatty acid methyl ester	(-)
FMEP	Frictional mean effective pressure	(bar)
FP	Flash point	(ºC)
GHG	Greenhouse gas emissions	(-)
H_2O	Water	(-)
HC	Hydrocarbon	(ppm)
HCCI	Homogeneous charge compression ignition engine	(-)
HLH	Higher latent heat	(-)
HRR	Heat release rate	(J/deg)
HV	Heating value	(MJ/kg)
ICE	Internal combustion engine	(-)
ICP	In-cylinder pressure	(bar)
ICT	In-cylinder temperature	(K)
ID	Ignition delay	(degrees)
KOH	Potassium hydroxide	(-)
LHV	Lower heating value	(MJ/kg)
MNHHR	Maximum net heat release rate	(J/deg)
NaOH	Sodium hydroxide	(-)
NDIR	Nondispersive infrared spectroscopy	(-)
NO	Nitric oxide	(ppm)
NO_2	Nitrogen dioxide	(ppm)
NO_x	Nitrogen oxides	(ppm)
O_2	Oxygen	(%vol)
PM	Particulate matter	(g/kWh)
PP	Pour point	(ºC)

P_{max}	Maximum cylinder pressure	(bar)
R	Gas constant	(J/mol-K)
REN21	Renewable Policy Network of 21st Century	(-)
SB100	Soybean biodiesel	(-)
SOC	Start of combustion	(degree)
STP	Spray tip penetration	(mm)
T	Temperature	(K)
TDC	Top dead centre	(-)
V_I	Current velocity	(m/s)
V_c	Clearance volume	(m^3)
V_m	Medium velocity of spray	(m/s)
V_s	Swept volume	(m^3)
V_0	Initial velocity	(m/s)
WCOME	Waste cooking oil methyl ester	(-)
WVB100	Waste vegetable biodiesel	(-)

Symbols

$\dot{m}_{cyl}$	Cylinder gas mass flow	(-)
$\dot{m}_{exh}$	exhaust mass flow rate	(-)
$\dot{m}_{in}$	Inlet air mass flow	(-)
$\dot{m}_f$	Fuel mass flow	(kg/s)
ρ	Density	(kg/m^3)
ν	Specific volume	(m^3/kg)
$\frac{dQ}{d\theta}$	Heat release rate	(J/ ^{0}CA)
θ	Crank angle	(degree)
V_d	Displacement volume	(m^3)
V	In-cylinder volume	(m^3)
T	Temperature	(K)
S	Stroke	(m)
A/F	Air fuel ratio	(-)
N	Engine speed	(rev/sec)
ω	Angular velocity	(rpm)
λ	Crank radius ratio	(-)
γ	Specific heat ratio	(-)
U	Internal energy	(kJ)
P	Pressure	(MPa)
η_{th}	Brake thermal efficiency	(%)

PUBLICATIONS

1. Shumani Ramuhaheli, Veeredhi Vasudevarao, Christopher Enweremadu. Experimental Assessment of Performance and Emission Characteristics of a Diesel Engine Fueled with Hybrid Biodiesel and its Blends with Ethanol, AIP Conf. Proc.2643, 050042-1-050042-8 (2023).

2. Shumani Ramuhaheli, Veeredhi Vasudevarao, Christopher Enweremadu. The Performance and Emission Characteristics Assessment of Hybrid Biodiesel/Ethanol Blends in a Diesel Engine. Environmental and Climate Technologies, 2022, vol 26, no. 1, pp. 670-683.

CHAPTER ONE

1.0 Introduction

1.1 Background of the Study

Most research conducted on renewable energy sources looks at finding a substitute for the diminution of fossil fuel reserves and lower the toxic gas from these fossil fuels on human health. This is very important as the daily greenhouse gas emission to the atmosphere continues to adversely impact on global warming (Cihan, 2021). The quest for renewable energy sources has led to the production of biodiesel, a close alternative to diesel fuel. Biodiesel can be made using waste cooking oil, fresh vegetable oils, or animal fats through the transesterification method, and it does not have aromatics and sulphur (Rashedul et al., 2014). It has an oxygen content of about 10 to 15% (Al-Dawody and Bhatti, 2014). Biodiesel fuel is described as renewable, and its properties are like standard diesel. It can be directly applied or mixed with standard diesel and run on engines (Mahmudul et al., 2017). Moreover, biodiesel shows similar combustion behaviours to standard diesel. However, biodiesel exhibits negative properties such as high viscosity, poor low temperature, and high density (Liu et al., 2017). The application of pure biodiesel in diesel engines has been limited all over the world. This is attributed to the fact that diesel engines were produced and optimized to run on diesel fuel. Hence, most scientists have suggested the use of diesel–biodiesel blends as a replacement for pure biodiesel in a diesel engine (Ali et al., 2016, Acharya et al., 2017).

The primary source of energy accounts for almost 85% of natural gas and renewable energy. However, renewable energy is increasing and becoming the preferred source of energy with an increase of 7.1% per annum, which provides for half of the increase around the world (Bilgen, 2014). Its share of primary energy is estimated to have grown from 6% in 2020 and is predicted to reach nearly 15% by 2040, as shown in Figure 1.1. The increase of 1.7% per annum in natural gas has been growing quicker compared to oil or coal. The figure below shows that oil has increased by 0.3 % per annum and this was much lower compared to decades before the 2030s. Coal consumption is roughly flat over the reflected timeframe, which is beneficial to the global energy system, and declining to its lowest level since before the industrial revolution (Economics, 2018).

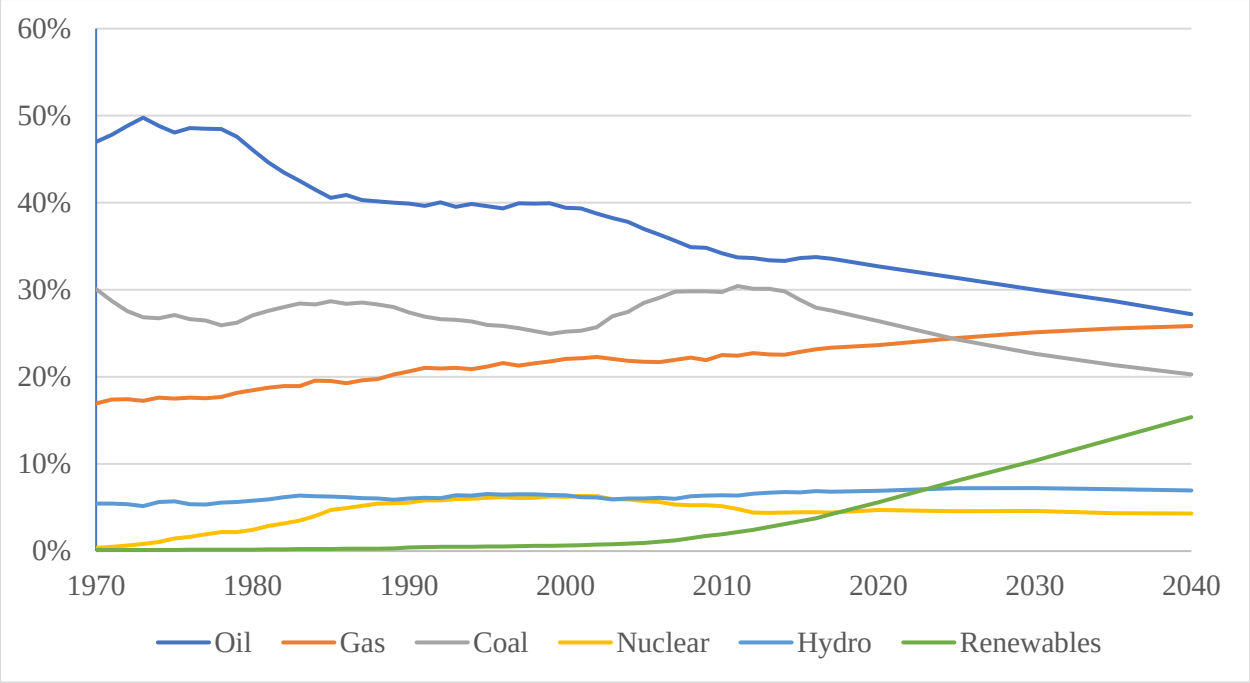

Figure 1.1: Shares of primary energy (Economics, 2018)

The drastic increase in global energy demand from oil, industrial, transportation, and building sectors is shown in Figure 1.2. Capuano (2018) predicted that by 2040, the global energy demand would have increased by 25% and require over $2 trillion US dollars in investment per year. The increase in primary energy consumption provided through different sources of energy is shown in Figure 1.3. The automotive sector has the largest energy demand compared to other sectors and is likely to grow in the coming years as shown in Figure 1.4. The scientific community understands the current situation of harmful emissions. However, the world needs to be aware of the necessity for renewable energy and the substitute for diesel fuel. The alternative fuel source of energy must be cost-effective, environmentally friendly, and simply accessible (Meher et al., 2006). To solve the challenge of energy demand and environmentally harmful substances, biodiesel and alcohol blends are considered, since they are reliable and affordable.

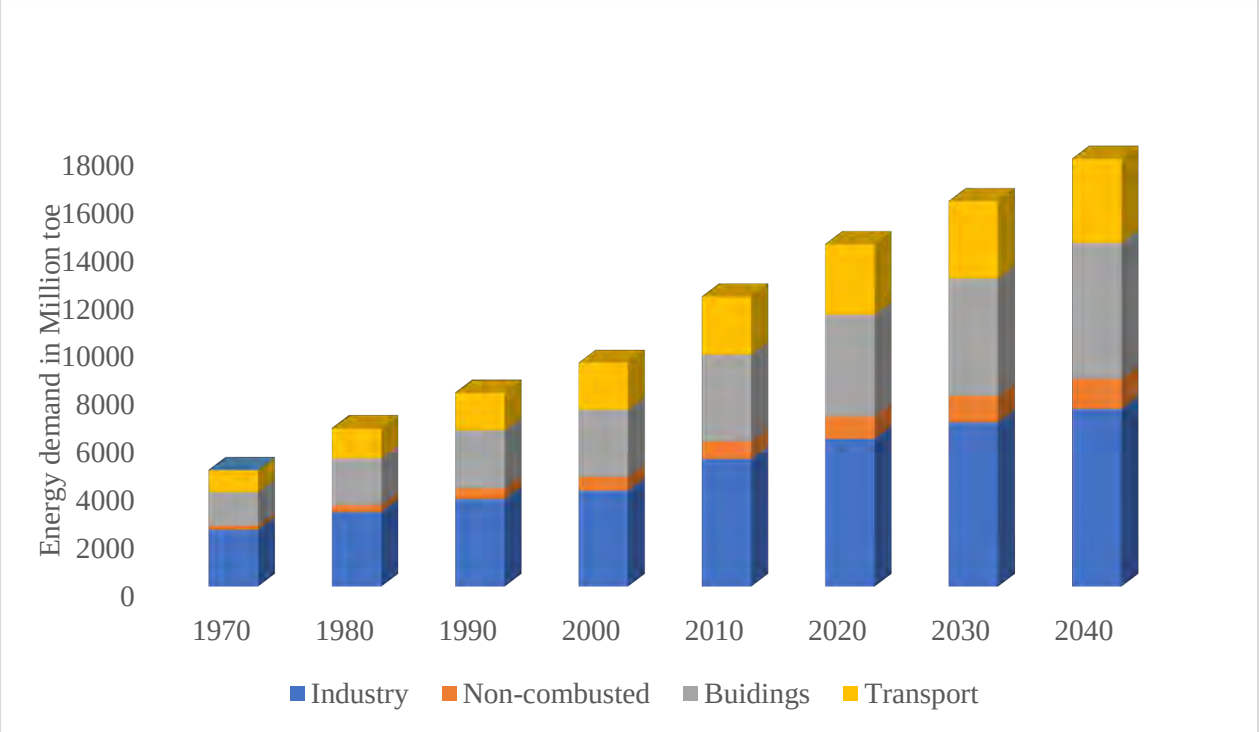

Figure 1.2: Primary energy consumption by end-use sector (BP, 2019)

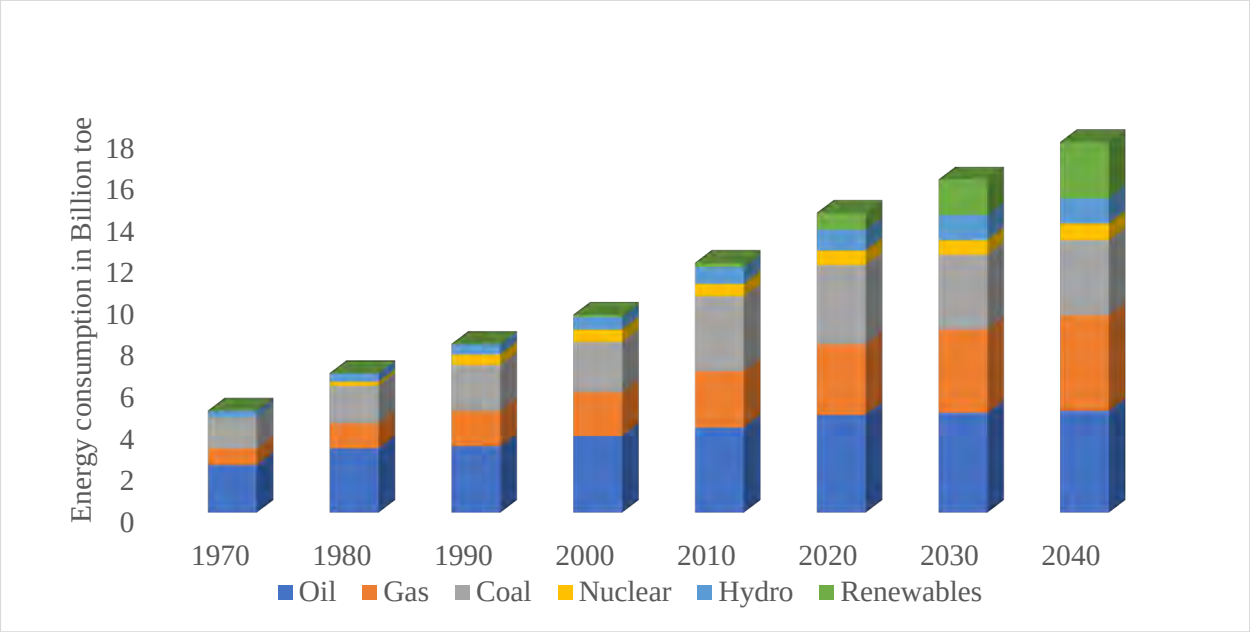

Figure 1.3: Primary energy consumption by fuel

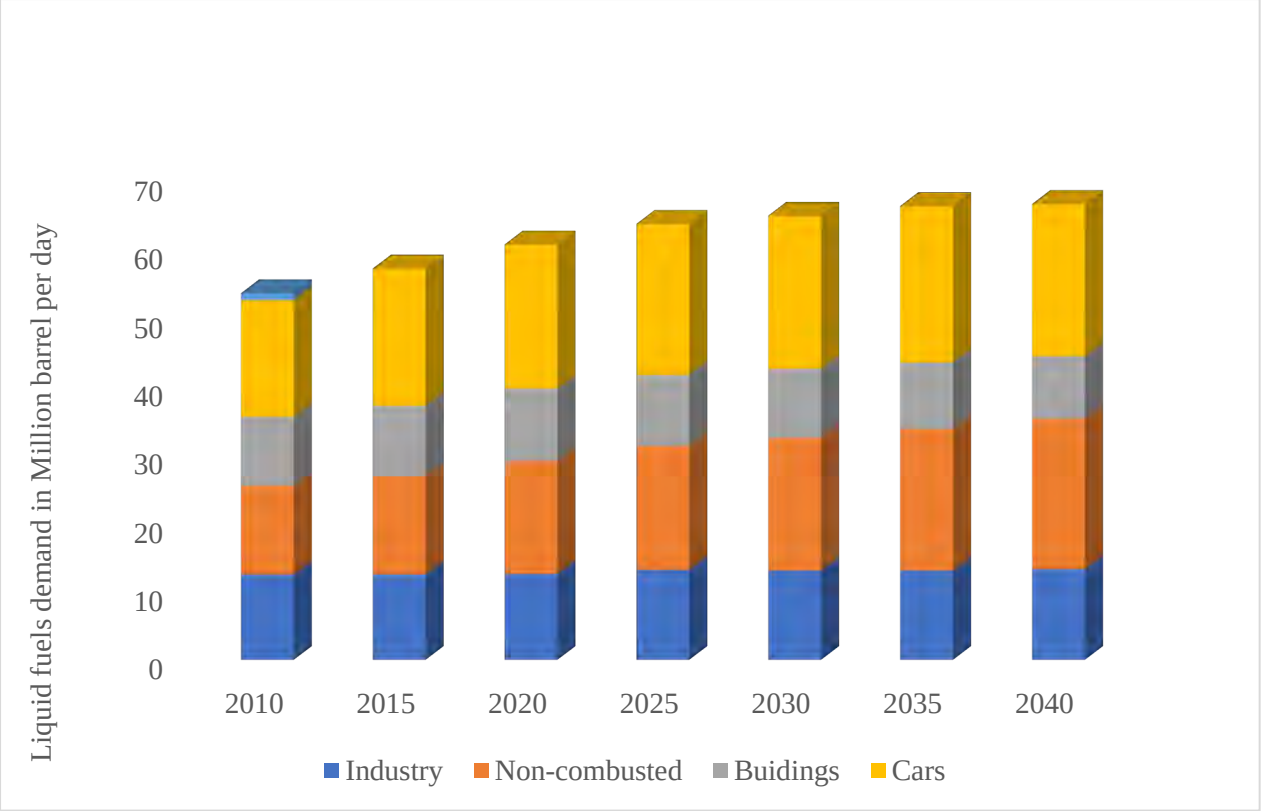

Figure 1.4: Liquid fuel demands by sectors (BP, 2019)

1.2 Biodiesel Production

Biodiesel was first introduced by the United States of America (USA) in 1992 through the National Biodiesel Board. Biodiesel fuel is produced from animal fats, fresh vegetable oil, waste vegetable oil, and some raw materials. In addition, it is mainly composed of long-chain fatty acid methyl ester. Biodiesel can be produced from waste cooking oil or fresh vegetable oil through the transesterification method, and it does not have aromatics and sulphur (Rashedul et al., 2014). It has an oxygen content of around 10–15% (Al-Dawody and Bhatti, 2014). It is renewable in nature and non-harmful, and its properties are marginally close to standard diesel. Biodiesel can be blended with standard diesel due to its similar features (de Araújo et al., 2013). Biodiesel can be applied straight or blended to standard diesel to run diesel engines (Mahmudul et al., 2017). Furthermore, compared to standard diesel, biodiesel attained a comparable combustion performance. Besides the advantages stated above, there are some disadvantages of biodiesel such as high viscosity, high density, and low temperature (Liu et al., 2017). The use of biodiesel in diesel engines has been restricted all over the world. Several researchers have recommended the use of diesel blended with biodiesel instead of biodiesel only, to run diesel engines (Ali et al., 2016, Acharya et al., 2017).

1.3 Properties of Fuels

Fuel properties are the most important parameters during the process of atomization in diesel engines. For example, the viscosity of biodiesel is more effective on the distribution of fuel droplet volume, fuel injection quality atomization, and uniformity blend (Mat Yasin et al., 2013). However, the viscosity of the fuel is required to meet the global biodiesel standards according to ASTM D6751 and EN 14214. One of the critical approaches to decreasing the viscosity and density of biodiesel fuel is to blend it with additives such as alcohol to improve the fuel properties (Emiroğlu and Şen, 2018). Even though alcohols are not used directly to run diesel engines, they are recommended as good fuel additives to biodiesel to improve the engine parameters and decrease emissions due to their high oxygen content (Mat Yasin et al., 2013).

The use of alcohol fuels in compression ignition engines has some limitations due to low cetane number and low miscibility (Pinzi et al., 2018, Datta and Mandal, 2017). For this reason, alcohols used as additives to improve fuel properties such as density and viscosity should be below 20% in biodiesel blends (Pinzi et al., 2018).

1.4 Impacts of Ethanol on Diesel Engines and the Environment

Ethanol is derived from corn, wheat, cassava, sweet potato, sugarcane, or sugar beet and is an alternative oxygenated fuel with an oxygen content of 35%, which is higher than the (11%) oxygen content standard diesel. Ethanol fuel properties have low density, viscosity, cetane number, flash point, and low heating value, which limits its application straight to diesel engines. To overcome these complications, ethanol could be blended with biodiesel to enhance the viscosity, density, and cetane number. However, when engine combustion lowers the temperature of biodiesel due to being ethanol-blended, the NO_x and Particulate Matter (PM) emissions might decrease simultaneously (An et al., 2015a). Biodegradation of ethanol is quick in the soil, borehole water, and surface water, which can be recovered within a maximum period of 10 days. The risk of ethanol is very low for the natural environment and living organisms. Only a few incidents have been reported of the death of fish on the water surface contaminated with ethanol due to the reduction of oxygen in the water (Parish et al., 2013, Olivares et al., 2015).

1.5 Effects of Biodiesel on Engine Performance

The substitute fuels used in diesel engines are normally evaluated based on performance and environmental impact. The most significant parameters considered by the scientists on internal combustion engines are brake power (BP), brake torque (BT), brake specific fuel consumption (BSFC), brake thermal efficiency (BTE), and brake mean effective pressure (BMEP) while its combustion characteristics are in-cylinder pressure (ICP), heat release rate (HRR), in-cylinder temperature (ICT), ignition delay (ID), spray tip penetration (STP), start of combustion (SOC), combustion duration (CD), and frictional mean effective pressure (FMEP). Biodiesel has the advantage of high combustion efficiency, high cetane number, and high lubrication impacts. The literature review sections will present and discuss the results of different studies related to the above engine parameters with the use of biodiesel-diesel-alcohol blends, and biodiesel-alcohol blends.

1.6 Effects of Biodiesel on Engine Emissions

The use of crude oil in the form of diesel fuel continues to grow particularly in the automotive sector and continues to increase emissions from the exhaust pipe of diesel engines. It has also caused numerous diseases and poverty throughout the world. The hydrocarbon emitted from the diesel engine forms ground-level ozone, which is the leading effect of smoke emission. Ozone layers also affect human health, and they can cause numerous infections such as lung diseases, eye irritation, and breathing complications. It is now nearly compulsory for any fuel used in the automotive sector to face harsh emissions targets set by various regulating authorities throughout the world. The major pollutants from the engine exhaust have been recognized and considered as carbon monoxide (CO), carbon dioxide (CO_2), NO_x, particulate matter (PM), hydrocarbon (HC), and smoke. The impact of alcohol added to biodiesel in various proportions on emissions of diesel engines will be discussed in the next sections of the literature review.

1.7 Setup of a Diesel-RK Software

Diesel-RK can be explained as the modelling and simulation software used to analyse internal combustion engines. This software was developed by the Department of Internal Combustion Engines at the Bauman Technical University, Russia. The software has been developed to

simulate and optimize the operating procedure of internal combustion engines with all types of boosting. This software tool could be used to predict the performance parameters, combustion, and emission characteristics. It can also be used to optimize fuel injection profiles such as multiple injections, sprayer design, and piston bowl shape optimization models of diesel engines. The Diesel-RK tool uses a multi-zone fire model, depending on the blend, with the combustion model, as developed by Razleisev and, thereafter by Kuleshov, which leads to the recognition of the tool as the Razleisev-Kuleshov or RK model (Hoang and Pham, 2018). The RK model takes into consideration the parameters, which influence the procedure of blend formation and burning of the diesel engine in full detail namely fuel distribution, the shape of the combustion chamber, spray distribution, the effect of spray in the combustion chamber surface, and contact between the adjacent sprays (Reham et al., 2015, Chin et al., 2012).

Currently, several specialised commercial CFD software tools such as Ansys, SOLIDWORKS, Sim scale, Autodesk CFD, CHEMKIN, and OpenFOAM are available all over the world. However, CFD procedures are normally capable accurately explaining characteristics such as the distribution of pressure, heat release, ignition delay, combustion duration, and discharge gases of the diesel engine. Even though they are accurate, CFD tools are expensive and take time to complete the process. According to Al-Dawody and Bhatti (2014), Diesel-RK can be used as an optimization tool due to its less time consumption and lower cost. It is a good commercial software tool that can be used to simulate diesel engines (single-cylinder or multi-cylinder conditions).

1.8 Motivation for the Study

Many studies from literature concentrate on performance parameters, combustion, and exhaust gas emissions by applying biodiesel-alcohol blends and biodiesel-diesel-alcohol blends of the diesel engine. Even though biodiesel has been blended with diesel and alcohols to reduce its limitations and improve fuel properties, it appears that only a few studies have been reported on the ternary mixture (biodiesel-biodiesel-alcohol). For that reason, the motivation for this study is to evaluate the performance, combustion, and emitted gases of the diesel engine fuelled with hybrid biodiesel (biodiesel-biodiesel), and ternary blend (biodiesel-biodiesel-ethanol blends). Furthermore, for improving insights and reducing the costs from the experimental processes, Diesel-RK simulation software was applied, and the results attained from the simulation software were compared with experimental data. The diesel engine performance

parameters considered were BP, BT, BSFC, BTE, and BMEP whereas the combustion parameters were ICP, HRR, ICT, ID, STP, SOC, and CD. The emission characteristics were CO_2, CO, HC, NO, PM, NO_x, and smoke.

1.9 Problem Statement

Experimental works are not always possible as they need manpower, are time-consuming, and are expensive to run. Furthermore, a numerical tool with proper mathematical modelling software might be an accurate process to predict engine parameters and exhaust gas emissions. Several scientists have stated that engines powered by biodiesel emit high levels of NO_x and PM. NO_x and PM were reported as the main harmful emissions from biodiesel engines that need to be controlled. Therefore, it is important to have an additional fuel that can be blended with biodiesel to lessen the NO_x, PM, and other emissions both experimentally and numerically. However, no numerical study has been conducted on a diesel engine fuelled with hybrid biodiesel (biodiesel-biodiesel) and biodiesel mixture and ethanol (biodiesel-biodiesel-ethanol) fuel blends. No comparison of these forms of fuel blends with standard diesel, in diesel engines, has been carried out in previous studies. Therefore, the computational tool of Diesel-RK is utilized in this study. This numerical study will use Diesel-RK software techniques to predict the engine performance parameters, combustion, NO_x, PM, and other emission characteristics using the different fuel blends under this study.

Alcohol fuel has been defined by researchers as a suitable addition to biodiesel fuel to enhance engine parameters and reduce emission characteristics because of high oxygen content. Normally, ethanol fuel can be produced from starch harvests obtainable from sugarcane, wheat, and maize. Both biodiesel, and ethanol are renewable in nature and environmentally friendly. Due to the argument and dispute among food and biofuels, several scientists have conveyed their preference of biodiesel production from a hybrid feedstock of waste vegetable oil and fresh vegetable oil for use as a hybrid biodiesel (biodiesel-biodiesel). They have also suggested that such mixtures improve the properties of biodiesel.

In this current study, an economically suitable technique will be employed to improve engine parameters and decrease emission characteristics powered by individual biodiesels (waste vegetable biodiesel (WVB100) and soybean biodiesel (SB100)), hybrid biodiesel (biodiesel-

biodiesel), and hybrid biodiesel-ethanol blends (biodiesel-biodiesel-ethanol) compared to standard diesel.

1.10 Research Aim

The aim for this research was to enhance the engine parameters and exhaust gas emissions using hybrid biodiesel and its blends with ethanol, and hence assess numerically and experimentally, the engine performance, combustion, and exhaust gases of the fuels in a diesel engine.

1.11 Objectives of the Study

The research was aimed to achieve the following objectives.

- To assess the thermophysical properties of a hybrid biodiesel (biodiesel-biodiesel mixture) from waste vegetable and soya bean oils and its blends with ethanol.
- To conduct laboratory studies on the engine performance, combustion, and emission characteristics of a diesel engine fuelled with the hybrid biodiesel-ethanol blends.
- To carry out numerical studies on the engine performance, combustion, and emission characteristics of a diesel engine fuelled with the biodiesel-biodiesel-ethanol blends.
- To validate and compare the results obtained from experimental and numerical studies on the engine performance, combustion, and emission characteristics of a diesel engine fuelled with the hybrid biodiesel-ethanol blends.

1.12 Justification for the Research

The continued high energy consumption is a result of global population density and living habits. The utilization of fossil fuels to satisfy this energy need has created a significant hurdle due to the rising expense of fossil fuels. Additionally, the toxic substances released by burning fossil fuels have led to smoke creation, global warming, and environmental impacts such an increase in greenhouse gas (GHG) emissions, ozone depletion, deforestation, and acid rain (Al-Dawody and Edam, 2022). This raises the issue of whether renewable energy sources can be used to replace diesel, a fossil fuel, in the automotive industry. As the global automotive industry expands, numerous countries are already under pressure from the international environmental regulating agencies to reduce their GHG emissions and other harmful discharges

(Change, 2014). It is well recognized that despite their continual decline, fossil fuels will not be able to remedy this issue because, as long as they are used, their emission standards will likely continue to deteriorate (Pan et al., 2009). By employing biofuels in diesel engines, this issue can be somewhat managed.

1.13 Scope of the Research

It has been reported that the properties of biodiesel and its blends differ from standard diesel fuel. This research's initial step is to evaluate the thermophysical characteristics of individual biodiesels, biodiesel mixtures, and ethanol blends, such as density, viscosity, heating value, and flash point. The second aspect of this research is to conduct laboratory studies on the engine performance, combustion, and emission characteristics of a diesel engine running on hybrid biodiesel-ethanol blends. The effects of fuel properties on the diesel engine's in-cylinder pressure, heat release rate, brake power, brake torque, brake specific fuel consumption, brake thermal efficiency, brake mean effective pressure, carbon monoxide (CO), hydrocarbon (HC), nitric oxide (NO), carbon dioxide (CO_2), and Bosch Smoke Number will be discussed based on the findings of their experiments. Most investigations on biodiesel-alcohol and biodiesel-diesel-alcohol blends engines and emissions have been published in the literature. As a result, there are few studies that specifically address the usage of ternary mixtures of biodiesel, biodiesel, and ethanol. A numerical analysis of the engine performance, combustion, and emission characteristics of a diesel engine running on biodiesel-biodiesel-ethanol blends makes up the third component of this research. The fourth aspect study compares some of these features with those discovered through experimentation using numerical simulation tools.

1.14 Organisation of the Thesis

The fundamental framework of this dissertation is as follows:

Chapter 1: Introduction

Introduction of the recent situation of biodiesel, the production of biodiesel from different feedstocks, properties of fuels, impacts of ethanol on the diesel engine and environment, the impact of biodiesel fuel on engine characteristics, and the impact of biodiesel fuel on exhaust gas emissions of the diesel engine. Lastly, the problem statement, aims, objectives, and justification of the research have been presented.

Chapter 2: Literature Reviews

This chapter shows the reviews on several aspects of literature that parallels the research questions in this study. The first section reviews the global status of biodiesel, the production of biodiesel, classification of biodiesel production feedstocks, and biodiesel production methods. The second section reviews the properties of biodiesel and its blends. The third section reviews the influences of biodiesel-diesel-ethanol blends on engine characteristics and exhaust gas emissions. The fourth section reviews the influences of biodiesel-ethanol blends on the performance, combustion parameters, and exhaust gas emissions. The fifth section reviews the numerical modelling on performance, combustion parameters, and emitted gases of the diesel engines.

Chapter 3: Experimental Studies on Performance, Combustion, and Emission Characteristics of Sample Fuels on a Diesel Engine

This chapter gives a brief explanation of materials, titration process, biodiesel production, fuel blend preparation, measurements of fuel properties, the experimental setup of a diesel engine, measurement procedure on combustion parameters, performance, and exhaust gas emissions. Results and discussions of fuel properties, combustion parameters, performance, and emitted gases of the diesel engine fuelled with D100, WVB100, SB100, BM100, BME5, BME10, and BME15 are also presented in this chapter.

Chapter 4: Prediction of Performance, Combustion, and Emission Characteristics

This chapter presents the numerical techniques to predict the performance, combustion parameters, and emitted gas of the diesel engine. It also provides the results and discussions on the engine parameters and exhaust gas emissions of the fuel samples.

Chapter 5: Validation of Numerical with Experimental Results

This chapter presents the validation of numerical with experimental results.

Chapter 6: General Discussions and Future Perspective

This chapter presents the conclusions and recommendations for further studies.

Appendices and References

1.15 Summary of Chapter One

Chapter one introduced the research conducted in this study. It gives a general introduction concerning the significance of biofuel in the automotive sector and environment, the production techniques and its fuel properties, performance, combustion parameters, and emission characteristics of the diesel engine. The overall introduction of numerical modelling, the significance of the study, problem statement, research aim, objectives of the study, and justification for the research have been identified. In the next chapter, the literature that was reviewed is identified.

CHAPTER TWO

2.0 Literature review

2.1 Introduction

Chapter two presents reviews on several aspects of the studies discussed in Chapter one. The objective of this research chapter is to review the previous works conducted by several researchers on biodiesel characteristics, performance, combustion parameters, and exhaust gas emissions of the diesel engine powered by biodiesel-diesel-alcohol blends and biodiesel-alcohol blends. This chapter further reviews the numerical modelling of engine parameters and exhaust gas emissions powered by biodiesel-diesel-alcohol blends and biodiesel-alcohol blends. According to the reviews, the specific problems of this research have been identified. The first section reviews the overview of biodiesel around the world and the production of biodiesel. The second section reviews the basic properties of biodiesel and its blends. The third section reviews experimental studies on the influences of biodiesel-diesel-alcohol blends on the engine performance, combustion parameters, and emitted gases. The fourth section reviews experimental studies on the effects of biodiesel and its ethanol blends on the engine performance, combustion, and emission characteristics. The fifth section reviews the numerical modelling of the diesel engines powered by biodiesel-diesel-alcohol blends and biodiesel-alcohol blends on performance, combustion, and exhaust gas emissions.

2.2 Overview of the Global Status of Biodiesel Production

According to the Renewable Energy Policy Network of 21st Century (REN21) 2009 report, the most renewable fuels used globally in the automotive sector are biodiesel and ethanol (Burrett et al., 2009). Countries such as the United States of America (USA), Brazil, China, and other European nations show that their biofuel market share is growing. De Oliveira and Coelho (2017) indicate that in the last decade, biodiesel is the leading growth among biofuels and is growing 15 times more in production capacity from 2002 to 2012. In 2013, the report showed that the automotive sector increased the production and consumption of biofuels by 7% worldwide. The total amount of biofuel production was 116 billion litres of which biodiesel fuels represented 26 billion litres. The main production and consumption of biofuels belongs to the European market. The European Union market has overseen being the leading region of

biodiesel production for many years. The European Union market had an estimated amount of 10.5 billion litres of biodiesel production in 2013, while its global share market remains stable in the current year. Nonetheless, in United States, the production of biodiesel increased quickly, and represented 17% of the total global production in 2013. In the same year, the United States market reached a total number of 115 biodiesel producers, with a total installation volume of approximately 8.5 billion litres. Besides the increase in United States biodiesel production, Asian countries are also growing rapidly. Countries such as Indonesia have improved their biodiesel production greatly ever since 2013, due to their new domestic biofuel policies, putting the country among the world's largest biodiesel market producers (Rico and Sauer, 2015). In the same year, Thailand had a 30% growth in both biodiesel and ethanol production.

In countries such as China, the demand for biofuels was motivated by tax and business reasons as it commemorates its small annual local biodiesel production of fewer than 0.2 billion litres of biodiesel production with just around 1.9 billion litres of imported fossil fuels. However, biodiesel in China has suffered a setback as the government agreed to tax the trade of biodiesel due to political motivation to assist local refinery producers of fossil fuels for the local market. REN21 stated that vegetable oil such as jatropha, soybean, coconut, and sunflower oils are mostly used in several countries to substitute fossil fuels to supply and run generators. A country such as Thailand generates its electricity using biodiesel produced from waste cooking oil, whereas in London, biodiesel from frying oil has been used to power the urban bus fleets. In Gauteng province, Johannesburg, South Africa, biogas, and biodiesel have been used to run the farmers' tractors (De Oliveira and Coelho, 2017).

2.3 Production of Biodiesel

Biodiesel fuel is produced from animal fats, fresh vegetable oil, waste vegetable oil, and some raw materials, and it is mainly composed of long-chain fatty acid methyl ester or ethyl ester (Ghazali et al., 2015). Table 2.1 shows the classification of various feedstocks for biodiesel production. Several scientists have noticed that vegetable oil could not be used straight into diesel engines due to its high density and viscosity as it would affect fuel spray atomization (Jayed et al., 2009, Bhuiya et al., 2016). The challenges of using vegetable oil directly in the diesel engine are presented in Table 2.2. To lessen the viscosity of vegetable oil, various techniques of biodiesel production were applied. The techniques that were used to produce biodiesel fuel from different feedstocks are pyrolysis techniques, micro-emulsification

techniques, dilution, and transesterification techniques (Demirbas, 2005, Demirbas, 2009, Silitonga et al., 2011, Balat, 2011).

Table 2.1: Classification of different feedstocks for biodiesel production (Athar and Zaidi, 2020)

Edible oils	Animal fats	Non-Edible oils	Microbial feedstocks
Sunflower	Beef tallow	Jatropha	Fungi
Soybean	Fish oil	Cottonseed	Microalgae
Canola	Poultry fat	Jojoba	Chlorellavulg
Rapeseed	Pork lard	Tobacco seed	Chlamydomonas
Sunflower	Waste frying oil	Moringa	Nostoc
Palm		Rubber seed tree	Botryococcus braunii
Coconut		Mahua	Crypthecodinium cohnii
Peanut		Castor	Cylindrothec
Wheat		Cofee ground	Dunaliella primolecta
Sorghum		Linseed	Isochrysis
Rice bran		Karanja	Monallanthus salina
Sesame		Passion seed	Nannochloropsis
Hazelnut		Croton megalocarpus	
Walnut		Cumaru	

Table 2.2: Challenges of using vegetable oils on diesel engines (Masjuki and Mofijur, 2010, Liaquat et al., 2013, Fazal et al., 2014)

Engine Problems	Reasons
Carbon deposits on automotive components.	High viscosity.
Filter plugging, injector coking, and nozzle blocking.	Polymerization products and free glycerine.
Failure of engine lubricating oil.	Polyunsaturated fatty acid vegetable oil.
The complication of starting during the cold weather.	Higher viscosity.
Delivery of fuel challenges, poor nozzle spray atomization.	Higher viscosity.
Elastomers such as nitrile rubber softening and swelling, hardening, and cracking.	Free methanol and free water in the blend.

Pyrolysis is defined as the method where a single substance was directly transformed into another by the way of heat in the presence of oxygen, and sometimes in the presence of catalyst (Mofijur et al., 2013, Atabani et al., 2013b). This production method is easier compared to the others.

Dilution is a method whereby vegetable oil and diesel fuel are blended to reduce viscosity. Micro-emulsification is defined as the creation of micro-emulsions and it is found as a possible answer to the high viscosity issue of vegetable oil (Abbaszaadeh et al., 2012). Transesterification is similarly identified as alcoholysis, it can be described as the consecutive reversible reaction among waste vegetable or vegetable oil and alcohol blends with the content of a catalyst. However, with the transesterification method, triglycerides were transformed into monoglycerides (Shahid and Jamal, 2011, Silitonga et al., 2014, Sanjid et al., 2014). The transesterification process can be characterized by three transesterification catalysts such as acid, alkali, and lipase. The standard procedure for biodiesel production methods from vegetable oil is illustrated in Figure 2.1. However, out of four conversion procedures, the transesterification process seems to be the best method for biodiesel production since it is an economical and efficient process (Sharma and Singh, 2009, Atabani et al., 2013a, Verma and Sharma, 2016). The contrast of the biodiesel production methods is presented in Table 2.3.

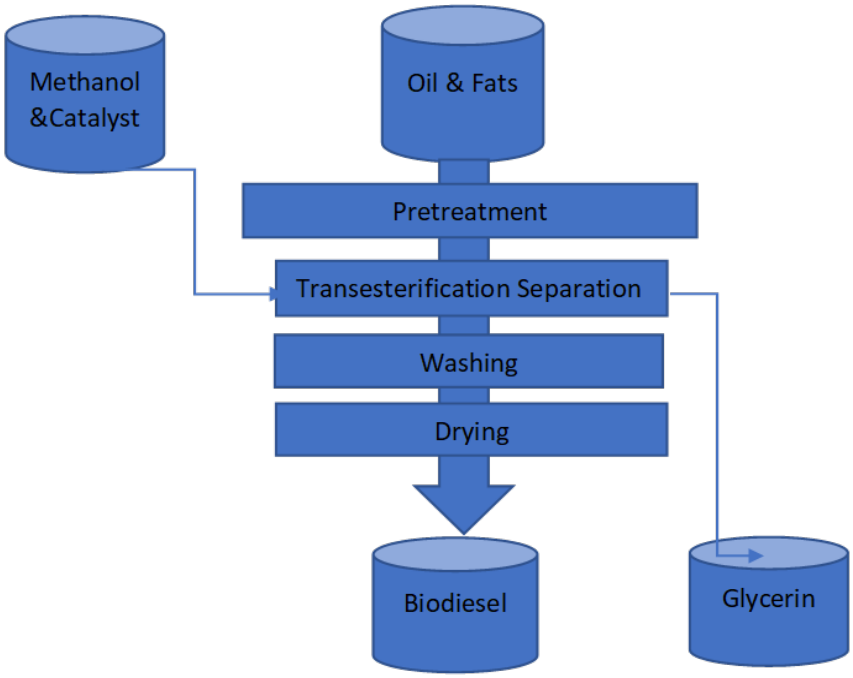

Figure 2.1: Standard procedure of biodiesel production from vegetable oils (Mofijur et al., 2016)

Table 2.3: Contrast of the biodiesel production techniques (Jayed et al., 2011, Mahmudul et., 2017)

Technologies	Dilution or micro-emulsion	Pyrolysis	Transesterification	Supercritical methanol
Advantages	Easy procedure.	Easy procedure and no pollution.	Biodiesel properties are marginally close to diesel, less costly, and low free fatty acid.	Catalysts are not necessary and short reaction time.
Disadvantages	High viscosity and poor volatility.	A high level of temperature is needed, and the apparatus is expensive.	Goods needs to be neutralised and cleaned. Difficult reaction for separation.	The apparatus is expensive, and the energy consumption is high.

2.3.1 Transesterification

Transesterification of fresh vegetable or waste vegetable oils, known as triglycerides, with the blend of alcohol, is rated among the best-developed techniques of biodiesel production. However, biodiesel fuel is known by another term as fatty acid alkyl esters (FAME). Transesterification reactions occur in vegetable oil, animal fat, and light alcohols (methanol or ethanol) with the addition of catalysts such as sodium hydroxide (NaOH) or potassium hydroxide (KOH). The final reaction formed from the transesterification method is glycerol, also called glycerine (Jain and Sharma, 2010). The entire biodiesel or transesterification process is presented in Figure 2.2. According to Abbaszaadeh et al. (2012) the NaOH or KOH catalysts were used to boost the reaction and accelerate the reaction period.

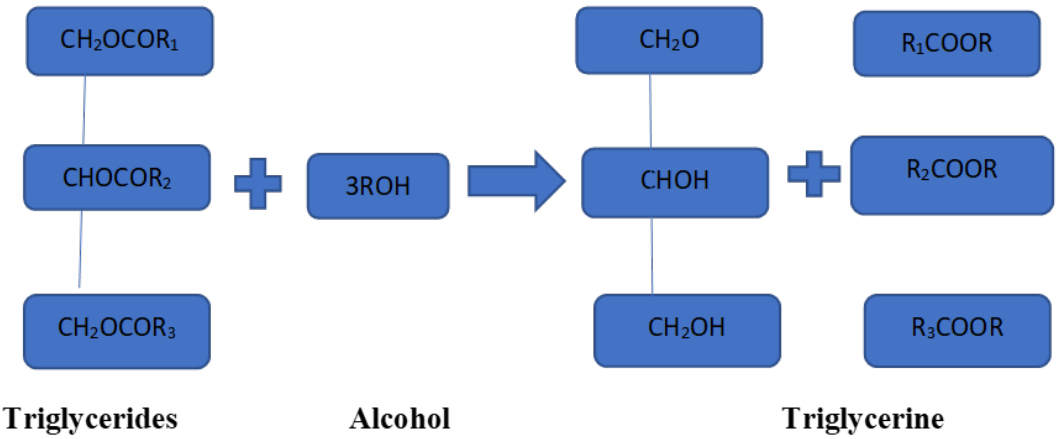

Figure 2.2: Transesterification reaction

2.3.2 Micro-Emulsification

The micro-emulsion can be defined in the same way as colloidal equilibrium diffusion, optically isotropic fluid microstructures, and its dimension range is between 1 to 150 nm. It was established freely in two generally immiscible liquid forms and with more than one ionic or non-ionic emulsifier (Ma and Hanna, 1999, Jain and Sharma, 2010). Micro-emulsions have been divided into three aspects such as aqueous phase, oil phase, and surfactant. Certain light alcohol solvents such as methanol or ethanol were used for the micro-emulsion method to fulfill the highest viscosity restriction of the diesel engines (Jain and Sharma, 2010).

2.3.3 Direct Application and Blending of Oils

The direct application of biodiesel to diesel engines as a fuel is inappropriate as it might cause injector blocking, formation of carbon deposits, oil ring spiking, and thickening of lubrication in long-term running (Ma and Hanna, 1999). However, the blending of biodiesel-diesel fuel blend might resolve the viscosity difficulties in a diesel engine. In addition, the heating up of vegetable oils could decrease the viscosity problems and improve engine fuel atomization as well as the mixing process, which gives better combustion parameters (Martin and Prithviraj, 2011). Peters et al. (1982) tested soybean biodiesel oil blended with standard diesel using the fractions of 1:2 and 1:1 in a direct injection (DI), turbocharged diesel engine. The authors noticed that lubricating oil becomes thick at a 1:1 ratio, but it did not occur at a 1:2 ratio. The 1:2 ratio was suitable for agricultural equipment.

2.3.4 Pyrolysis

Pyrolysis is defined as the heating system with a catalyst and the absence of oxygen to transform one substance into another (Liu et al., 2016). The pyrolysis procedure is not difficult, it is wasteless, has no air pollution, and it is useful in association with other cracking procedures. The types of pyrolyzed items are fresh vegetable oils, animal fats, pure fatty acids, bio-waste, and fatty acids methyl ester (Maher and Bressler, 2007). The pyrolysis techniques have been used by several scientists to produce biodiesel fuels (Maher and Bressler, 2007, Lappi and Alén, 2011, Mihaela et al., 2013).

2.4 Advantages of Using Biodiesel

The advantages of the biodiesel in a diesel engine are significant and based on the following features:

- The engine life and efficiency are lengthy due to biodiesel usage, although accompanied with less savings due to early replacements of parts needing to be procured.
- Biodiesel is environmentally friendly to the atmosphere (Hanaki and Portugal-Pereira, 2018, Ali et al., 2019).
- It improves thermal efficiency since the friction declines due to the diesel-biodiesel blend's higher lubricating quality (Enweremadu et al., 2011, Ogunkunle and Ahmed, 2019a).
- It is made from raw materials that are natural and easy to find (Hamze et al., 2015).
- It is renewable and does not affect global warming due to the closed carbon cycle, and the quantity of carbon carried by the plant is restored to the environment. Biodiesel fuel is carbon neutral as zero gases are emitted into the atmosphere (Ogunkunle and Ahmed, 2019b).
- It is not dangerous for transportation from one location to another due to a high flash point.

2.5 Disadvantages of Using Biodiesel (Mahmudul et al., 2017)

- It produces high NO_x emissions compared to standard diesel fuel.
- High cloud point and pour point freezing of biodiesel influence cold weather starting.
- The high chemical structure of vegetable oil increases the viscosity and density, and this increase affects the fuel pump complications, combustion, and atomization injector system of the engine.

- The brake torque and brake power of the diesel engines fuelled with biodiesel are less compared to standard diesel.
- The brake-specific fuel consumption is higher compared to standard diesel owing to its low heating value.
- Long-term use of the diesel engine powered with biodiesel causes clogging of filters, fuel injectors, and incompatibility due to high viscosity.

2.6 Classification of Biodiesel Production Feedstocks

The feedstocks of biodiesel production are mainly sourced from biomass of renewable origins such as oil plants, algae, and fats. Depending on the source of feedstock, they can be classified into four different categories. The specific purity and composition of each feedstock can be beneficial towards a better understanding of the production processes for the different generations of biodiesel (Bashir et al., 2022).

2.6.1 First-generation Feedstocks

Edible oils such as soybean oil, sunflower oils, rapeseed oils, peanuts, palm oils, and coconut oils are the first harvests to be applied for producing biodiesel. The cultivation of these edible feedstocks is highly known in several nations such as Germany, Malaysia, China, South Africa, and United States. Currently, it is known that edible oils make up 95% of biodiesel all over the world. The fractions of feedstocks utilised globally for biodiesel production consist of 16% rapeseed, 26% soybean, 35% palm, 7% animal fats, 11% used cooking oil, and 5% additional feedstocks (Syafiuddin et al., 2020). Nonetheless, the edible oils that are used to produce biodiesel raise the concern of food against fuel, the devastation of soil sources, and deforestation. Furthermore, the significantly increased rate of edible oils in the past 10 years has had an impact on the biodiesel industry market (Balat and Balat, 2010, Balat, 2011). The use of these oils to produce biodiesel is not possible in the long-term due to the rising gap between their need and supply in several biodiesel producing nations.

2.6.2 Second-generation Feedstocks

Feedstocks such as poultry fat, fish oil, lard, and waste vegetable oils are considered the second generation of biodiesel feedstocks. The free fatty acids (FFA), and other impurities of these

oils are lower compared to edible oils. Non-edible oils with a high level of FFA undergo an esterification process or are normally processed using a two-step esterification technique or transesterification technique to produce biodiesel. The quantity of FFA available through the feedstocks does not only portray the possible reactions, but also guides the choice of catalyst to be applied. Regardless of the accessibility of plentiful feedstocks, the huge task is the feedstocks collection at the designated area to ease the logistic problems. However, edible oils do not experience this problem as they have already established production and supply areas. The pre-treatment cost of non-edible oils is another concern that must be kept lesser than the savings that could be made from the feedstock option (Athar and Zaidi, 2020).

2.6.3 Third-generation Feedstocks

One of the solutions to lower the dependence on edible oil for biodiesel production is to use non-edible oils. Nowadays, non-edible oils are gaining attention globally due to their massive accessibility in various parts of the world. In addition, the advantage of non-edible crops is that they can be grown mostly in wastelands whereas edible crops cannot be suitable for wastelands. They can eliminate their race for food versus biodiesel fuel, and their production is more economical compared to edible oils. The major source of non-edible oils includes jatropha, castor, rice bran, mahua, jojoba, tobacco seed, karanja, cottonseed, neem, coffee ground, kusum, and eucalyptus oil (Kibazohi and Sangwan, 2011, Kumar and Sharma, 2011).

2.6.4 Fourth Generation Feedstocks

Microalgae feedstocks could be described as a promising fourth generation of biodiesel feedstock and they are faster and easier to grow (Bhushan et al., 2020). Microalgae contain the highest oil-yielding feedstocks for biodiesel production and could produce 250 times extra oil per acre than soybean oil (Khan et al., 2017). Photosynthetic microorganisms can produce algal biomass through water, CO_2, and sunlight, but more efficiently than plants. The advantage of microalgae is that its production output is higher than edible and non-edible oils. Microalgae could solve the crisis of biodiesel production and food production. Furthermore, microalgae are the only source of feedstock that has the potential to meet the world's need for transportation fuels and could be sustainably developed quickly. The major bottlenecks for microalgae commercialization are the high costs of biodiesel production required for high oil-yielding algae strains. This process requires a huge quantity of freshwater and huge bioreactors. Several

studies have indicated that microalgae can be grown in flue gas and, therefore, can consume feedstock greenhouse gas (Atabani et al., 2012, Lim and Teong, 2010).

2.7 Catalytic Biodiesel Production Methods

2.7.1 Biodiesel Production Using Homogeneous Catalysts

Homogeneous catalysts are described as the first conventional method for biodiesel production. In this process, the acid and base catalysts are in the form of a liquid. The selection between the base and acid catalysts is mostly based on the amount of FFA content of oil, which usually differs from the origin of the oil, cultivation, processing, and storage systems (Athar and Zaidi, 2020). The current large volume of FFA of the non-edible oils restricts the application of a highly active base catalyst. The base catalysts are mostly recommended for oils that have an amount of less than 0.5 wt.% of FFA (Helwani et al., 2009). The availability of alkaline catalysts and free fatty acids in feedstocks generates soaps that reduce fatty acid alkyl esters (FAAE) yield and makes the separation complicated. Catalysts such as sodium hydroxide (NaOH) and potassium hydroxide (KOH) are suitable to produce biodiesel for low FFA of oils (Sharma et al., 2010, Qian et al., 2010, Silitonga et al., 2013a). Table 2.4 shows some homogenous alkaline catalysts used with different oil feedstocks at various operational parameters and yields for biodiesel production.

Table 2.4: Biodiesel production with homogeneous catalysts

Catalyst	Feedstocks	Catalyst (wt%)	Temperature (ºC)	Alcohol: oil molar ratio	Reaction time (h)	Yield (%)	References
KOH	Karanja	1	60	10:1	1.5	92	(Karmee and Chadha, 2005)
KOH	Waste cooking oil	1	60	3:1	1	94	(Sadaf et al., 2018)
KOH	Jatropha	1	50	6:1	2	97.1	(Berchmans et al., 2013)
KOH	Tobacco seed oil	0.5	50	5:1	1	96.5	(Anwar et al., 2018)
NaOH	Jatropha	0.8	45	9:1	0.5	96.3	(Tapanes et al., 2008)
NaOH	Sunflower	1	60	6:1	2	97.1	(Rashid et al., 2008)
NaOH	Used frying oil	1.1	70	7.5:1	0.5	85.3	(Leung and Guo, 2006)
NaOH	Tobacco seed oil	1	50	5:1	1	97	(Parlak et al., 2009)
CH_3ONa	Rice bran	0.88	55	6:1	1	83.3	(Rashid et al., 2009a)
CH_3ONa	Cottonseed	0.75	65	6:1	1.5	96.9	(Rashid et al., 2009b)
CH_3ONa	Castor oil	1	30	16:1	0.5	93.1	(de Lima da Silva et al., 2009)

2.7.2 Biodiesel Production Using Heterogeneous Catalysts

Various concerns associated with the use of homogeneous catalysts with the mixture of biodiesel are soap formation for high FFA of oil, complications of catalyst separation, and the huge quantity of wastewater during the washing process. However, the use of heterogeneous catalysts might be an alternative solution to that matter. Heterogeneous catalysts could be applied several times, and their separation can be easy. The application of heterogeneous catalysts leads to lower production rates due to both the esterification and transesterification processes that could be done at the same time (Yan et al., 2010, Endalew et al., 2011). Solid heterogeneous catalysts are normally categorized as alkaline, acidic, and bifunctional solids. The acidic solid catalyst could catalyze the existence of FFA by esterification process and the alkaline solid catalyst could catalyze the transesterification process, whereas the bifunctional solid catalyst can catalyze both concurrent esterification and transesterification reactions (Borges and Díaz, 2012). The analysis of heterogeneous acid solid reagents, for producing biodiesel, includes sulfated zirconia-alumina (SZA), tungstated zirconia-alumina (WZA), and perfluorinated alkane sulfonic acid resin (Nafion-NR50) (Chai et al., 2007). An acid solid catalyst such as SZA and WZA can simultaneously assist the transesterification process and esterification process (Kouzu et al., 2008). The alkaline solid catalysts can be categorized as the metal complexes [Sn/Zn/Pb(3-hydroxy-2 methyl-2 pyrone)$_2$ (H_2O_2)], alkaline metal carbonates [Na_2CO_3, K_2CO_3], alkaline earth metal oxides [CaO, MgO, SrO, BaO], transition metal oxides [ZnO, TiO, ZrO_2, Na_2MoO_4)], and alkaline earth metal carbonates [$CaCO_3$] (Tantirungrotechai et al., 2013, Wang et al., 2012). Table 2.5 indicates the biodiesel production methods from different feedstocks under different working conditions of heterogeneous catalysts.

Table 2.5: Biodiesel production using heterogeneous catalysts.

Catalyst	Feedstock	Catalysts (wt.%)	Temperature (ºC)	Alcohol: oil molar ratio	Reaction time (h)	Yield (%)	References
H_2SO_4 impregnated Delinix regia pods	Karanja oil	3	50	12:1	0.75	99.86	(Karmakar et al., 2020)
(ZS/Si) zinc stearate immobilises on silica gel	Waste cooking oil	3	200	18:1	10	98	(Jacobson et al., 2008)
CaO	Jatropha	1.5	70	9:1	2.5	93	(Marinković et al., 2016)
CaO	Soybean	8	65	12:1	3	95	(Liu et al., 2008)
CaO	Sunflower oil	2	60	12:1	2	99.6	(Reyero et al., 2014)
SO_4^{2-} /TiO_2-SiO_2	Waste oil	3	200	9:1	5	92	(Peng et al., 2008)
Sulfonated biochar	Microalgae	5	100	10:1	1	98.2	(Dong et al., 2015)
Li/TiO_2	Canola oil	5	65	24:1	3	98	(Alsharifi et al., 2017)
Calcide dolomite	Canola oil	5.3	60	7.6:1	2.5	96.6	(Korkut and Bayramoglu, 2018)
Ti/SiO_2	Waste cottonseed oil	5	65	30:1	3.4	98	(Kaur et al., 2018)
CaO	Palm oil	9	60	12:1	2	90	(Uprety et al., 2016)

2.7.3 Biodiesel Production Using Enzymatic Catalysts

The transesterification process using enzymatic catalysts does not have a challenge with the purification, washing, saponification, and neutralization of biodiesel. Enzyme catalysts could be applied in high FFA feedstocks. It can be used under mild working conditions and could transform more oil into biodiesel (Aransiola et al., 2014, Rathore et al., 2016). However, due to some complications associated with enzymatic catalysts such as long reaction periods and high costs, they are not highly commonly used (Leung et al., 2010). Lipases such as *Candida rugosa*, *Pseudomonas cepacia*, *Candida antarctica*, *Rhizopus oryzae*, and *Rhizomucor miehei* are all enzymes that are normally capable of catalyzing the transesterification process (Amini et al., 2017). The recycling and constancy of enzymatic catalysts are the major problems for their commercialization. Immobilization can enhance the reusability and stability of the enzymatic catalysts for transesterification reaction (Ranganathan et al., 2008). The enzymatic process at a mild reaction parameter includes alcohol to-oil ratio of 3:1, a temperature of between 40-50ºC, an enzymatic catalyst of 12.5-25 wt%, a reaction time of 4-8 hours, and a stirring speed of 200 rpm (Rathore et al., 2016). The different enzymatic catalysts for the transesterification process are summarised in Table 2.6.

Table 2.6: Biodiesel synthesis using enzymatic catalysts.

Catalysts	Feedstock	Catalyst (wt.%)	Temperature (ºC)	Alcohol: oil molar ratio	Reaction time (h)	Yield (%)	References
Lipozyme RMIM	Soybean	7	4	3:1	50	60	(Zhao et al., 2017)
Lipozyme TLIM	Waste cooking oil	6	40	12:1	2	90.1	(Subhedar and Gogate, 2016)
CalleraTM Trans L lipase	Soybean oil	1.45	35	4.5:1	24	96.9	(Wancura et al., 2018)
(Lipozyme TL IM) + candida antarctica (Novozym 435)	Rapeseed	3+1	35	4:1	12	95	(Li et al., 2006)
Candida antartica (Novozym 435)	Cotton seed	30	50	4:1	7	91.5	(Köse et al., 2002)
Pseudomonas cepacia	Jatropha	5	8	4:1	50	98	(Shao et al., 2008)
Pseudomonas fluorescens	Sunflower oil	10	40	4.5:1	48	91	(Gryglewicz et al., 2013)
Pseudomonas fluorescens	Palm	20	58	18:1	24	98	(Galeano et al., 2017)
Novozym 435	Waste cooking oil	15	12	3.8:1	44.5	100	(Azócar et al., 2010)
Novozym 435	Waste oil	40	50	6:1	14	72	(Taher et al., 2017)

2.8 Properties of Biodiesel

The characteristics of the performance of the diesel engine depend on the properties of fuels. The density and viscosity of biodiesel are higher than standard diesel. Biodiesel fuels are much safer to use compared to standard diesel due to their high flash point. Qi et al. (2010) stated that when light alcohols are mixed with biodiesel, there is poor miscibility.

Due to that fact, the maximum percentage blending of alcohol to biodiesel needs to be limited to 15%, some fuel properties such as diesel, ethanol, soybean, and waste cooking oil biodiesel are presented in Table 2.7, Table 2.8, and Table 2.9 for comparison evaluation (Al-Dawody and Bhatti, 2014, Tutak et al., 2017, Prabu et al., 2017). It can be clearly understood that ethanol has low density and viscosity compared to standard diesel and biodiesel fuels as presented in Table 2.9.

Table 2.7: Properties of diesel fuel and soybean methyl ester (Al-Dawody and Bhatti, 2014)

Properties	Diesel fuel	Soybean methyl ester
Chemical formula	$C_{13.77}H_{23.44}$	$C_{19}H_{35}O_2$
C/H ratio	6.9	6.51
Density at 15 ºC (g/cm)	860	876
Viscosity at 40 ºC (Cst)	3	4.25
Molecular weight (kg/kmol)	190	292.2
Surface tension factor (N/m)	0.028	0.0433
Calorific value (MJ/kg)	42.5	36.22
Flash point (ºC)	76	130
Cetane number	48	51.3

Table 2.8: Properties of waste cooking oil methyl ester (WCOME) and diesel fuel (Kathirvel et al., 2016)

Properties	WCOME	Diesel
Flash point ºC	130	68
Fire point ºC	132	76
Kinematic viscosity at 40 ºC in (mm/sec)	5.87	3.9
Calorific value (MJ/kg)	38.2	45.2
Density (kg/m)	844	830

Table 2.9: Properties of diesel (D100: 100% Diesel), biodiesel (B100: 100% Biodiesel), and ethanol fuel (Tutak et al., 2017)

Properties	D100	B100	Ethanol
Molecular formula	$C_{14}H_{25}$	$CH_3(CH_2)NCOOH_3$	C_2H_5OH
Cetane number	51	56	11
Heating value (MJ/kg)	42.5	37.1	26.9
Density at 20 ºC (kg/m^3)	840	855	789
Viscosity at 40 ºC (mPa s)	3.11	4.51	1.1
Heat of evaporation (kJ/kg)	250	300	840
Stoichiometric air fuel ratio	14.5	12.5	9
Flash point (ºC)	78	>101	425
Auto-ignitron temperature (ºC)	250	363	420
Oxygen content (wt %)	0	10.8	34.8
Carbon content (wt %)	87	77.1	52.2
Hydrogen content (wt %)	13	12.1	13

Venkata Subbaiah and Raja Gopal (2011) described ethanol fuel as an oxygenated compound easily made from renewable resources. It has an improved oxygen chemical element of 35% oxygen content in weight. However, when the biodiesel fuel was blended with ethanol, the combustion process gave more oxygen, which led to a leaning effect. The leaning effect is known to improve combustion characteristics. Ethanol has a low heating value estimated at an average of 27 MJ/kg, which is lesser, when compared, than the heating value of biodiesel (Tutak et al., 2017). The cetane number of ethanol is much lesser than that of biodiesel and of standard diesel, when

compared, as presented in Table 2.9. The lower percentage of cetane number leads to acceptable limits and creates no operational difficulties for biodiesel-alcohol blends.

2.8.1 Density

Density can be described as a significant fuel property that influences engine performance parameters. The properties of the fuel cetane number and calorific value have been correlated with density. Density affects engine combustion parameters and atomization efficiency (Alptekin and Canakci, 2009). It can also affect engine brake power due to the mass of fuel injected. Normally, high density might affect a large flow of fuel resistance that leads to high viscosity, and this can also cause low fuel injection. Ethanol has a lower density than that of diesel, but biodiesel has a density that is higher than the density of standard diesel (Shahir et al., 2014).

Kwanchareon et al. (2007) investigated the influence of biodiesel blends on standard diesel, biodiesel, and ethanol blend properties. The results indicated that the addition of ethanol-blended to biodiesel decreased the density of biodiesel and this might be possible due to the low density of ethanol. Furthermore, the addition of biodiesel fractions means an increase in density. The authors revealed that the density values of all fuel blends are suitable and within the acceptable standard restrictions of the engines. Those results match with the studies carried out by Guarieiro et al. (2009), and Cheenkachorn and Fungtammasan (2009).

Park et al. (2012) evaluated the effects of the biodiesel-diesel-ethanol blend by fixing the ethanol fraction to 20% by volume. The authors observed that the mixing of bioethanol usually decreased the density, viscosity, heating value, and cetane number (Park et al., 2009, Lapuerta et al., 2010, Barabas et al., 2010). As the biodiesel fraction increased then the density, viscosity, and cetane number increased, and in the interim, heating value decreased. The density and viscosity of the fuel decreased due to an increase in bioethanol blends.

Kandasamy et al. (2019) evaluated the impact of blending ethanol with biodiesel (B5E20) and compared it with cotton seed methyl ester 5%-95% pure diesel (B5), pure diesel, and ethanol

properties. The results showed that B5E20 fuel density decreased compared to biodiesel-diesel and pure diesel. The reduction might be caused by the mixture of ethanol to biodiesel-diesel.

Madiwale et al. (2018) investigated the properties of 5% ethanol added to the different feedstock of biodiesel with varying proportion (ranging from 75% down to 15%) of pure diesel fuel. Among the fuel properties investigated, it was found that the 5% replacement of diesel by ethanol in varying proportions of diesel-biodiesel blends decreased the densities of the blends for all the studied proportions of the different feedstocks of biodiesel employed in that published work. biodiesel decreased the density of biodiesel blends for all proportions. This decrease might be caused by the addition of ethanol blends.

(Ramuhaheli, et al. (2023) worked on the qualities of hybrid biodiesel blends that contained 5%, 10%, and 15% ethanol. The findings showed that the low density of ethanol caused the addition of ethanol-blended with hybrid biodiesel to decrease density.

2.8.2 Viscosity

The viscosity of the fuel can be explained as the resistance to allow fuel to flow easily from the engine. Normally biodiesel viscosity is higher compared to standard diesel, but roughly low compared to fresh vegetable oils. Viscosity has a large influence on lower temperatures, which can disturb the fuel from flowing easily from the fuel reservoir to the engine. Mat Yasin et al. (2013) observed that poor fuel spray atomization and erroneous fuel injectors are caused by higher viscosity.

Barabas et al. (2010) tested the viscosity of diesel-biodiesel-ethanol blends and compared to straight diesel. The results suggest that the viscosity of ethanol blends was marginally closed to straight diesel, and the difference gets smaller with the increase in temperature due to the small vaporizing temperature of ethanol. The density of diesel-biodiesel-ethanol blends were also marginally closed to the density of straight diesel due to the additional ethanol fraction.

Zöldy (2011) measured the viscosity by adding the percentage of ethanol blend to biodiesel-diesel using EN ISO 3104:1994 standards. The author set numerous biodiesel blends to measure their viscosity. The results showed that the viscosity of diesel fuel was nearly the same as the biodiesel-diesel-ethanol blend. This might be due to the addition of an ethanol blend.

Mat Yasin et al. (2013) tested the viscosity of biodiesel with the addition of an ethanol blend. The results indicated that the addition of an alcohol blend to biodiesel decreases the density and viscosity. This might be due to alcohol added to biodiesel fuel.

2.8.3 Cetane Number

The cetane number (CN) of fuel indicates the conditions of fuel, if it has a long or short ignition delay period during the engine combustion. The increase in CN is related to the rise of carbon chain length. Normally, diesel engines accept a CN ranging from 40 to 55, but if it is under 38, the ignition delay will increase quickly. However, alcohol has a low CN compared to standard diesel and pure biodiesel fuel. The consequences of low cetane number are noise and long ignition delay. The CN of light alcohols such as ethanol and methanol are low where their range is between 8 and 3, which describes them as a poor CI engine fuel. Additionally, the CN of the diesel-alcohol blend relies on the base of diesel ignition quality and the fraction of alcohol in the blend (Mat Yasin et al., 2013).

Barabas et al. (2010) evaluated the CN of diesel-biodiesel-ethanol blends and compared them with standard diesel. The results indicated that the cetane number of the diesel engine fired with diesel-biodiesel-ethanol blends was decreased with bioethanol content due to the low CN of ethanol. Cetane number has an impact on the engine performance and combustion parameters. However, biodiesel fuel, due to high CN, could improve fuel properties. The blend can fulfill the standard condition of 51 CN for diesel.

2.8.4 Heating Value

The heating value (HV) is another important aspect for evaluation in terms of suitability as an option for diesel fuel. The low heating value of fuel can influence the engine performance, more

particularly on power output. The heating value of biodiesel and alcohol fuels is less compared to straight diesel. Nevertheless, the mixture of biodiesel and standard diesel decreased the heating value compared to standard diesel. The increased percentage of ethanol blended into biodiesel highly reduced the heating value (Fernando and Hanna, 2004, Cheenkachorn and Fungtammasan, 2009, Kannan, 2013). This decrease might be caused by the low heating value of ethanol. Zhu et al. (2011a) indicated that the lower heating value of the biodiesel-ethanol blend decreased compared to pure biodiesel and standard diesel. This might be caused by the addition of ethanol blend to biodiesel fuel.

2.8.5 Flash Point

The flash point (FP) has been applicable in shipping for safety standards that specify flammable resources. It also can be explained as the starting of fuel burn temperature, with the contact aflame and air. It shows the existence of highly explosive substances (Srivastava and Prasad, 2000). The standard methods that were normally applied to measure the flash point are ASTM D93 and EN ISO 3697. It does not have an impact on the caliber of combustion. Nonetheless, it is crucial for the storage, treatment, and transportation of fuel. Numerous factors can influence the FP of biodiesel and one of them is alcohol content (Boog et al., 2011). The quantity of carbon atoms and binary bonds of the biodiesel can influence the biodiesel flash point (Carareto et al., 2012).

2.8.6. Cloud Point (CP)

The cloud point can be defined as the temperature where wax crystals come out when fuel is cool. The formation of wax crystals stiffens the oil and blocks the engine fuel injectors and fuel filters (Hassan and Kalam, 2013). The measurement of CP is mostly reliable to estimate biodiesel cold flow properties as it reveals the tendency of oil to block fuel injectors and filters of the engine during the low temperature operating conditions. The CP could be measured using ASTM standards such as D5771, D5772, D5773, and D2500 (Sierra-Cantor and Guerrero-Fajardo, 2017). Verma et al. (2016) studied the development of palm biodiesel cold flow properties by using ethanol as an additive. The results showed an increase in the ethanol percentage gradually increases the cloud point and pour point of biodiesel. The authors suggested that using an 80% biodiesel and

20% ethanol blend at low-temperature conditions is the best for cold flow properties. Dwivedi and Sharma (2016) reported similar results to enhance cold flow properties of biodiesel from waste cooking oil. Their studies showed that a similar additional percentage of ethanol to waste cooking oil biodiesel contributed to the improvement of cloud point and pour point.

2.8.7 Pour Point (PP)

The Pour Point (PP) is the coldness temperature at which the crystal groups are formed in the fuels, blocking fuel from flowing and later losing its pumping capability (Dwivedi and Sharma, 2015). It is a significant parameter to assess the flow conduct of biodiesel in the pipeline supplies and storage (Edith et al., 2012). Biodiesel PP could be measured using the ASTM standards such as D5853, D5949, D5950, D5985, D6749, D6892, and D97 (Monirul et al., 2015). Out of all these standards, ASTM D5853 and ASTM D97 are the most applied to assess the pour point (Sia et al., 2020).

Ali et al. (2014) evaluated the addition of ethanol, butanol, and diethyl ether to enhance the pour point of biodiesel. The results show that the addition of 5% diethyl ether to biodiesel improved the cold flow behavior of pour point reduction. The addition of ethanol, butanol, and diethyl ether decreases the viscosity and density of the biodiesel. Their experimental results also showed that fuel properties such as density, acid value, and viscosity improved with the addition of ethanol, butanol, and diethyl ether.

2.8.8 Cold Filter Plugging Point (CFPP)

CFPP is described as the cold temperature at which the fuel leads to block filters and crystallizes in diesel engines. It is commonly used as an indicator of the low temperature of fuels, and it is a significant concern in countries with extreme cold weather, where the ambient temperature would be low enough to crystallize and block the fuel filters (Bukkarapu and Krishnasamy, 2021). The CFPP measurements provide the lowest temperature of fuels at which engine operational problems occur after lengthy exposure to lower ambient temperature conditions. The test method to measure the CFPP is ASTM D6371 standards (Subramaniam et al., 2013).

Pradelle et al. (2019) evaluated the CFPP by adding 5% and 10% of ethanol blends to biodiesel-diesel fuel and compared it to standard diesel. The results proved that the CFPP of biodiesel and 10% of ethanol blend decreased but was higher compared to 5% of ethanol blend. This decrease could have been due to the decreasing miscibility of the diesel fuel and biodiesel when ethanol content is increased.

2.8.9 Acid Value (AV)

The acid value measures the free fatty acids contained in fuel samples. The FFA are either saturated or unsaturated acids that normally take place in fats and oils. Fatty acids differ in carbon chain length and the quantity of unsaturated bonds. The higher value of free fatty acids could lead to a larger amount of acid value. The AV is stated as mg KOH required to neutralize 1 g of FAME. The consequences of higher acid content in the fuel supply system might cause a serious corrosion problem in a diesel engine. The acid value can be evaluated by using ASTM D664 and EN 14104 standards. These two standards accepted the maximum acid value of 0.50 mg KOH/g for biodiesel fuel (Ali et al., 2016). Mat Yasin et al. (2013) evaluated the acid value of standard diesel, biodiesel, biodiesel-diesel blend, and biodiesel-alcohol blend. The results indicated that the acid value of the biodiesel-alcohol blend attained the highest value compared to other testing fuels, while the biodiesel-diesel blend attained the minimum value, which is 16.7% lower compared to standard diesel.

2.9 Fuel Blending Techniques

Currently, three key methods are used for biodiesel blend preparation, namely splash, in-line and in-tank bending (Micic, 2020). These methods were used to blend ethanol and biodiesel mixture fuel to the required percentage.

Splash blending can be defined as the process where two fuels (biodiesel mixture and ethanol) are loaded into separate vessels, with relatively slight blending occurring as the fuel lay in a vessel. With this blending method, it is important to consider that biodiesel has higher specific gravity compared to ethanol. The basis of this blending technique is that biodiesel must be sprayed at the

top layer of ethanol already loaded into the tank. If this order is not respected, fuel cannot be properly blended.

The second technique is in-line blending. For this technique, ethanol was added to the stream of biodiesel mixture as it flows through the tube in a way that the ethanol and biodiesel mixture become fully blended by the turbulent flow through the tube. Then the ethanol blend was continuously added slowly into the flowing stream of biodiesel mixture flowing through a small line inserted in a large tube. Ethanol was added in a slight amount of volume throughout the time while the biodiesel mixture was loaded.

The third technique is in-tank blending, which loads two fuels separately (ethanol and biodiesel mixture). These techniques do not need additional recirculation as it results in a satisfactory blending of two fuels. Out of those three techniques, the splash blending technique is widely used for commercial purposes due to its effectiveness and well-planned. The experimental ethanol blend purpose needs high measurement perfection, a huge amount of testing batches, and low biodiesel quantities.

2.10 Influences of Biodiesel-Diesel-Ethanol Blend on Performance, Combustion, and Emission Characteristics

Randazzo and Sodré (2011a) investigated the impact of ethanol in diesel-soybean biodiesel blends on the fuel consumption of a diesel engine. The cold-starting period was evaluated as it was seen as one of the significant problems of engines powered by biodiesel and ethanol blends. Fuel blends containing 3% to 20% of soybean biodiesel-diesel-ethanol fuel were experimentally tested. It was noticed that the increase of 20% biodiesel blend to diesel fuel attained a long cold-starting period. This result has an impact on the high distillation temperature of 20% biodiesel blend (B20), in comparison with 3% biodiesel blend (B3) and 10% biodiesel blend (B10). An increase in the ethanol blend could increase the cold-start period. The specific fuel consumption of the 5% ethanol blend and B20 increased. Similar results have been reported by Lapuerta et al. (2007) who used ethanol blends ranging from 5% to 30% in a diesel engine and attained an increase in fuel consumption.

Fang et al. (2013) evaluated the effect of adding ethanol to diesel and biodiesel on the combustion characteristics and exhaust gas emissions of a diesel engine. The ethanol and diesel fuel were blended with biodiesel to avoid the stratification of alcohol and diesel blends. Due to the low combustion temperature of biodiesel-diesel-ethanol (BDE) blends, the authors indicated that NO_x emissions decreased compared to pure diesel. This could be caused by the higher latent heat of vaporization of ethanol, while the smoke emitted by BDE blends also decreased because of high oxygen content of ethanol. However, the maximum heat release rate of BDE blends increased compared with pure diesel. It was also noticed that the ignition delay was higher due to the low cetane number of alcohol blends.

Khoobbakht et al. (2019) investigated the effect of ethanol blend to biodiesel and diesel on the performance and emitted gases. An experimental design was conducted as central composite rotatable designs using the response surface method. The results showed that the brake power of biodiesel-diesel-ethanol blends decreased compared to pure diesel and this was possibly due to lower heating value. The brake specific fuel consumption of biodiesel and ethanol blends increased compared to pure diesel. The BSFC increase might have been possibly caused by lower heating value of alcohol blends and the higher viscosity of biodiesel. The low volumetric ratio of biodiesel and ethanol blends enhanced the brake thermal efficiency of the diesel engine.

Kavitha et al. (2019) experimentally evaluated and compared the diesel engine fuelled with a biodiesel-diesel-ethanol blend using standard diesel as a reference fuel. The test was conducted to evaluate the engine parameters and exhaust gas emissions under different load conditions. The 90%diesel-7.5%biodiesel-2.5%ethanol (D90B7.5E2.5) was associated with a highly significant decrease in BSFC compared to standard diesel at a power output of 0.937 kW. Usually, BSFC decreases with an increase in engine loads. Due to the low density and viscosity of ethanol blends, the BSFC decreased with a highly concentrated biodiesel blend (Yuvarajan and Ramanan, 2016). A decrease in NO_x for emission was observed for D90B7.2E2.5 compared to straight diesel, while D95B3.72E1.25 slightly increased compared to straight diesel fuel. These results could be explained by the maximum in-cylinder pressure of biodiesel compared to standard diesel leading to high NO_x emission (Siva et al., 2019, Ganesan et al., 2019, Devarajan et al., 2019). The HC, CO_2, and NO_x of ethanol blend decreased with an increase in biodiesel blend, although it released

less CO with a reduction of the biodiesel blend. Such results could be attributed to the complete combustion process of fuel and variation to the engine oxygen supply.

Noorollahi et al. (2018) evaluated the impact of diesel fuel blends (biodiesel-diesel-ethanol) on engine characteristics. Full load conditions were experimentally used to evaluate the engine parameters and exhaust gas emissions at various speeds of 1700, 2100, 2500, and 2900 rpm. The results showed that the brake power of BDE decreased compared to standard diesel. This reduction could be possibly due to the high oxygen content of bioethanol and the high volatility of ethanol. With an increase in ethanol blends, the torque ratio was initially increased and later decreased due to the lower heating value of biodiesel. The biodiesel-diesel-ethanol blend gave a high specific fuel consumption compared to standard diesel. This increase could be explained by the increased percentage of biodiesel blends. It was also observed that NO_x emissions increased with an increased fraction of biodiesel.

Bhurat et al. (2019) investigated the impacts of BDE blends on engine performance and exhaust gas emissions. The results showed the enhancement of BTE of a diesel engine powered by ethanol blends compared to standard diesel. This improvement might be possible due to the low alcohol boiling point, which gives a better-quality spray of alcohol blend. However, the BSFC of BDE increased compared to standard diesel due to long ignition delay and low heating value. The NO_x emission of BDE decreased compared to standard diesel and this decrease might be due to ethanol addition to biodiesel, which leads to the cooling effect. The hydrocarbon emissions were considerably higher at all engine load conditions due to an inadequate quantity of oxygen, which leads to air-fuel mixture content. The CO emissions were significantly higher than standard diesel, which certainly reflects inadequate oxygen in the combustion period leading to inefficient combustion.

Barabas et al. (2010) investigated the impact of biodiesel-diesel-ethanol blend and diesel fuel to evaluate the performance parameters and exhaust gas emissions of the diesel engine at a fixed speed of 1400 rpm. The authors observed that the BSFC of the diesel engine powered by biodiesel-diesel-bioethanol blends was higher compared to standard diesel at low load conditions. This might be due to the lower heating value of alcohol blend. Furthermore, CO emission results were lower

at a high load condition, whereas NO_x emissions were marginally increased. However, less HC and smoke were emitted at all engine loads, and this might be caused by the alcohol blend.

Jha et al. (2009) experimentally compared the emitted gases of a new diesel engine and an old diesel engine fuelled with different ethanol blend ratios. It was reported that NO_x emissions were low for ethanol blends with the use of the new engine while the emissions were high for the old engine. The increasing fraction of ethanol blends leads to an increase of CO emissions for both the new and old engines.

Cheenkachorn and Fungtammasan (2010) experimentally investigated engines powered with biodiesel-diesel-hydrous-anhydrous ethanol blends, compared to standard diesel on performance characteristics and exhaust gas emissions. The authors concluded that the engine fuelled with BDE blends exhibited a decrease in brake power compared to diesel fuel. Those results could be explained by the low heating value and longer ignition delays of ethanol blends. The BSFC of ethanol blends increased compared to standard diesel due to their higher oxygen content and low heating value. It was found that the PM and CO gases emitted were less compared to standard diesel and this reduction might be due to improved combustion of alcohol blend. Moreover, NO_x emissions of biodiesel-diesel-alcohol blends were increased compared to standard diesel, and this might be caused by the fuel-air equivalence ratio.

Yilmaz et al. (2014b) studied the impacts of BDE blends on performance parameters and exhaust gas emissions. The ethanol blends percentage were 3%, 5%, 15%, and 25%, compared to standard diesel. The results showed that the exhaust gas temperature (EGT) of ethanol blends was higher compared to standard diesel, and this might be due to the low CN and higher latent heat of vaporization produced by ethanol blends. However, the ethanol blends of CO emissions were higher compared to standard diesel. This behavior might be the reason for lower CN and higher latent heat of vaporization produced by alcohol blends. In addition, BDE blends emitted less NO compared to standard diesel due to the ethanol cooling effect, which leads to low cylinder combustion.

Hulwan and Joshi (2011) experimentally evaluated the impact of ethanol percentage additive on biodiesel-diesel fuel in a diesel engine. The engine parameters and emitted gases of the BDE blend were evaluated and compared to normal diesel as a reference fuel. The data indicated that the BTE of the diesel engine fuelled with BDE blends improved compared to standard diesel. The possible explanation for this improvement was the high oxygen content of ethanol blend. The BSFC of BDE fuel blends increased compared to standard diesel and this action was attributed to the low heating value of the ethanol blend. The authors discovered that the increase of in-cylinder pressure was caused by the increase of engine load. However, low CN and high latent heat of ethanol blends increased ignition delay at low load conditions. The start of combustion delayed with the application of BDE fuel blends compared to standard diesel. The low viscosity of ethanol blends gives an improvement of the air-fuel mixture, and the high percentage of fuel was burned through the premixed burning phase. Smoke emissions of BDE decreased compared to standard diesel, especially at a maximum load condition. Availability of alcohol oxygen content might be the reason for this decrease.

Guarieiro et al. (2014) evaluated the use of oxygen containing fuels such as ethanol and biodiesel on performance parameters and exhaust gas emissions of a diesel engine powered by biodiesel-diesel, BDE blend, and compared to neat biodiesel. The authors observed that NO_x emitted by BDE slightly decreased compared to diesel fuel. Furthermore, both higher latent heat of vaporization and lower heating value of ethanol blends might contribute to this decrease. The CO emissions of BDE decreased compared to biodiesel fuel and this might be due to improved combustion of the ethanol blends. It was also noticed that the biodiesel-diesel recorded high power output due to improved heating value compared to other test fuels. The BSFC of biodiesel-diesel fuel was decreased compared to neat biodiesel and BDE blends due to the high calorific value.

Geo et al. (2017) experimentally compared a diesel engine fuelled by biodiesel and ethanol portion to evaluate the performance parameters and exhaust gas emissions. The test was done at a fixed speed of 1500 rpm and different percentages of engine load. The authors found that the brake specific energy consumption (BSEC) of the engine fuelled by ethanol blends decreased compared to neat diesel, and the increase of the BSEC observed from these neat fuels (without ethanol) was attributed to the high level of density and viscosity, which has an impact on mixture formation,

leading to a major diffusion combustion phase. The NO_x emitted from the ethanol blends at full load conditions was lesser than that emitted by neat diesel due to reduced premixed burning rate, which helped to slow the heat release. Higher HC emission was noticed with the use of biodiesel-ethanol blends compared to normal diesel. This increase in HC emissions might be caused by the formation of a destruction layer of unburned ethanol in the combustion chamber.

2.11 Influences of Biodiesel-Ethanol Blends on the Performance, Combustion, and Emission Characteristics

Zheng et al. (2016) evaluated the engine characteristics and exhaust gas emissions of ethanol and butanol, each to biodiesel and biodiesel 2,5-dimethylfuran, pure biodiesel, and normal diesel. The test was conducted using different ratios of exhaust gas recirculation (EGR) (0%, 30%, and 50%), three different loads of 20, 40, and 60 mg per cycle diesel fuel, and two blending fractions (20% and 50%). It was concluded that the three binary blends and pure biodiesel fuel emit less smoke compared to normal diesel. All alcohol blends emitted low NO_x gas, and this might be caused by low viscosity, which has an impact on the high ignition delay of the engine to sustain low combustion temperature to the cylinder. It was observed that the engine fuelled with neat biodiesel, 20% butanol blend (Bu20), and dimethylfuran (DMF20) emitted higher NO_x compared to diesel. The HC and CO gas emissions of binary fuels were higher compared to normal diesel at low load conditions. On the other hand, they emitted less than normal diesel at a high load condition. The fuel sample of biodiesel and ethanol blends attained low BTE compared to normal diesel at low load conditions and medium load conditions. However, all percentages of EGR were increased during the high load conditions. The peak compression ratio (CR) value of 20% ethanol blend was roughly the same as neat diesel and HRR was like ethanol blends (20% ethanol-80% diesel) at low load conditions.

Venkata Subbaiah and Raja Gopal (2011) experimentally evaluated the effects of biodiesel and its 2.5%, 5%, and 7.5% ethanol blends on engine performance parameters and exhaust gas emissions. The test was operated at different engine load conditions from 0% to 100%. According to the findings, the BTE of alcohol blends was improved compared to pure diesel. Nevertheless, the BSFC of engines powered by biodiesel-ethanol blends increased compared to pure diesel. The lower heating value (LHV) of ethanol blends might be the reason for this increase. The CO

emissions of 2.5 and 5% of ethanol blends were lower, whereas 7.5% of ethanol blend emissions were higher compared to pure diesel. The NO_x emissions of biodiesel-ethanol blends attained lower values compared to pure diesel at all load conditions, and this might be possible due to high latent heat that gives an indication of a high cooling effect leading to low combustion temperature, which improved oxygen molecules. The HC gas emitted by biodiesel-ethanol blends attained less compared to neat diesel. This might be possible due to the improvement of engine combustion, higher HRR, and in-cylinder temperature of alcohol molecules.

Ramuhaheli et al. (2022) evaluated the performance and emission characteristics of ternary blends of hybrid biodiesel mixture ethanol (biodiesel-biodiesel-ethanol). The results were compared with experimental data analysis using the Diesel-RK software. Pure hybrid biodiesel was shown to have the highest brake power among the alternative fuels at a maximum speed of 2500 rpm. The higher brake power of hybrid biodiesel was caused by its high heating value when compared to that of individual biodiesel and hybrid biodiesel-ethanol blend fuels. When compared to individual biodiesels and diesel, the NO emissions of experimental and anticipated values for the hybrid biodiesel-ethanol blend attain the lowest value. Low in-cylinder combustion temperature caused by ethanol vaporization heat is the cause of this drop.

Zhu et al. (2011a) investigated and compared the combustion parameters, performance, and exhaust gas emissions of the diesel engine powered by biodiesel-ethanol blends, pure biodiesel, and Euro V diesel fuel. The results showed that the diesel engine fuelled with biodiesel-ethanol blend led to higher maximum ICP and HRR compared to biodiesel. The authors also found that the biodiesel-ethanol blends exhibited a longer ignition delay. This could be clarified by the low CN of ethanol blends (Yilmaz et al., 2014b). The brake specific fuel consumption of the diesel engine fuelled with pure biodiesel and biodiesel-ethanol blends was higher compared to standard diesel. This increase might be due to LHV of ethanol blends and higher density of biodiesel. The BTE of biodiesel and biodiesel-ethanol blends were marginally close, but higher than pure diesel due to biodiesel oxygen content of alcohol blends. In addition, the biodiesel-ethanol blends reduced the NO_x and PM emissions compared to pure biodiesel and pure diesel. The authors observed that biodiesel oxygen content is an important parameter to decrease NO_x and PM. The

low percentage of ethanol blends emitted lower CO and HC compared to biodiesel in all test methods whereas a high percentage of ethanol blends led to an increase in HC and CO.

Prbakaran and Viswanathan (2018) evaluated and compared the effect of the various proportions of biodiesel and ethanol blends on the engine performance, combustion parameters, and emitted gases of various proportions at a fixed speed and various engine loads. The diesel engine was fuelled with biodiesel-ethanol blends compared to normal diesel as base fuel. The results showed that the fuel samples of biodiesel-ethanol blend increased BTE with engine load increase compared to normal diesel. This increase in BTE might be explained by the lower viscosity of ethanol mixture percentage. It has been pointed out that the BSFC from biodiesel-ethanol blend increased compared to normal diesel. The low heating value of alcohol blend could explain this increase. It was found that the maximum ICP and HRR of all biodiesel-ethanol blends increased at high load conditions due to better reactivity of oxygen at those high load conditions where the combustion chamber temperature was high. The NO_x emissions from the 50% biodiesel and 50% ethanol attained lesser value than from normal diesel at all load conditions. It was suggested that the 50% proportion of ethanol addition to the biodiesel fuel blend led to NO_x emissions reduction. The diesel engine powered by 90% biodiesel and 10% ethanol fuel blend had smoke emission that rose to attain the emission from normal diesel at full load (100%), but the 50% and the 30% blends of ethanol with biodiesel exhibited lower smoke emissions than the emission from normal diesel at all load conditions. This low smoke might be due to low viscosity of the alcohol blend, which causes better atomization and improves reactivity for blends containing oxygen.

Wei et al. (2018) experimentally evaluated biodiesel and its ethanol blends of 5%, 10%, and 15% by its volume on a diesel engine with constant speed at various load conditions on combustion parameters, performance, and exhaust gases. It was discovered that the biodiesel-ethanol blends achieved maximum HRR, maximum ICP, long ignition delay, and short combustion duration. The maximum combustion parameters of biodiesel-ethanol blends might be caused by low CN. The authors observed that the BSFC of biodiesel-ethanol blends increased when compared to biodiesel possibly caused by the low heating value. The BTE difference between biodiesel and biodiesel-ethanol blends were marginally close. The BTE of diesel engines powered with biodiesel-ethanol blends decreased compared to standard diesel at low load conditions due to low combustion

temperature and higher latent heat of evaporation of ethanol. In addition, biodiesel-ethanol blends emitted high CO and HC gases, while their NO_x emissions decreased.

Yilmaz and Sanchez (2012) investigated the influence of ethanol and methanol to biodiesel on a diesel engine to evaluate the engine parameters under various load conditions. These two alcohol blends were experimentally compared to pure diesel and pure biodiesel fuel to evaluate the performance and exhaust gas emissions. The authors observed that the BSFC of the biodiesel-ethanol blend was marginally less compared to biodiesel-methanol blend but higher compared to neat diesel. This could be clarified by alcohol's higher latent heat of evaporation. The EGT of biodiesel-alcohol blends was marginally higher than neat diesel and pure biodiesel due to short combustion period of alcohol blends. The CO emissions of biodiesel-alcohol blends were improved marginally compared to diesel and pure biodiesel under 70% engine load. Low NO_x was emitted by alcohol blends compared to diesel and pure biodiesel. The possible explanation for this decrease might be the ICT of the latent heat.

Alptekin (2017) evaluated the emitted gases, injection, and combustion parameters of the turbocharged common rail engine powered by biodiesel with oxygenated solketal and ethanol fuel blends. The results indicated that both oxygenated fuel blends have high BSFC compared to normal diesel. Yilmaz et al. (2014a), Lei et al. (2016) found that higher BSFC of the diesel engine powered by biodiesel, biodiesel-diesel, and diesel-oxygenated fuel blends was achieved compared to diesel. The maximum cylinder pressure of the biodiesel-ethanol blend was higher compared to standard diesel. Venkanna and Venkataramana Reddy (2012) obtained similar results from their investigations. The authors found that the maximum net heat release rate (MNHRR) values were marginally similar, and the different positions for MNHRR were less than 1° crank angle (CA) of different fuels with the same testing circumstances. The NO_x emissions of biodiesel-ethanol blends increased compared to standard diesel and this might be attributed to the availability of high oxygen content. Moreover, CO_2 and CO emitted by biodiesel-ethanol blends were slightly lower compared to biodiesel, and this might be caused by high oxygen present in the biodiesel and oxygenated fuels.

2.12 Numerical Modelling on Performance, Combustion, and Emission Characteristics of Diesel Engine Powered by Biodiesel and Alcohol Fuel Blends

Computer simulation is the process of building a model of a physical system representing real processes and evaluating the processes. Frequently, the model is based on mathematical procedures to represent the real procedures applying a set of differential equations, and the analysis is processed by a computer. Computer simulations save time and are more economical compared to experimental studies. Nevertheless, simulation is only a step before measurements and the results attained from numerical simulation must be validated with measurement results to verify accuracy. Once validated, computer simulation can be used to evaluate the engine parameters of a system. Numerical simulations are extremely beneficial in the case of internal combustion engine analyses (Ganesan, 2000).

2.12.1 Single-dimensional Model

Single-zone dimensional models are commonly used in preference of more accurate models such as multi-dimensional thermodynamic models due to being less complicated, numerically more efficient, and mostly yield comparable results. The single-zone models do not include spatial variations, and, hence, assume a uniform blend of temperature and composition in the whole combustion chamber. The first law of thermodynamics is used in cylinder gases by assuming the combustion chamber as the control volume (Maurya et al., 2019). The condition of the cylinder is described in terms of average properties, and the engine cylinder is assumed as a single zone, where there is no temperature gradient occurring, and the reactants and products are entirely mixed (Gatowski et al., 1984, Thor et al., 2009, Gautam et al., 2022). Hence the ideal gas equation and thermodynamic laws form the basis of engine combustion modelling in a single zone.

2.12.2 Single-dimensional Model Equations

In-cylinder volume

The in-cylinder volume can be computed using equation (2.1) (Thakkar et al., 2021)

$$V(\theta) = V_C + \frac{V_S}{2}.\left(1 + \lambda - cos\theta - \sqrt{\lambda^2 - sin^2\theta}\right) \quad (2.1)$$

Where V_C is the clearance volume, V_S is the swept volume, λ is the ratio of the radius of the crank over the connecting rod length and θ is the crank angle.

In-cylinder temperature

The in-cylinder temperature could be obtained using the first law of thermodynamics, which is given by equation (2.2) (Gautam et al., 2022)

$$\frac{dT}{d\theta} = \frac{T}{PV}(\gamma - 1)\frac{dQ}{d\theta} - \frac{T}{V}(\gamma - 1)\frac{dV}{d\theta} \quad (2.2)$$

Rate of heat release

The heat release rate can be computed by equation (2.3) (Cuddihy, 2014)

$$\frac{dQ}{d\theta} = \frac{1}{\gamma - 1}p\frac{dV}{d\theta} + \frac{1}{\gamma - 1}V\frac{dp}{d\theta} \quad (2.3)$$

Where $\frac{dQ}{d\theta}$ is the heat release rate (J/^{o}CA), γ represents the specific heat ratio, P represents the in-cylinder pressure (bar), and V represents the in-cylinder volume (m^3).

In-cylinder pressure

In-cylinder pressure can be computed using equation (2.4) (Cuddihy, 2014)

$$\frac{dP}{d\theta} = \frac{\gamma - 1}{V}\left(\frac{dQ}{d\theta}\right) - \gamma\frac{P}{V}\left(\frac{dV}{d\theta}\right) \quad (2.4)$$

2.12.3 Multi-dimensional Model

Multi-dimensional CFD codes are accurate and more realistic simulations of the liquid fuel spray, particle collision, oscillation, atomization, and evaporation encountered by highly turbulent reactive fluid flow in diesel engines. The KIVA is a computer code used for numerical computation of transient, two and three-dimensional chemically reactive flows along with sprays. It uses a time-marching, finite volume scheme, which resolves the conservation equations of mass, momentum, and energy, and accounts for turbulence using an Arbitrary Lagrangian Eulerian (ALE) process in three solution phases (Maghbouli et al., 2013).

2.12.4 Multi-dimensional Model Equations

The equation of species m and the energy equation in terms of specific internal energy are formulated in the KIVA code as given by Equation (2.5) and (2.6), respectively (Amsden et al., 1985, Maghbouli et al., 2013).

$$\frac{\partial \rho_m}{\partial t} + \nabla.(\rho_m u) = \nabla.\left[\rho D \nabla\left(\frac{\rho_m}{\rho}\right)\right] + \dot{\rho}_m^c + \dot{\rho}^s \delta_{ml} \quad (2.5)$$

$$\frac{\partial}{\partial t}(\rho l) + \nabla.(\rho u l) = -P\nabla.u + (1 - A_0)\sigma : \nabla u - \nabla.J + A_0 \rho \varepsilon + \dot{Q}^c + \dot{Q}^s \quad (2.6)$$

Where $\dot{\rho}_m^c$ in equation (2.5) and $\dot{Q}^c$ in equation (2.6) are the parameters that need to be computed through the combustion model. Numerical explanations of these phrases are as follows:

$\dot{\rho}_m^c = W_m \dot{\omega}_m$

$\dot{Q}^c = -\sum_{m=1}^{M} \dot{\omega}_m \left(\Delta h_f^o\right)_m$

Venkatraman and Devaradjane (2011) built a zero-dimensional, single-dimensional model for DI diesel engines to predict the performance and emitted gases of any biodiesel with minimum inputs such as density, calorific value, molecular formula, and engine specifications. The developed simulation model was used to predict the engine parameters and exhaust gas emissions for ICEs. Experiments were performed in a diesel engine fuelled with diesel and different blends of pungam biodiesel to validate the simulation model. The results show that heat release rate increased during premixed combustion and decreased during diffusion combustion. The increase in the rate of heat release rate was because of the decrease in the ignition delay period. Biodiesel and its biodiesel-diesel blends showed low specific fuel consumption compared to diesel and this might be due to better in-cylinder combustion. The predicted NO_x data were slightly higher compared to the experimental results. The addition of the biodiesel blends decreased HC values with respect to load increase. The emitted CO attained lower biodiesel-diesel blends compared to standard diesel. It was observed from the results that there is a good agreement between simulated and experimental data, which reveals the fact that the simulation model developed predicted the engine characteristics and emitted gas of any biodiesel and diesel fuel, given engine specifications as input.

Sudeshkumar and Devaradjane (2011) developed a two-zone-computer simulation model to predict the performance, combustion, and gas emissions of a diesel engine powered by an ignition

improver blend of 12% 2-ethoxy ethanol. Results were validated using experimental data. A good agreement was found between the predicted and experimental values. The operational range of the model was wide, and the computational run time was short. It was concluded that the simulation model would be suitable to be used for thermodynamically based cycle simulations in CI engines fuelled with ignition improver blends and diesel fuel.

An et al. (2015b) investigated the consequence of methanol addition to biodiesel on engine parameters and exhaust gas emissions. A 3D CFD numerical simulation was conducted using the KIVA-CHEMKIN model code coupled with CHEMKIN II to simulate biodiesel and 5%, 10%, and 20% of methanol blends at different load conditions at a speed of 2400 rpm. The results showed a decrease in ICP and indicated thermal efficiency with an increase in ethanol blend percentage due to long ignition delay and low heating value. The CO emissions generally increased in the ethanol blend ratio while the NO_x emissions declined. The increase in CO emission was due to the low heating value of ethanol. With improvement in fuel injection timing, the combustion process seems to improve under low and high load conditions.

Zhou et al (2015) built a three-dimensional numerical model based on the KIVA4-CHEMKIN code connected with the newly built skeletal chemical kinetics process to examine the compression ignition engine characteristics. Methanol was fed through the intake port of the engine whereas biodiesel was injected straight to the engine system towards the end of the compression stroke. The CO, NO_x emissions and soot formation from the biodiesel and methanol binary fuel were compared. The results showed that under 10% load, the in-cylinder pressure decreased with an increase in methanol mass fraction, and this was due to more unburned fuel and low thermal efficiency from low reactivity and temperature.

Datta and Mandal (2017) evaluated the impacts of methanol and ethanol blends on engine characteristics. Diesel-RK simulation software was used to predict the engine performance parameters. Light alcohols (methanol and ethanol) were added individually to biodiesel and compared. It was pointed out that the maximum in-cylinder temperature decreased with the addition of ethanol or methanol to biodiesel. This decrease might have been caused by the cooling effect formed by the high latent heat of the alcohols when compared to that of biodiesel. The HRR

increased with the increase in alcohol blends and occurs further away from the TDC. This increase might be due to the longer ignition delay of alcohol blends. The higher latent heat of evaporation and lower CN of alcohols might also be the reason for this kind of behavior. The addition of 15% methanol and 15% ethanol separately showed that NO_x emission decreased by 30% and 19%. This decrease might be due to the reduction of in-cylinder temperature with alcohol-blended fuels. This study concluded that ethanol and methanol can be blended with biodiesel to improve engine parameters and decrease NO_x emissions.

Rajak et al. (2021) evaluated experimentally and numerically, the performance, combustion, and exhaust gas emissions of diesel fuel with biodiesel blends (B20) from first, second, and third-generation feedstocks, on the diesel engine. Numerical modelling of Diesel-RK was used to investigate the engine parameters and emitted gas at different compression ratios and loads. Numerical data were validated with experimental data under the same working conditions. The results showed that the ICP of pure diesel was higher compared to the first, second, and third-generation feedstock blend of B20 and this might be due to the high calorific value of the diesel fuel. The BMEP showed lower values for the first, second, and third generation of feedstock blends (B20) compared to standard diesel due to lower energy. The NO_x emissions showed reductions for soybean at a ratio of 16.5, and jatropha curcas at a ratio of 17.5 compared to diesel. However, the NO_x emissions for jojoba, karanja, and fish oil attained the maximum value compared to diesel fuel with CR of 17.5 and full load condition. Additionally, the numerical results attained a good agreement with the experimental results.

According to Al-Dawody and Bhatti (2011), the performance parameters and emission characteristics of a diesel engine powered with diesel and soybean biodiesel blends were theoretically investigated using Diesel-RK simulation software. The results showed that particulate matter and Bosch smoke emissions of biodiesel blends decreased compared to standard diesel fuel. On an average basis, there is a reduction in the brake thermal efficiency, brake power, and brake-specific fuel consumption for all soybean biodiesel blends by 2%, 3%, and 12%, respectively, compared to that obtained from standard diesel fuel. The NO_x emissions of all biodiesel blends were higher compared to standard diesel fuel. Among all tested fuels, it was noticed that B20% soybean biodiesel was the best-tested fuel, which gave the same performance

results with a good reduction in emissions as compared to standard diesel operation. A very good agreement was obtained between the theoretical and experimental results.

2.13 Summary of Chapter Two

The literature review has revealed the key conclusions in this study, and they are summarised as follows:

The biodiesel and ethanol blends lead to the reduction of density and viscosity and are marginally close to standard diesel. The addition of ethanol percentage to biodiesel attains high latent heat of vaporization and high oxygen content, which result in better combustion of diesel engines. The maximum in-cylinder pressure is variable with biodiesel-ethanol blends. The ignition delay period mostly relies on the fuel properties, which could have an impact on combustion parameters such as peak cylinder pressure, HRR, and cylinder temperature. High auto-ignition temperature and low CN of ethanol have long ignition delays and have an impact on engine combustion chamber behaviour. The BTE of alcohol blends improved better with the increase in engine load. The use of a low percentage for ethanol blends affects a slight delay of start in combustion. The addition of ethanol blends decreases NO_x, smoke, and PM emissions, based on the amount of percentage blending. The use of biodiesel-ethanol blends leads to a high oxygen zone in the combustion chamber and leads to producing lower exhaust gas emissions through the combustion process.

Computer simulation methods such as zero-dimensional models, single-dimensional models, multi-dimensional models, KIVA-CHEMKIN and Diesel-RK models have been presented in the literature review to provide results closely related to results from the experimental analysis. This proved that computer simulations can be effectively used to verify results from experimental analysis.

The literature review reveals that numerous researchers have conducted their experimental works using biodiesel-ethanol blends or biodiesel-diesel-ethanol blends. However, there is still a lack of investigations on comparing the effects of the biodiesel-biodiesel blend (biodiesel mixture) and the ternary mixture (biodiesel-biodiesel-alcohol blends). Only a few studies might have been conducted on the ternary mixture of diesel-biodiesel-biodiesel-alcohol blends (Swarna et al.,

2022). Therefore, to fill in the knowledge gap, the purpose of this research was to evaluate the performance, combustion, and emission characteristics of biodiesel mixture (biodiesel-biodiesel) and ternary blends of biodiesel mixture-ethanol blends (biodiesel-biodiesel-ethanol blends) with different percentages of 5%, 10%, and 15%, using standard diesel as a baseline for comparison. To have better knowledge and reduce costs that occurred during experiments, Diesel-RK simulation software was used, and the results from the experiment were validated using computer simulation. The performance parameters studied were BT, BP, BSFC, BTE, and BMEP. The combustion characteristics investigated included in-cylinder pressure and heat release rate. The emissions characteristics investigated included CO_2, NO, and smoke emissions.

CHAPTER THREE-METHODOLOGY

3.0 Experimental studies on performance, combustion, and emission characteristics of sample fuels on a diesel engine

3.1 Introduction

This chapter discusses the laboratory setup and methods used in the production of soybean biodiesel and waste vegetable oil biodiesel samples that were experimentally used on a diesel engine. It gives detailed descriptions of the experimental procedure required for D100, WVB100, SB100, BM100, BME5, BME10, and BME15 characterization. It also discussed the titration process, fuel blends preparation, measurements of fuel properties, engine operation procedures, X-Tract extreme software procedures, performance, combustion, and emission characteristics' procedures. The methods to ensure the accuracy of measurements are also explained.

3.2 Materials

Potassium hydroxide (KOH), sodium hydroxide (NaOH), and soybean vegetable oil were purchased from Jezreel Eduscience, South Africa. Waste vegetable oil was collected from the science campus cafeteria, University of South Africa, South Africa. The diesel (D100) fuel was purchased from Shell gas station, in South Africa. Biodiesel fuels from waste vegetable oil and soybean oil were produced through the transesterification method using methanol as a reagent and KOH as a catalyst. The biodiesel pilot plant, supplied by Pignat®, assisted in producing biodiesel fuel from soybean oil (SB) and waste vegetable oil (WVO) as shown in Figure 3.1 and the schematic diagram of the biodiesel processor is presented in Figure 3.2. The sample fuels were named diesel (D100); 100% waste vegetable biodiesel (WVB100); 100% soybean biodiesel (SB100), 50% waste vegetable and 50% soybean biodiesel (BM100); 80% waste vegetable, 15% soybean biodiesel and 5% ethanol (BME5); 70% waste vegetable, 20% soybean and 10% ethanol (BME10); 60% waste vegetable, 25% soybean and 15% ethanol (BME15).

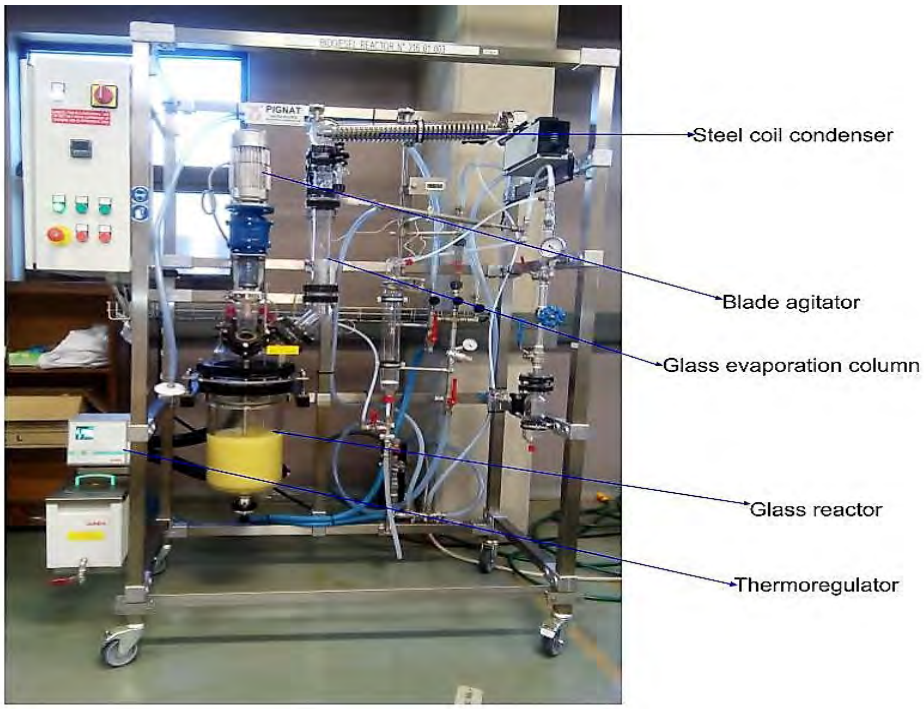

Figure 3.1: Experimental Pignat® biodiesel plant

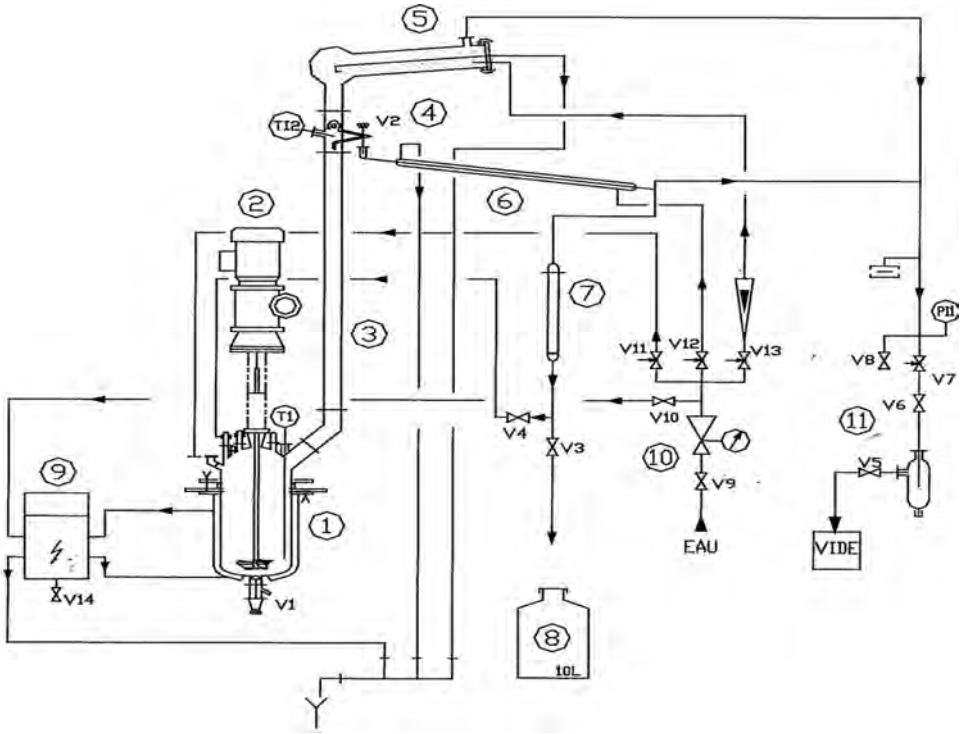

Figure 3.2: Principal schematic of biodiesel processer

Components of the Pilot Plant Unit

1. Double jacketed glass reactor, reaction capacity 10 litres
2. Variable speed triple-blade agitator
3. Glass evaporation column
4. Reflux head with a manual reflux valve, temperature measurement
5. Glass shell and steel coil condenser with a surface area of 0.2 m^2
6. Steel Liebig exchanger with distillate removal
7. 4 A molecular sieve, Ø 1.3mm beads, glass column, emptying valve
8. 10L reception vessel in PE
9. 3 kW thermoregulator; heating using a heat-conducting mineral oil; cooling by cold water circulation
10. Cooling water circuit includes: general cut-off valve, reducing valve equipped with a manometer, cut-off valve towards the thermoregulator, control valve for filling the reactor, control valves and flowmeters towards the condenser
11. Vacuum circuit includes: main cut-off valve, vacuum trap, vacuum control valve for the reaction process, venting valve, automatic pressure relief valve, pressure measurement

Description of the valves

V1 reactor emptying valve “crust-breaking type”.
V2 manual reflux valve
V3 emptying or cut-off valve for the « molecular sieve» column.
V4 cut-off valve for the output of the molecular sieve towards the reactor
V5 main cut-off valve for the vacuum circuit
V6 cut-off valve for the vacuum for the reaction process
V7 control valve for the reduced pressure
V8 valve for venting the unit.
V9 main cut-off valve for the cold-water feed (cooling water)
V10 cut-off valve for the cold-water feed to the thermoregulator
V11 control valve for filling or cleaning the reactor.
V12 valve controls the flow rate of water to the Liebig condenser.

V13 valve controls the flow rate of water to the condenser.

V14 valve for emptying the oil from the thermoregulator.

Description of the measurements

TI1 temperature of the reaction medium by PT100 probe

TI2 temperature at the head of the column

PI1 process pressure: 0 to 1 bar

FI1 water flow rate entering the condenser.

3.3 Titration Process and Biodiesel Production

3.3.1 Titration Process

The method described by Aworanti et al. (2019) was used to analyze the free fatty acids (FFA) in waste vegetable oil. The free fatty acid was determined by the titration process. This process required the exact amount of catalyst to prepare and to avoid incorrect results and unused fuel. Figure 3.3 present the equipment and materials used to perform the titration tests. One gram of potassium hydroxide (KOH) was dissolved in one litre of distilled water. 10 ml of isopropanol alcohol was added to 1 ml of waste vegetable oil. Three drops of phenolphthalein indicator were added to form a white solution. The mixture of distilled water and KOH was then put in a burette and titrated with the white solution until it turned pink. The titration process was experimentally repeated three times to determine the average amount of KOH used in the titration. The results of the first, second, and third titrations were 2.4 ml, 3.4 ml, and 2.4 ml, respectively. However, the average amount was 2.7 ml, and this value was acceptable to proceed with the transesterification procedure for biodiesel production from waste vegetable oil.

The free fatty acid was calculated using the equation 3.1.

$$\%\text{FFA} = \frac{(1^{st}+2^{nd}+3^{rd})\text{titrations}}{3} \qquad (3.1)$$

$$\%\text{FFA} = \frac{(2.4+3.4+2.4)\text{ml}}{3}$$

$$\%\text{FFA} = 2.7\ \text{ml}$$

Figure 3.3: Titration kit process

3.3.2 Biodiesel Production

The neat biodiesel fuels (WVB100 and SB100) were produced by transesterification process using methanol as an alcohol and KOH as a catalyst. From the direct use and blending, micro-emulsions, pyrolysis of vegetable oil and transesterification, he most important and effective current technology for biodiesel production is the transesterification of oils with alcohol to give biodiesel as main product and glycerine as by product. The oil was filtered by filter funnel 155 mm plastic fuel funnel to remove solid impurities. The oil was heated to 100°C to evaporate the water present. The nonexistence of water and impurities was critical for good transesterification reactions. Methanol was used for the reaction since it is cheaper compared to other alcohols, and it contains better physicochemical properties. KOH was used as a superior performance reagent in transesterification reactions. The temperature of the oil was set at 55°C in the heating tank before the reaction started. The prepared solutions of methanol and KOH catalyst were blended in the reactor tank and mixed. The entire test was carried out at a temperature of 55°C for a period of one to two hours. Then, the blend was allowed to settle or cooled overnight to allow biodiesel and glycerol separation. The oil methyl ester floated on the upper layer in the separation tank and the glycerol settled down at the lower layer as shown in Figure 3.4. The biodiesel was washed with warm distilled water to eliminate contaminations and glycerine. The lid of the tank was opened, and 50% volume of distilled water was sprayed throughout the ester and stirred gently. After five minutes, the drain valve was opened to recover the soapy water in the recipient. The washing procedure was repeated up until the lower layer had similar pH of distilled water and this shows

that the biodiesel fuel was free from catalysts. The drying process for biodiesel took at least 4-5 hours while the agitator was working. After 4-5 hours, the mixture was cooled by lowering the thermoregulatory setting the temperature to 20ºC. When the temperature was less than 20^0C, the valve was opened to collect the biodiesel in an appropriate recipient.

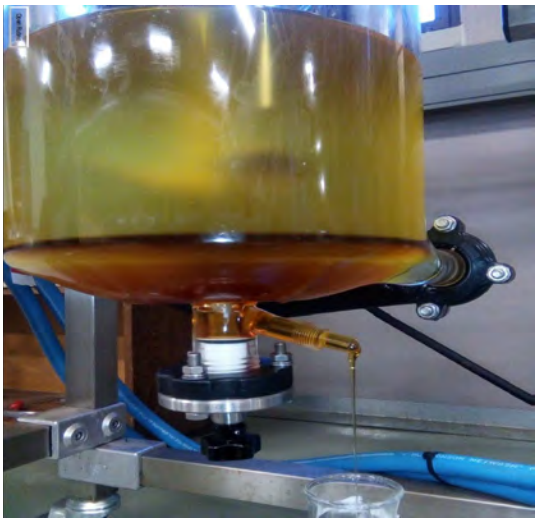

Figure 3.4: Biodiesel and glycerol separation

3.4 Blending of the Fuel Samples

In this work, the in-tank blending method was used to prepare biodiesel mixture (BM100) and biodiesel mixture-ethanol fuel blends (BME5, BME10, and BME15) in various tanks as shown in Figure 3.5. Based on the fraction of the blend, biodiesel mixture volume and ethanol were calculated. For instance, to prepare 10 litres of biodiesel mixture and ethanol fuel blends, BME5, 80% waste vegetable oil biodiesel (WVB) (8 litres), 15% soybean oil biodiesel (SB) (1.5 litres), and 5% ethanol (E) (0.5 litres) were used. The ethanol was measured by volume and poured into an empty tank. The use of volume percent in the blends stems from the fact that the industry standard for biodiesel blends is to use volume percent to blend fuels. Also, fuel injection pumps meter fuel by volume.

The hybrid biodiesel was poured on top of the ethanol fuel surface. This method improved the blending of ethanol and biodiesel mixture and avoided settling down of the biodiesel mixture at the lower end of the tank due to its higher density (Tutak et al., 2017). The lid tank was closed

tightly and agitated for three minutes. The complete biodiesel mixture-ethanol blends were finally poured into the fuel tank that connects the fuel supply system.

Figure 3.5: Biodiesel fuel blends preparation

1. Ethanol (E) 0%, waste vegetable biodiesel (WVB) 50%, and soybean biodiesel (SB) 50% (BM100)
2. Ethanol (E) 5%, waste vegetable biodiesel (WVB) 80%, and soybean biodiesel (SB) 15% (BME5).
3. Ethanol (E) 10%, waste vegetable biodiesel (WVB) 70%, and soybean biodiesel (SB) 20% (BME10).
4. Ethanol (E) 15%, waste vegetable biodiesel (WVB) 60%, and soybean biodiesel (SB) 25% (BME15).

3.5 Measurement of Fuel Properties

The quality of biodiesel is influenced by feedstock composition, oil extraction technique, biodiesel synthesis, refining procedures, etc. To assess biodiesel quality, important standards were formulated. The property values of D100, WVB100, SB100, BM100, BME5, BME10, and BME15 were taken for this study. All biodiesel fuel samples need to meet the standards of biodiesel set by ASTM D6751. These standards set the guidelines for testing biodiesel fuels and recommend suitable ranges for various fuel properties used in the engines. The quality of fuels produced was certified by measurement of their physico-chemical properties according to the ASTM specifications. Fuel density was measured using the Digital Density Meter, Densitometer Model DDM2910, obtained from Rudolph Research Analytical®, viscosity was measured according to

the viscometer standard, the flashpoint was measured according to the ASTM D93 flash point standard, using the Pensky-Martens automatic flash point apparatus, and the heating value was measured by the IKA C1 oxygen bomb calorimeter.

3.5.1 Operating Procedure for Densitometer Model DDM2910 for Density Meter Measurement

To test the fuel samples, 2 ml of fuel sample was injected using a syringe to ensure that no bubbles occurred. A green button was pushed to start the test measurements. The density meter has a density range of 0 g/cm^3 to 3 g/cm^3 and a temperature range of 0ºC to 100ºC. The DDM 2910 was set at a temperature of 20ºC to test the fuel samples as shown in Figure 3.6. An average of one minute was taken to complete the process of a single test. The experiment was conducted three times, and the average value was taken as a representative value.

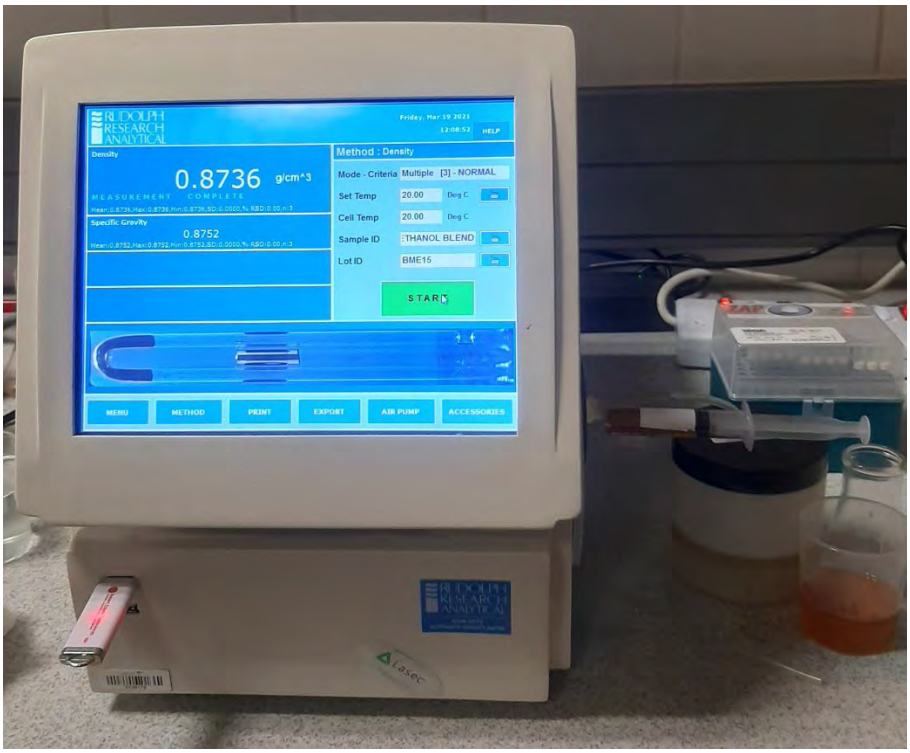

Figure 3.6: DDM2910 density meter

3.5.2 Operating Procedure for ASTM D93 Flash Point Measurement

To start the flash point test, the main switch was switched on and windows were launched immediately at the main menu of the display screen, of an Pensky-Martens automatic flash point apparatus, as shown in Figure 3.7. The push button was pressed from the main menu to start the experiment. Method A was selected to test all the fuel samples. The experimental data of the fuel sample and the maximum temperature were recorded. The experiment was conducted three times, and the average value was taken as the representative value.

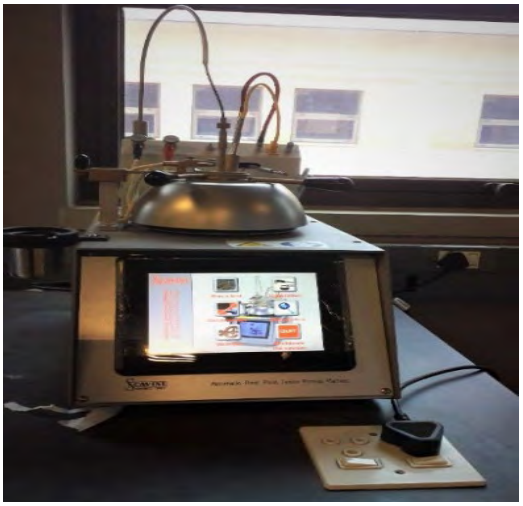

Figure 3.7: Automatic flash point Pensky-Martens apparatus

3.5.3 Operating Procedure for IKA Oxygen Bomb Calorimeter Measurement

The calorific values of D100, WVB100, SB100, BM100, BME5, BME10, and BME15 fuel was measured by IKA C1 bomb calorimeter. The components of the oxygen bomb calorimeter are shown in Figure 3.8. A fuel sample of 0.2 grams was measured and entered using a numeric keypad. The cotton thread was attached to the ignition wire and fuel sample. A fuel sample was loaded into the calorimeter container to evaluate the potential energy. The measurements of calorific value started automatically after the ignition wire and the calorimeter closed. The calorific value was measured using the official standards of DIN 51900 and ISO 1928.

Figure 3.8: IKA oxygen bomb calorimeter apparatus

3.6 Experimental Setup of a Diesel Engine and Parameter Measurement Procedure

The diesel engine experimental setup is available at the Mechanical Engineering Laboratory, Department of Mechanical Engineering, University of South Africa (UNISA), South Africa. The experimental study was performed in a single-cylinder, compression ratio of 17, four stroke, diesel engine, at a maximum load condition where the output shaft was connected to eddy current dynamometer to evaluate the speed, brake power, and brake torque. The measurements were conducted at various speeds starting from 1000, 1500, 2000, and 2500 rpm. Full technical descriptions of the diesel engine are presented in Table 3.1 whereas the experimental engine setup and schematic diagram are presented in Figure 3.9 and Figure 3.10.

Table 3.1: Technical Descriptions of Yanmar Diesel engine

Parameters	Technical data
Model	L48N6CF1T1AA
Type	4 Stroke, vertical cylinder, Air cooling by flywheel fan Diesel engine
No. of cylinders	1
Rated Power	3.5 kW@3600 rpm
Compression Ratio	17
Bore	57 mm
Stroke	70 mm
Connecting rod length	332 mm
Fuel	2.4 litre
Displacement	0.219 litre

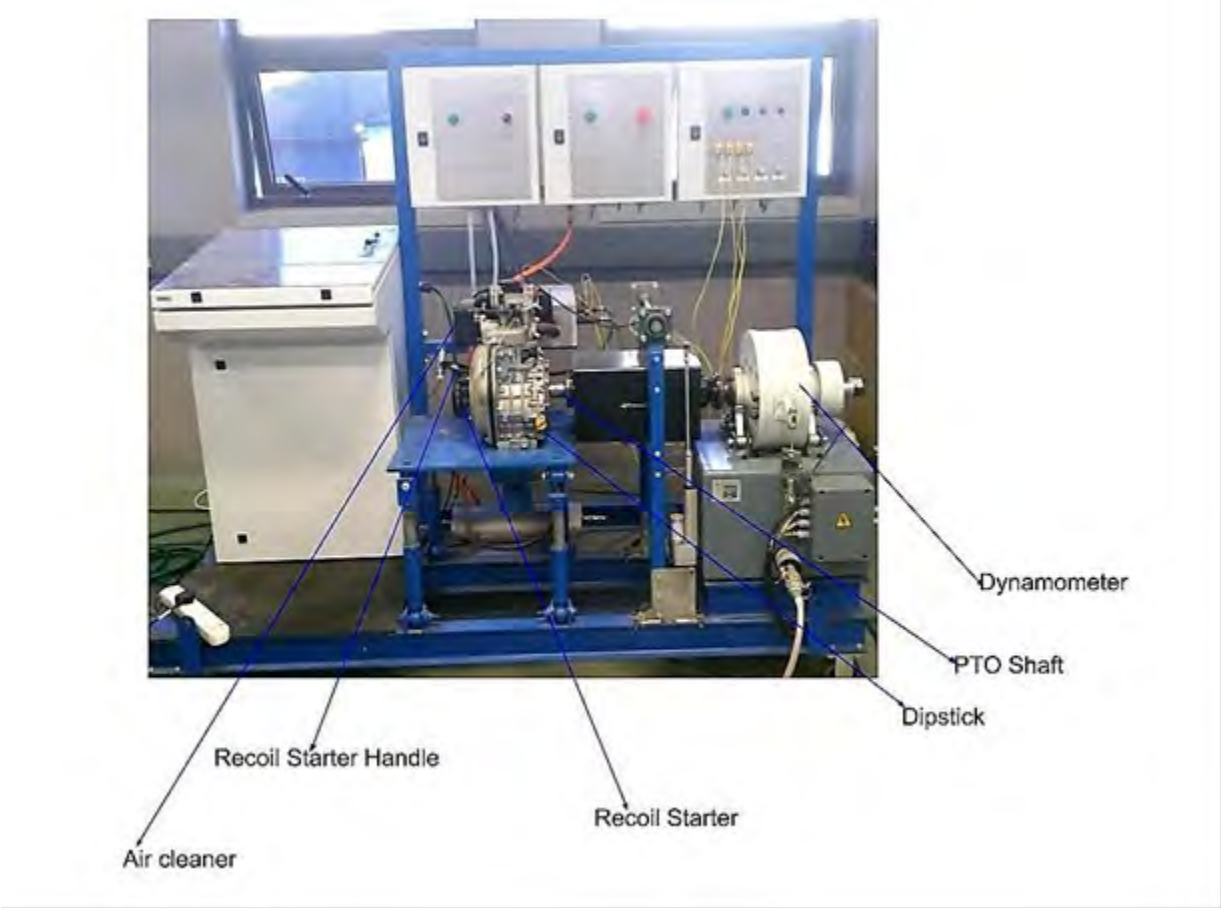

Figure 3.9: Experimental YANMAR diesel engine facilities

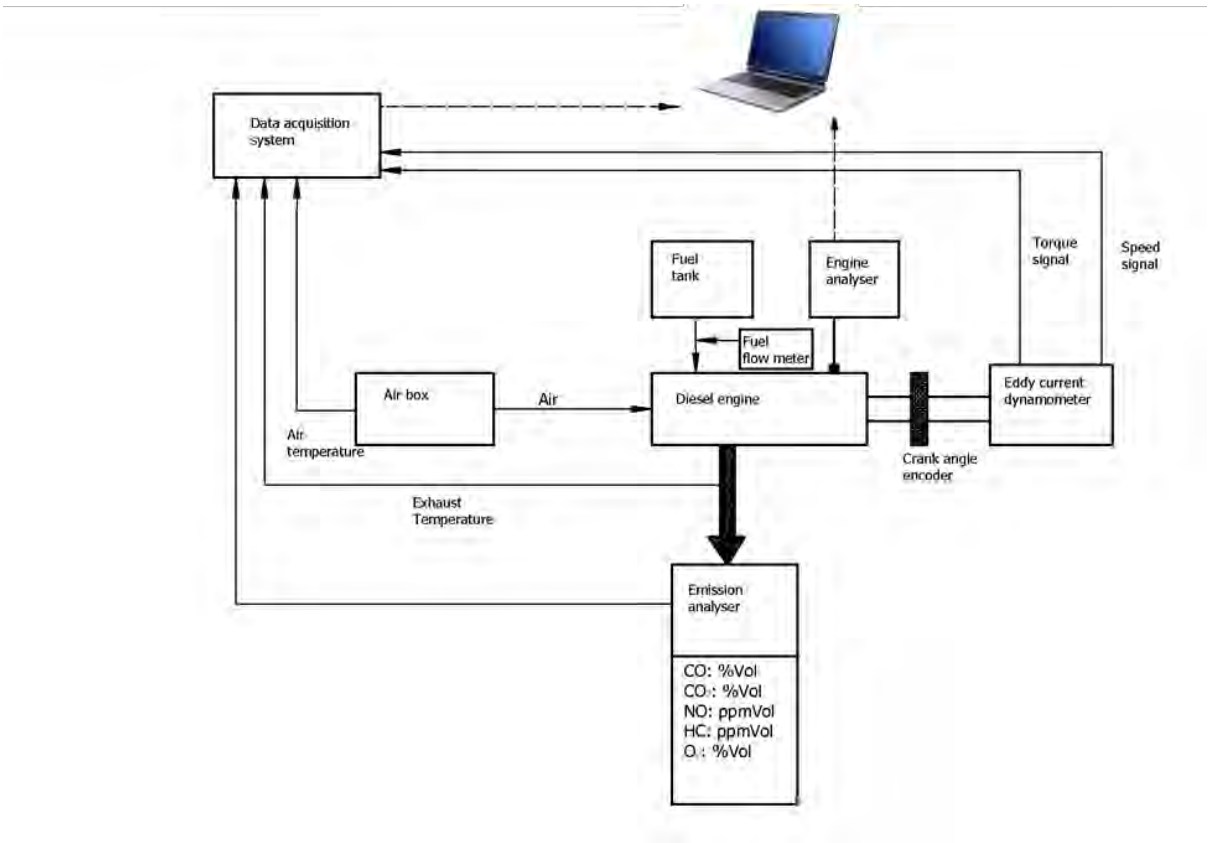

Figure 3.10: Schematic diagram of a Yanmar diesel engine

The fuel samples of D100, WVB100, SB100, BM100, BME5, BME10, and BME15 were run in the diesel engine according to the test programme. The engine was warmed up for a period of 20 minutes with 100% of diesel fuel following which the fuel line was changed to WVB100, SB100, BM100, BME5, BME10, and BME15. The engine speed was adjusted in compliance with the test programme. Through each test run of the diesel engine, sampling and measurement of the various parameters were carried out. After each experiment, the engine was once again fuelled and operated with standard diesel to remove all the outstanding fuel blends through the fuel tubes. The data acquisition was started after five minutes of the fuel change over to make sure that the fuel lines were free from the previous fuel (diesel). After each experiment, the engine was once more fuelled and run with standard diesel to drain all the remaining fuel blends in the fuel line. This process was followed for every blend until all samples were completed. Three rounds of experiments were performed in the same circumstances to check for the repeatability of all results. The experiment was thoroughly monitored to be sure of its accuracy, that no error occurred, and

complete data was transferred to a computer unit. The exhaust gas emissions were monitored and measured three times to make sure each emission data at the same time and average were taken. The operational settings were automatically programmed into a test cycle with the X-Tract extreme software for data collection. This test cycle was applied for every different fuel sample.

The test was carried out on a diesel engine as indicated in section 3.6. Using the different fuels, the engine parameters and emitted gases were measured. The detailed specification of the diesel engine parameters is presented in Table 3.2. However, the parameters have been chosen due to the significance of the design, performance, and emission assessment of the diesel engine.

Table 3.2: Parameters of the diesel engine

	Measured parameters	Calculated parameters
1	Torque	Heat release rate
2	Engine speed	Brake thermal efficiency
3	Fuel mass flow rate	Brake-specific fuel consumption
4	Exhaust temperature	Brake power
5	Inlet Pressure	
6	In-cylinder pressure	
7	Crank angle	
8	TDC mark	
9	Exhaust emissions	
	CO	
	CO_2	
	HC	
	NO_x	
	Smoke	

3.7 X-Tract Extreme Software

The X-Tract Extreme software can be described as the generic engineering software programme for measures, record, exhibit, and monitors, according to the evaluation of physical indicator namely engine speed, engine torque, engine power, temperatures, pressures, fuel flow, airflow, and emitted gases.

3.8 Measurement System for Combustion and Performance of Diesel Engine Parameters

The combustion characteristics such as ICP and HRR with crank angle are the significant parameters measured. The diesel engine performance parameters such as BT, BP, BSFC, BTE, and BMEP were also significant parameters measured.

3.8.1 In-Cylinder Pressure

The ICP was monitored and measured through a piezoelectric transducer pressure sensor mounted to the cylinder head of the engine. The ICP indicator was connected through the charge amplifier to send the output voltage in the range of 0.5-4.5 volts. The ICP was measured through the fiber-optic pressure transducer with a range of 0-1500 psi and a sensitivity of 2.64 mV/psi. The ICP data was measured and monitored in each work cycle of up to 720°CA (where CA is Crank Angle) at 1°CA resolution. The ICP data were monitored and recorded with the support of a digital hantek1008 oscilloscope. The technical specifications of the pressure sensor are shown in Table 3.3 and Figure 3.11 presenting the AutoPSI-S Pressure Sensor.

Table 3.3: Technical specifications of the pressor sensor

Pressure sensor	
Brand	Optrand
Model	H32294-Q
Type	AutoPSI-A
Pressure range (psi)	0-1500
Input voltage (V DC)	9-18V
Output voltage (V DC)	0.5-4.5
Sensitivity (mV/psi)	2.64
Bandwidth (Hz)	0.1-20000
Operating temperature (°C)	(-40) -(+350)

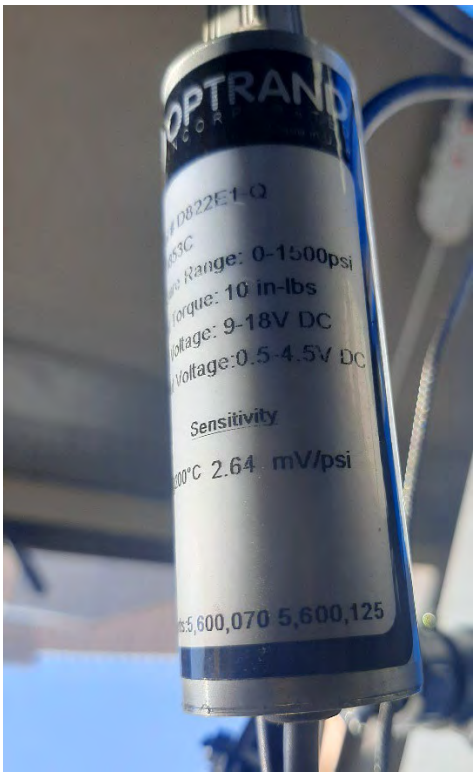

Figure 3.11: AutoPSI pressor sensor

To determine the in-cylinder pressure with the support of the sensor's output voltage, the ICP is presented by:

$$P = \frac{(V - V_{min})}{S} \quad (3.2)$$

Where P is Cylinder Pressure [psi], V is the Output Voltage [V], Vmin is the Minimum Output Voltage [V], and S is Sensitivity[V/psi].

3.8.2 Crank Angle (CA), Engine Speed (N), and Top dead Centre (TDC) Mark

The CA, engine speed, and TDC of the engine were recorded by the rotary encoder (Type: ARC S 50 360 TTL38) as shown in Figure 3.12. The rotary encoder was connected to the crankshaft of the engine. The crankshaft was connected directly to the crank angle sensor. which monitored and measured the engine in-cylinder pressure and the position of the crank angle.

Figure 3.12: Rotary encoder

3.8.3 Heat Release Rate

The heat release rate is estimated from the first law of thermodynamics as given in equations 3.3 and 3.4 using the in-cylinder pressure and crank angle obtained through a piezoelectric sensor attached to the cylinder head (Heywood, 2018).

$$\frac{dQ_n}{d\theta} = \frac{1}{\gamma-1} P \frac{dV}{d\theta} + \frac{1}{\gamma-1} V \frac{dP}{d\theta} \tag{3.3}$$

Where $\frac{dQ_n}{d\theta}$ represents the heat release rate (J/^{o}CA), P is the in-cylinder pressure (bar), γ is the specific heat ratio, V represents the in-cylinder volume (m^3), and $\frac{dP}{d\theta}$ represents the pressure as a function of crank angle. The specific heat ratio for heat release analysis with the value of $\gamma = {C_P}/{C_V}$ will be taken as 1.35.

In-cylinder volume (V) at any crank position can be obtained using the empirical relation of the cylinder piston model derived from its geometry based on equation 3.4 (Abbaszadehmosayebi, 2014).

$$V = V_C \left\{1 + \frac{1}{2}(r-1)\left[R + 1 - cos\,\theta - (R^2 - sin^2\theta)^{\frac{1}{2}}\right]\right\} \tag{3.4}$$

Where V_C is the clearance volume (m^3), r is the compression ratio, R is the connecting rod length ratio to crank radius, and θ is the crank angle.

$$\frac{dV}{d\theta} = \frac{V_d}{2} sin\theta \left[1 + \frac{cos\theta}{\sqrt{R^2 - sin^2\theta}}\right] \quad (3.5)$$

Where $\frac{dV}{d\theta}$ is the volume as a function of crank angle and V_d is the displacement volume (m^3).

3.9 Engine Performance

3.9.1 Power and Torque

The performance parameters such as engine speed (N) and brake torque (BT) of the engine were measured through experimental techniques monitored by X-Tract extreme software as shown in Figure 3.13.

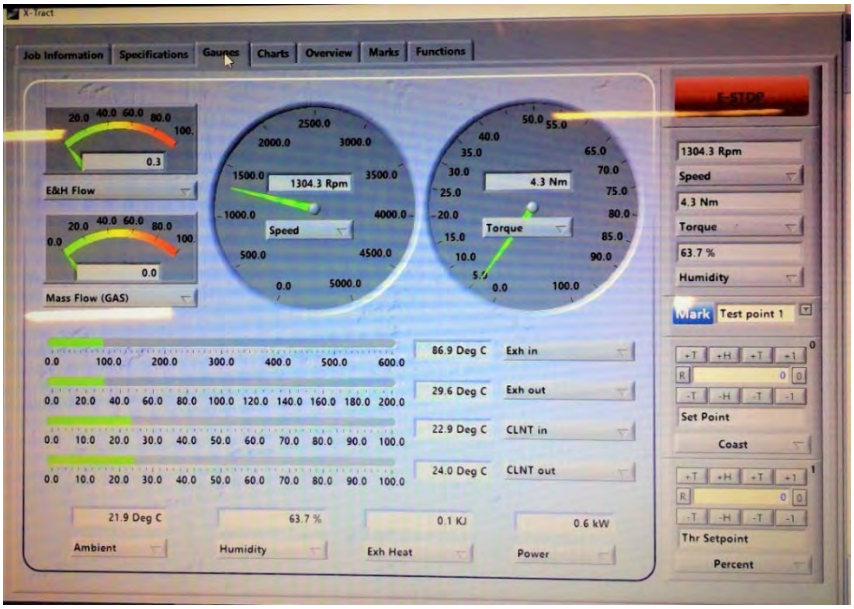

Figure 3.13: Screenshot of X-Tract extreme software

The brake torque was measured through the dynamometer of the diesel engine and monitored by X-tract extreme software. The brake power (kW) of the engine is assessed by equation 3.6.

$$BP = 2\pi NT \quad \text{kW} \quad (3.6)$$

Where, N symbolise engine speed (rev/sec), and T symbolise engine torque measured through dynamometer (Nm).

3.9.2 Fuel Mass Flow Rate

The mass flow rate was measured using Promass 83 Endress and Hauser fuel, meter which was connected to X-Tract extreme software. Figure 3.14 shows the apparatus of Promass 83 Endress and Hauser fuel meter and Table 3.4 presents the specifications of Promass fuel meter.

Figure 3.14: Promass 83 fuel meter apparatus and specifications

Table 3. 4: Specifications of the Promass fuel meter

Measuring principle	Range
Compatible fuel types	Petrol and Diesel
Ambient temperature range	-20-40 ºC
Fluid density range	0-5000 kg/m³
Pressure range of secondary containment	25 bar
Weight	5 Kg

3.9.3 Brake Specific Fuel Consumption

The BSFC can be explained as the measures of conversion efficiency of different fuel samples fuelled into diesel engines to produce great power output and it describes the economy of the fuel to the engine. The BSFC was evaluated using equation 3.7:

$$BSFC = \frac{\dot{m}_f}{BP} \quad \text{(kg/kWh)} \quad (3.7)$$

where:

$\dot{m}_f$ represents the mass flow rate of the fuel (kg/h)

BP represents the brake power of the engine power (kW)

3.9.4 Brake Thermal Efficiency

The BTE has been explained by the power output of the engine to the crankshaft per chemical energy produced from the fuel consumption. The BTE is evaluated using equation 3.8:

$$\eta_{th}(\%) = \frac{BP}{\dot{m}_{f(HV)}} x\ 100 \text{ or } \quad \eta_{th}(\%) = \frac{3600}{bsfc\ x\ (HV)} x\ 100 \tag{3.8}$$

3.10 Emissions

3.10.1 Emission Characteristics Measurement

The exhaust gas emissions were measured using Bosch BEA 060 shown in Figure 3.15 whereas Bosch BEA 070 was used to measure the smoke number, see Figure 3.16. The exhaust gas components measured include CO, HC, CO_2, O_2, and NO. The section line of the equipment was directly placed to the exhaust pipeline, and it was heated to maintain the temperature of the wall to try and avoid condensation of HC in the pipeline. The insulated line was stretched from the exhaust pipeline to the apparatus where the analyser was positioned. All emissions analysers were set on one bench. The CO, CO_2, HC, and NO emissions were measured using the non-dispersive infrared system. The BEA 060 is equipped with an O_2 sensor and the O_2 sensor is a wearing part. The oxygen was measured using the sensor with an electro-chemical action sensor. The oxygen measurement is automatically adjusted to an air oxygen content of 20.9% by volume. All emission experiments were measured three times at a constant speed. The results were averaged over three readings.

Figure 3.15: BOSCH BEA 060 Emission analyser

Figure 3.16: BOSCH BEA 070 Emission analyser

3.11 Uncertainty Analysis

It is important to measure an uncertainty assessment of the experimental techniques to spread out the accuracy of the data. Accountabilities may be ineluctable while using measurement apparatus. For that reason, it is critical to evaluate the uncertainty of the experimental process to expand the accuracy of the results. Furthermore, the measurements were carried out three times to expand the accuracy of the data obtained. The uncertainty assessment was performed at various features such as range, accuracy, and uncertainty of the tools as presented in Table 3.5 (Heywood, 2018).

Utilising the proportion uncertainties of different instruments, the total proportion uncertainties of various parameters were evaluated. By applying the theory of propagation of errors, the overall percentage of uncertainty for the measured and assessed parameters is as follows:

$$\% = \sqrt{\begin{matrix}(T)^2 + (speed\ sensor)^2 + (load)^2 + (pressor\ sensor)^2 + (CA\ encoder)^2 \\ +(dynamometer)^2 + (co)^2 + (co^2)^2 + (HC)^2 + \\ (NO)^2 + (O_2)^2 + (smoke)^2\end{matrix}} \quad (3.9)$$

$$\% = \sqrt{\begin{matrix}(0.15)^2 + (1)^2 + (0.2)^2 + (0.5)^2 + (0.2)^2 + (0.15)^2 + (0.3)^2 + (1)^2 + \\ (0.1)^2 + (0.5)^2 + (0.2)^2 + (0.1)^2\end{matrix}}$$

$$\% = 1.67$$

Table 3.5: Uncertainties of the parameters

Number	Instrument	Type	Range	Accuracy	Uncertainty (%)
1	Temperature sensor	K	0-600 °C	±1 °C	±0.15
2	Speed sensor	Rotary encoder	0-3600 rpm	±10	±1.0
3	Load indicator		0-20 kg	±0.1 kg	±0.2
4	Pressor sensor	Piezoelectric	0-100 bar	±1 bar	±0.5
5	Crank angle encoder		0-360 ppr	±1°	±0.2
6	Dynamometer	Load cell	0-50 kg		±0.15
7	Fuel gas analyser				
	CO		0-10,000 %vol	±0.001 %vol	±0.3%
	CO_2		0-18 %vol	±0.01 %vol	±1.0%
	HC		0-9999 ppm	±1 ppm vol	±0.1%
	NO		0-5000 ppm	±1 ppm vol	±0.5%
	O_2		0-22 %vol	±0.01 %vol	±0.2
	Smoke		0-100 %vol	±1%vol	±0.1

3.12 Prediction of performance, combustion, and emission characteristics

3.12.1 Introduction

Several research has been carried out on the use of numerical tools to analyse the performance parameters, combustion, and gas emission by ICEs. Numerical modelling of compression ignition engines is usually applied in computational fluid dynamics or one-dimensional gas dynamics and thermodynamics-based models. However, these days, many specialised commercial

Computational Fluid Dynamics (CFD) tools are available. Software simulations tools such as KIVA (Jeon et al., 2016, Katrašnik, 2016), ECFM-3Z of model of STARCD (Sharma et al., 2015), CONVERGE and ENSIGHT (Chowdary et al., 2016), and AVL FIRE™ (Petranović et al., 2017, Petranović et al., 2015, Soni and Gupta, 2016) have been used to compute air flow and fuel spray in combustion chambers of internal combustion engines. Vujanović et al. (2016) performed the optimization of the combustion engine at various models such as Eulerian-Lagrangian and Eulerian-Eulerian. Computational fluid dynamics (CFD) simulations are mostly capable of clarifying the accurate characteristics such as ICP, HRR, SOC, ID, CD, and exhaust gas emissions working procedures of the ICEs. Even though CFD simulation tools are accurate and detailed, they are expensive and take longer to process (Rajak et al., 2018a). Several researchers have been using CFD software for numerical modelling for their investigations on internal combustion engines with various fuels. As an alternative to the expensive nature of the commercial CFD software, and to have a better knowledge while also saving the costs from intense experimentation, Diesel-RK software has proven to be a useful tool.

Diesel-RK could be explained as the modelling simulation software applied to analyse ICEs. The Diesel-RK software uses the multi-zone fire model based on the combination and combustion model of Razleisev and which was modified by Kuleshov that made the model to be known as the Diesel-RK model (Al-Dawody and Bhatti, 2013, Kuleshov and Mahkamov, 2008, Kuleshov et al., 2010, Datta and Mandal, 2017, Kuleshov, 2005, Kuleshov, 2009). Diesel-RK software is not expensive, is quick at computing, and is computationally less costly.

3.12.2 Physical Properties Used as Input Data

Physical properties of the fuels are necessary as input data for the simulation of in-cylinder pressure, heat release rate, in-cylinder temperature, ignition delay, spray tip penetration, the start of combustion, and combustion duration.

3.12.3 Diesel-RK Computer Simulation Model

Diesel-RK software was built according to the first law of thermodynamics calculations to analyse the combustion parameters, performance, and exhaust gas emissions of the diesel engine. The Diesel-RK model analyses the formation mixture and combustion of the diesel engine. This software can be used in a multi-parameter optimization characteristics process. The multi-zone combustion model was used where the spray is distributed into seven different zones. Three different steps were used to divide the spray assessment like the initial formation of a solid axial flow, cumulative spray assessment with the period of spray interaction through the combustion chamber wall, and circulation of fuel walls. The multi-zone model was built to simulate or predict the combustion processes of the engine.

3.12.4 Methodology for Diesel-RK

The proposed study of computational software is applied to evaluate the combustion parameters, performance, and emitted gases of the engine fuelled with diesel fuel (D100) and six biofuels: 100% waste vegetable oil biodiesel (WVB100), 100% soybean oil biodiesel (SB100), 50% waste vegetable oil biodiesel-50% soybean oil biodiesel (BM100), 80% waste vegetable oil biodiesel-15% soybean oil biodiesel-5% ethanol (BME5), 70% waste vegetable oil biodiesel-20% soybean oil biodiesel-10% ethanol (BME10), 60% waste vegetable oil biodiesel-25% soybean oil biodiesel-15% ethanol (BME15) at a full load condition, a constant compression ratio of 17 and various engine speeds. To perform the use of the DRK software, numerical modelling of Yanmar engine, four-stroke single-cylinder diesel engine model was loaded to the DRK-software together with D100, WVB100, SB100, BM100, BME5, BME10, BME15, and fuel properties namely viscosity, density, and heating value to run the simulation. The software was set up to predict the performance, combustion parameters, and exhaust gas emission of the diesel engine. The details of the engine characteristics are presented in Table 3.1. The initial input conditions for simulation are presented in Table 3.6.

Table 3.6: Input boundary condition for simulation

Parameters	Values
Initial pressure	1 bar
Initial temperature	300 K
Fuel injection timing	23° CA before TDC
Fuel spray angle	136°
Piston	Bowl shape
Fuel injected	0.00791 g/cycle

The first law of thermodynamics is used to calculate thermodynamic properties. For each crank angle, properties like pressure and temperature are computed. To compute its coefficients, it makes use of empirical and semi-empirical correlations that were discovered through experimental studies. Additionally, the R-K model, a multi-zone diesel fuel spray mixture generation and combustion model, is used in the Diesel-RK simulation (Adham and Mabsate, 2017, Kuleshov, 2006, Kuleshov, 2007).

The governing equations

The governing equations are based on the fluid flow to the combustion chamber in a multi-zone model. The following governing equations are used as follows (Rajak et al., 2018b, Salam and Verma, 2019):

Conservation of mass equation (Adham and Mabsate, 2017):

$$\dot{m}_{cyl} = \dot{m}_{in} + \dot{m}_{exh} + \dot{m}_{bb} + \dot{m}_{fuel} \quad (3.10)$$

Where: $\dot{m}_{cyl}$ represents mass flow rate of the cylinder gas, $\dot{m}_{in}$ represents the inlet air mass flow rate, $\dot{m}_{exh}$ represents the exhaust mass flow rate, $\dot{m}_{bb}$ is the blow by rate, and $\dot{m}_{fuel}$ represent the fuel mass flow injected in the cylinder during the cycle.

Conservation of species equation (Adham and Mabsate, 2017):

$$\dot{Y}_j = \sum_j \left(\frac{\dot{m}_j}{m_{cyl}}\right)\left(Y_i^j - Y_i^{cyl}\right) + \dot{\omega}_j \quad (3.11)$$

Where: $\dot{Y}_j$ is the time derivative of the mass fraction of the species, $\dot{m}_j$ is the time derivative of the mass of species, m_{cyl} mass of the cylinder gas, Y_i^j and Y_i^{cyl} are the stoichiometric coefficients for products and reactants, respectively, and $\dot{\omega}_j$ is the source term.

Conservation of energy equation (Adham and Mabsate, 2017):

$$\dot{U}_{cyl} = \dot{Q}_w + \dot{Q}_{chem} - P_{cyl}\dot{V}_{cyl} + h_{in}\dot{m}_{in} + h_{exh}\dot{m}_{exh} \quad (3.12)$$

Where: $\dot{U}_{cyl}$ is the time derivative of the internal energy, $\dot{Q}_w$ is the heat transferred from the cylinder to the wall, $\dot{Q}_{chem}$ is the heat released by combustion, P_{cyl} is the cylinder pressure, $\dot{V}_{cyl}$ is the time derivative of the cylinder volume, h_{in} and h_{exh} are the enthalpies of the inlet and exhaust gas, respectively.

The in-cylinder combustion modelling equations

The basic governing equations defining the small change in cylinder gas temperature, pressure, and composition are derivable from the equation of state. The general quasi-steady flow energy equation in differential form for any control volume may be written following (Yamin, 2022):

$$\sum \frac{dQ_i}{dt} - 2\sum \frac{dW_k}{dt} = \frac{d}{dt}(m.u) - \sum \frac{dm_j}{dt}\left(h_j - \frac{V_j^2}{2g_c} + \frac{z.g}{g_c}\right) \quad (3.13)$$

Assuming negligible change in kinetic and potential energy of the streams and zero shaft work, the energy equation can be written as:

$$\sum \frac{dQ_i}{dt} - 2\sum \frac{dW_k}{dt} = \frac{d}{dt}(m.u) - \sum \frac{dm_j}{dt}\left(h_j\right) \quad (3.14)$$

$$\sum \frac{dW_k}{dt} = P\frac{dV}{dt} \quad (3.15)$$

By using the equation of state and expressing internal energy u as a function of temperature and composition, the rate of change of temperature with crank angle θ is given by:

$$\frac{dT}{d\theta} = \sum \frac{dQ_i}{d\theta} - \frac{mRT}{V}\frac{dV}{d\theta} + \sum \frac{dm_j}{d\theta}\left(h_j\right) - u\sum \frac{dm_j}{dt}\frac{m.\frac{\delta udF}{\delta Fd\theta}}{m.C_v} \quad (3.16)$$

Where m represents the mass (kg), R represents the gas constant (J/mol-K), T represents the temperature (K), V represents the volume (m^3), u is the internal energy (kJ), and h is the specific enthalpy (kJ/kg).

The gas pressure and temperature during the compression stage are calculated using the following equations (Yamin, 2022), from which the pressure and temperature of the crank angle at every point are solved numerically by the Runge-Kutta method:

$$\frac{dP}{d\theta} = \frac{\left[-\left(1+\frac{R}{C_v}\right).P.\frac{dV}{d\theta} - \frac{RdQ_{cr}}{C_v} + \frac{RdQ_{ht}}{C_v d\theta}\right]}{V} \tag{3.17}$$

$$\frac{dT}{d\theta} = T.\left(\frac{1}{P}\frac{dP}{d\theta} + \frac{1}{V}\frac{dV}{d\theta}\right) \tag{3.18}$$

In-cylinder volume (V) at any crank position can be attained using the empirical relation of the cylinder piston model derived from its geometry based on equation 3.19 (Abbaszadehmosayebi, 2014).

$$V = V_C\left\{1 + \frac{1}{2}(r-1)\ \left[R + 1 - cos\ \theta - (R^2 - sin^2\theta)^{\frac{1}{2}}\right]\right\} \tag{3.19}$$

Where V_C is the clearance volume (m^3), r is the compression ratio, R is the connecting rod length ratio to crank radius, and θ is the crank angle.

The rate of change of cylinder volume with crank angle is given by:

$$\frac{dV}{d\theta} = \frac{V_d}{2} sin\theta\left[1 + \frac{cos\theta}{\sqrt{R^2 - sin^2\theta}}\right] \tag{3.20}$$

Where $\frac{dV}{d\theta}$ is the volume as a function of crank angle and V_d is the displacement volume (m^3).

3.12.5 Heat Release Model

Figure 3.17 shows the distribution of fuel in each section through the spraying period. The fuel was sprayed into two stages: the first stage was before jet impingement and the second stage was after impingement.

The following governing equations (3.21)– (3.24) were considered for this model to assess the heat release in a cycle from the time when the fuel is burning at various stages (Al-Dawody and Bhatti, 2013, Kuleshov and Mahkamov, 2008, Datta and Mandal, 2017).

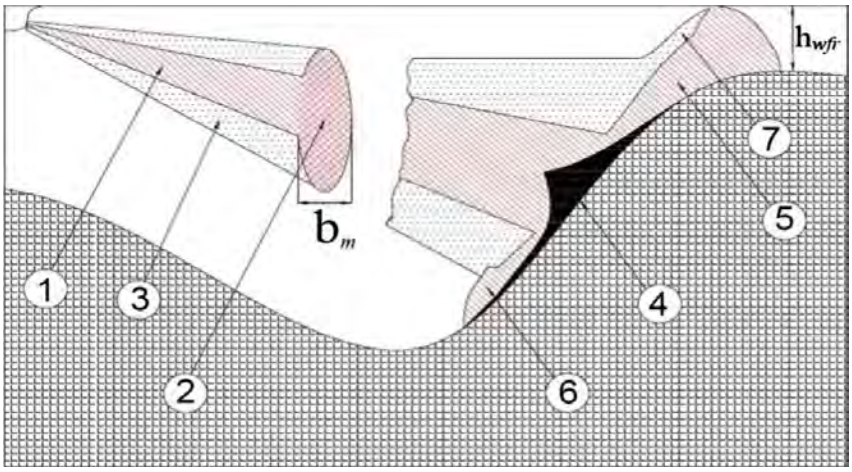

Figure 3.17: The different zones of diesel spray (Kuleshov et al., 2010)

Heat model:

(a) Before impingement

1. Dense conical core
2. Dense forward front
3. Dilute outer sleeve

(b) After impingement

4. The axial conical core of the near-wall flow
5. The dense core of the near-wall flow
6. Dense forward front of the near-wall flow
7. Dilute the outer sleeve of the near wall flow

where: b_m = spray depth (m)

h_{wfr} = height of the near-wall flow

Diesel-RK simulation software can operate by multi-zone combustion model where the heat release procedure is defined into four major stages (Kuleshov et al., 2007). Each stage has its own physical and chemical features.

The auto-ignition delay period represents the first stage of the heat release rate, and is computed by modified Tolstov's equation (Al-Dawody and Bhatti, 2013) as follows:

$$\tau = 3.8X10^{-6}(1 - 1.6X10^{-4}.n)\sqrt{\frac{T}{P}}exp\left(\frac{E_a}{8.312T} - \frac{70}{CN+25}\right) \quad (3.21)$$

Where, P represents the in-cylinder pressure in (MPa) units and T represents the in-cylinder temperature in (K) as a function of crank angle θ, E_a represents the activation energy in the auto-ignition process (kJ/kmol), n represents engine speed in (rpm), CN represents cetane number of fuels.

During the premixed combustion stage period (second stage), the heat release rate is as follows (Kuleshov, 2009):

$$\frac{dx}{d\tau} = \Phi_0 X \left(A_0 \left({}^{m_f}/_{V_i} \right) X(\sigma_{ud} - X_0) \right) + \Phi_1 X \left(\frac{d\sigma_u}{d\tau} \right) \quad (3.22)$$

Where, m_f represents fuel mass per cycle, V_i is cylinder volume at injection timing, $\sigma_{ud,}$ and σ_u represent fuel fractions evaporated through the ID period up to the recent moment, respectively.

During the mixing-controlled combustion stage period (third stage), the heat release rate is as follows (Kuleshov, 2009):

$$\frac{dx}{d\tau} = \Phi_1 \, X \, \left(\frac{d\sigma_u}{d\tau} \right) + \Phi_2 \, X \, \left(A_2 \left({}^{m_f}/_{V_c} \right) \, X \, (\sigma_u - X) \, X \, (\alpha - X) \right) \quad (3.23)$$

where V_c is cylinder volume at TDC.

Following the fuel injection, at the late combustion stage, the last stage of the heat release rate is as follows (Kuleshov, 2009):

$$\frac{dx}{d\tau} = \Phi_3 A_3 K_T (1 - X)(\xi_b \alpha - X) \quad (3.24)$$

Where, ξ_b represent the efficiency of air use and α represent the air-fuel equivalence ratio.
In heat release model equations, the parameter, which defines how completely the fuel vapour combusts in the zones is expressed by Φ_0 and the four-stage period equations are given as $\Phi_0 = \Phi_1 = \Phi_2 = \Phi_3$. A_0, A_1, and A_2 represent the empirical factors reliant on the speed of the engine and swirl intensity, and also, A_3 can be found in equation (3.24). The heat transfer of the cylinder is brought into account, and the corresponding heat transfer coefficients for its various zones are assessed utilising Woschni's correlation (Woschni, 1967).

The simulation also assesses the engine characteristics such as brake power (BP), brake specific fuel consumption (BSFC), brake thermal efficiency (BTE), brake mean effective pressure (BMEP) and frictional mean effective pressure (FMEP) (Heywood, 2017, Gad et al., 2021):

Brake power is assessed using equation (3.25) (Heywood, 2017) as follows:

$$BP = 2\pi NT \tag{3.25}$$

Where T represents the brake torque (Nm), and π is pi.

Brake thermal efficiency is assessed using equation (3.26) (Heywood, 2017) as follows:

$$\eta_{th} = \frac{3600 \text{ x } BP}{\dot{m}_f \text{ x } HV} \tag{3.26}$$

Where BP is the BP (kW) and HV represents the heating value (kJ/kg).

The Frictional Mean Effective Pressure (FMEP) is assessed using equation (3.27) (Heywood, 2017) as follows:

$$\text{FMEP} = \alpha + \beta P_{max} + \gamma V_p \tag{3.27}$$

Where, α, β and γ are constants, P_{max} represents the maximum cylinder pressure, and V_p is the mean piston velocity in m/s.

The brake-specific fuel consumption is assessed using equation (3.28) (Datta and Mandal, 2017, Rajak and Verma, 2019) as follows:

$$\text{BSFC} = \frac{\dot{m}_f}{P_b} \tag{3.28}$$

Where $\dot{m}_f$ represents the mass flow rate of the fuel (kg/h and P_b is the brake power (kW).

The Brake Mean Effective Pressure (BMEP) is assessed in equation (3.29) (Heywood, 2017) as follows:

$$\text{BMEP} = \frac{2\text{BP}}{V_d \text{ x N}} \tag{3.29}$$

Where BP is the brake power (kW), V_d is the swept volume (m^3), and N is the engine speed (rpm).

The equivalence ratio (α_1) is assessed using equation (3.30) (Heywood, 2017) as follows:

$$\alpha_1 = \frac{(A/F)}{(A/F)_s} = \frac{\left(\dot{m}_a/\dot{m}_f\right)}{\left(\dot{m}_a/\dot{m}_f\right)_s} \tag{3.30}$$

Where α is the A/F Equivalence ratio, and A/F is the air-to-fuel ratio.

3.12.6 Spray Tip Penetration Model

Figure 3.18 indicates the current speed of the elementary fuel mass (EFM) injected through the small-time step and moving from the injector towards the STP and its equation can be written as follows (Kuleshov and Mahkamov, 2008):

$$\left(\frac{V_1}{V_0}\right)^{\frac{2}{3}} = 1 - \frac{l}{l_m} \tag{3.31}$$

where $V_1 = {dl}/{d\tau_k}$ represents the recent velocity of the EFM.

V_m = Medium velocity of spray in meters per second

V_o = Initial velocity in meters per second

V_1 = Current velocity in meters per second and l_m = penetration length

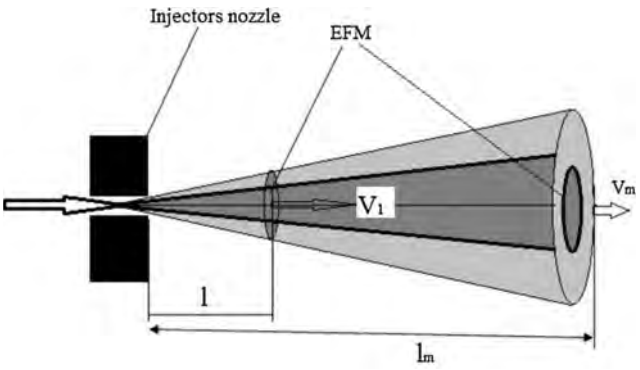

Figure 3.18: The vaporization of spray evaluation of the engine (Kuleshov and Mahkamov, 2008, Al-Dawody and Bhatti, 2013)

3.12.7 NO_x Formation Modelling

Nitrogen oxides such as NO and NO_2 were both normally created and named NO_x. Heywood (1988) states that both nitrogen oxide emissions and nitric oxide (NO) are the main emitted gases from the engine (Heywood, 2018). The NO emission is the only formation that can be formed through various mechanisms. However, the prediction model that can be used to take care of NO formation is the thermal or Zeldovich mechanism. Kuleshov (2009) used similar techniques for the NO formation model to simulate the DI diesel engine. The equilibrium structure of combustion products of eighteen species during the burnt gas zone was first analysed by this model followed

by the kinetic of thermal NO following the Zeldovich mechanism. The nitrogen oxides are on the chain mechanism and the basic reactions are as follows:

$$O_2 \leftrightarrow 2O$$

$$N_2 + O \leftrightarrow NO + N$$

$$N + O_2 \leftrightarrow NO + O \quad (3.32)$$

The reaction rates of equation (3.33) depend on atomic oxygen. The concentration of NO volume in combustion products formed in the recent evaluation step is attained from the following equation (Datta and Mandal, 2017):

$$\frac{d[NO]}{d\theta} = \frac{p \times 2.333\times10^{7}.e^{-\frac{38020}{T_Z}}[N_2]_e.\{1-([NO]/[NO]_e)^2\}}{R.T_Z.\left(1+\frac{2365}{T_z}.e^{\frac{3365}{T_z}}.\frac{[NO]}{[O_2]e}\right)}.\frac{1}{\omega} \quad (3.33)$$

Where P represents the cylinder pressure in Pa, T_Z represents the temperature of the burnt gas zone in K, R represents the gas constant in J per (mole K) units; ω represents the angular of the crank velocity in 1/sec; $r_{NO}, r_{N_2}, r_O, r_{O_2}$ named as equilibrium concentrations of nitrogen oxide, molecular nitrogen, atomic and molecular oxygen, consequently.

The specific NO emission in g/kWh is computed as follows (Kuleshov and Grekhov, 2013):

$$e_{NO} = \frac{30 r_{NO} M_{bg}}{L_C \eta_M} \quad (3.34)$$

Where M_{bg} represent the mass of burnt gas inside of a combustion cylinder (kmol), L_C represent the operational cycle (kJ) and η_M represent mechanical efficiency.

3.12.8 Soot and Particulate Matter Formation Model

The possible formation of soot emissions in a diesel engine is the incomplete combustion of unburnt hydrocarbon fuel. Soot formation of the fuel sample can be defined as the good distribution of black carbon atoms in the form of vapour. Mostly soot formation is formed due to the chain of destruction transformation of fuel molecules circulating from surface droplets to the front of the flame and high-thermal temperature of polymerization and dehydrogenization vapour-liquid of evaporating droplets. Equation (3.35) was formed to analyse the amount of soot formation through the burning zone (Al-Dawody and Bhatti, 2013, Datta and Mandal, 2017).

$$\left(\frac{d[C]}{d\tau}\right)_K = 0.004\frac{q_c}{V}\frac{dx}{d\tau} \quad (3.35)$$

Where V is the volume of cylinder; q_c is the mass of fuel for the cycle; $dx/d\tau$ represent the heat release rate of the fuel.

Soot formation level can be stated as Hartridge smoke level (HSL) or Bosch smoke number. Hartridge smoke level or Bosch smoke number is attained from the Hartridge smoke equation in Diesel-RK simulation software using suitable relation (Datta and Mandal, 2018).

$$\text{Hartridge} = 100\,[1 - 0.9545\exp(-2.4226\,[\text{C}])] \tag{3.36}$$

The equation (3.37) presented by Alkidas (1984) predicts the level of particulate matter emission attained from Bosch smoke number (Datta and Mandal, 2018).

$$[\text{PM}] = 565\left(\text{In}\frac{10}{10-\text{Bosch}}\right)^{1.206} \tag{3.37}$$

Another important emission characteristic is air pollutant emissions (SE) as summarised by PM and NO_x emissions (Al-Dawody and Bhatti, 2013) in Equation (3.38):

$$\text{SE} = \text{C}_{\text{PM}}\left[\frac{\text{PM}}{0.15}\right] + \text{C}_{\text{NO}}\left[\frac{\text{NO}_\text{X}}{7}\right] \tag{3.38}$$

Where C_{PM} is an empiric factor for PM 0.5 and C_{NO} is an empiric factor for NO_x 1.0.

CHAPTER FOUR-RESULTS AND DISCUSSION

4.1 Experimental Studies of Characterization, Performance, Combustion, and Exhaust Gas Emissions.

The results of fuel characterization, combustion parameters, performance, and emitted gases of the diesel engine powered by standard diesel (D100), waste vegetable biodiesel (WVB100), soybean biodiesel (SB100), biodiesel mixture from waste vegetable biodiesel and soybean biodiesel (BM100), biodiesel mixture-ethanol blends (BME5, BME10, and BME15) at the full load conditions are discussed in this section. The combustion parameters, performance, and exhaust gas emissions of the diesel engine powered by these fuel samples were investigated and compared to D100 as a base fuel. Results were presented for all experiments done and attempts have been made to highlight the influence of fuel samples and the fuel properties on engine characteristics during the full load conditions. The results presented are based on the experimental data obtained from the diesel engine.

4.1.1 Properties of the Fuel Samples

Table 4.1 presents the results of the key properties of the fuel samples studied. These properties, especially viscosity, density, and heating value are known to have major effects on engine brake power and brake torque.

Table 4.1: Fuel properties

Properties	D100	WVB100	SB100	BM100	BME5	BME10	BME15
Density (kg/m³)	0.8263	0.8868	0.8865	0.8857	0.8814	0.8771	0.8714
Viscosity at 40°C (mm²/s)	2.66	4.72	4.238	4.411	4.065	3.629	3.255
Heating value (MJ/kg)	42.5	37.5	39.6	41.5	37.1	36.7	36.2
Flash Point (°C)	78.5	193	130	150	119	110	90.5

Viscosity

The viscosity of the different fuel samples has been measured. The viscosity of WVB100, SB100, BM100, BME5, BME10, and BME15 increased by 77.4%, 59.3, 65.8%, 52.8%, 36.4%, and 22.4% compared to D100. The viscosity of the hybrid biodiesel-ethanol blends decreased compared to WVB100, SB100, and BM100 whereas the viscosity of these biodiesel fuels increased compared to diesel (D100). Wei et al. (2018) reported that the viscosity of biodiesel-ethanol blends attained lower values compared to biodiesel but higher than diesel fuel. Higher values of viscosity could negatively affect the volume flow and injection spray characteristics of the engine (Silitonga et al., 2013b). In addition, BME15 attained the lowest value compared to WVB100, SB100, BM100, BME5, and BME10. The possible decrease of the viscosity from BME15 might be due to the presence of higher percentage of alcohol blend.

Densities

The density of WVB100, SB100, BM100, BME5, BME10, and BME15 fuels has been measured and compared to the density of D100 at a constant temperature of 20^{o}C. Compared to D100, the density of WVB100, SB100, BM100, BME5, BME10, and BME15 increased by 7.3%, 7.3%, 7.2%, 6.7%, 6.1%, and 5.5%, respectively. However, the densities of BME5, BME10, and BME15 decreased compared to WVB100, SB100, and BM100. This might be due to ethanol being added to the hybrid biodiesel. Similar results were obtained by Zhu et al. (2011b), Wei et al. (2018) reported that compared to the density of biodiesel, the density of biodiesel-ethanol fuel blends decreases, and tends towards the density of standard diesel, as the percentage of ethanol blending in the biodiesel increases from 5% up to 15%. The density values of all test fuels are suitable for the limitation standard of the diesel engine.

Heating Value

The heating values of D100, WVB100, SB100, BM100, BME5, BME10, and BME15 fuels have been measured. Compared to D100, the heating values of WVB100, SB100, BM100, BME5, BME10, and BME15 decreased by 11.8%, 6.8%, 2.4%, 12.7%, 13.6%, and 14.8% respectively.

The oxygen content of ethanol blends was the reason behind the lowest heating value of BME15 fuel. This is proved in Table 15 as the heating value of all feedstock fuel samples are lower compared to standard diesel. The results reported by Geng et al. (2021) show that the higher oxygen content of biodiesel-ethanol blends could reduce the heating value compared to biodiesel and standard diesel. The heating value of the biodiesel mixture was marginally close to that of D100 at just a 2.4% decrease in value.

Flash Point

The flash point fuel samples of D100, WVB100, SB100, BM100, BME5, BME10, and BME15 were measured. The results show that the flash point of WVB100, SB100, BM100, BME5, BME10, and BME15 increased by 145.9%, 65.6%, 91.1%, 51.6%, 40.1%, and 15.3%, respectively, compared to that of diesel fuel. The results show that the flash point fuel samples for WVB100, SB100, and BM100 were much higher compared to D100 and these results are also in agreement with those attained by Mat Yasin et al (2013) who indicates that the biodiesel blend with alcohol additive attained higher flash point compared to standard diesel. However, in this case, the WVB100, SB100, and BM100 were difficult to ignite with the high flash point. The high flash point of biodiesel might be due to the presence of predominate unsaturated acid chain length in the vegetable oil (Hoekman et al., 2012). The flash point of BME5, BME10, and BME15 attained lower values compared to WVB100, SB100, and BM100 but higher than D100. This might be due to ethanol being added to the hybrid biodiesel. The results reported by Atmanli and Yilmaz (2020) are in line with the current results that discovered that the flash point of biodiesel and higher alcohol blends are lower than biodiesel but higher compared to standard diesel.

4.1.2 Combustion Characteristics Under Full Load Conditions

The engine combustion for D100, WVB100, SB100, BM100, BME5, BME10, and BME15 was investigated with the combustion parameters such as ICP and HRR. Furthermore, based on ideal gas and the first law of thermodynamics, in-cylinder pressure can be applied in complicated calculations such as estimation of air mass flow, combustion analysis, as well as NO_x prediction

(Brunt et al., 1998, Desantes et al., 2010). In these studies, the variation of ICP and HRR was studied for WVB100, SB100, BM100, BME5, BME10, and BME15 and compared to D100.

In-Cylinder Pressure

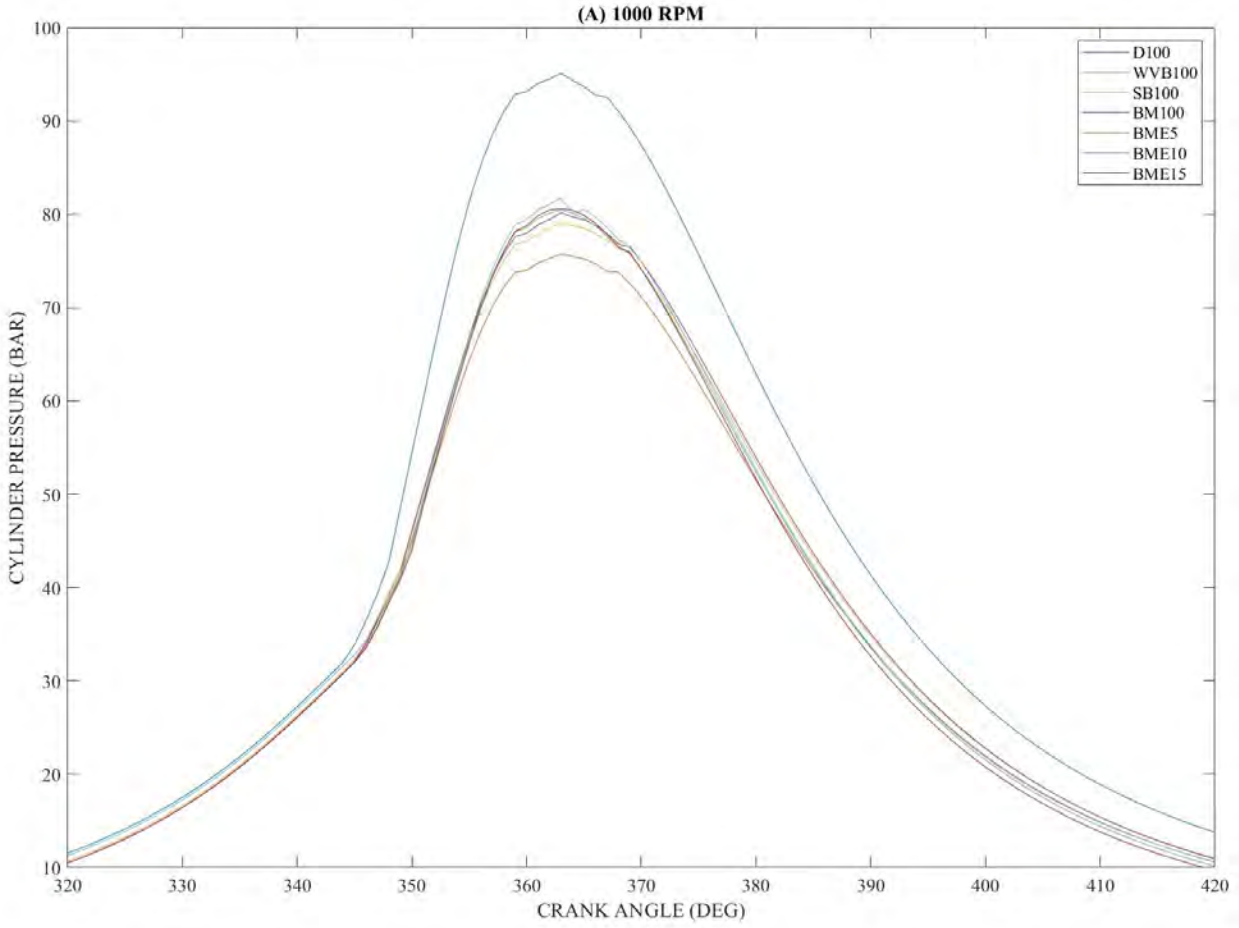

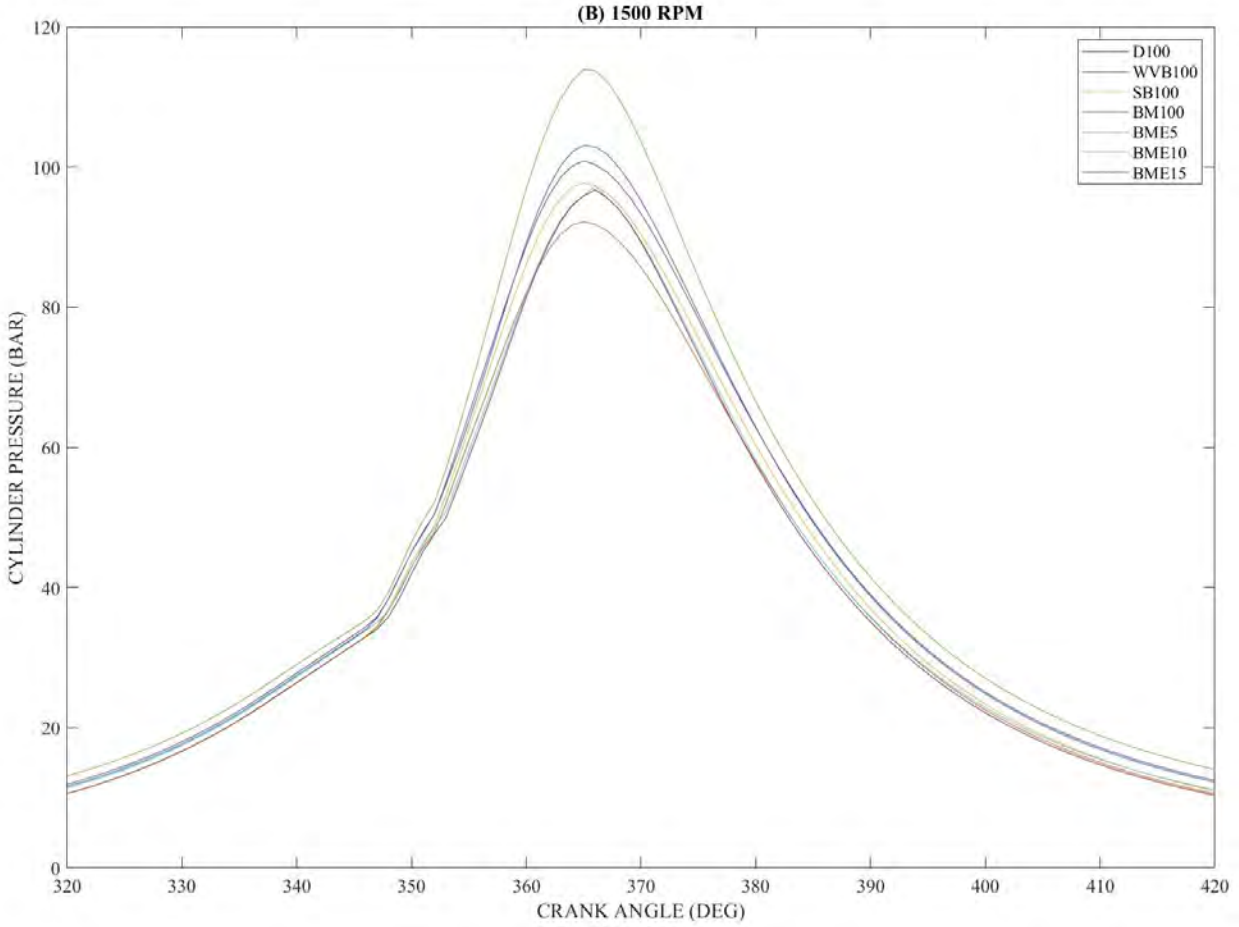
(B) 1500 RPM
D100
WVB100
SB100
BM100
BME5
BME10
BME15
CYLINDER PRESSURE (BAR)
CRANK ANGLE (DEG)
0
20
40
60
80
100
120
320
330
340
350
360
370
380
390
400
410
420

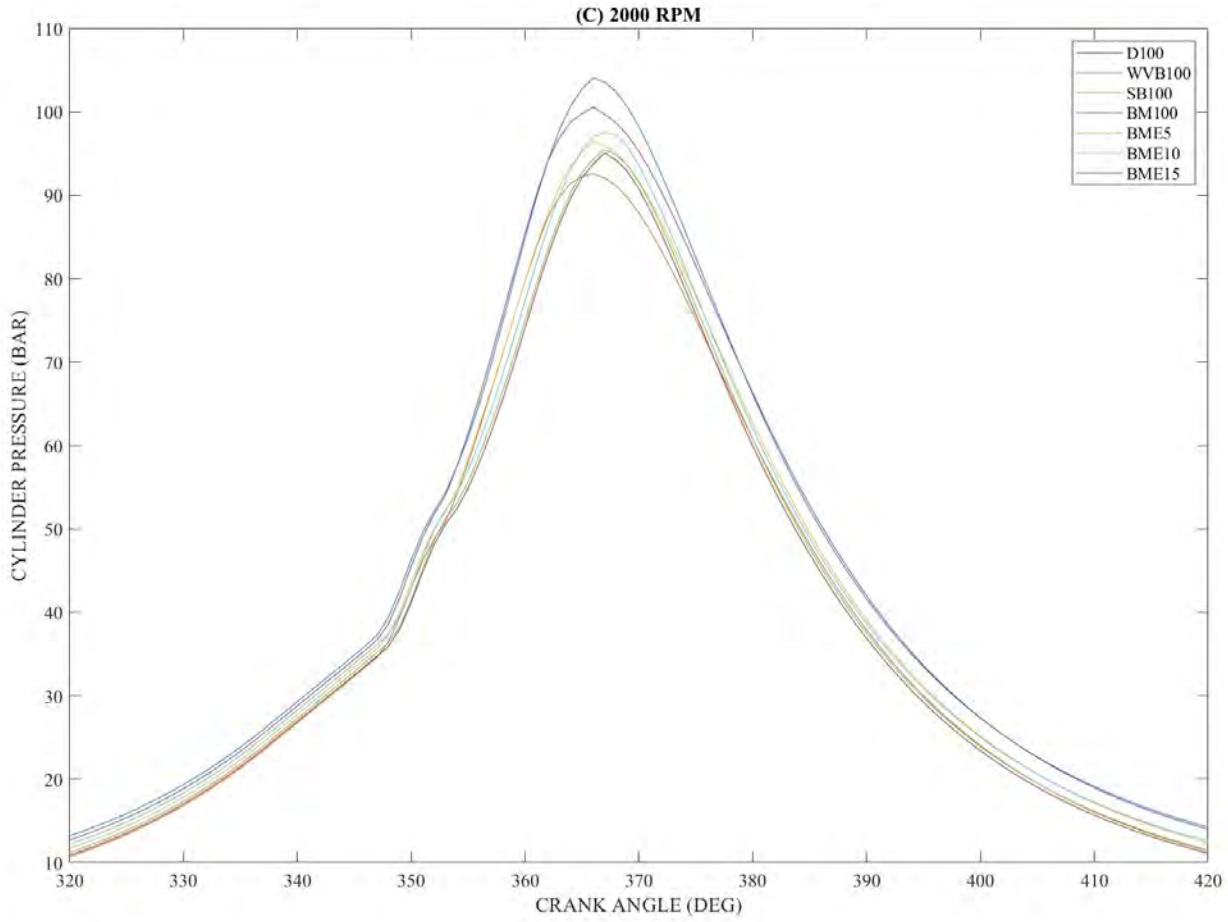
(C) 2000 RPM
D100
WVB100
SB100
BM100
BME5
BME10
BME15
CYLINDER PRESSURE (BAR)
CRANK ANGLE (DEG)
110
100
90
80
70
60
50
40
30
20
10
320
330
340
350
360
370
380
390
400
410
420

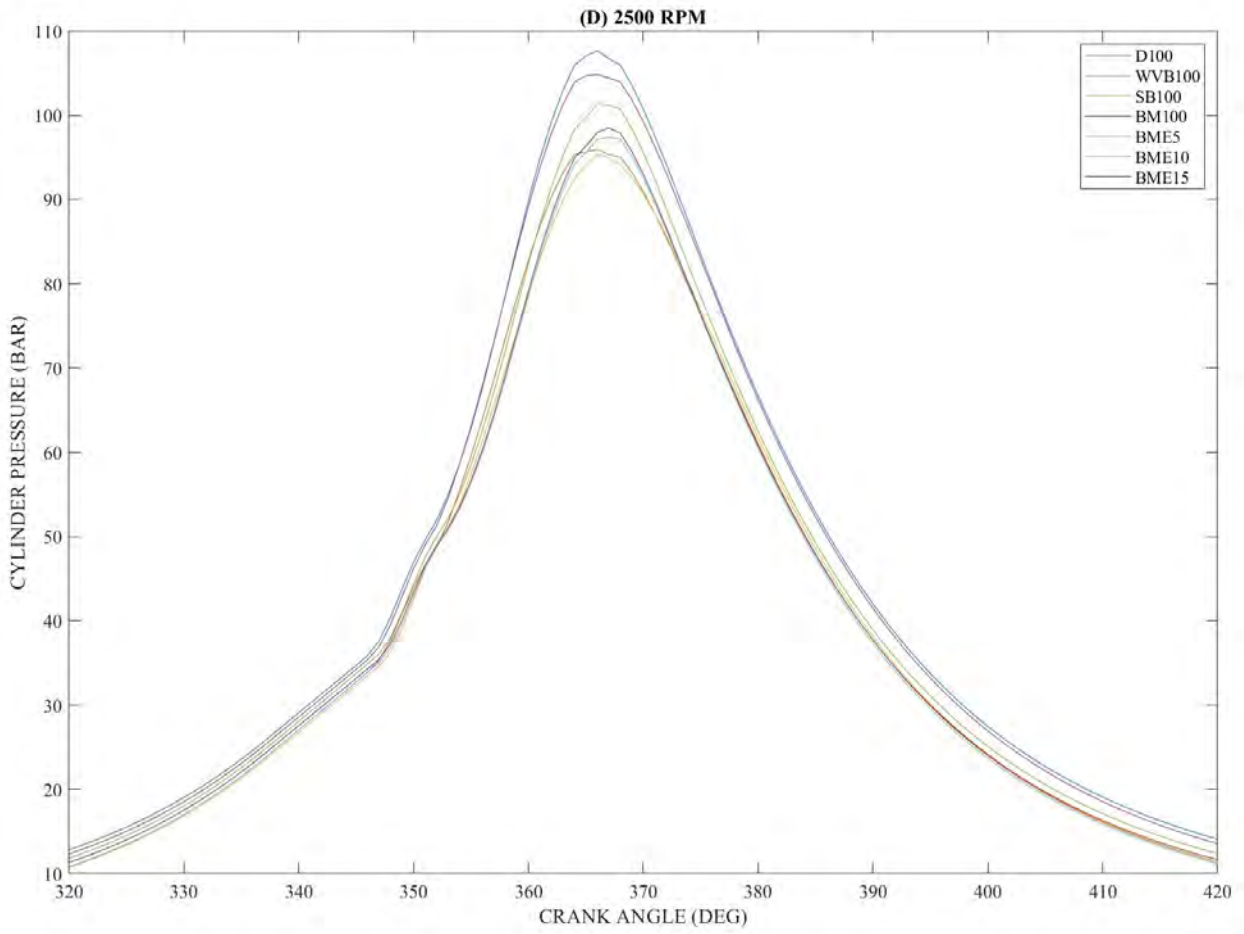

Figure 4.1: Variation of in-cylinder pressure with crank angle

Figure 4.1 shows the variation of ICP for D100, WVB100, SB100, BM100, BME5, BME10, and BME15 at different crank angle positions. The experimental results show that the peak ICP of D100 attained the highest value compared to WVB100, SB100, BM100, BME5, BME10, and BME15 at all engine speeds. The possible reason for this maximum value of D100 might be due to higher heating value, low density, low viscosity, and better fuel atomization (Swarna et al., 2022). At the maximum speed, the peak ICP of SB100 attained the lowest value compared to D100, SB100, BM100, BME5, BME10, and BME15. This could be possible due to low energy content, high viscosity, and poor fuel atomization of biodiesel. At the same operating condition, the fuel samples of BME5, BME10, and BME15 exhibited higher in-cylinder pressure compared to individual biodiesels (WVB100 and SB100). This improvement might be due to higher oxygen content of ethanol to hybrid biodiesel that encouraged the combustion process. Moreover, the

BM100 fuel sample attained the maximum value of in-cylinder pressure compared to WVB100, SB100, BME5, BME10, and BME15 due to the high calorific value of hybrid biodiesel. Thiyagarajan et al. (2020) mentioned, in their experiment that the diesel engine powered with safflower biodiesel-methanol blend attained the maximum in-cylinder peak pressure compared to pure biodiesel. At the minimum speed of 1000 rpm, the peak in-cylinder pressure of fuel samples for D100, WVB100, SB100, BM100, BME5, BME10, and BME15 was 95.11 bar at 363º aTDC, 76.72 bar at 363º aTDC, 79.93 bar at 363º aTDC, 81.16 bar at 363º aTDC, 81.45 bar at 363º aTDC, 81.93 bar at 363º aTDC, and 81.59 bar at 363º aTDC. However, at the maximum speed of 2500 rpm, the peak in-cylinder pressure fuel samples of D100, WVB100, SB100, BM100, BME5, BME10, and BME15 was 106.67 bar at 366º aTDC, 96.95 bar at 366º aTDC, 95.45 bar at 366º aTDC, 104.32 bar at 366º aTDC, 101.34 bar at 366º aTDC, 98.37 bar at 367º aTDC, and 99.01 bar at 367º aTDC, respectively. At the maximum speed of 2500 rpm, the in-cylinder pressure of the diesel engine powered by WVB100, SB100, BM100, BME5, BME10, and BME15 decreased by 9.1%, 10.5%, 2.2%, 5.0%, 7.8%, and 7.2% compared to D100. The position of the maximum ICP indicates the pace at which the energy is released as it mostly depends on the tested fuel properties (Swarna et al., 2021).

Heat Release Rate

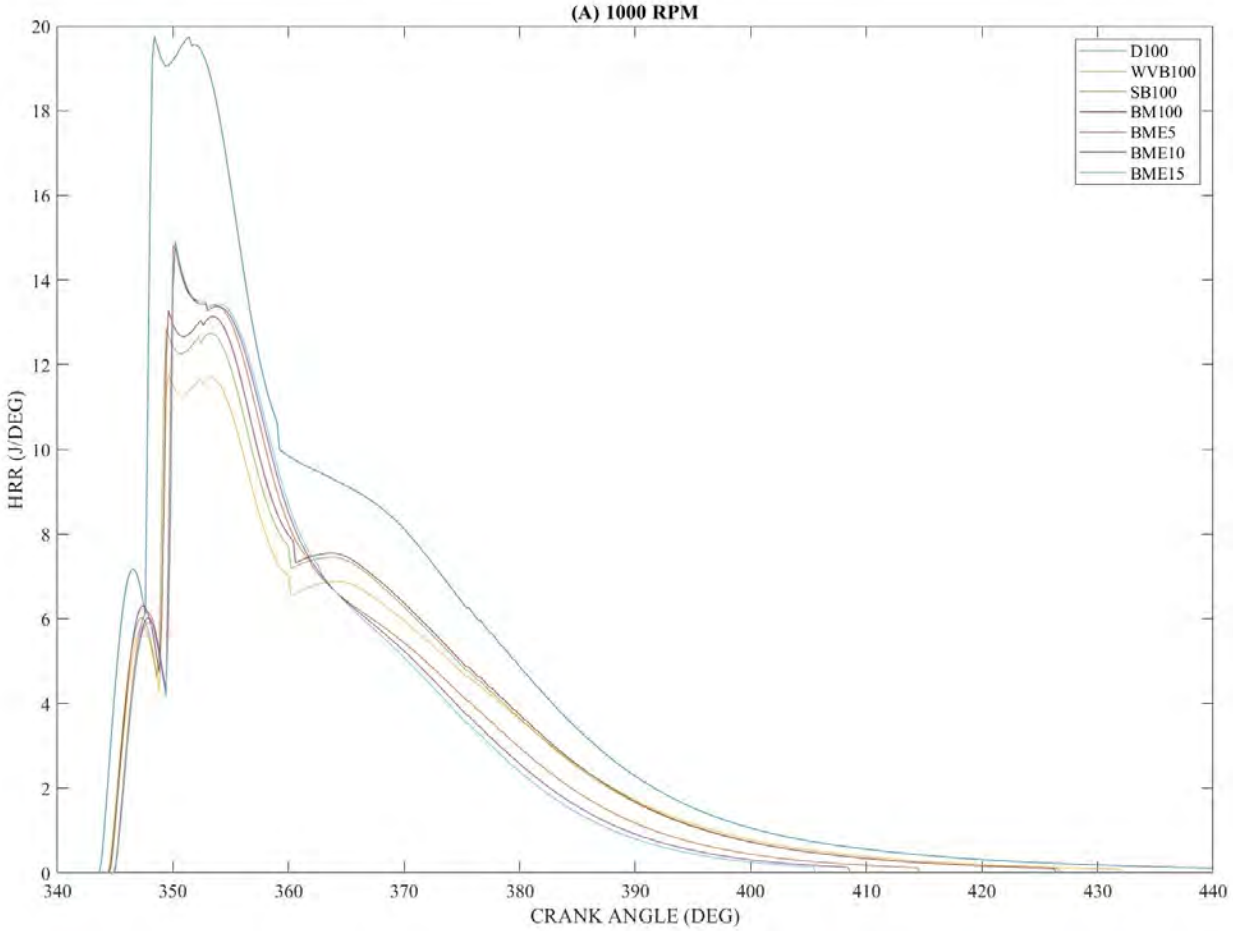

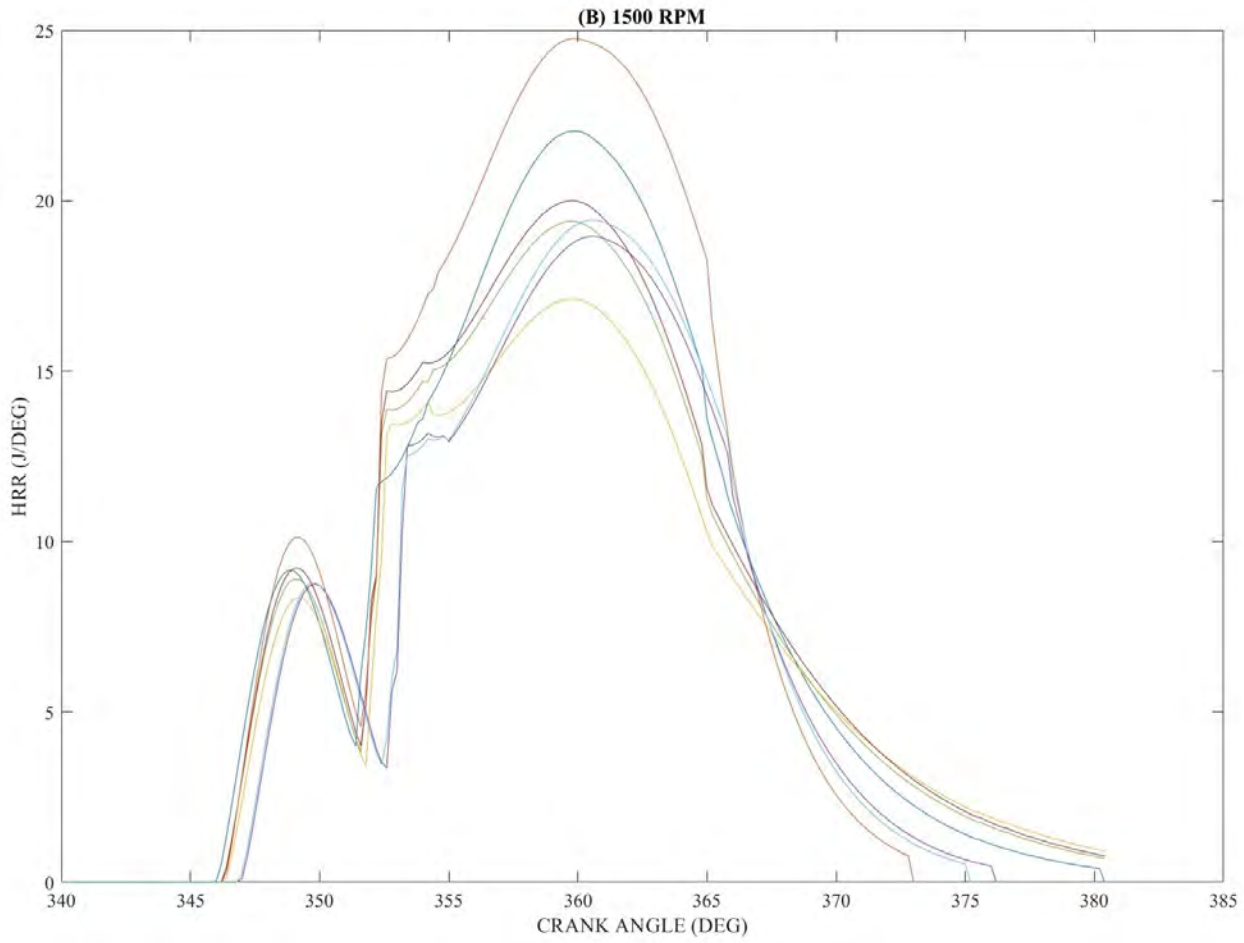
(B) 1500 RPM
HRR (J/DEG)
CRANK ANGLE (DEG)
0
5
10
15
20
25
340
345
350
355
360
365
370
375
380
385

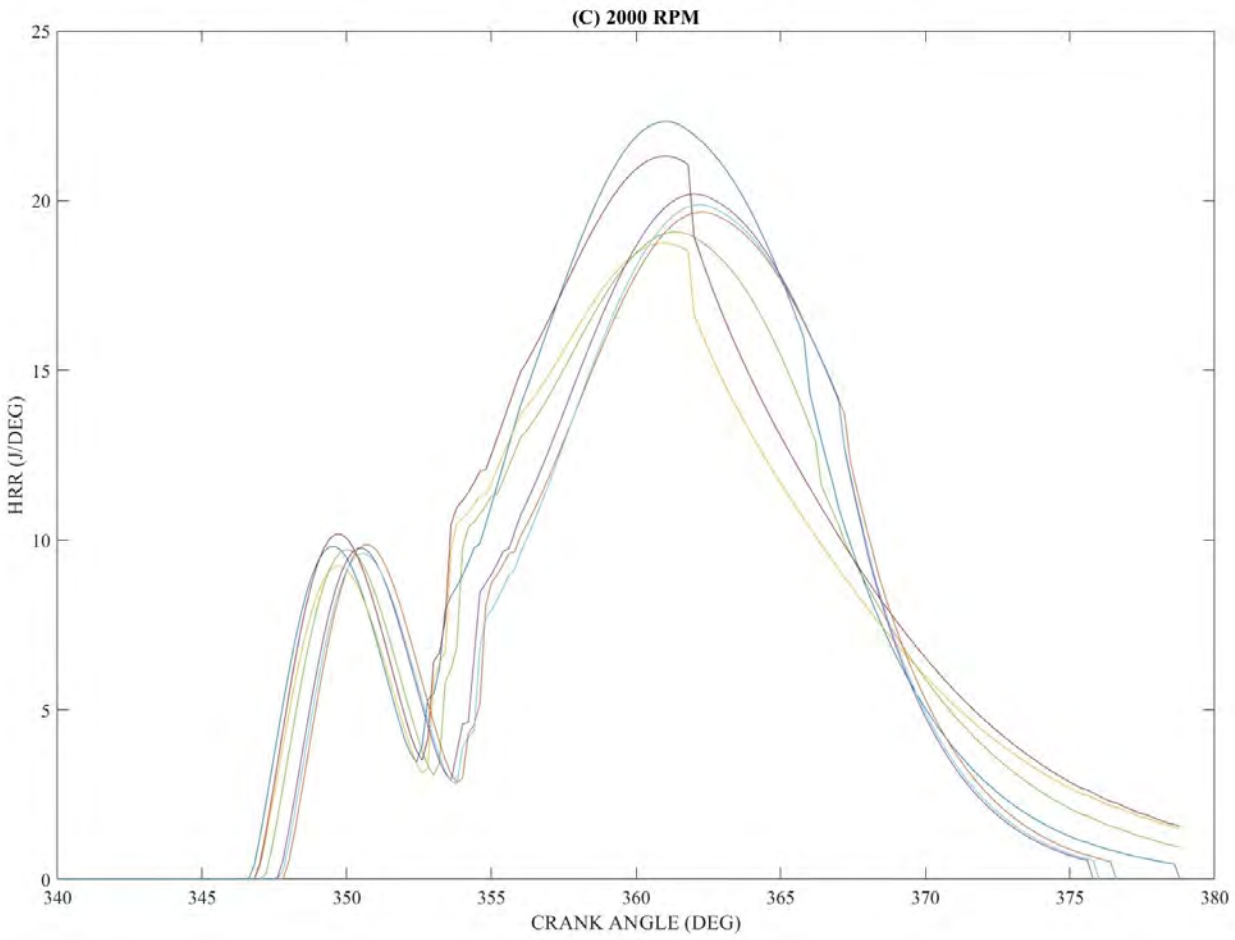
(C) 2000 RPM
HRR (J/DEG)
CRANK ANGLE (DEG)
0
5
10
15
20
25
340
345
350
355
360
365
370
375
380

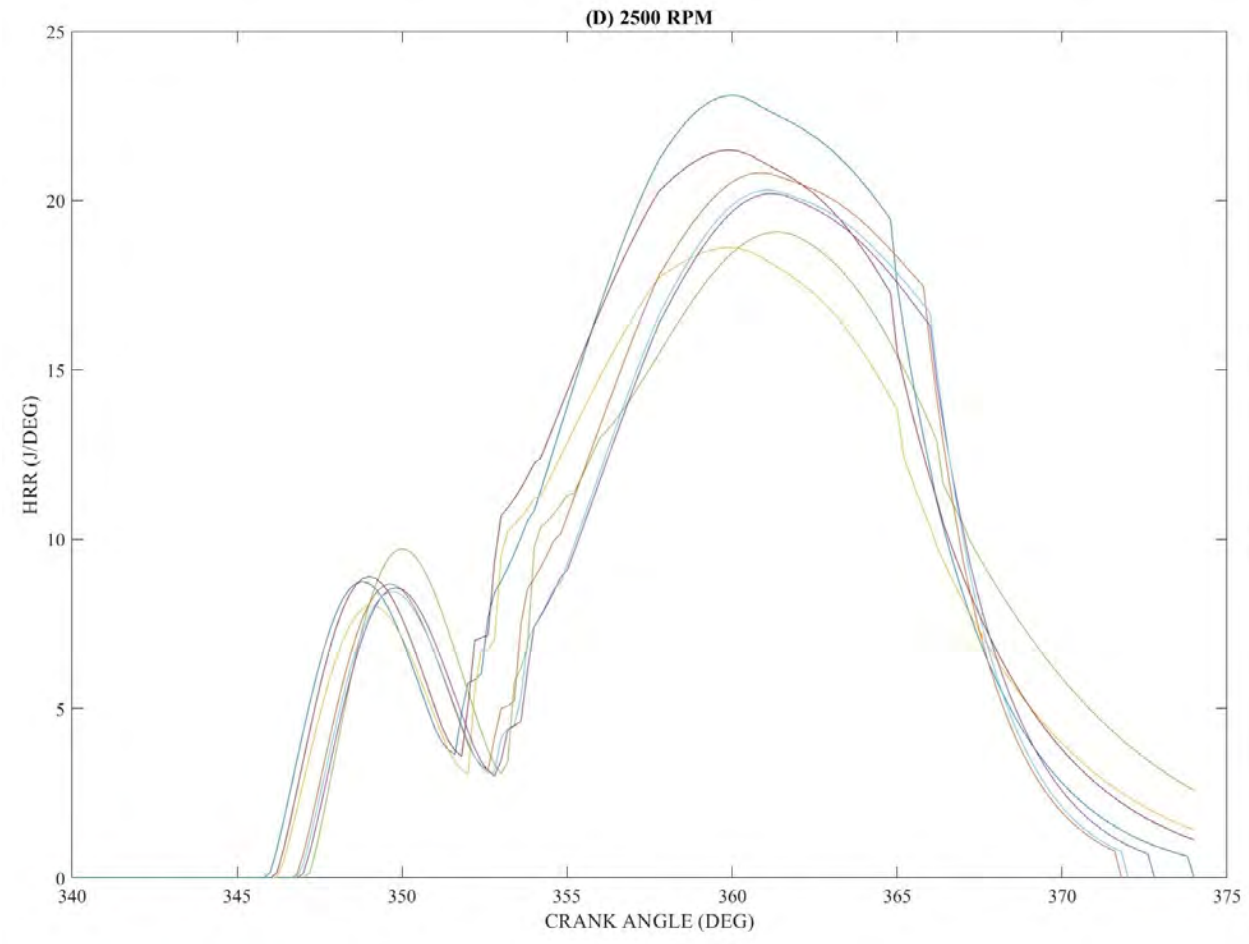

Figure 4.2: Variation of heat release rate with crank angle

The heat release rate can be defined as a significant combustion aspect derived from the first law of thermodynamics as a working procedure of in-cylinder pressure to evaluate the combustion process, which occurs inside of combustion chamber. The variation of HRR for D100, WVB100, SB100, BM100, BME5, BME10, and BME15 with the crank angle at full load conditions is depicted in Figure 4.2. The results show that the HRR of the D100 fuel sample attained the maximum value compared to the HRR of all the tested fuels at all engine speeds. The possible explanation for this maximum value of D100 was due to higher heating value, low cetane number, and short ignition delay that improved fuel atomization due to lower viscosity (Yesilyurt et al., 2020). At the minimum speed of 1000 rpm, the fuel sample of BME15 attained a higher value of HRR compared to all tested fuel blends. The possible increase might be due to higher ignition delay caused by the low cetane number of ethanol. The higher volatility, lower viscosity, and lower

surface tension of ethanol promote the evaporation of fuel droplets, which lead to better air-fuel blending (Wei et al., 2018). Zhu et al. (2010a), Zhu et al. (2011a) obtained similar kinds of results. At the maximum speed of 2500 rpm, the maximum HRR fuel samples of D100, WVB100, SB100, BM100, BME5, BME10, and BME15 were 23.11 J/deg, 18.61 J/deg, 18.97 J/deg, 21.49 J/deg, 20.82 J/deg, 20.21 J/deg, and 20.31 J/deg, respectively. The HRR of hybrid biodiesel-ethanol blends was higher compared to individual biodiesel (WVB100 and SB100) at the minimum and maximum speed.

These maximum values were due to longer ignition delay and higher oxygen content of ethanol that enhanced the heat release rate. Meanwhile, BME5, BME10, and BME15 attained longer ignition delay and high oxygen content of ethanol, which enhance the diffusion stage of combustion and high volatility leading to a high volume of fuel consumption through the premixed stage combustion and higher HRR (Sivalakshmi and Balusamy, 2012, Zhu et al., 2011a). However, the lowest values of individual biodiesels might be due to higher viscosity, which directly disturbs the combustion process. It can also be noted from the figure that the HRR fuel samples of WVB100, SB100, BM100, BME5, BME10, and BME15 decreased by 19.5%, 17.9%, 7.0%, 9.9%, 12.5%, and 12.1% compared to D100 at the maximum speed of 2500 rpm.

4.1.3 Performance Characteristics Under Full Load Conditions

In this section, various engine parameters have been assessed using experimental measurements. The most common parameters used to evaluate the engine characteristics are BP, BSFC, BT, BTE, and BMEP. However, the impacts of fuel properties such as density, viscosity, and heating value of D100, WVB100, SB100, BM100, BME5, BME10, and BME15 were evaluated on a diesel engine.

Brake Power

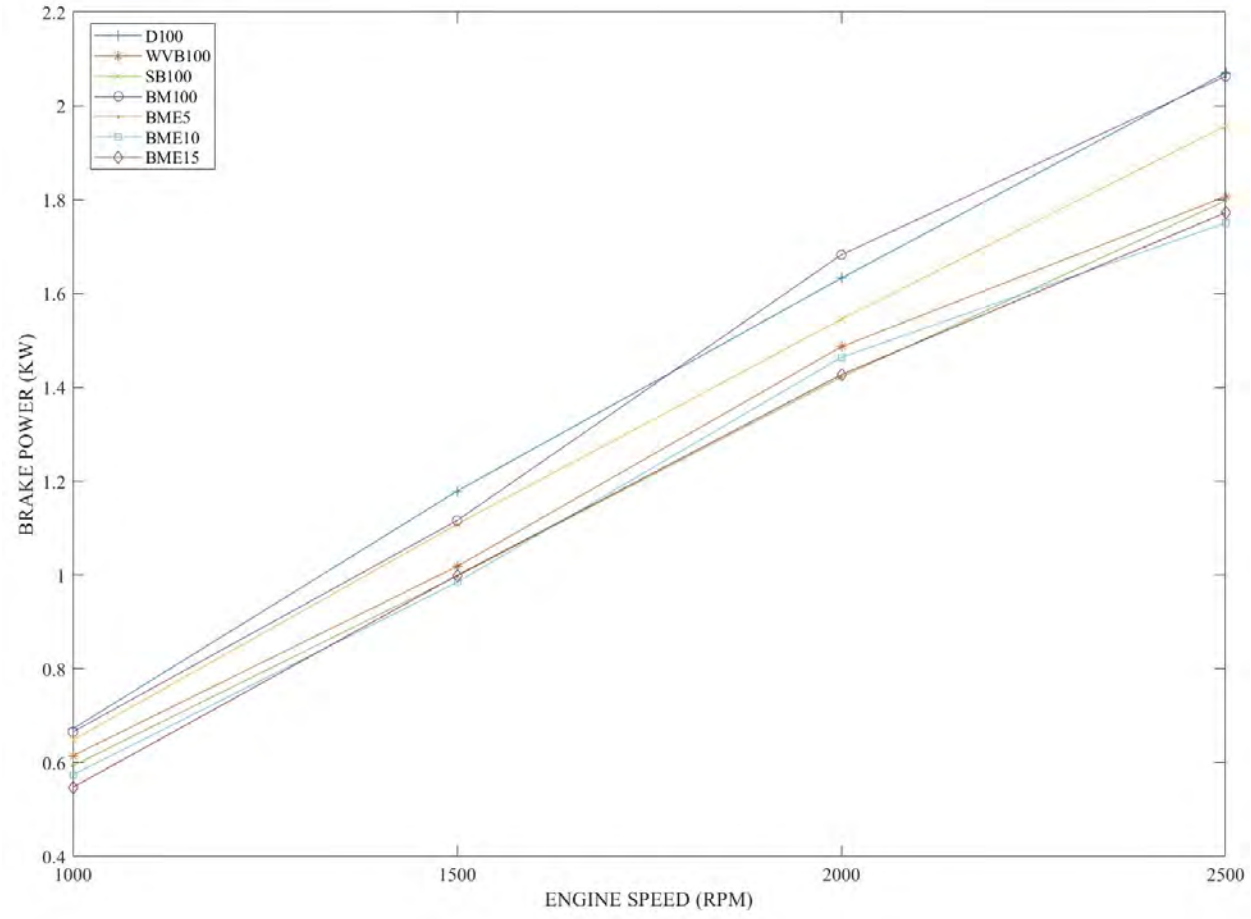

Figure 4.3: Variation of brake power with engine speed

The variation of brake power with engine speed for D100, WVB100, SB100, BM100, BME5, BME10, and BME15 is depicted in Figure 4.3. From the figure, with the increase in engine speed, brake power increased for all the fuel samples. The results show that D100 attained the maximum BP compared to all the fuel samples tested at the minimum and maximum speed. The possible increase of BP might be due to the higher heating value of D100. For green fuels assessment, BM100 attained the maximum value of brake power compared to other fuel blends at maximum speed. It can be noted that hybrid biodiesel has a high CN, and this might possibly lead to the better performance of brake power. Furthermore, the higher heating value of hybrid biodiesel compared to the individual biodiesels (WVB100 and SB100) and hybrid biodiesel-ethanol blends might be the reason for higher brake power. The minimum value for BME15 of brake power might be caused by low calorific value. All hybrid biodiesel-ethanol blends attained the lowest values of BP

compared to all fuel samples tested. The reason might be low cetane number of ethanol that affect the hybrid biodiesel-ethanol blends resulting to low power output. This result agrees with Shirneshan et al. (2021) who showed that the brake power of biodiesel continuously decreased with a higher percentage of ethanol blends compared to diesel fuel due to the low calorific value. It can also be noted from the graph that the values of D100, WVB100, SB100, BM100, BME5, BME10, and BME15 were 2.07 kW, 1.81 kW, 1.96 kW, 2.06 kW, 1.80 kW, 1.75 kW, and 1.77 kW at the maximum engine speed of 2500 rpm. Compared to D100, the WVB100, SB100, BM100, BME5, BME10, and BME15 decreased by 12.7%, 5.5%, 0.3%, 13.2%, 15.4%, and 14.4% at a maximum speed of 2500 rpm. This decrease was due to low heating value, low cetane number, and higher latent heat (Dwivedi et al., 2018).

Brake-Specific Fuel Consumption

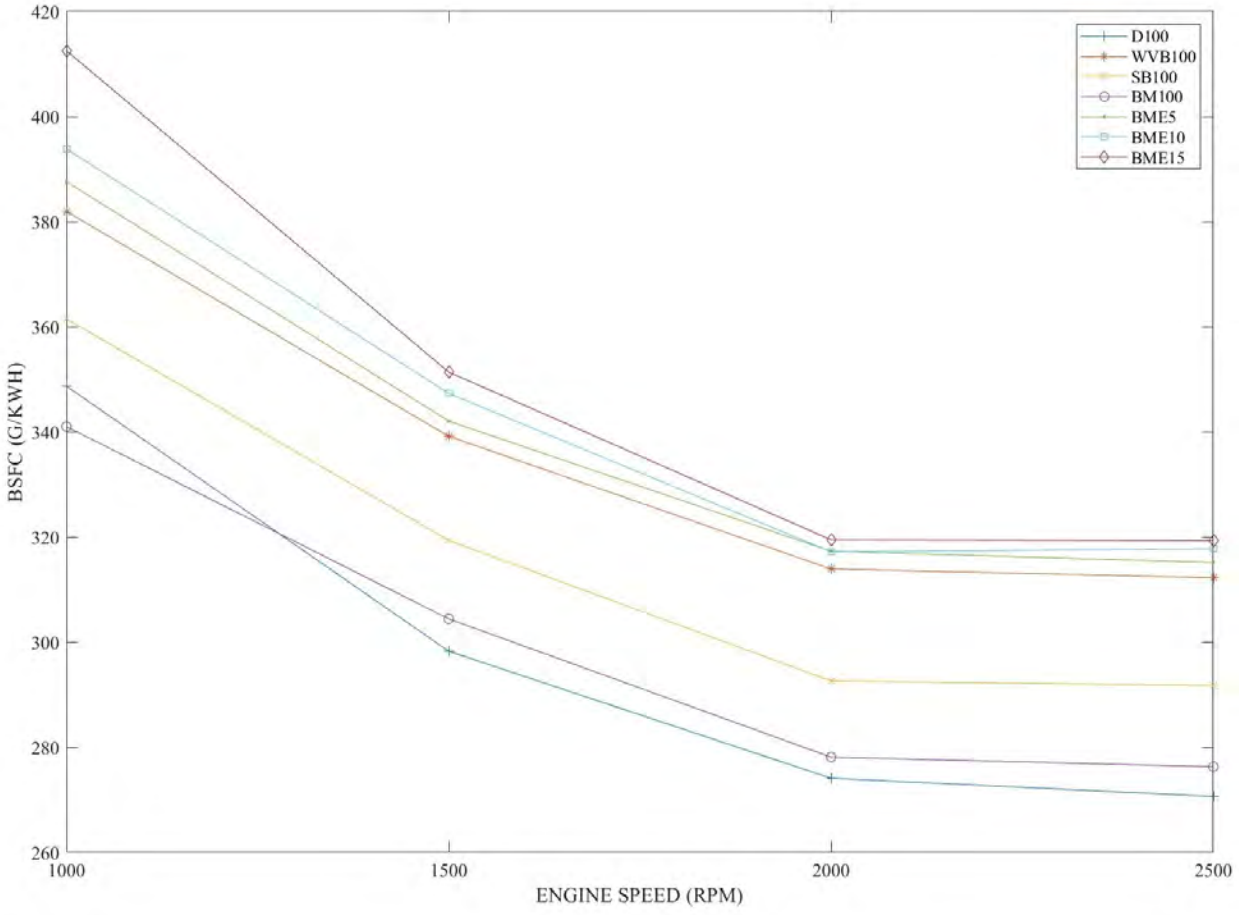

Figure 4.4: Variation of brake specific fuel consumption with engine speed

Figure 4.4 shows the comparison of BSFC for D100, WVB100, SB100, BM100, BME5, BME10, and BME15 with engine speed at full load conditions. The BSFC for all the fuel samples tested showed similar trends at all engine speeds. It can be noted from the figure that all fuel samples slowly decreased with the increase of speed due to the good quality of air-fuel mixture. At the maximum speed of 2500 rpm, the BSFC of WVB100, SB100, BM100, BME5, BME10, and BME15 increased by 15.4%, 7.8%, 2.1%, 16.4%, 17.4%, and 18.0% compared to D100. The possible increase might be due to lower heating values of tested fuels. Another reason for this increase in BSFC of green fuels might be due to the larger volume of fuel consumed to produce the necessary quantity of energy. Wei et al. (2018) reported that the BSFC of biodiesel-alcohol blends increased compared to standard diesel. However, compared to BM100 at the maximum speed of 2500 rpm, the BSFC of BME5, BME10, and BME15 increased by 14.1%, 15.0%, and 15.6%, respectively. The possible increase was caused by the high latent heat of evaporation since the heat was lost from the combustion chamber due to evaporation, which causes the cooling effect and reduces combustion efficiency (Atmanli and Yilmaz, 2020). At 2500 rpm, the BSFC of D100, WVB100, SB100, BM100, BME5, BME10, and BME15 was 270.674 g/kWh, 312.276 g/kWh, 291.764 g/kWh, 276.312 g/kWh, 315.169 g/kWh, 317.782 g/kWh, and 319.321 g/kWh, respectively.

Brake Torque

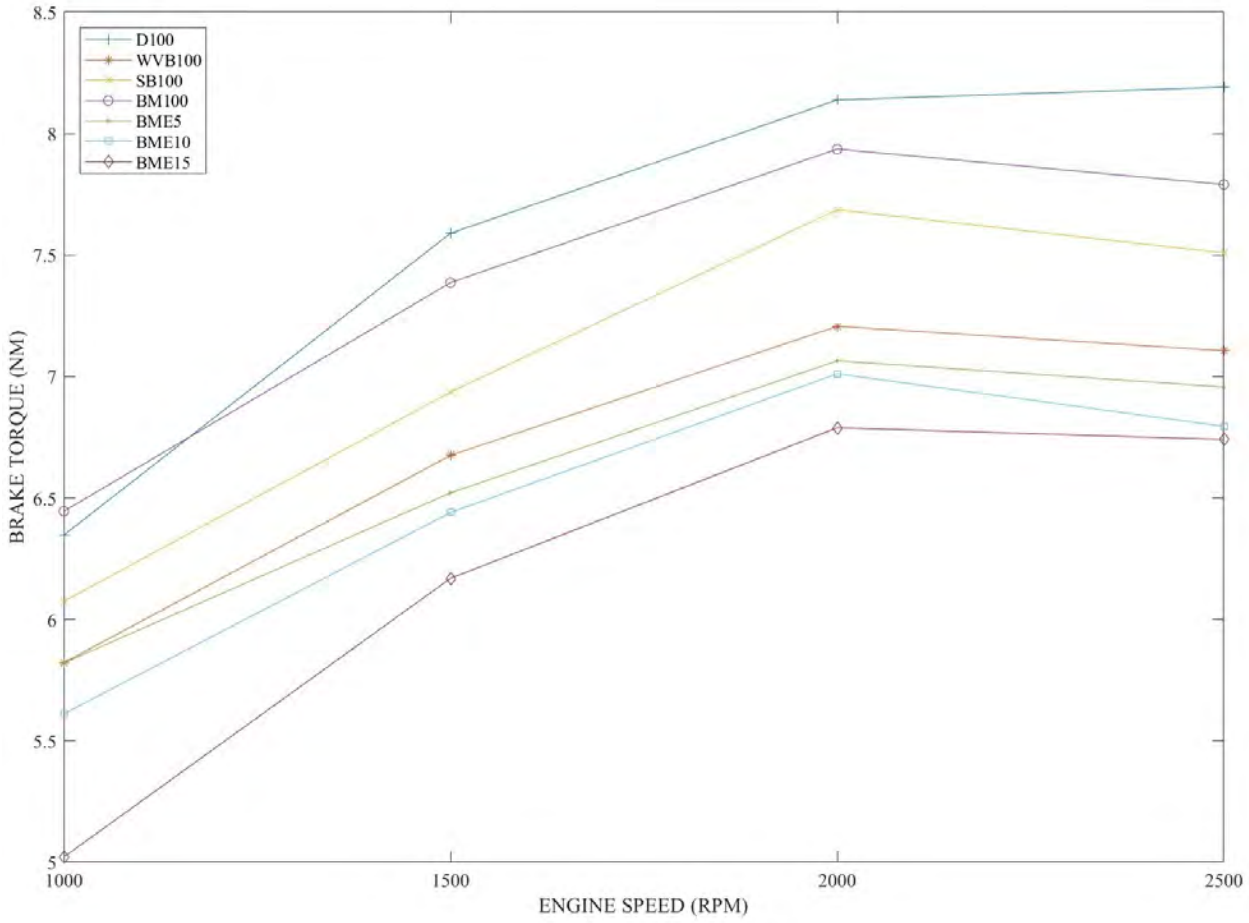

Figure 4.5: Variation of brake torque with engine speed

Figure 4.5 shows the variation of BT of the diesel engine fuelled with D100, WVB100, SB100, BM100, BME5, BME10, and BME15 at various speed conditions. The results show that the BT for all the fuel samples shows similar trends. However, the BT for all the fuel samples increased to a maximum at 2000 rpm and started to decrease to a maximum speed of 2500 rpm. The BT decreased at a maximum speed because the engine was unable to consume the full charge of air. At the maximum speed of 2500 rpm, the BT of D100 was 8.192 Nm, WVB100 (7.106 Nm), SB100 (7.509 Nm), BM100 (7.790 Nm), BME5 (6.957 Nm), BME10 (6.795 Nm), and BME15 (6.741 Nm). The maximum BT was attained at 2000 rpm with a value of 8.219 Nm for D100 fuel. The BT of WVB100, SB100, BM100, BME5, BME10, and BME15 fuels decreased by 13.3%, 8.3%, 4.9%, 15.1%, 17.1%, and 17.7% compared to D100 at the maximum speed of 2500 rpm. The low heating value, low cetane number of alcohols, and high latent heat might be the cause of longer

ignition delay, which influences the engine combustion and hence decreases the brake torque (Kandasamy et al., 2019). Furthermore, the BT of the biodiesel mixture (BM100) attained the highest values compared to individual biodiesel and biodiesel mixture-ethanol blends. These results agree with studies reported by Fazal et al. (2013) who stated that the high lubricity and shorter ignition delay of biodiesel may result in better combustion efficiency, which boosts the brake torque.

Brake Thermal Efficiency

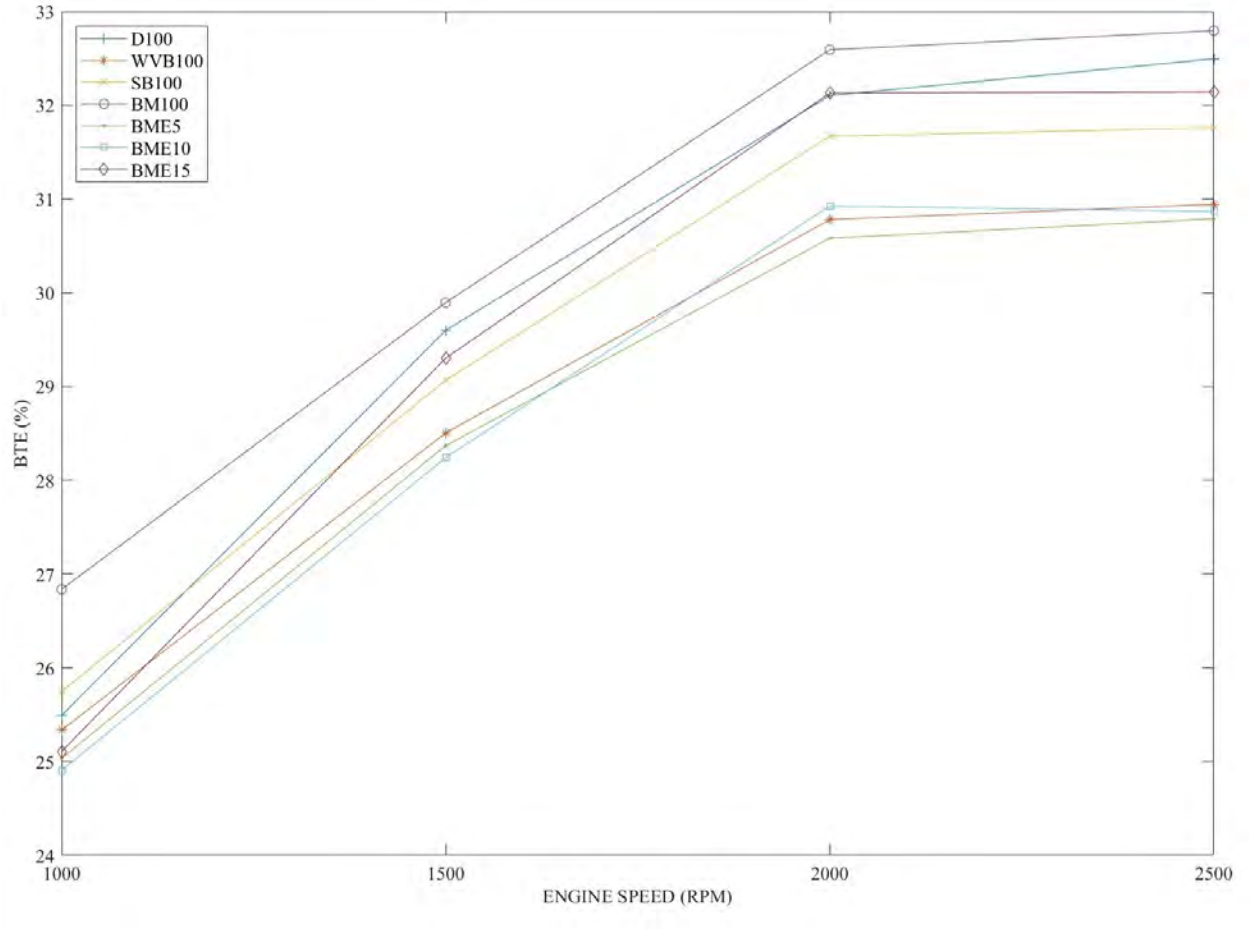

Figure 4.6: Variation of brake thermal efficiency with engine speed

The BTE is usually defined as the ratio of engine mechanical power as a role of energy input of fuel consumption in unit time. The high BTE of the engine represents the optimization of fuel consumption and enhanced transition of fuel to energy. The comparison of BTE with respect to engine speed of D100, WVB100, SB100, BM100, BME5, BME10, and BME15 fuels is shown in

Figure 4.6. It can be discovered from the graph that with the increase of engine speed, the BTE of all fuel samples increases up to the maximum speed due to high combustion quality of ethanol. The increase of ethanol blends decreases the density and viscosity of hybrid biodiesel, which improves the injection better and this might lead to better atomization of the charge (Paul et al., 2017). The results show that BM100 attained the highest BTE compared to all testing fuel samples at the minimum and maximum speed. At the minimum speed of 1000 rpm, the BTE of D100, WVB100, SB100, BM100, BME5, BME10, and BME15 was 25.49%, 25.34%, 25.75, 26.84%, 25.03%, 24.91%, and 25.11% whereas, at the maximum speed of 2500 rpm, the BTE of D100, WVB100, SB100, BM100, BME5, BME10, and BME15 was 32.49%, 30.94%, 31.76%, 32.79%, 30.79%, 30.87%, and 32.14%, respectively. The test results reported by Anand et al. (2010) were in line with the current test results. The BM100 and BME15 attained higher thermal efficiency compared to individual biodiesels, BME5 and BME10. The high BTE of the BM100 and BME15 may be due to the improved atomization through injection and the decrease in friction loss is related to higher lubricity. In addition, BME15 attained high oxygen content of ethanol, which could boost the combustion process.

Brake Mean Effective Pressure

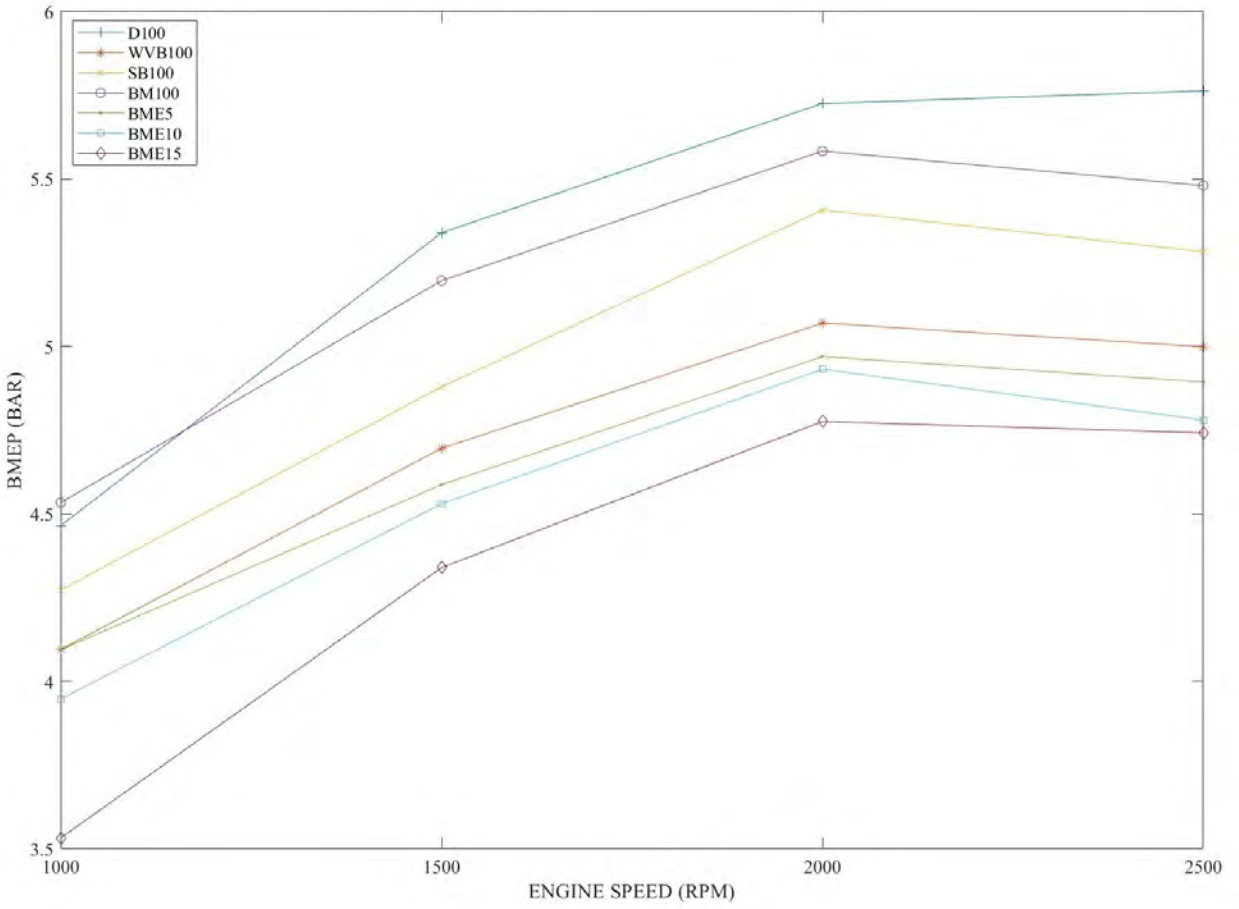

Figure 4.7: Variation of brake mean effective pressure with engine speed.

The product of brake torque and displacement volume of the diesel engine is described as BMEP (Islam et al., 2015). Figure 4.7 shows the comparison of BMEP for D100, WVB100, SB100, BM100, BME5, BME10, and BME15 with respect to engine speed. The results show that the BMEP values of WVB100, SB100, BM100, BME5, BME10, and BME15 for all tested engine speed was decreased compared to D100. The maximum value of BMEP is attained at D100 with the value of 5.65 bar at a speed of 2000 rpm. At the maximum speed of 2500 rpm, the BMEP of D100 was 5.76 bar, WVB100 (5.0 bar), SB100 (5.28 bar), BM100 (5.48 bar), BME5 (4.89 bar), BME10 (4.78 bar), and BME15 (4.74 bar). At the same maximum speed, the BMEP of WVB100, SB100, BM100, BME5, BME10, and BME15 decreased by 13.3%, 13.3%, 4.9%, 15.1%, 17.1%, and 17.7%, respectively, compared to that of D100. The possible decrease for all fuel samples might be due to lower heating values and high viscosity (Rajak et al., 2021).

4.1.4 Effects of the Fuel Samples on the Engine Emission Characteristics

In this section, exhaust gas emitted by the diesel engine powered by WVB100, SB100, BM100, BME5, BME10, and BME15 was investigated and compared with D100 fuel. The tested exhaust gases were carbon monoxide (CO), hydrocarbon (HC), nitric oxides (NO), carbon dioxide (CO_2), and smoke.

CO Emissions

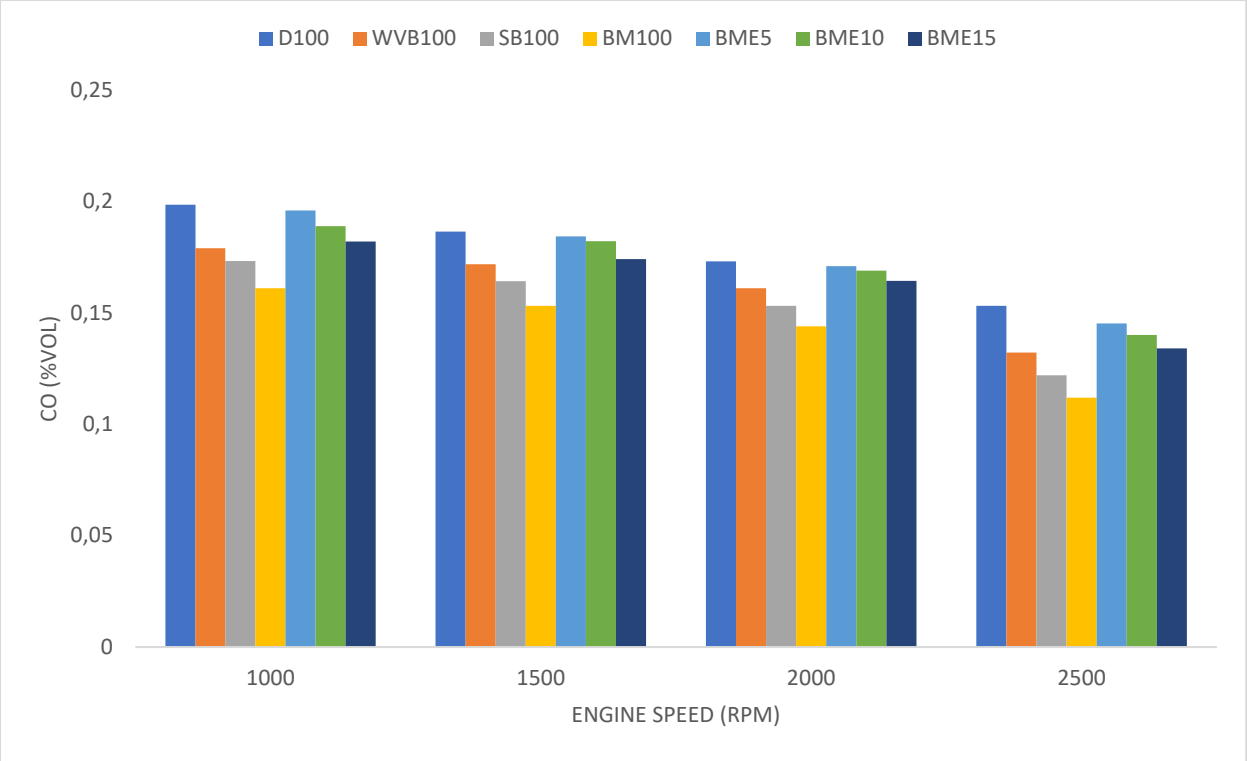

Figure 4.8: Variation of CO emission with engine speed

Figure 4.8 presents the variation of CO emissions of the diesel engine powered by D100, WVB100, SB100, BM100, BME5, BME10, and BME15 under full load conditions at different speeds. It can be noted from the figure that the CO emissions at the minimum speed attained higher values for all fuel samples owing to air-fuel mixture, which causes worsening in the fuel atomization and formation of larger fuel drop size (Tutak et al., 2017). At the maximum speed, there is a drastic reduction for all tested fuel samples due to the early flame-out duration, and at maximum speed high BTE in which higher ICP is built and caused the reduction in CO emissions. Compared to

D100, it was found that the CO emissions of WVB100, SB100, BM100, BME5, BME10, and BME15 decreased by 13.8%, 20.4%, 26.9%, 5.2%, 8.5, and 12.5%, respectively at the maximum speed of 2500 rpm. The increase in CO emissions for D100 was due to higher heating value that increased the combustion chamber temperature and improved efficiency with the shortfall of excess oxygen and resulted in the formation of rich blend that increased CO emission without transforming carbon to CO_2. The CO emissions for all the biodiesel blends tested decreased due to the early spark-out period compared to D100 at the maximum speed (Swarna et al., 2021). At the same operating conditions, the CO emissions for D100, WVB100, SB100, BM100, BME5, BME10, and BME15 were found to be 0.15%vol, 0.13%vol, 0.12%vol, 0.11%vol, 0.15%vol, 0.14%vol, and 0.13%vol. However, BM100 attained the lowest CO emission compared to the other fuels tested and this might be due to high CN and the excess of oxygen content through chemical structure, which produce the lower value of CO emissions. In addition, BME5, BME10, and BME15 exhibited lower emissions compared to D100. This decrease was caused by high oxygen content and low CN of ethanol and the improvement of the combustion process. This result agrees with that obtained by Ramírez et al. (2014), Li et al. (2015), who tested the diesel engine indicating that the CO emissions of diesel-biodiesel-pentanol blends decreased compared to standard diesel due to oxygenated fuels that offer higher local oxygen concentration.

HC Emissions

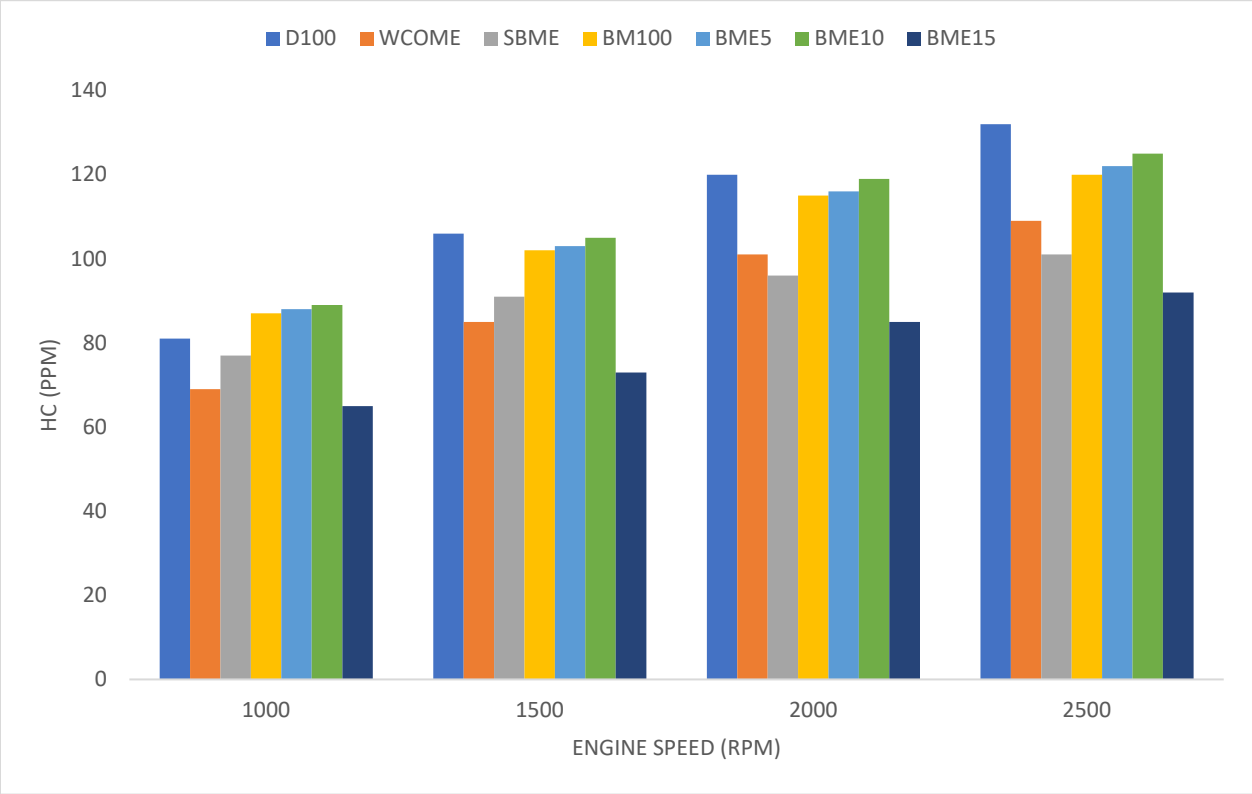

Figure 4.9: Variation of HC emissions with engine speed

Figure 4.9 shows the variation of HC emissions of the diesel engine fuelled with D100, WVB100, SB100, BM100, BME5, BME10, and BME15 under full load conditions. It can be seen from the figure that the formation of HC emissions was higher at the maximum speed of 2500 rpm. This may be possibly due to air-fuel mixture and high in-cylinder temperature, which leads to an increase in incomplete combustion of the engine. The results also showed that at 1500 rpm, 2000 rpm, and 2500 rpm engine speeds, D100 emitted the highest hydrocarbon compared to all other fuels tested. This might be due to the air-fuel mixture and low oxygen content that led to higher hydrocarbon emissions (Li et al., 2015). Nonetheless, there was decrease in HC emissions for WVB100, SB100, BM100, BME5, BME10, and BME15 compared to D100. This might be due to the high oxygen content of ethanol and high cetane number of biodiesels that led to improvement in combustion. At the maximum speed of 2500 rpm, the HC emissions of D100, WVB100, SB100, BM100, BME5, BME10, and BME15 were found to be 132 ppm, 109 ppm, 101 ppm, 120 ppm, 122 ppm, 125 ppm, and 92 ppm, respectively. The HC emissions of WVB100, SB100, BM100,

BME5, BME10, and BME15 decreased by 17.4%, 23.5%, 9.1%, 7.6%, 5.3%, and 30.3% compared to D100 at the maximum speed of 2500 rpm.

The excess of oxygen content improved the combustion of biodiesel that led to low HC emissions. The HC emissions of WVB100, SB100, and BM100 were slightly lower compared to BME5 and BME10 at all engine speeds. The possible decrease in HC emissions of biodiesels was due to the high cetane number, the lower latent heat of vaporization, the availability of oxygen content, and the improvement of auto-ignition properties. These findings are like the previous work reported by Atmanli (2016), Nour et al. (2019), and Yesilyurt (2020). However, BME15 emitted less HC emissions compared to WVB100, SB100, BM100, BME5, and BME10 at the minimum and maximum speeds. This decrease might be due to the higher percentage of ethanol blend, which increased the oxygen content and reduced viscosity and density of the hybrid biodiesel, leading to improved fuel spray and atomization, better combustion, and hence lower hydrocarbon emissions. Shudo et al. (2007) reported similar findings of HC emission with the palm oil methyl ester and ethanol blends.

NO Emissions

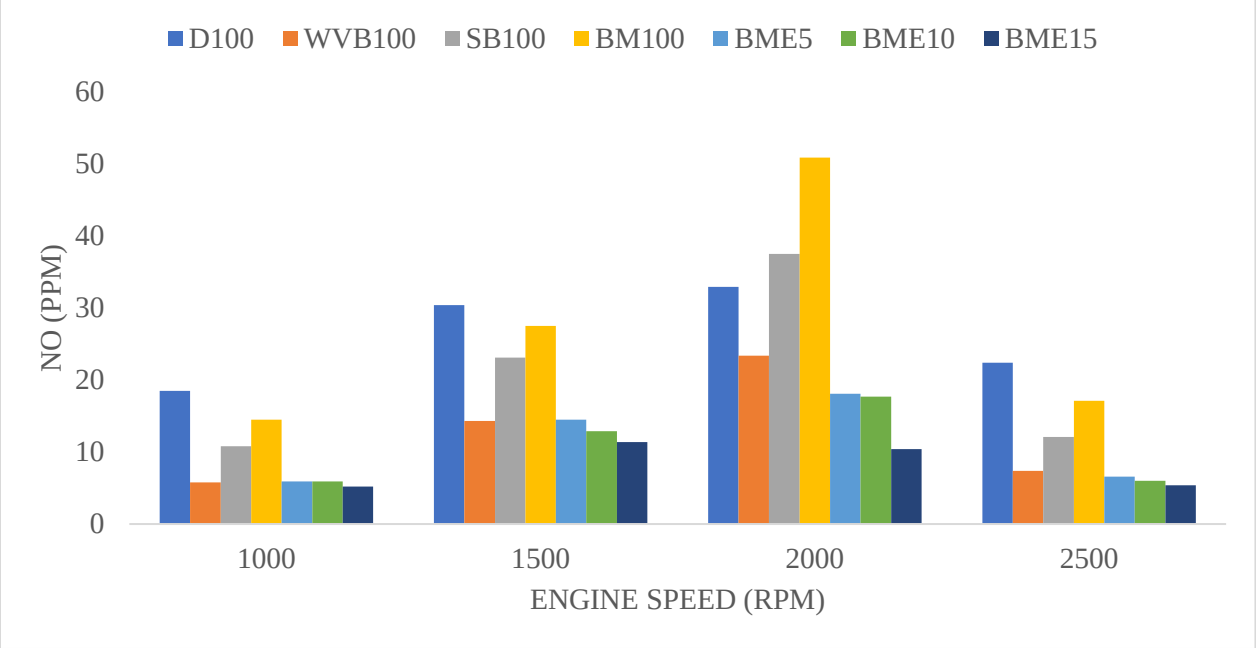

Figure 4.10: Variation of NO emissions with engine speed

Figure 4.10 shows the variation of nitric oxide (NO) emissions of D100, WVB100, SB100, BM100, BME5, BME10, and BME15 fuels, respectively. NO is the main component of NO_x (Heywood, 2018), and the emission trends for both gas species are expected to relate. It can be seen from the graph that BM100 attained the highest NO emission compared to all other fuels tested at a speed of 2000 rpm. The possible reason for the highest emission might be due to the availability of oxygen content through chemical structure and high cetane number, which cause long ignition delays in the premixed combustion stage leading to short time air-fuel mixture (Krishnamoorthi and Malayalamurthi, 2017). At the maximum speed of 2500 rpm, the fuel sample of BME5, BME10, and BM15 attained the lowest NO emissions compared to all other fuels tested. This might be possibly due to the cooling effect of ethanol blend associated with its lower heating value and higher latent heat of evaporation leading to the decrease of combustion temperature and hence reducing the NO emissions (Nanthagopal et al., 2019). This acknowledges alternative results noticed in the literature of biodiesel-ethanol blends and biodiesel-methanol blends (Venkata Subbaiah and Raja Gopal, 2011, Yilmaz and Sanchez, 2012). Datta and Mandal (2017) also reported similar kind of results for NO_x emission of the diesel engine powered by biodiesel-ethanol and biodiesel-methanol blending. The burning temperature of ethanol is lower compared to biodiesel and diesel fuel due to being partially oxidized (Arul Mozhi Selvan et al., 2009). At the same operating conditions, the NO emissions of D100, WVB100, SB100, BM100, BME5, BME10, and BME15 were 22.4 ppm, 7.4 ppm, 12.1 ppm, 17.1 ppm, 6.6 ppm, 6 ppm, 6 ppm, and 5.4 ppm, respectively. Compared to D100, the fuel sample of WVB100, SB100, BM100, BME5, BME10, and BME15 emissions decreased by 67%, 46%, 23.7%, 70.5%, 73.2% and 75.9% at the maximum speed of 2500 rpm.

CO_2 Emissions

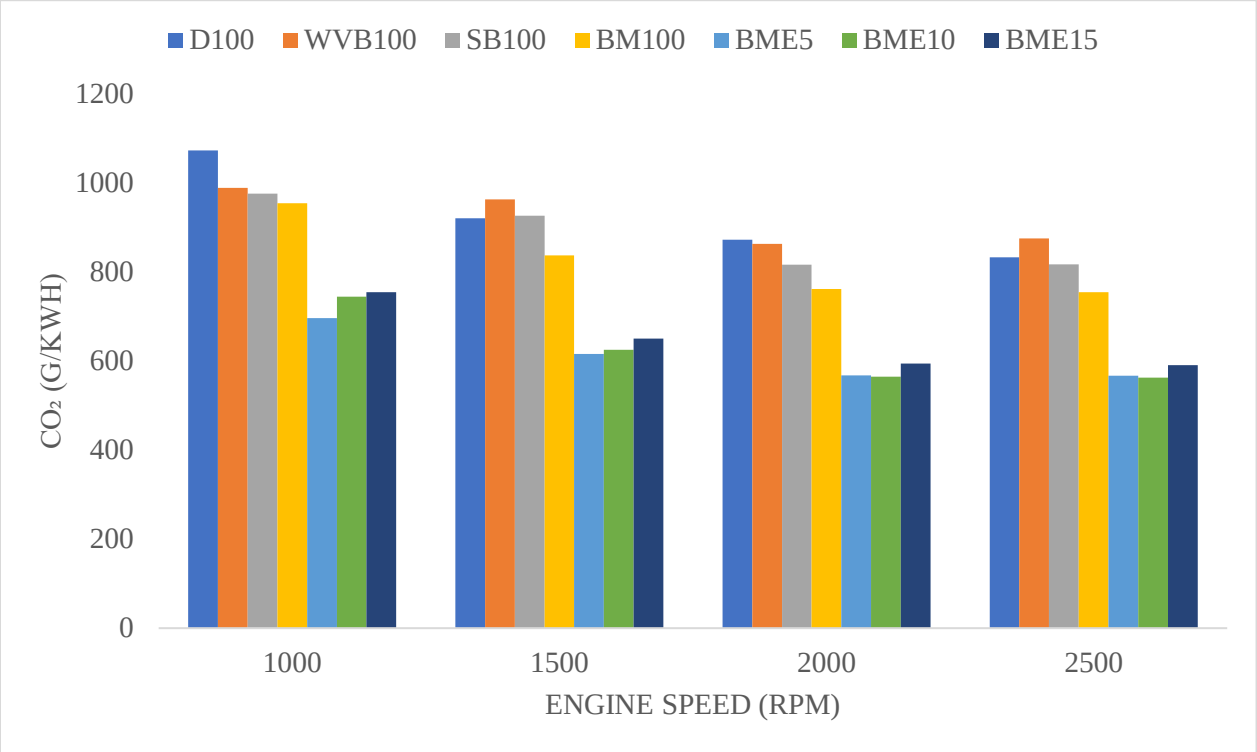

Figure 4.11: Variation of CO_2 emissions with engine speed

One of the significant indicators of knowing the entire combustion procedure within the cylinder is the availability of CO_2 emission. This gas emission was not meant to produce air pollution, but it was one of the major greenhouse gases (Pulkrabek, 2004). Figure 4.11 shows the variation of CO_2 emissions of D100, WVB100, SB100, BM100, BME5, BME10, and BME15 fuels, respectively. At the maximum speed of 2500 rpm, WVB100 attained the highest value of CO_2 emissions compared to other tested fuels. The highest value of WVB100 might be due to the inbuilt extra oxygen atoms in the chemical formation that lead to reaction of unburning carbon atoms through the combustion process. The addition of ethanol to hybrid biodiesel decreased the emissions compared to WVB100, SB100, and BM100 at the maximum speed. A possible reason for this decrease was the high oxygen content of ethanol. These results are also in agreement with those obtained by Alptekin et al. (2015) who indicated that the CO_2 emission of standard diesel-bioethanol-biodiesel fuels decreased compared to standard diesel. The CO_2 emissions of D100, WVB100, SB100, BM100, BME5, BME10, and BME15 were 832.7 g/kWh, 875.74 g/kWh, 816.90 g/kWh, 754.3 g/kWh, 567.3 g/kWh, 562.5 g/kWh, and 590.7 g/kWh at the maximum speed

of 2500 rpm. Compared to D100, it was found that the CO_2 of SB100, BM100, BME5, BME10, and BME15 decreased by 1.9%, 9.4%, 31.9%, 32.4%, and 29.1% while WVB100 increased by 5.2% at the maximum speed of 2500 rpm. This reduction was caused by the high oxygen content of ethanol added to the biodiesel mixture, which improves complete combustion. Another reason for this decrease is probably the improvement in the brake thermal efficiency. Zhu et al. (2011a) also reported similar outcomes using waste vegetable oil biodiesel and methanol blend as fuel for their test studies.

Bosch Smoke Emissions

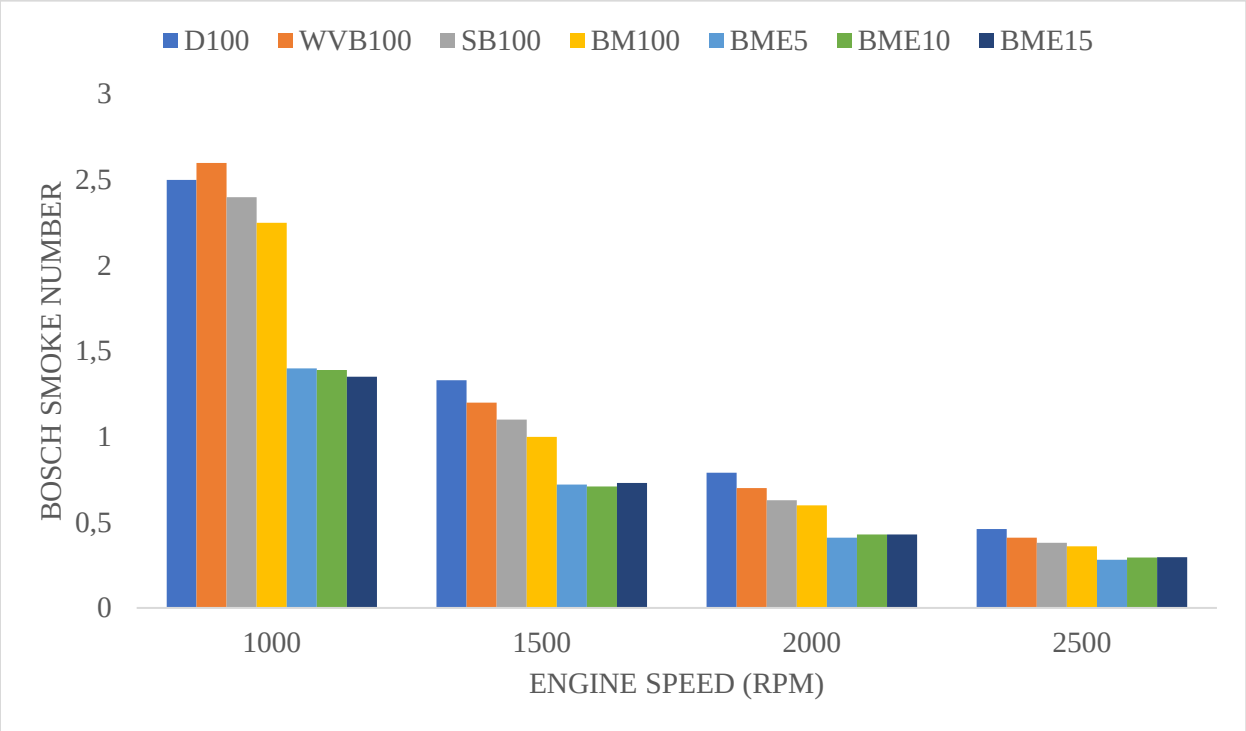

Figure 4.12: Variation of Bosch smoke number emission with engine speed.

The Bosch smoke number is a sign of dry soot emitted by the diesel engine, which is the core influence behind the PM formation. The variations of Bosch smoke number emission with respect to the engine speed of D100, WVB100, SB100, BM100, BME5, BME10, and BME15 fuels has been indicated in Figure 4.12. It can be noted from the graph that the smoke emission decreased with an increase in engine speed. The results show that D100 attained higher smoke emissions compared to WVB100, SB100, BM100, BME5, BME10, and BME15 at almost all engine speeds. This increase might be due to the high quantity of oxygen molecules present in the chemical

structure, which could assist in complete combustion inside the cylinder. It can be observed that BME5, BME10, and BME15 attained the lowest smoke emissions compared to all other fuels tested. The possible decrease of hybrid biodiesel-ethanol blends might be due to higher latent heat of evaporation and low cetane of ethanol. The addition of ethanol might increase the oxygen content and decrease the viscosity and density of the blended fuel, favouring complete and cleaner combustion (Kandasamy et al., 2019). Zheng et al. (2016) obtained similar results by comparing standard diesel, biodiesel, butanol, and ethanol blends at various load conditions. At the same operating condition of 2500 rpm, the Bosch smoke number of D100, WVB100, BM100, BME5, BME10, and BME15 were 0.46%, 0.41%, 0.38%, 0.36%, 0.281%, 0.295%, and 0.296%, respectively. The smoke emissions of WVB100, SB100, BM100, BME5, BME10, and BME15 decreased by 10.9%, 17.4%, 21.7%, 38.9%, 35.9% and 35.7% compared to D100 at the maximum speed of 2500 rpm. Ashok et al. (2019) reported similar kind of results and concluded that the smoke emission from fuel samples of diesel-biodiesel-high alcohol blends decrease compared to diesel and biodiesel due to the high oxygen content of alcohol.

4.2 Prediction of performance, combustion, and emission characteristics

This section presents and discusses the numerical modelling of combustion, performance, and exhaust gas emissions of the diesel engine powered by diesel (D100), waste vegetable biodiesel (WVB100), soybean biodiesel (SB100), biodiesel mixture from waste vegetable oil, and soybean oil (BM100) and biodiesel mixture-ethanol fuel blends (BME5, BME10, and BME15). The combustion parameters such as ICP, HRR, ICT, ignition delay, spray tip penetration, the start of combustion, combustion duration, and frictional mean effective pressure has been computed using Diesel-RK software as the simulation tool. Performance parameters such as BP, BSFC, BT, BTE, BMEP, and emission characteristics such as CO_2, PM, NO_x, and Bosch smoke number have also been evaluated using the same software (Diesel-RK).

4.2.1 Combustion Parameters

The analysis of cylinder pressure was considered the main parameter of engine combustion since its pressure could directly affect the engine parameters (Bora et al., 2014). The combustion

parameters such as ICP, HRR, ICT, ID, STP, SOC, CD, and FMEP were used to assess the D100, WVB100, SB100, BM100, BME5, BME10, and BME15 at full load conditions. The numerical results of combustion parameters for tested fuel samples were discussed and compared with standard diesel as a reference fuel.

In-Cylinder Pressure

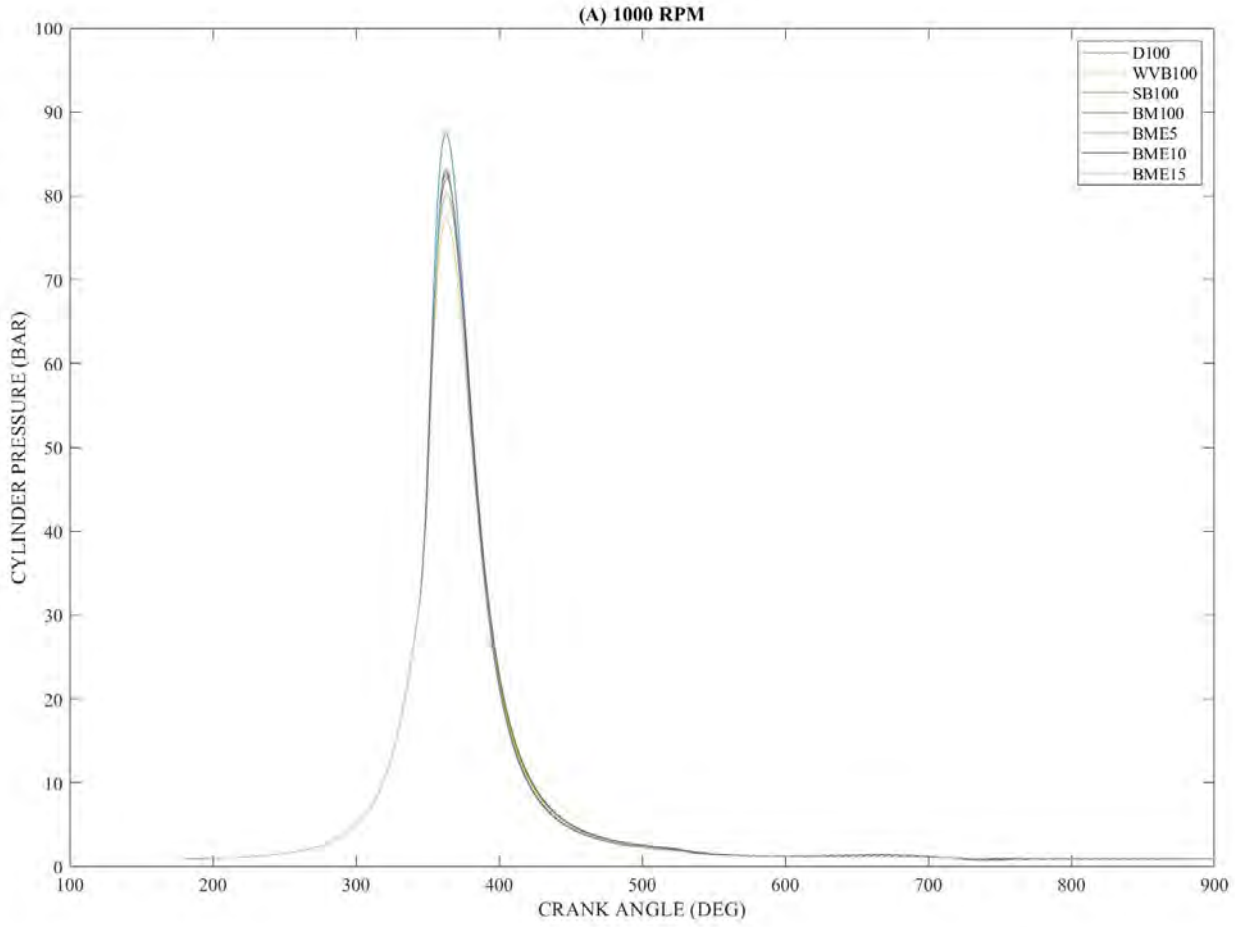

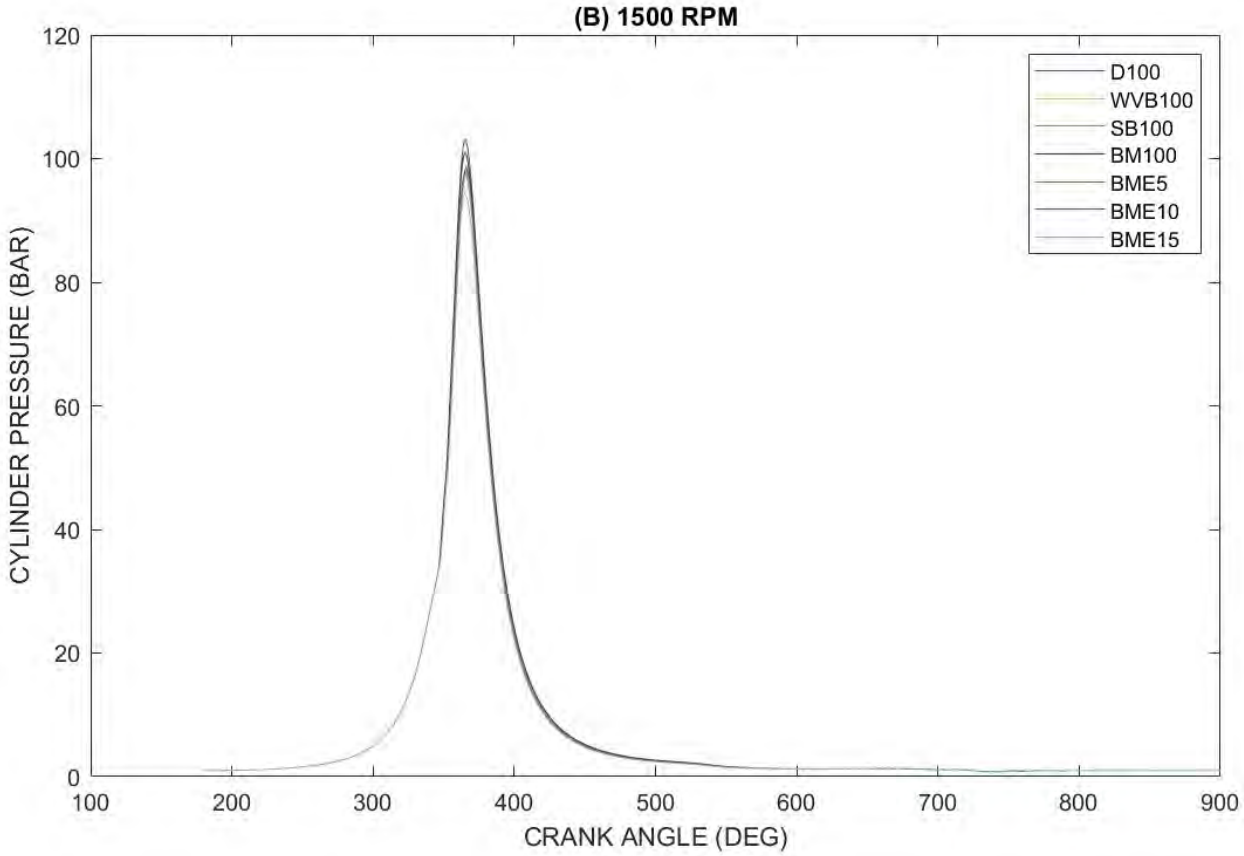
(B) 1500 RPM
D100
WVB100
SB100
BM100
BME5
BME10
BME15
CYLINDER PRESSURE (BAR)
CRANK ANGLE (DEG)
0
20
40
60
80
100
120
100
200
300
400
500
600
700
800
900

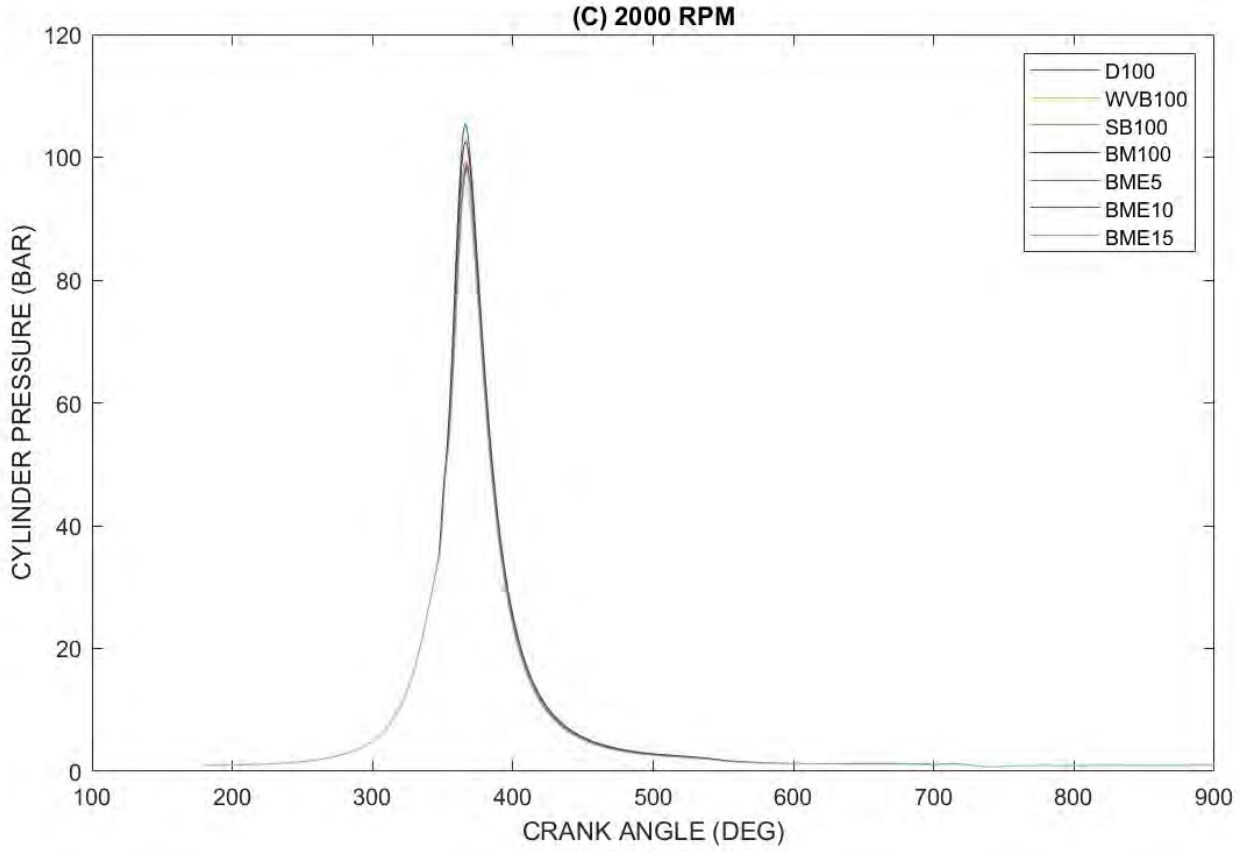
(C) 2000 RPM
CYLINDER PRESSURE (BAR)
CRANK ANGLE (DEG)
D100
WVB100
SB100
BM100
BME5
BME10
BME15
0
20
40
60
80
100
120
100
200
300
400
500
600
700
800
900

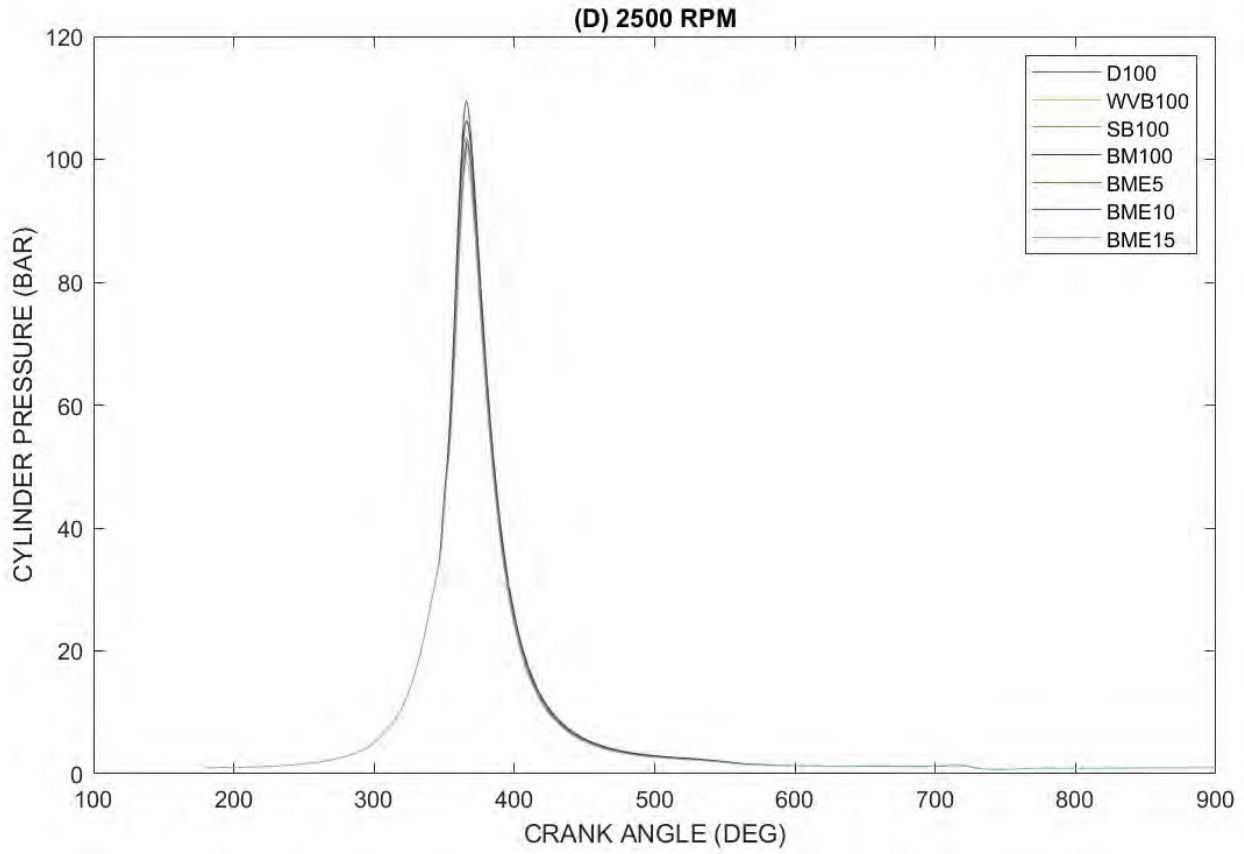

Figure 4.13: Variation of in-cylinder pressure with the crank angle of simulated data

The in-cylinder pressure relies on fuel burning through the premix burning phase to ensure better combustion and heat release (Al-Dawody and Bhatti, 2013). The position of the in-cylinder peak pressure indicates the speed to release the energy. The in-cylinder pressure was predicted using the Runge-Kuta method in equation (3.17). Figure 4.13 shows the variation of in-cylinder pressure for D100, WVB100, SB100, BM100, BME5, BME10, and BME15 at different crank angles using the Diesel-RK computer simulation model. In general, blended fuels lead to higher maximum ICP compared to biodiesel and diesel fuels. This maximum value was due to alcohol oxygen content, which promotes the combustion process. But the maximum in-cylinder pressure differs very little with increasing ethanol concentration due to blended fuels, which lead to better-premixed combustion. The predicted results attained from Diesel-RK software show that at the minimum speed of 1000 rpm, the fuel samples of D100 attained the highest in-cylinder pressure of 87.54 bar at 363º aTDC whereas WVB100, SB100, BM100, BME5, BME10, and BME15 attained the values of 77.04 bar at 363º aTDC, 80.27 bar at 364º aTDC, 82.06 bar at 364º aTDC, 82.69 bar at 363º

aTDC, 82.93 bar at 363º aTDC, and 83.39 bar at 363º aTDC. At the maximum speed of 2500 rpm and 366º aTDC, the maximum in-cylinder pressure of D100, WVB100, SB100, BM100, BME5, BME10, and BME15 were 109.5 bar, 99.72 bar, 103.59 bar, 106.32 bar, 103.01 bar, 102. 35 bar, and 101.52 bar, respectively. Compared to D100, the in-cylinder pressure of WVB100, SB100, BM100, BME5, BME10, and BME15 decreased by 8.9%, 5.4%, 2.9%, 5.9%, 6.5%, and 7.3%, respectively at the maximum speed of 2500 rpm.

The decrease of in-cylinder pressure might be due to combustion inhibited by the higher latent heat of vaporization; the lower cetane number postponed the starting point of combustion for the blended fuels. Besides, the combustion process for the diesel engine was divided into the premixed combustion mode and the diffused combustion mode. Swarna et al. (2022) experimentally used heptanol blended ternary fuel samples and attained higher in-cylinder pressure and temperature, where short ignition delay periods improved the premixed combustion compared to ethanol blends of ternary fuel and biodiesel blends' samples. In addition, all in-cylinder pressure figures were approximately comparable in profile.

Heat Release Rate

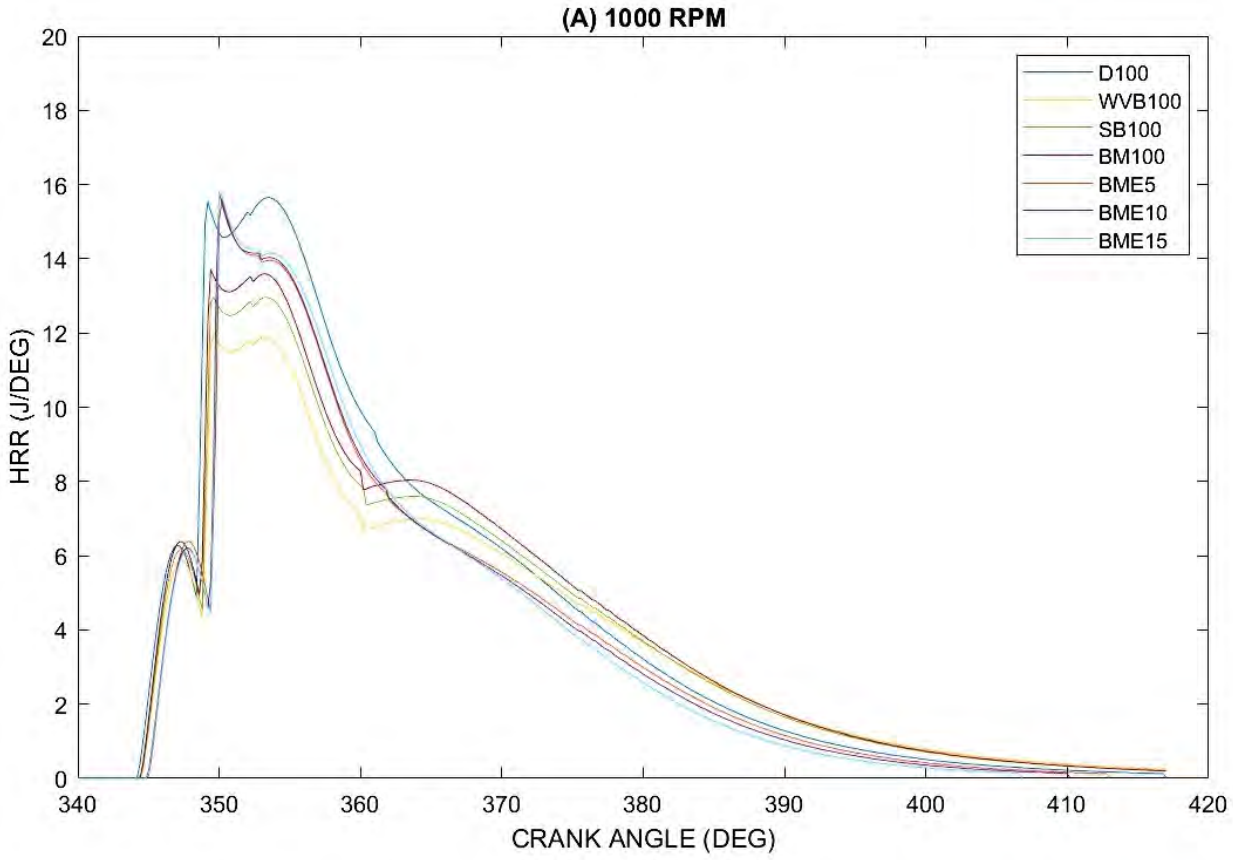

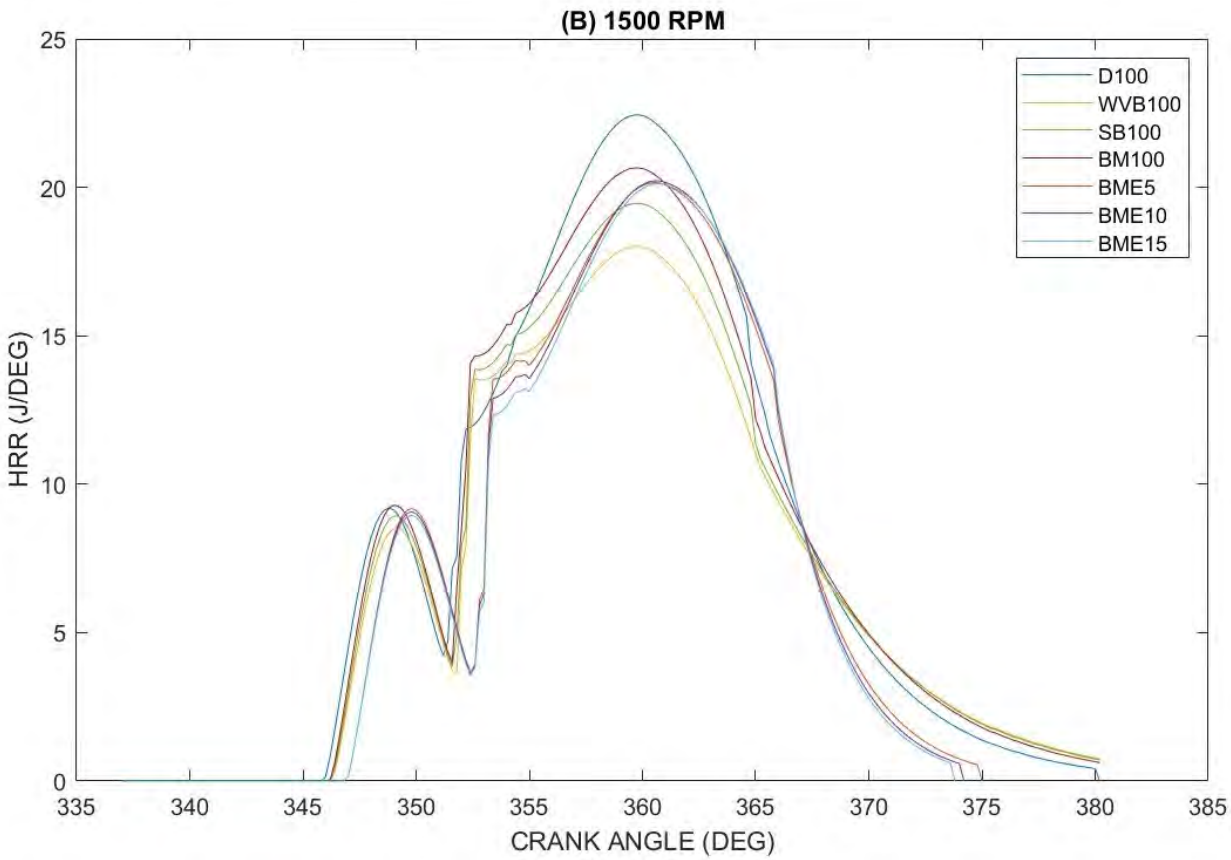
(B) 1500 RPM
D100
WVB100
SB100
BM100
BME5
BME10
BME15
HRR (J/DEG)
CRANK ANGLE (DEG)
0
5
10
15
20
25
335
340
345
350
355
360
365
370
375
380
385

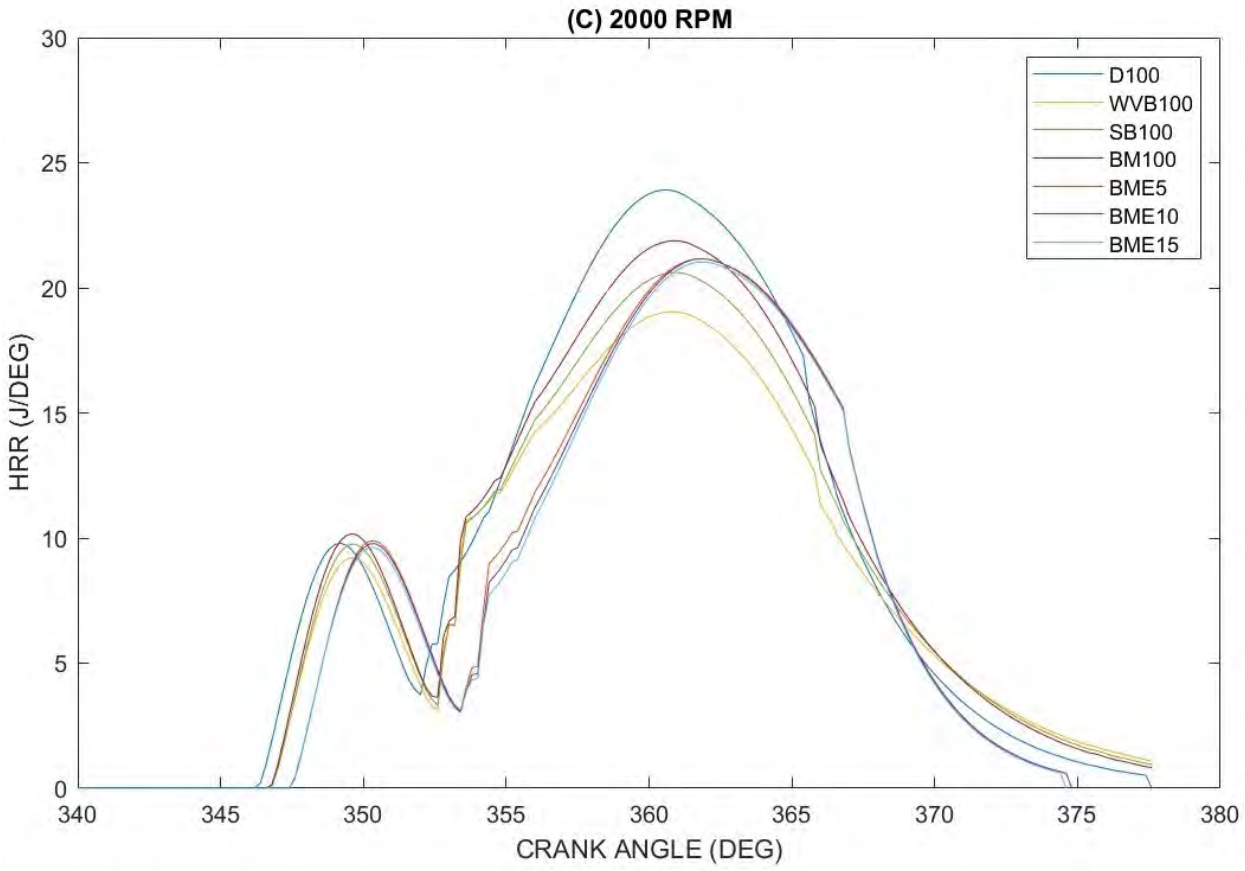
(C) 2000 RPM
HRR (J/DEG)
CRANK ANGLE (DEG)
D100
WVB100
SB100
BM100
BME5
BME10
BME15
0
5
10
15
20
25
30
340
345
350
355
360
365
370
375
380

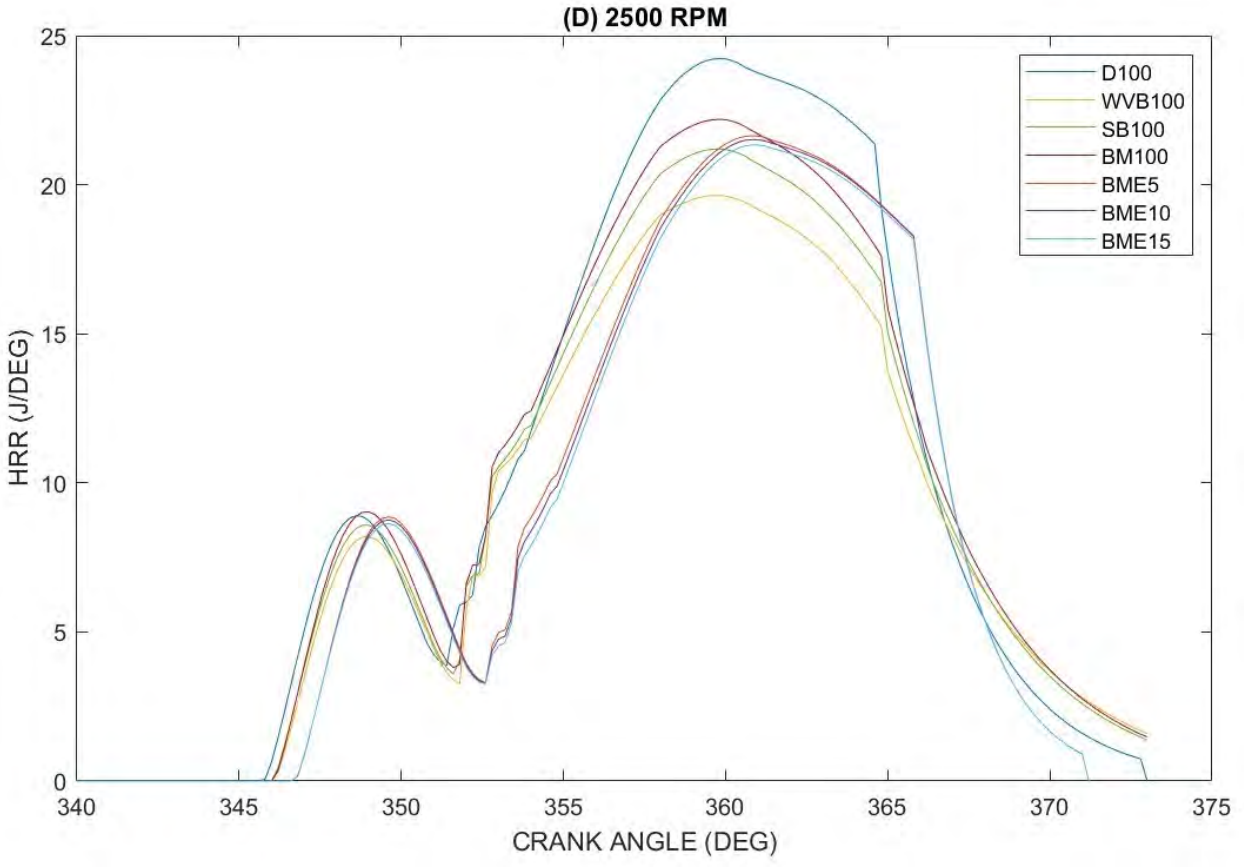

Figure 4.14: Variation of heat release rate with the crank angle of simulated data

The heat release rate helps to identify the point where combustion starts, the amount of fuel burned in the premixed mode, and variances in the fuel-burning rates. Figure 4.14 shows the variation of heat release rate for D100, WVB100, SB100, BM100, BME5, BME10, and BME15 at different crank angles using the DRK computer simulation model. The heat release rate was numerically simulated using a multi-zone combustion model in equation (3.24). The results show that BME10 and BME15 attained the maximum HRR compared to WVB100, SB100, BM100, and BME5 at the minimum speed of 1000 rpm. The higher latent heat of vaporization, auto-ignition temperature, and low cetane number of ethanol delayed the initiation of combustion and produced more fuel and air mixtures during ignition delay and promoted the premixed combustion process. These eventually lead to an increase in hybrid biodiesel-ethanol blends for premixed combustion (Xiao et al., 2020). The HRR fuel samples of D100, WVB100, SB100, BM100, BME5, BME10, and BME15 were found at 24.23 J/degree, 19.64 J/degree, 21.2 J/degree, 22.19 J/degree, 21.64 J/degree, 21.51 J/degree, and 21.33 J/degree, respectively. Compared to D100 at the maximum

speed of 2500 rpm, the HRR of WVB100, SB100, BM100, BME5, BME10, and BME15 decreased by 18.9%, 12.5%, 8.4%, 10.7%, 11.2%, and 12.0%, respectively. The possible reason for this decrease of individual biodiesels, and biodiesel mixture-ethanol blends might be due to low cetane number and low calorific value. Alcohol blends lead to a longer ignition delay compared to WVB100, SB100, and BM100 (Zhu et al., 2010a, Zhu et al., 2011a). Individual biodiesels (WVB100 and SB100) attained the lowest HRR at the maximum speed compared to BM100, BME5, BME10, and BME15. These decreases might be possible due to higher viscosity, density, and high cetane number.

The individual biodiesels properties directly affected the combustion procedure. The higher density and viscosity led to better atomization characteristics inside the cylinder. At all engine speeds, hybrid biodiesel-ethanol blends attained higher HRR compared to individual biodiesels. The increase of hybrid biodiesel-ethanol blends might be due to higher oxygen content, low viscosity, and lower cetane number. The low cetane number leads to long ignition delay, and the larger amount of fuel accumulation during the premixed phase combustion (Yilmaz and Sanchez, 2012). It can be noted that the oxygen molecules in the combustion chamber led to an improved combustion efficiency resulting in better performance characteristics (Yesilyurt et al., 2020).

Cylinder Temperature

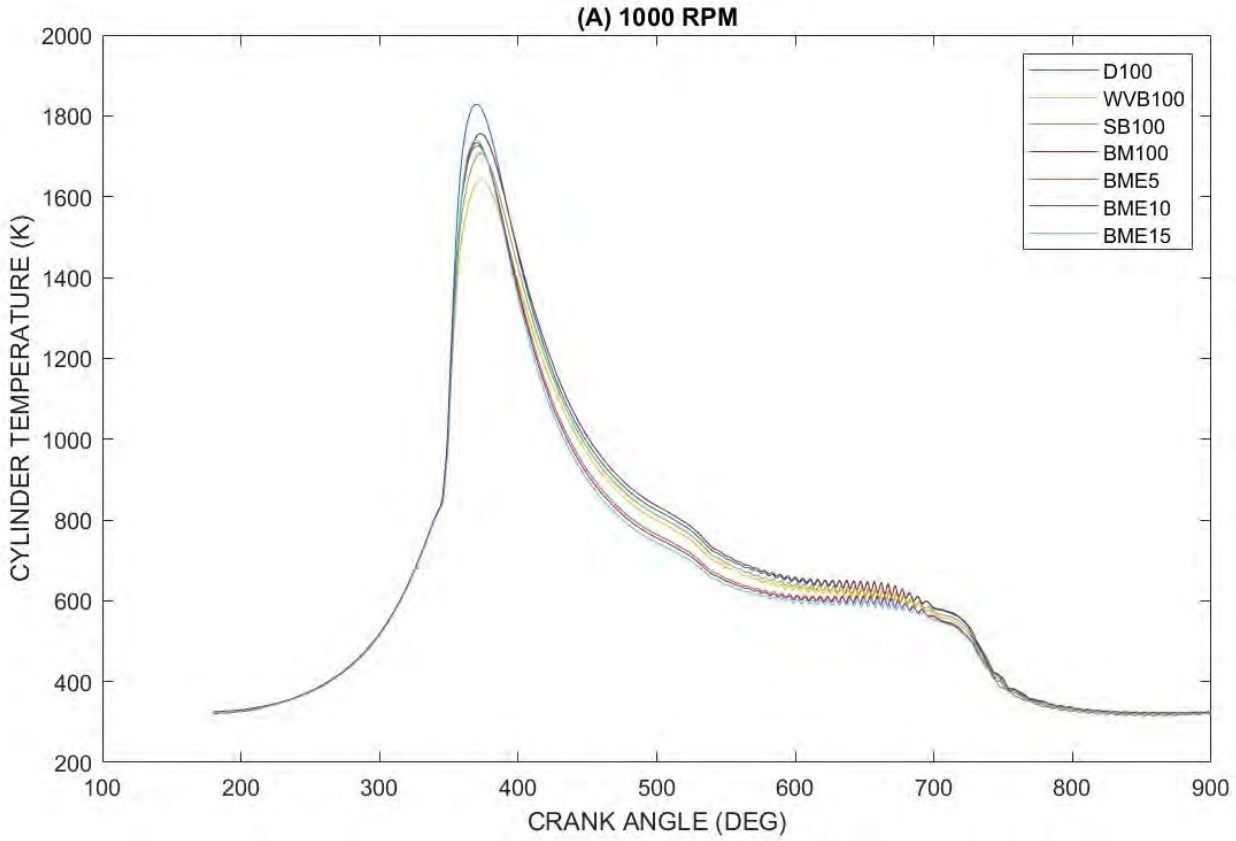

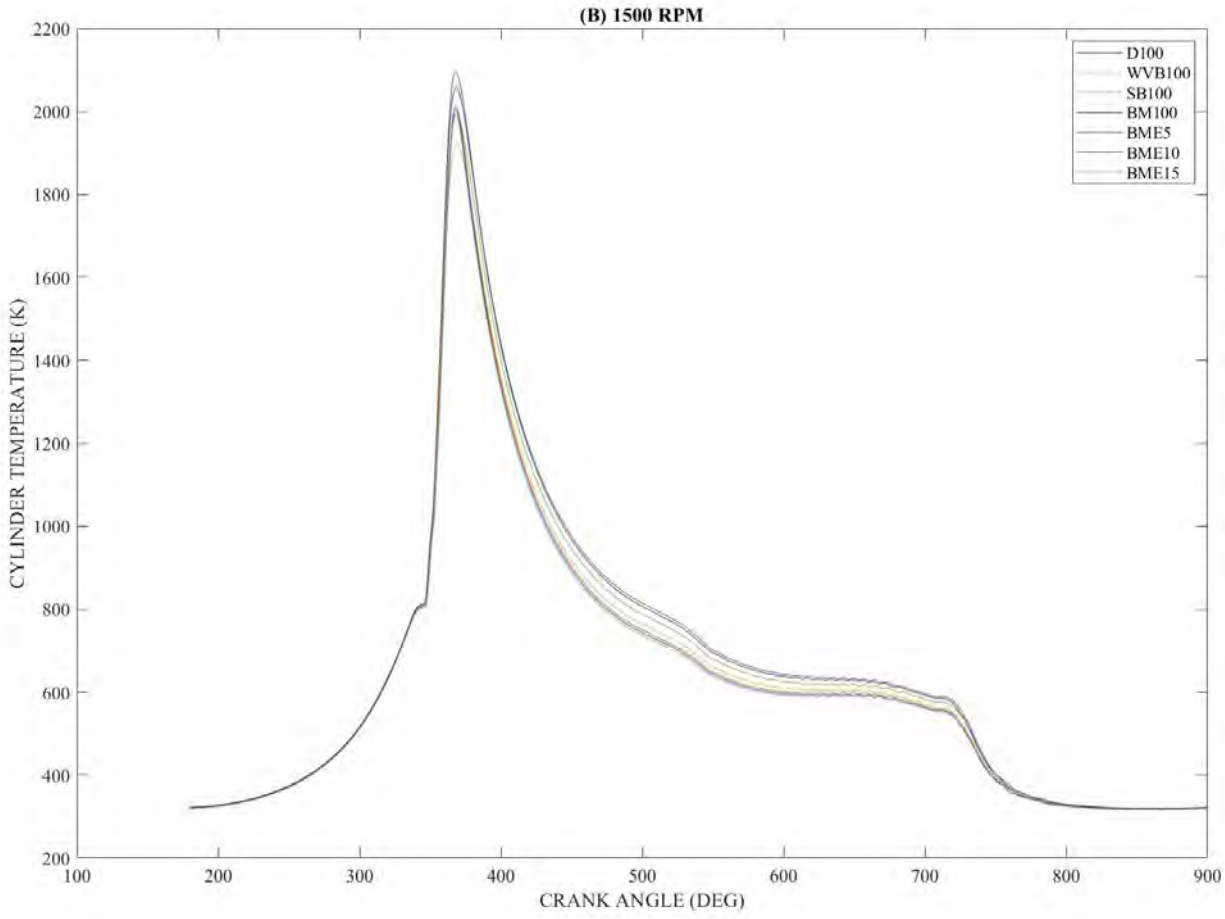
(B) 1500 RPM
D100
WVB100
SB100
BM100
BME5
BME10
BME15
CYLINDER TEMPERATURE (K)
CRANK ANGLE (DEG)
2200
2000
1800
1600
1400
1200
1000
800
600
400
200
100
200
300
400
500
600
700
800
900

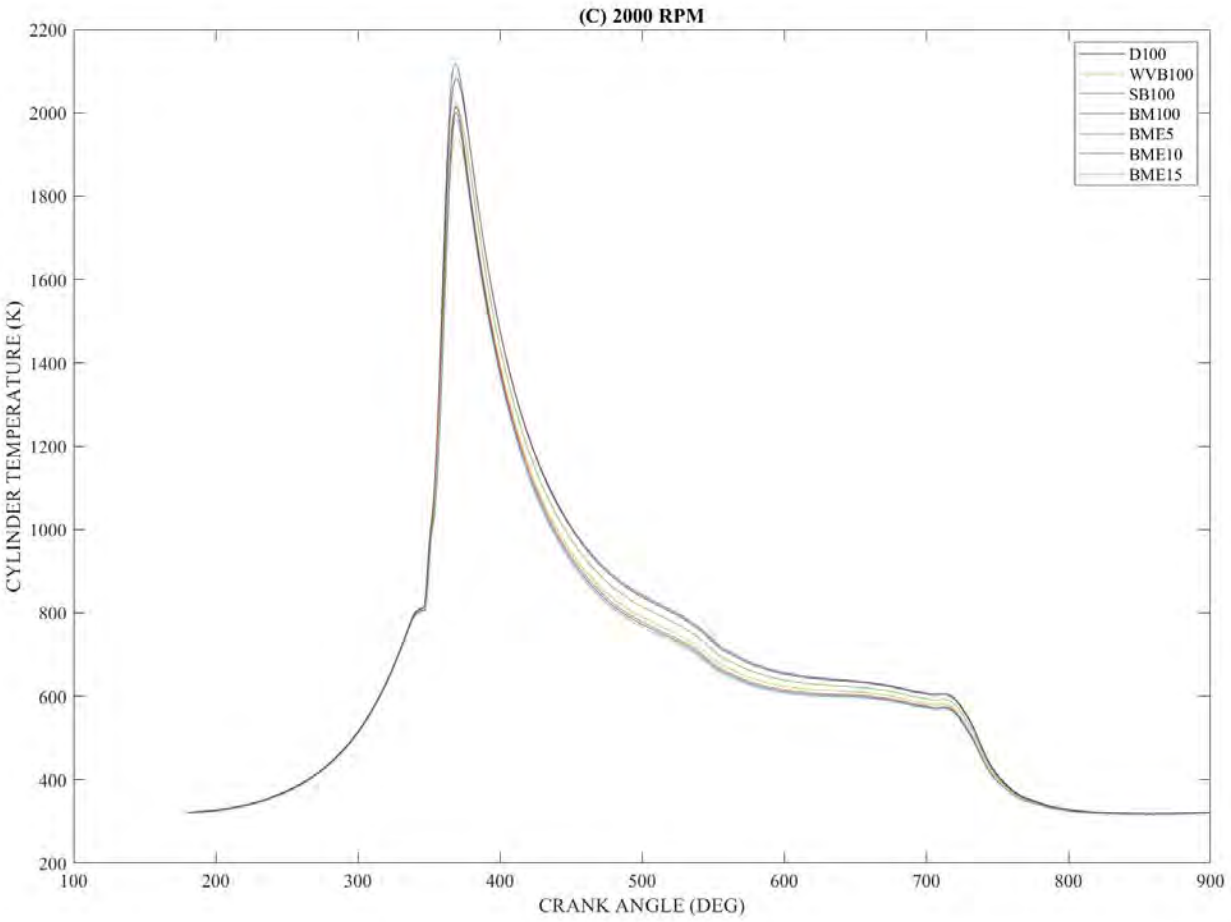
(C) 2000 RPM
D100
WVB100
SB100
BM100
BME5
BME10
BME15
CYLINDER TEMPERATURE (K)
CRANK ANGLE (DEG)
2200
2000
1800
1600
1400
1200
1000
800
600
400
200
100
200
300
400
500
600
700
800
900

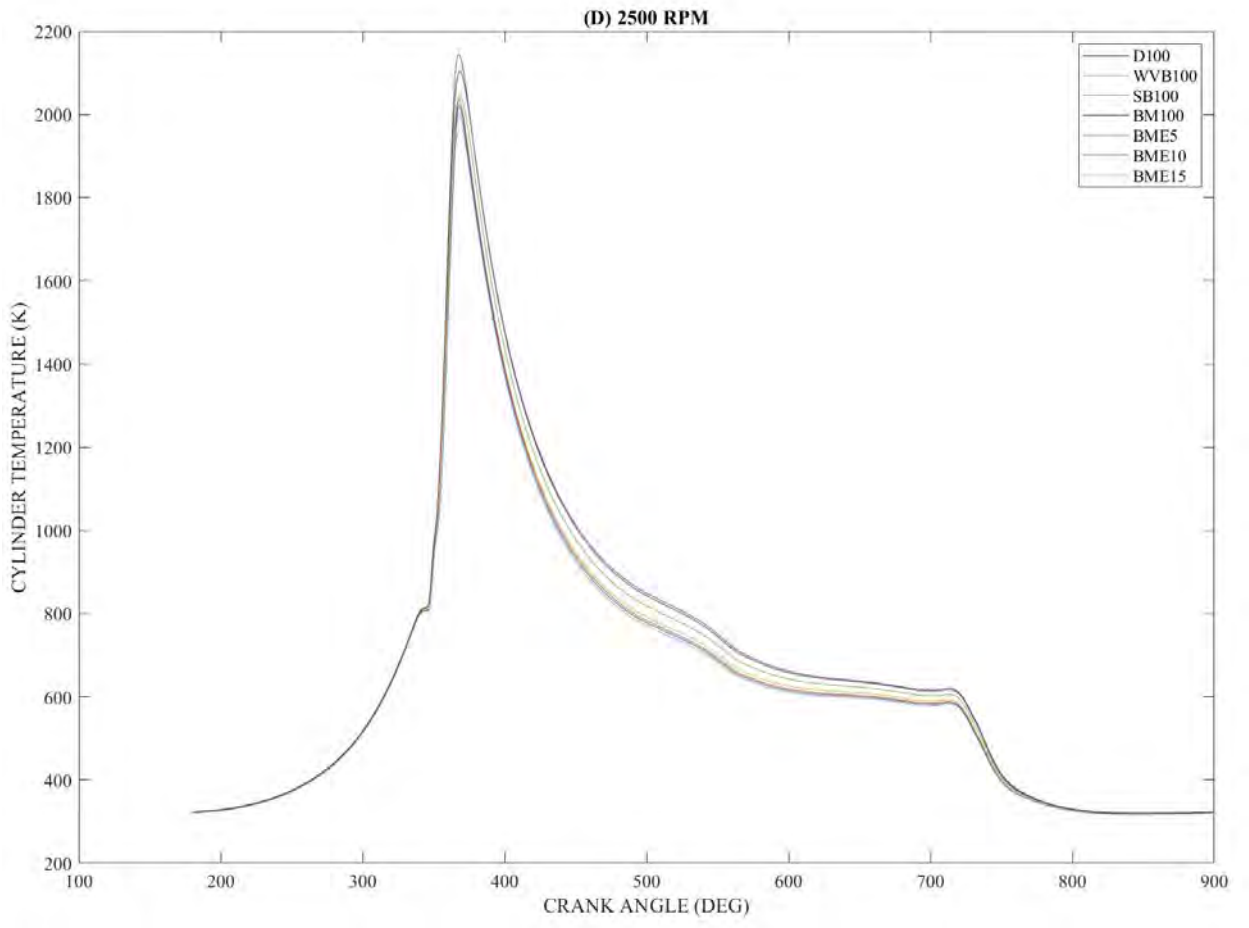

Figure 4.15: Variation of in-cylinder temperature with the crank angle of simulated data

The in-cylinder temperature of the engine has a great impact on the emission and knocking. High NO_x emission has been attributed to the maximum temperature in the combustion cylinder chamber (Al-Dawody and Bhatti, 2013). The variation of in-cylinder temperature with crank angles of D100, WVB100, SB100, BM100, BME5, BME10, and BME15 under full load is presented in Figure 4.15. The in-cylinder temperature was simulated using equation (3.18). The results show that D100 attained the maximum ICT at all engine speeds compared to WVB100, SB100, BM100, BME5, BME10, and BME15. This maximum in-cylinder temperature of D100 might be due to improved fuel atomization and lower viscosity (Karabektas et al., 2014). These results are in agreement with Krishnamoorthi et al., (2018) who discovered that the in-cylinder temperature of neat diesel was higher compared to diesel-biodiesel-diethyl ether blends at different compression ratios. The maximum in-cylinder temperature and at a maximum speed for D100 lead to an improvement of the combustion process (Rajak et al., 2021). At the maximum speed of 2500

rpm and 368^0 aTDC, the maximum in-cylinder temperature of D100, SB100, BM100, BME5, BME10, and BME15 was 2144.4 K, 2043.4 K, 2102.8 K, 2035.8 K, 2021.7 K, and 2003.7 K, while at 369^0 aTDC the maximum in-cylinder temperature of WVB100 was 1968 K, respectively. The in-cylinder temperature of WVB100, SB100, BM100, BME5, BME10, and BME15 decreased by 8.2%, 4.7%, 1.9%, 5.1%, 5.7% and 6.6% compared to D100 at maximum speed of 2500 rpm.

However, the cylinder temperature of BM100 fuel attained the highest cylinder temperature compared to all hybrid biodiesel-ethanol blends. These decrease of ethanol blends might be attributed to low cylinder temperature, higher latent heat of evaporation, higher specific heat, and lower heat of reaction (Anand et al., 2011).

Ignition Delay

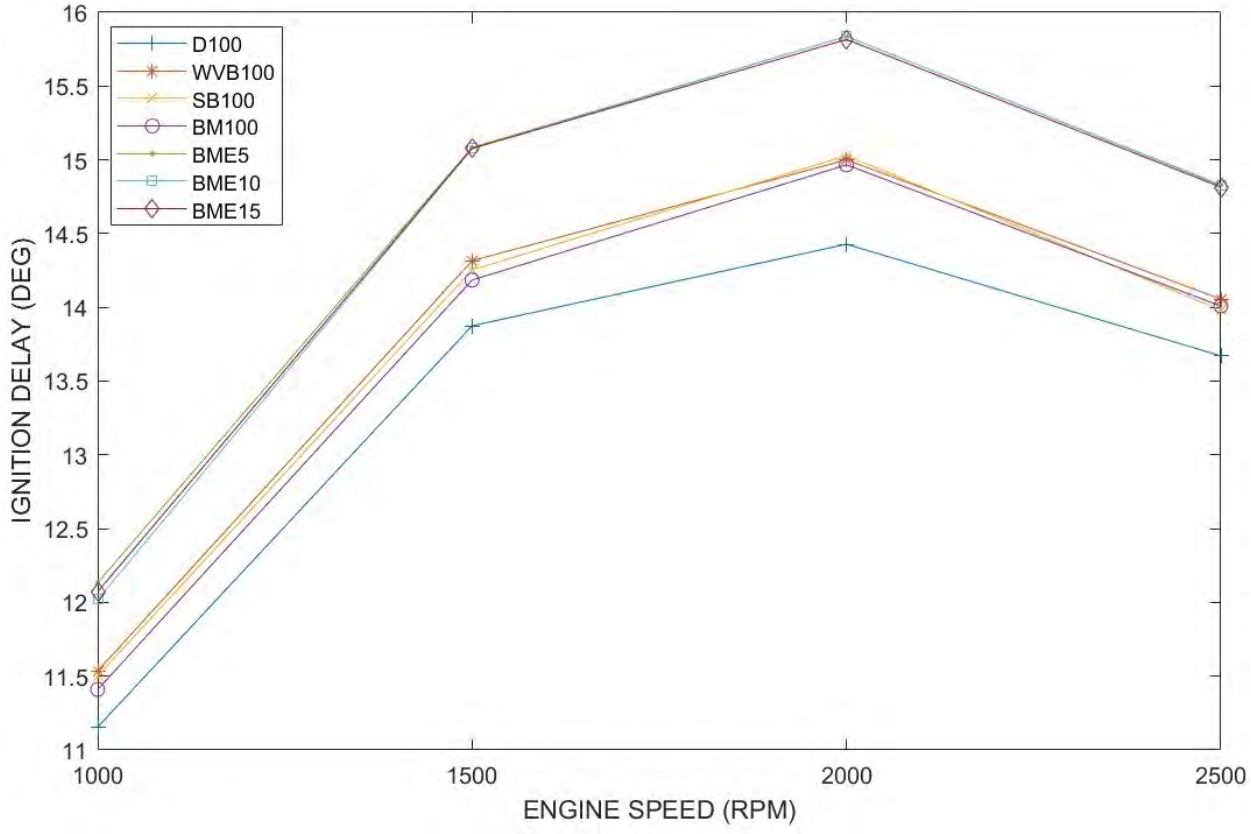

Figure 4.16: Variation of ignition delay period with an engine speed of simulated data

The ignition delay can be described as a qualitative amount of the combustion procedure. Figure 4.16 shows the variation of ignition delay for D100, WVB100, SB100, BM100, BME5, BME10, and BME15 with respect to engine speed. The ignition delay was predicted using Tolstov's equations model for simulation in equation (3.21). The predicted results obtained from Diesel-RK software show that the fuel samples of D100, WVB100, SB100, BM100, BME5, BME10, and BME15 were 13.67º, 14.06º, 13.98º, 14.01º, 14.83º, 14.83º, and 14.82º at the maximum speed of 2500 rpm. It can be seen from the graph that at the same operating conditions, the fuel samples of BME5, BME10, and BME15 attained the long ignition delay compared to WVB100, SB100, and BM100. The reason for the long ignition delay for hybrid biodiesel-ethanol blends might be due to the low cetane number of ethanol, which is far lower than that of diesel and biodiesel (Geng et al., 2021). A previous investigation conducted by Kuszewski (2019) shows that when the percentage of ethanol increased, the derived cetane number of the biodiesel-ethanol blends decreased. In the present study also, the addition of ethanol blends decreased the cetane number for biodiesel mixture-ethanol blends, which led to a long ignition delay period (Zhu et al., 2010a, Anand et al., 2011).

Compared to D100, the ignition delay of WVB100, SB100, BM100, BME5, BME10, and BME15 increased by 2.8%, 2.3%, 2.5%, 8.5%, 8.4%, and 8.4%, respectively. Long ignition delay may lead to a lengthier air-fuel mixing period, and this leads to a higher instantaneous HRR. Studies carried out by Sivalakshmi and Balusamy (2012) have shown that long ignition delays were due to the presence of alcohol in biodiesel-alcohol blends, which affects fuel burn during the premixed combustion phase and improves thermal efficiency. Xiao et al. (2020) compared the ignition delay of neat diesel, biodiesel, and biodiesel-butanol blends, and the results show that alcohol blends attained the long ignition delay periods due to higher latent heat of vaporization and low cetane number of alcohols. Since the higher latent heat of vaporization and low cetane number of alcohols delayed the starting of combustion, the ignition delay of blended fuels was longer.

Spray Tip Penetration

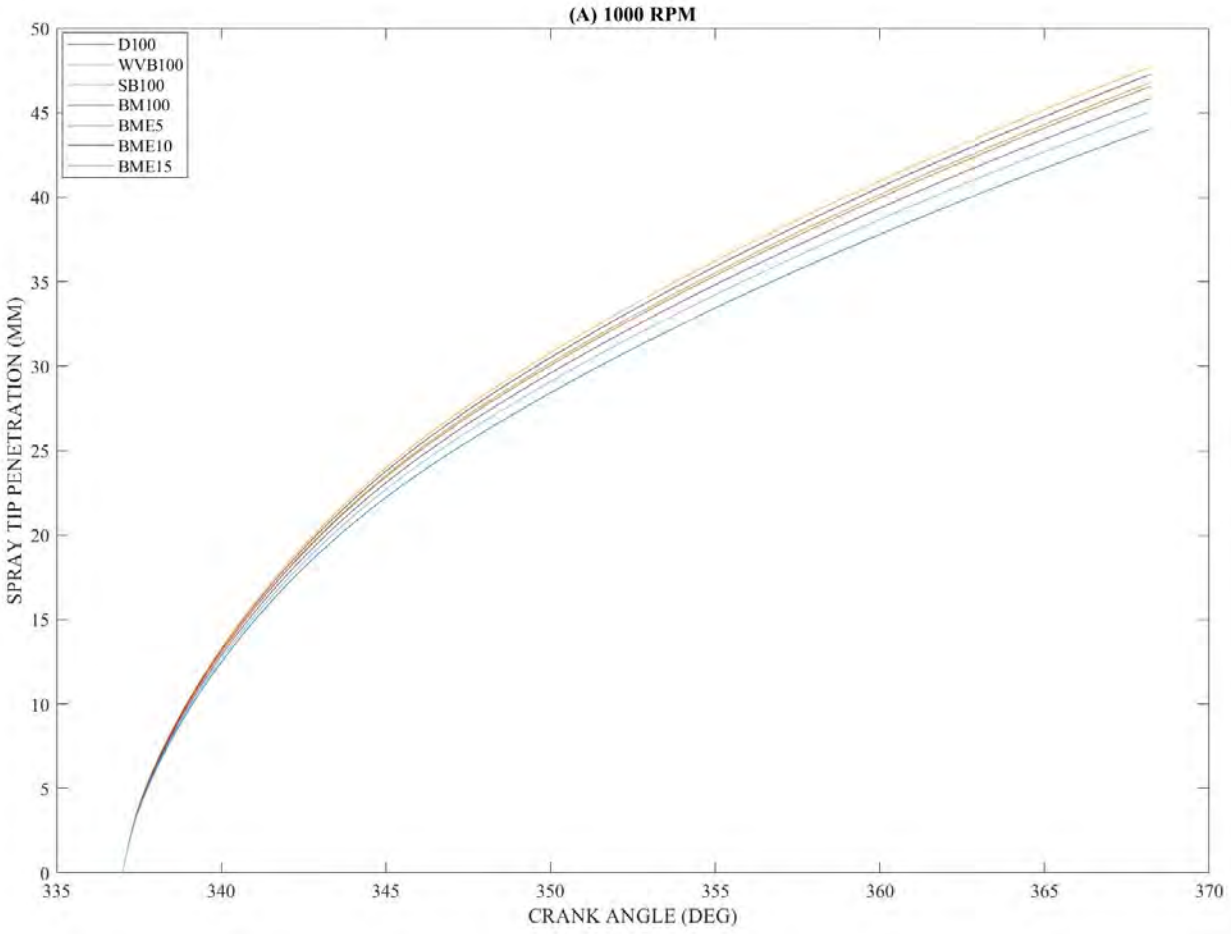

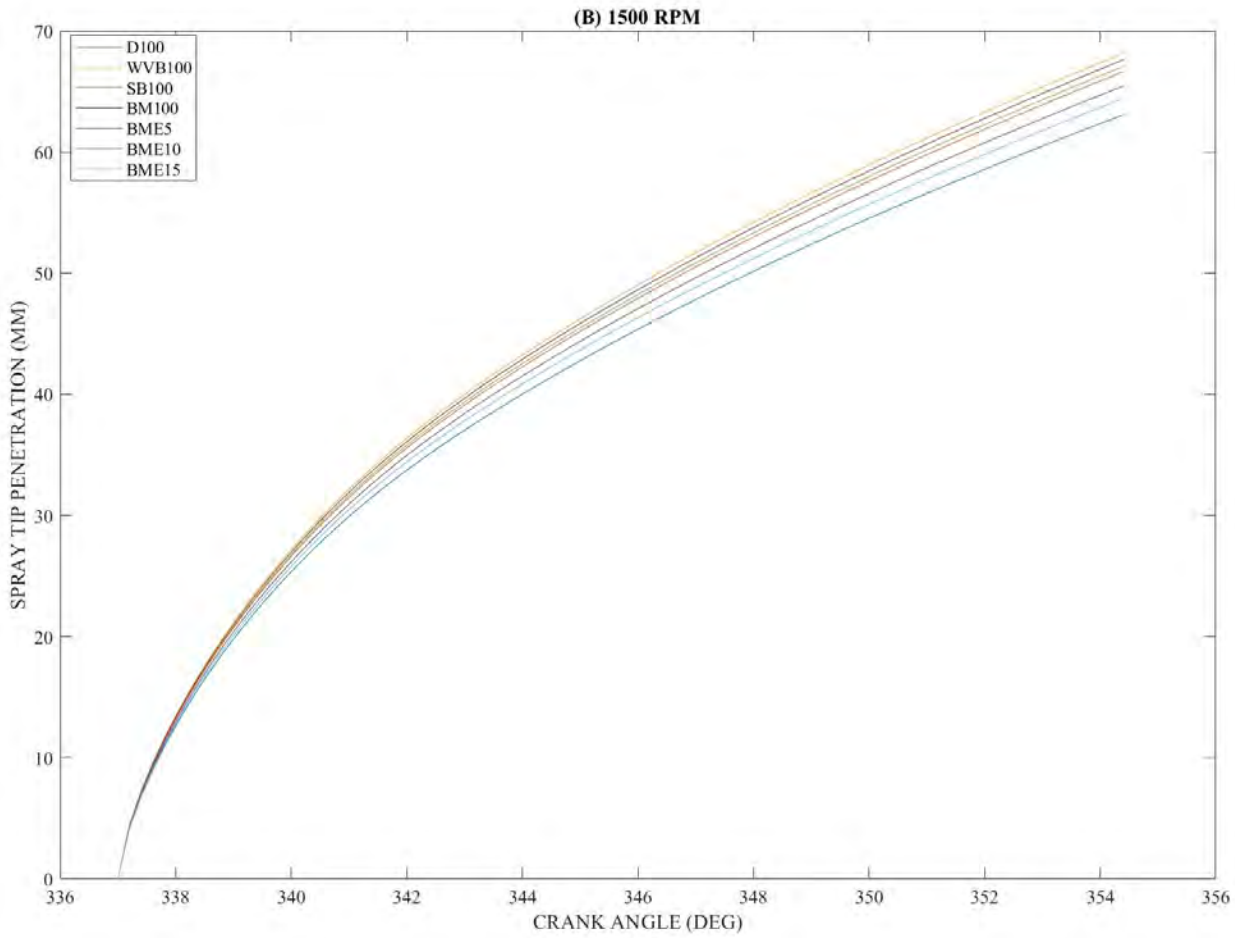
(B) 1500 RPM
D100
WVB100
SB100
BM100
BME5
BME10
BME15
SPRAY TIP PENETRATION (MM)
CRANK ANGLE (DEG)
0
10
20
30
40
50
60
70
336
338
340
342
344
346
348
350
352
354
356

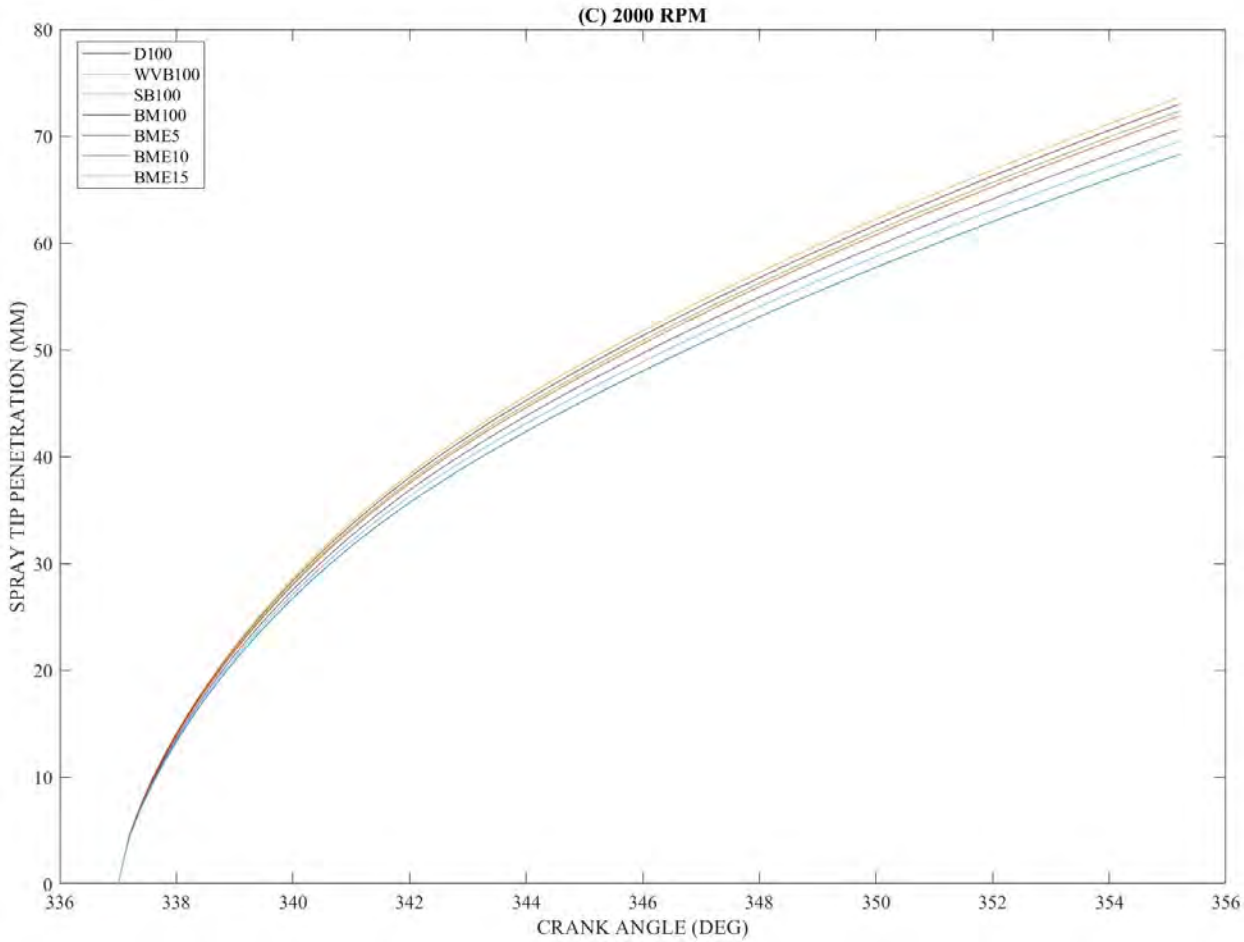
(C) 2000 RPM
D100
WVB100
SB100
BM100
BME5
BME10
BME15
SPRAY TIP PENETRATION (MM)
CRANK ANGLE (DEG)
0
10
20
30
40
50
60
70
80
336
338
340
342
344
346
348
350
352
354
356

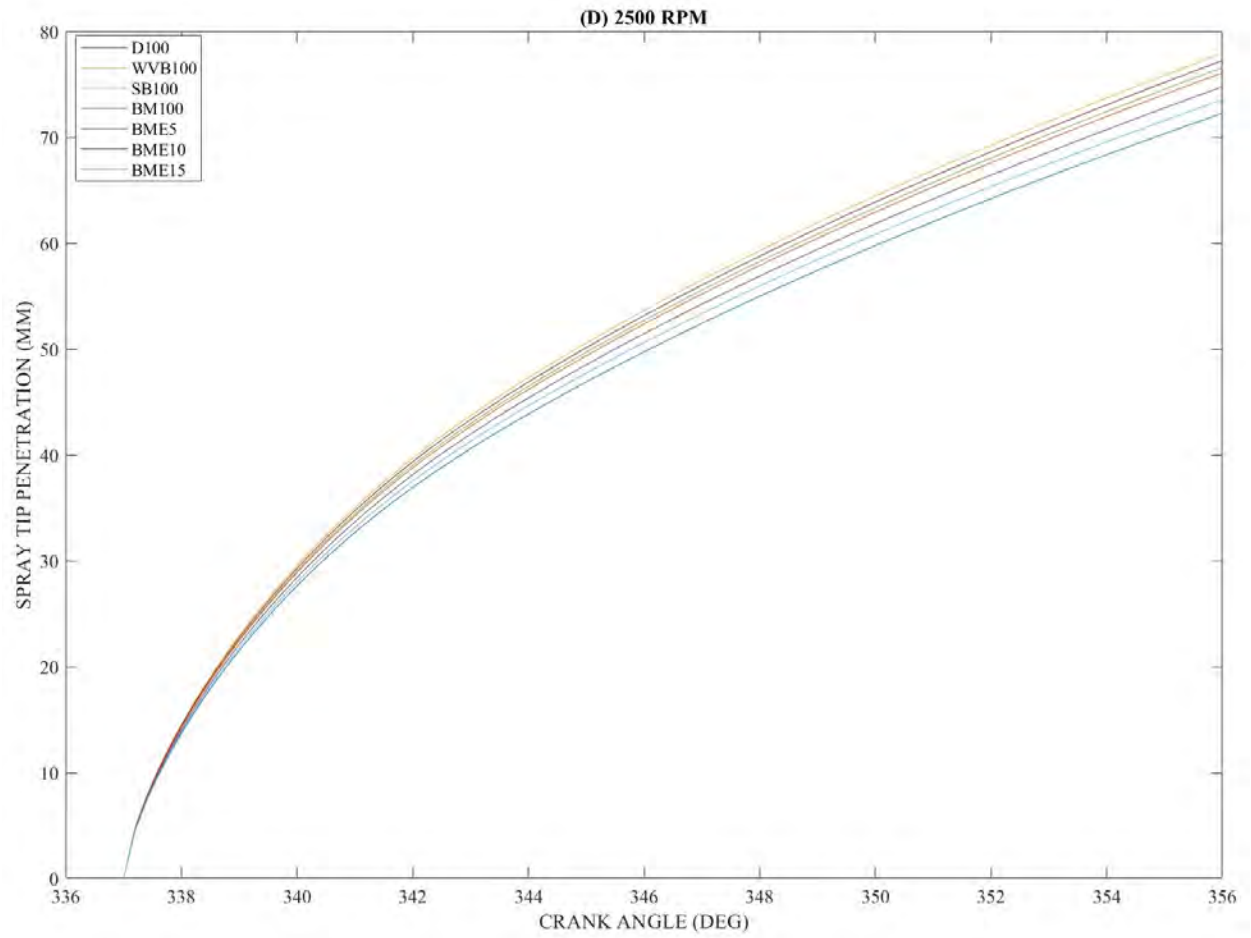

Figure 4.17: Variation of spray tip penetration with the crank angle of simulated data.

The spray tip penetration is defined as the significant parameter used to evaluate air-fuel mixture through the combustion process. The high level of STP may lead to pushing a large volume of fuel into the combustion chamber and increase the possibility of a fuel-rich zone on combustion chamber walls. The spray tip penetration was numerically simulated using equation (3.31). Figure 4.17 shows an increase of STP with an increase of the crank angle of the engine fuelled with D100, WVB100, SB100, BM100, BME5, BME10, and BME15. The results show that the STP of D100, WVB100, SB100, BM100, BME5, BME10, and BME15 were 72.26 mm, 77.92 mm, 76.57 mm, 77.23 mm, 76.08 mm, 74.76 mm, and 73.54 mm, respectively. The STP of individual biodiesels and biodiesel mixture are higher compared to hybrid biodiesel-ethanol blends. The reason for higher STP for biodiesel might be due to higher viscosity and surface tension, which makes biodiesel harder to break up into small droplets compared to other blended fuels (Zhan et al., 2018).

The radial extension of fuel spray from biodiesel is slower due to inferior atomization, the spray front is narrower, and the fuel spray encounters less air resistance, thus, the STP of biodiesel was the longest among diesel, biodiesel-alcohol blends (Geng et al., 2021). The STP of BME15 gradually decreased with an increase of ethanol blends, at which the STP tends towards that of D100 fuel. The increase of ethanol percentage leads to the reduction of viscosity for biodiesel-ethanol blends, the number of finer atomized droplets increased on the periphery of the fuel spray, and the entrainment effect between the atomized droplets and the ambient gas was intensified. Hence, the STP of biodiesel-ethanol blends gradually decreased with the increasing ethanol ratio (Geng et al., 2021). Compared to D100 at the maximum speed of 2500 rpm, the STP of WVB100, SB100, BM100, BME5, BME10, and BME15 increased by 7.8%, 6.0%, 6.9%, 5.3%, 3.5%, and 1.8%. All the STP of other tested fuels attained higher values compared to D100 at maximum engine speeds.

Start of Combustion

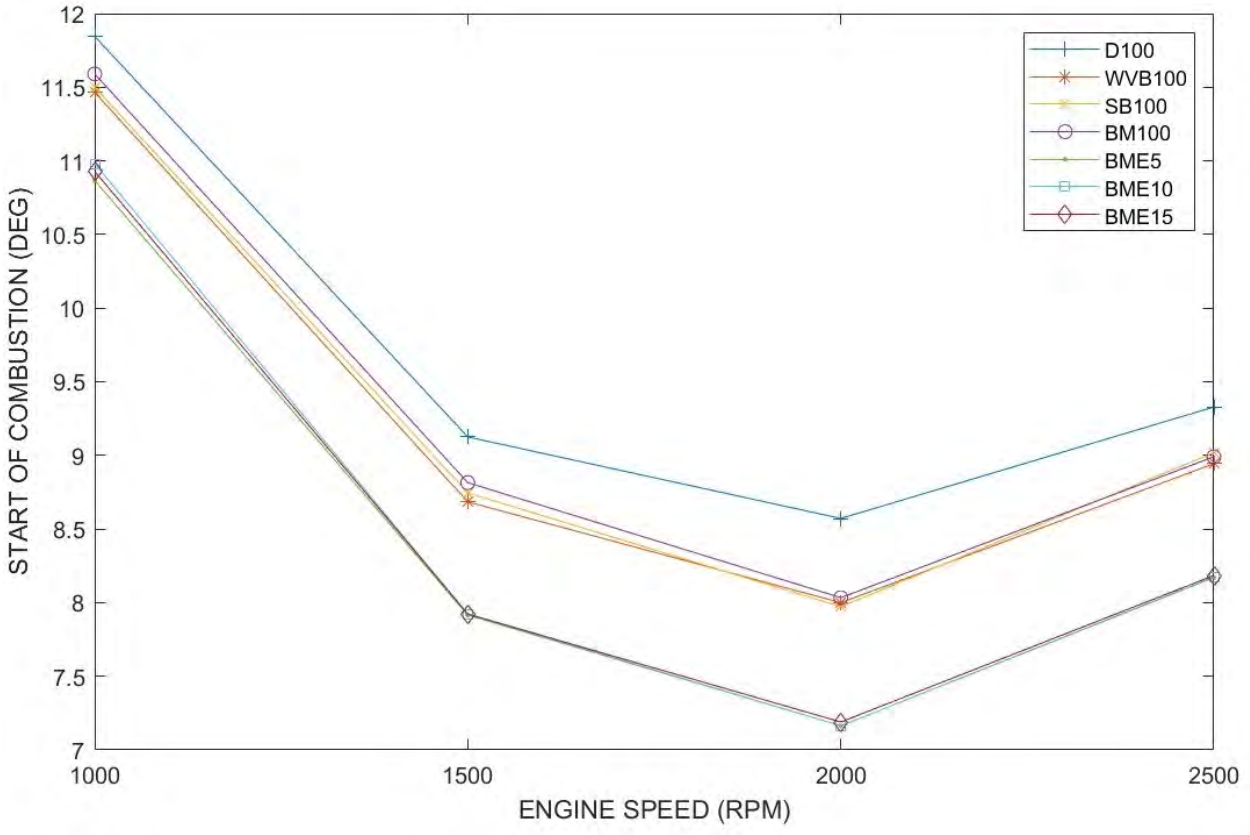

Figure 4.18: Variation of the start of combustion with an engine speed of simulated data.

The start of the combustion is described as the crank angle at which heat is released at the beginning of the premixed combustion phase. The start of combustion was numerically simulated using equation (3.22). Figure 4.18 shows that the SOC decreases up to 2000 rpm and started to increase to the maximum engine speed. At the same operating condition, the Diesel-RK simulation results show that the SOC of fuel samples for BME5, BME10, and BME15 (8.170 deg, 8.174 deg, and 8.185 deg) decreased compared to D100, WVB100, SB100, and BM100 (9.329 deg, 8.944 deg, 9.019 deg, and 8.991 deg). This decrease might be due to low cetane number and higher latent heat of evaporation of ethanol. Lapuerta et al. (2017) reported that the auto-ignition time of biodiesel blended with ethanol and butanol, respectively, at a fixed volume of the combustion chamber. The authors noticed that the increase of ID was due to alcohol blends. Compared to D100, the SOC of WVB100, SB100, BM100, BME5, BME10, and BME15 decreased by 4.1%, 3.3%, 3.6%, 12.4%, 12.4%, and 12.3% at the maximum speed of 2500 rpm.

Combustion Duration

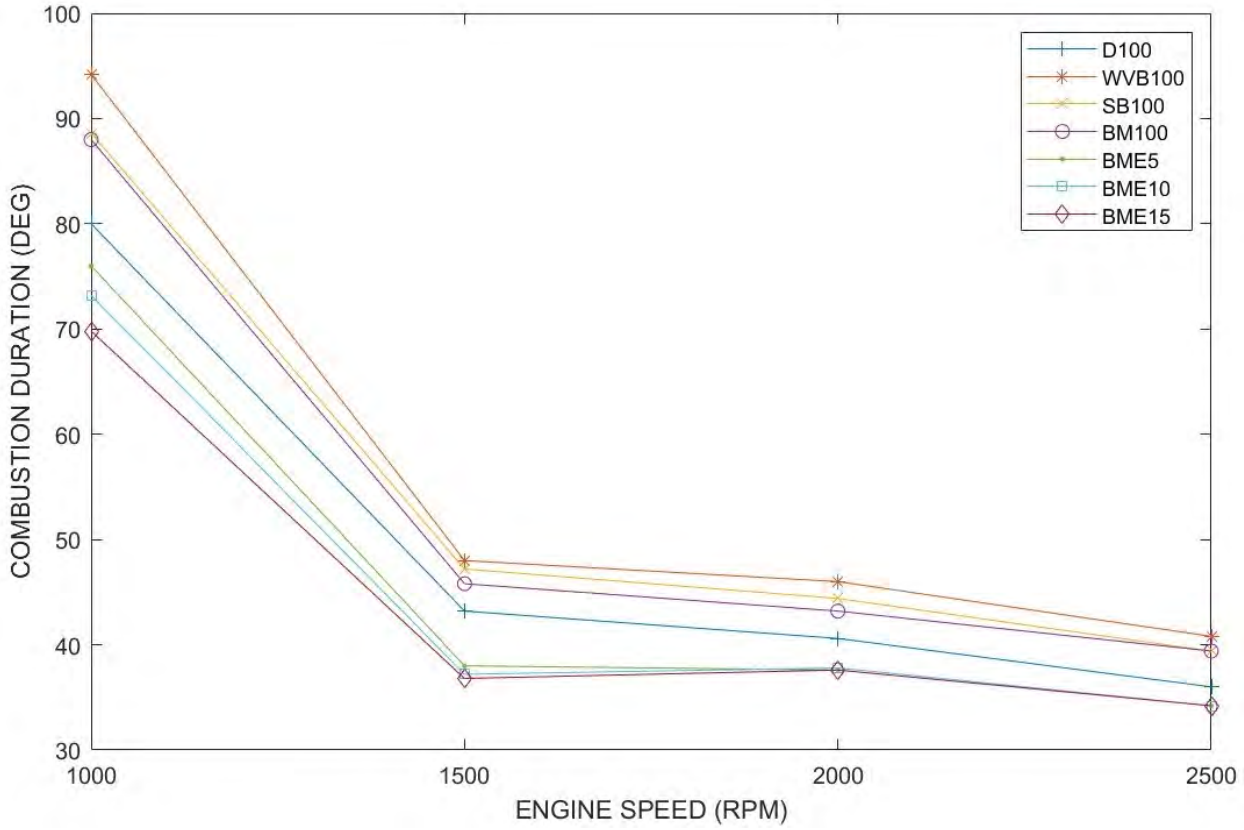

Figure 4.19: Variation of combustion duration with engine speed of simulated data.

The combustion duration refers to the time interval between the start of combustion and the end of combustion. The combustion duration was numerically simulated using equation (3.23). Figure 4.19 shows that the combustion duration decreases with an increase of engine speed. At the maximum speed, the results show that the combustion duration of BME5, BME10, and BME15 (34.2 deg, 34.2 deg, and 34.2 deg) attained short combustion duration compared to D100, WVB100, SB100, and BM100 (36 deg, 40.8 deg, 39.4 deg, and 39.4 deg). This could be due to the enhancement of the premixed combustion process where more fuel is burned in the premixed mode (Nour et al., 2019). Compared to those of D100, each of the combustion durations of BME5, BME10, and BME15 decreased by 5%, whereas those of WVB100, SB100, and BM100 increased by 13.3%, 9.4%, and 9.4% at the maximum speed. The possible reason for the short combustion duration of hybrid biodiesel-ethanol blends might be due to their higher oxygen content that promotes the combustion process leading to quick combustion that shortens particularly the diffusion combustion phase (Wei et al., 2018). Diesel-biodiesel-ethanol blends and biodiesel-ethanol blends generally have a longer ignition delay, a larger amount of fuel burned in premixed mode, and less burned in diffusion mode, which leads to a short combustion period compared to biodiesel and diesel fuel for all engine loads (Tse, 2016). The higher oxygen content of alcohol blends could also accelerate the combustion duration (Xiao-Ran et al., 2015). It has also been explained that micro-explosion could have improved the evaporation of the fuel droplets and subsequently accelerate the air-fuel mixing leading to a shorter combustion duration of alcohol blends (Liu et al., 2011).

Frictional Mean Effective Pressure

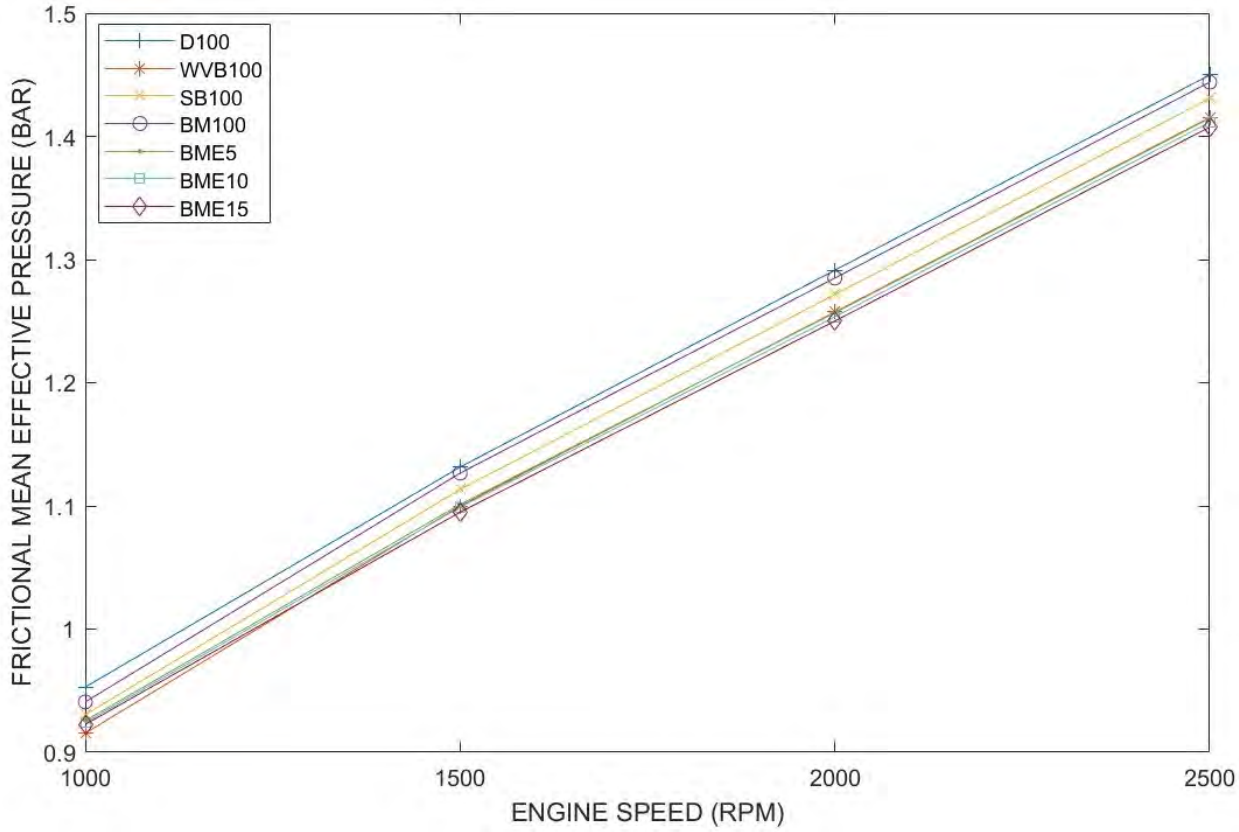

Figure 4.20: Variation of friction mean effective pressure with an engine speed of simulated data.

The frictional mean effective pressure can be stated as the quantity of energy attained for mean effective pressure to overcome the friction caused by the reciprocating apparatuses. The frictional mean effective pressure was evaluated using equation (3.27). The FMEP was assessed from the measurements of cylinder pressure and dynamometer brake torque. Figure 4.20 shows that the FMEP increases with an increase of engine speed. The values of FMEP of WVB100, SB100, BM100, BME5, BME10, and BME15 were found to be very close to that of D100 at all engine speeds. The results show that the Diesel-RK simulation of BME15 had the lowest FMEP of 1.408 bar compared to D100, SB100, BM100, BME5, and BME10 with values of 1.450 bar, 1.415 bar, 1.431 bar, 1.444 bar, 1.415 bar, and 1.411 bar at the maximum speed of 2500 rpm. Compared to D100 at the same operating conditions, the FMEP of WVB100, SB100, BM100, BME5, BME10, and BME15 decreased by 2.3%, 1.3%, 0.4%, 2.4%, 2.6 and 2.9%, respectively. The decrease of

FMEP values observed among the tested fuels in this study might be due to low cetane number, higher latent heat of evaporation, and low heating value.

4.2.2 Engine Performance Analysis

The predicted performance parameters of the diesel engine are discussed in this section. Parameters such as BP, BSFC, BT, BTE, and BMEP are presented and discussed.

Brake Power

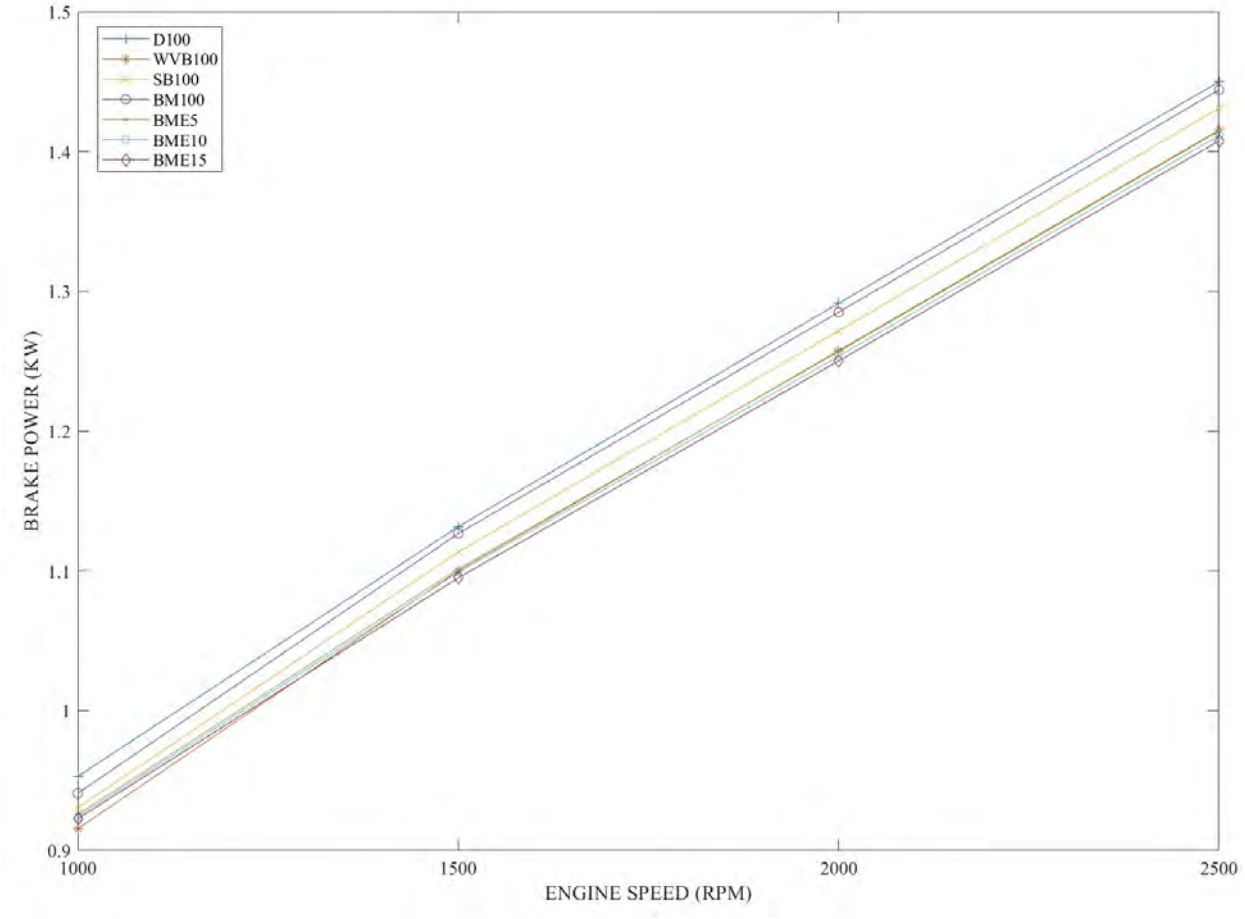

Figure 4.21: Variation of brake power with engine speed of simulated data.

The variations of BP with respect to an engine speed of D100, WVB100, SB100, BM100, BME5, BME10, and BME15 fuels are shown in Figure 4.21. The brake power was evaluated using equation (3.25). The Diesel-RK predicted results show that D100 (2.16 kW) attained the highest

BP compared to WVB100, SB100, BM100, BME5, BME10, and BME15 with the values of 1.87 kW, 2.0 kW, 2.12 kW, 1.85 kW, 1.82 kW, and 1.83 kW at the maximum engine speed of 2500 rpm. The heating value (HV) and cetane number (CN) of alcohol lead to a decrease in brake power (a derived parameter) (Yesilyurt et al., 2018). Another reason for low brake power in a diesel engine fuelled with alcohol blends is the high latent heat of vaporization, which was explained by Ghobadian et al. (2009). They indicated that a part of the energy was consumed for the vaporization of the fuels throughout the fuel injection due to the higher latent heat of alcohol. Since the engine power is proportional to brake torque and engine speed, the maximum engine BP depends not only on the explosion force but also on the engine speed. Due to the test conditions, the change in engine power will be affected by the engine BT (Heidari-Maleni et al., 2020). It can be noted from the graph that at the maximum speed of 2500 rpm, the BP of WVB100, SB100, BM100, BME5, BME10, and BME15 decreased by 13.4%, 7.4%, 2.0%, 14.3%, 15.5%, and 15.3%, respectively, compared to that of D100. The possible decrease was due to low heating value and cetane number of individual biodiesels, biodiesel mixture, and biodiesel mixture-ethanol blends. Similar kinds of results were reported by Maki and Shahad (2020).

Brake-Specific Fuel Consumption

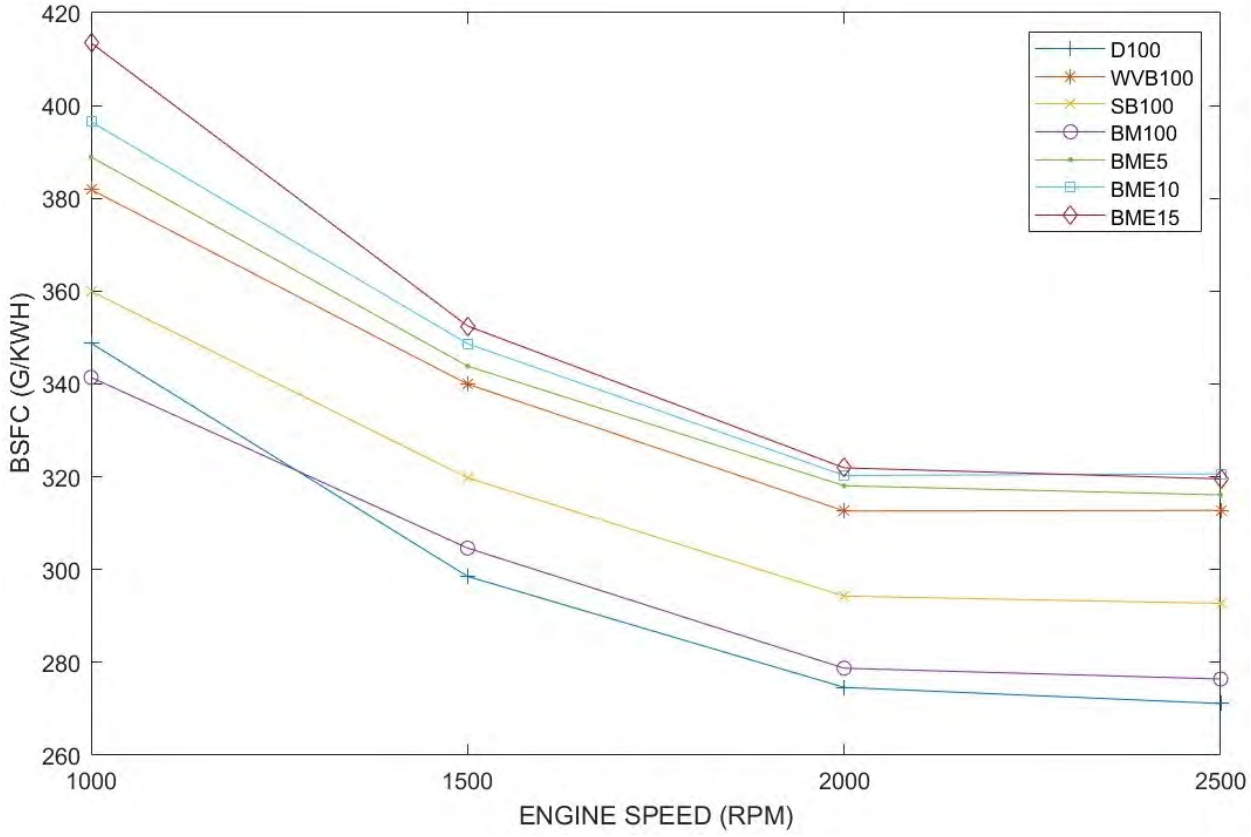

Figure 4.22: Variation of brake-specific fuel consumption with engine speed of simulated data.

Brake-specific fuel consumption is the quality volume of fuel consumed throughout the engine to release one Kilowatt of power in a period of one hour. It also measures the capability of the diesel engine to convert the chemical energy of the fuel to the desired work output (Hürdoğan et al., 2017, Singh et al., 2018). The brake-specific fuel consumption was evaluated using equation (3.28). Figure 4.22 shows that the BSFC of BME5, BME10, and BME15 increased BSFC compared to WVB100, SB100, BM100, and D100 throughout the entire speeds. This might be due to the high amount of fuel consumed to produce the required energy. Diesel fuel attained the lowest BSFC from minimum to maximum speed due to higher heating value. At the maximum speed of 2500 rpm, the Diesel-RK predicted values were 271.14 g/kWh, 312.77 g/kWh, 292.72 g/kWh, 276.43 g/kWh, 316.10 g/kWh, 320.63 g/kWh, and 319.56 g/kWh, respectively. Compared to D100, the BSFC of WVB100, SB100, BM100, BME5, BME10, and BME15 increased by 15.4%, 8.0%, 2.0%, 16.6%, 18.3%, and 17.9% at the maximum speed of 2500 rpm. This increase might

be due to lowering the heating values of individual biodiesels, and hybrid biodiesel-ethanol blends. Most of the studies by other researchers acknowledge that the increase in BSFC is on average like the decrease of the lower heating value for diesel engines powered by biodiesel (Zhu et al., 2011b). To compensate for the lower heating value of biodiesels, hybrid biodiesel-ethanol blends, and a large amount of fuel need to be injected to attain similar power output (Yilmaz and Sanchez, 2012). Compared to BM100, the BSFC fuel samples of BME5, BME10, and BME15 increased by 14.4%, 16%, and 15.6%, respectively. This increase might be due to the higher latent heat of evaporation of ethanol, the heat was lost from combustion chamber due to evaporation, which causes the cooling effect and reduces the combustion efficiency (Atmanli and Yilmaz, 2020).

Brake Torque

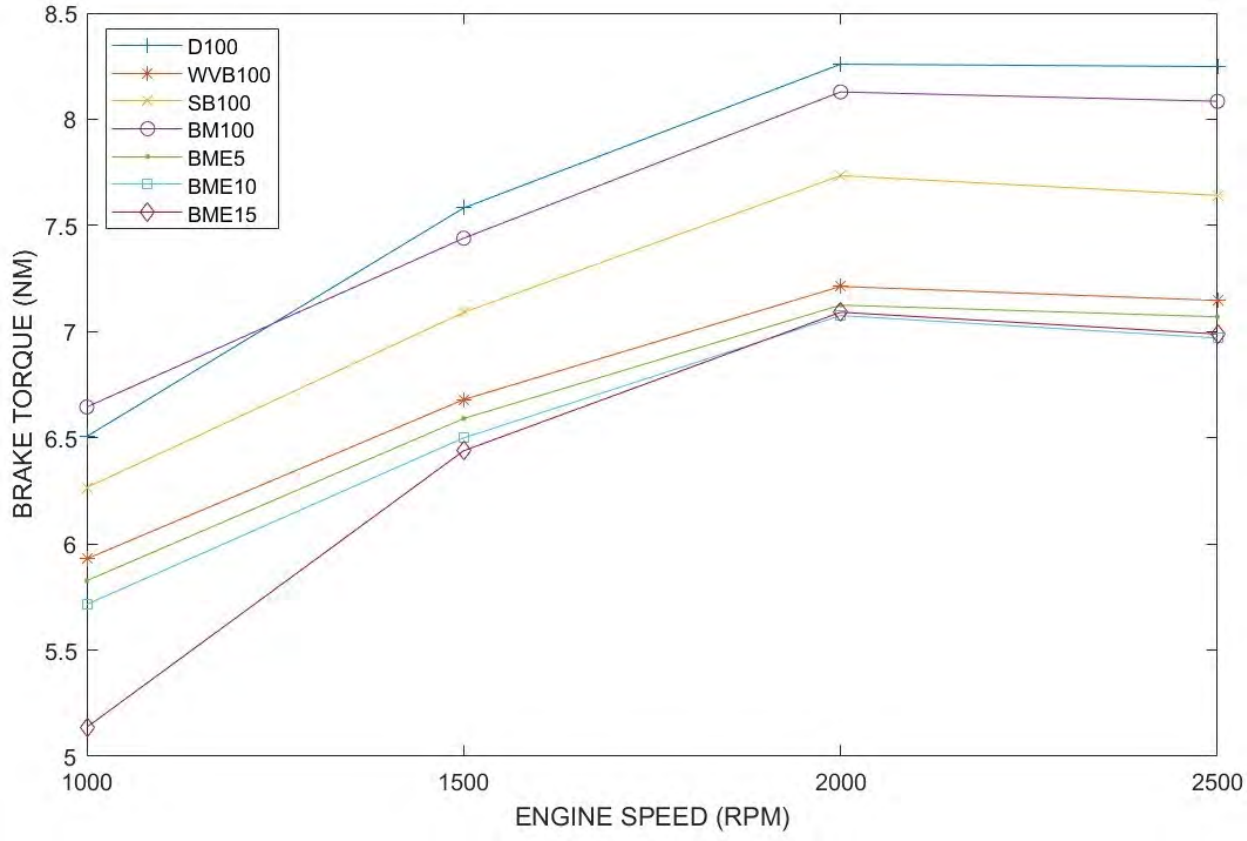

Figure 4.23: Variation of brake torque with engine speed of simulated data.

The variations of BT with respect to an engine speed of D100, WVB100, SB100, BM100, BME5, BME10, and BME15 fuels are shown in Figure 4.23. The BT increases engine speed due to higher

mechanical losses and is an indication of fuel being used efficiently during the ignition process to produce an output of the engine. At the maximum speed of 2500 rpm, the Diesel-RK simulation results show that the BT of D100 was 8.248 Nm, WVB100 (7.147 Nm), SB100 (7.642 Nm), BM100 (8.085 Nm), BME5 (7.070 Nm), BME10 (6.970 Nm), and BME15 (6.990 Nm). The brake torque values rely on the engine load, speed, energy contents, and fuel properties such as viscosity, and heating value according to the literature (Verma et al., 2015, Rajak and Verma, 2020). In comparison with D100, the BT of WVB100, SB100, BM100, BME5, BME10, and BME15 decreased by 13.4%, 7.4%, 2.0%, 14.3%, 15.5% and 15.3% at the maximum speed. A possible reason for this decrease might be due to the lower heating values of tested fuel samples. Appavu et al. (2021) reported that the brake torque of the biodiesel-pentanol blend decreased compared to pure diesel and biodiesel-diesel due to the lower energy content of pentanol. The BT was directly affected by lower calorific value and fuel consumption during the ignition process. Ignition is composite and depends on several characteristics such as turbulence, injection timing, fuel-air preparation, and injection pressure (Rajak et al., 2018a, Golimowski et al., 2013).

Brake Thermal Efficiency

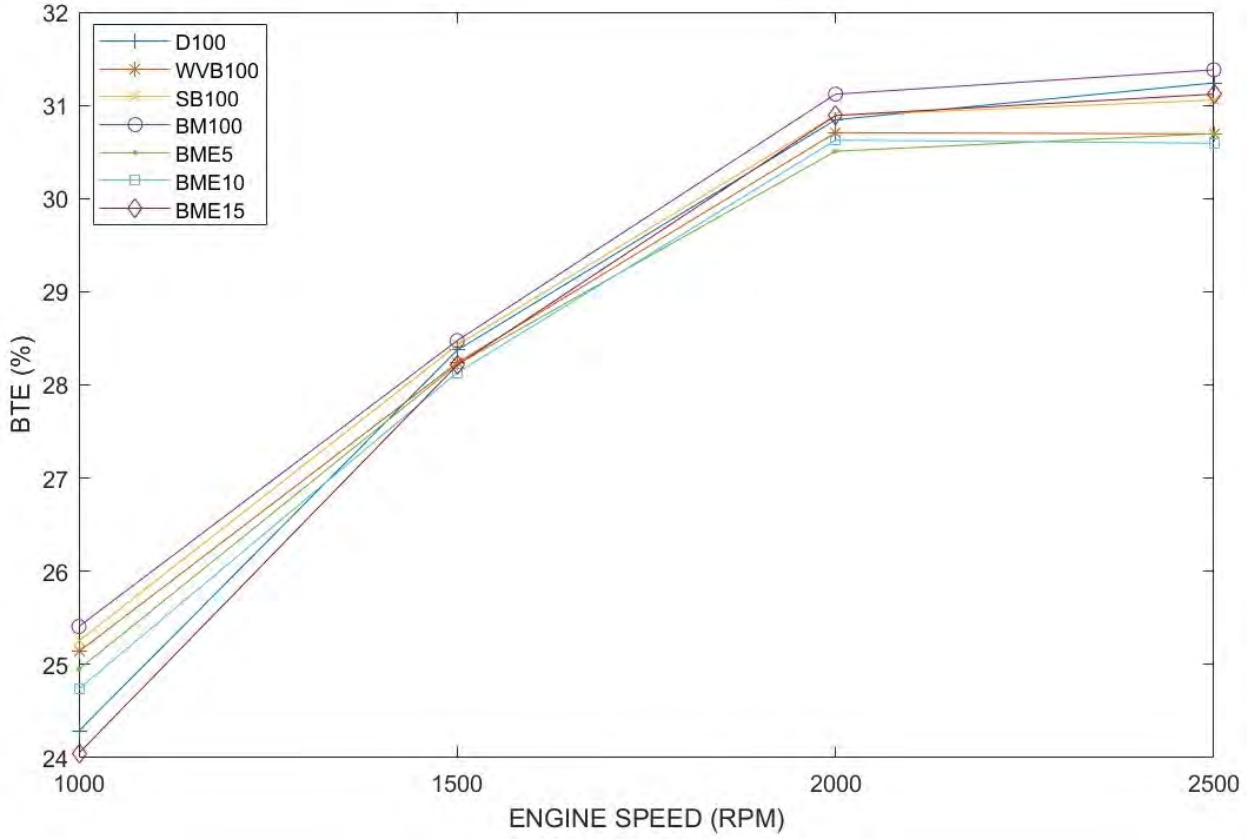

Figure 4.24: Variation of brake thermal efficiency with an engine speed of simulated data.

The variations of BTE with respect to an engine speed of D100, WVB100, SB100, BM100, BME5, BME10, and BME15 fuels are shown in Figure 4.24. The brake thermal efficiency was evaluated using equation (3.26). It was noted from the graph that at the maximum speed of 2500 rpm, the BTE of D100, WVB100, SB100, BM100, BME5, BME10, and BME15 was 31.2%, 30.7%, 31.1%, 31.4%, 30.7%, 30.6%, and 31.1%, respectively. Compared to D100, the BTE of BM100 increased by 0.4% at the maximum speed. This increase might be due to combustion improvement on account of increased oxygen content. At the same operating condition, WVB100, SB100, BME5, BME10, and BME15 decreased by 1.8%, 0.6%, 1.7%, 2.1%, and 0.4% compared to D100. Anand et al. (2010) reported that the BTE of diesel fuel attained higher value compared to biodiesel and these results were in line with the current numerical results. The BTE of BME15 increased compared to individual biodiesels (WVB100 and SB100). This increase might be due to higher oxygen content, higher flame speed, and improved fuel properties, which may lead to the

higher burning rate of alcohol blend over neat biodiesel. Anand et al. (2011) reported that the BTE of the biodiesel-methanol blend was higher compared to neat biodiesel at the high load. This successfully improves the combustion procedure, which consequently leads to improved BTE (Datta and Mandal, 2017). At the maximum speed, the results of BME15 are comparable to diesel fuel. This might be due to the reduction of the viscosity of the ethanol blends. This leads to better atomization and better fuel mixture leading to an increase in BTE (Prbakaran and Viswanathan, 2018).

Brake Mean Effective Pressure

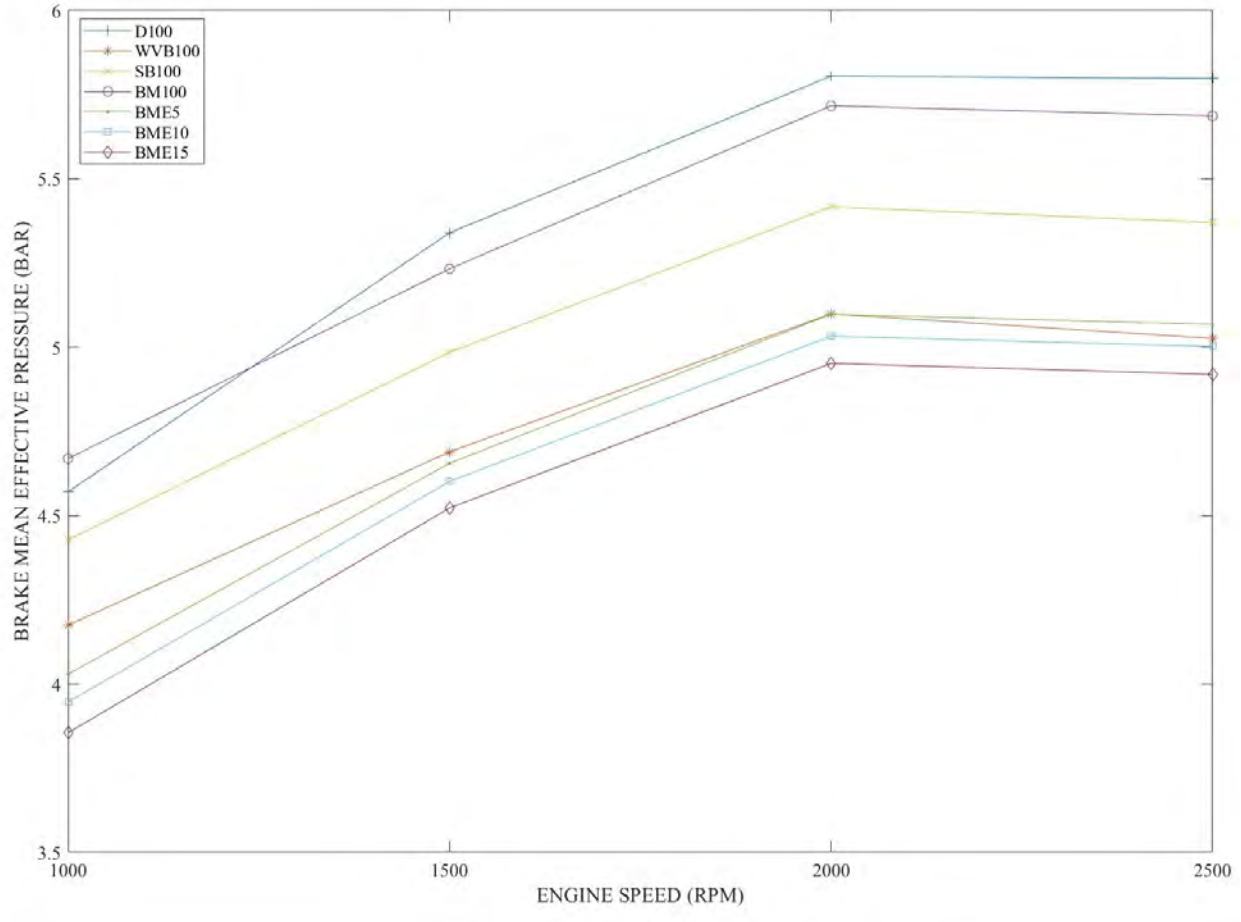

Figure 4.25: Variation of brake mean effective pressure with an engine speed of simulated data.

The variation of brake mean effective pressure with engine speeds of D100, WVB100, SB100, BM100, BME5, BME10, and BME15 is presented in Figure 4.25. The brake mean effective pressure was evaluated using equation (3.29). At the maximum speed of 2500 rpm, the Diesel-RK

predicted values of BMEP fuel samples for D100, WVB100, SB100, BM100, BME5, BME10, and BME15 were 5.80 bar, 5.03 bar, 5.37 bar, 5.69 bar, 5.07 bar, 5.0 bar, and 4.92 bar, respectively. At the same operating conditions, the BMEP of WVB100, SB100, BM100, BME5, BME10, and BME15 decreased by 13.3%, 7.4%, 1.9%, 12.6%, 13.7% and 15.2%, respectively, compared to the BMEP from D100. The possible decrease of individual biodiesels, hybrid biodiesel, hybrid biodiesel mixture, and ethanol blends might be due to low heating value and high oxygen content of alcohol. The higher density and viscosity of biodiesel lead to fuel atomization and vaporization problems hence decreasing BMEP (Gad et al., 2021). Another reason for this decrease might be because of brake power, which is directly proportional to BMEP at a given speed. Rajak et al. (2021) reported that the BMEP of diesel fuel attained higher values compared to first, second, and third-generation feedstocks blended on a diesel engine and these results were in line with the current numerical results.

4.2.3 Emission Analysis

The exhaust gas emissions such as CO_2, NO, NO_x, PM, and Bosch smoke number were numerically evaluated using Diesel-RK software and discussed.

CO_2 Emission

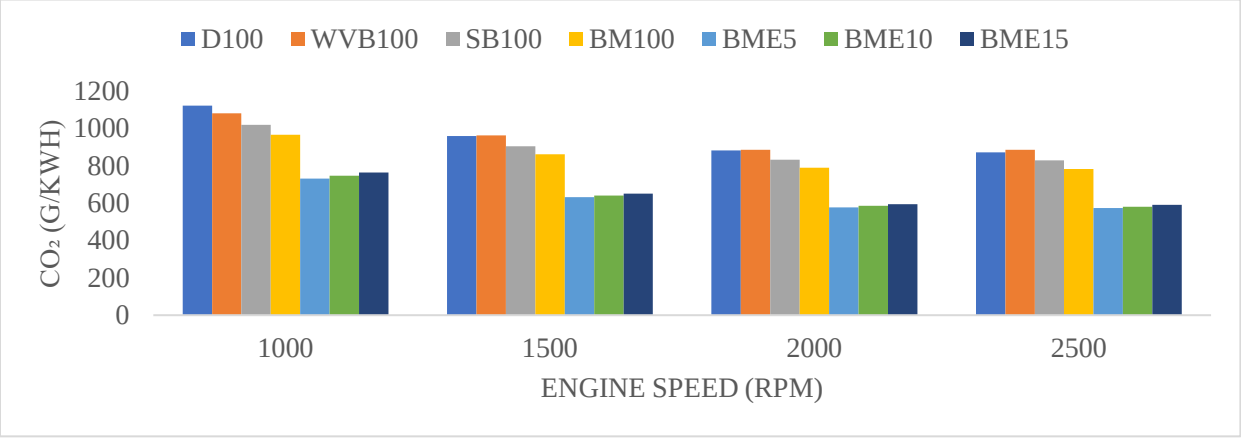

Figure 4.26: Variation of CO_2 with engine speed of simulated data.

The CO_2 emitted by diesel engines is one of the primary components of exhaust gas caused by the burning of HC fuels. This emission was not meant to produce air pollution, but it has since been found to be one of the crucial greenhouse gases (Pulkrabek, 2004). The variations of CO_2 with

respect to an engine speed of D100, WVB100, SB 100, BM100, BME5, BME10, and BME15 were presented in Figure 4.26. The graph showed that when the engine speed increased, the CO_2 emission levels decreased. The CO_2 emissions of D100, WVB100, SB100, BM100, BME5, BME10, and BME15 were 873.68 g/kWh, 887 g/kWh, 830.34 g/kWh, 784.13 g/kWh, 574.44 g/kWh, 581.97 g/kWh, and 591.78 g/kWh at the maximum speed. The CO_2 emissions of SB100, BM100, BME5, BME10, and BME15 decreased by 5.0%, 10.2%, 34.3%, 33.4%, and 32.3%, whereas WVB100 increased by 1.5% compared to D100 at the maximum speed. A possible reason for the decrease of BME5, BME10, and BME15 might be due to the high oxygen content of ethanol blends. Akar (2016) discovered that the CO_2 emissions of the diesel engine fuelled with diesel-biodiesel-butanol blend decreased compared to diesel fuel. Randazo and Sodré (2011b) stated that the increased percentage of ethanol in the B20 blend decreases the CO_2 emission level due to the lower C/H ratio of the ethanol molecule. This numerical study is also in agreement with the results attained by Alptekin et al. (2015) who indicate that the CO_2 emission of diesel-bioethanol-waste oil biodiesel decreased compared to biodiesel-diesel.

NO Emission

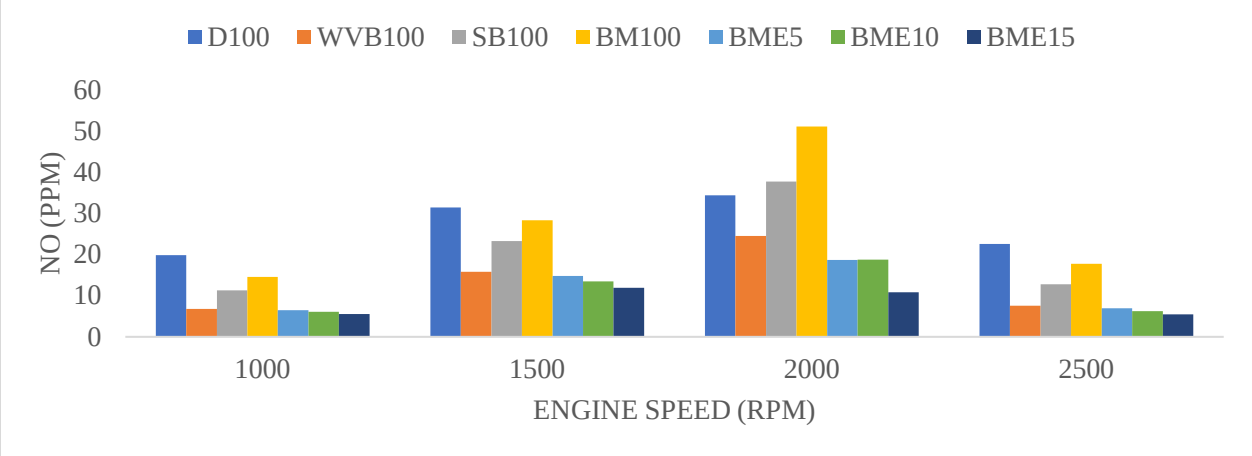

Figure 4.27: Variation of NO with engine speed of simulated data.

Figure 4.27 shows the variation of nitric oxide (NO) emissions of D100, WVB100, SB100, BM100, BME5, BME10, and BME15 fuels, respectively. The Diesel-RK prediction results show that D100 and BM100 emit the maximum values of NO emission compared to other testing fuel samples at the maximum speed of 2500 rpm. The possible increase might be due to the high cetane

number of biodiesel and the presence of oxygen content in the chemical structure. The hybrid biodiesel-ethanol blends attained the lowest NO emissions compared to other tested fuels at the maximum speed of 2500 rpm. The possible decrease for hybrid biodiesel-ethanol blends might be due to higher latent heat of vaporization, which is an indication of a high cooling effect leading to low combustion temperature with the improvement of oxygen molecules. Datta and Mandal (2017) stated that the diesel engine powered by biodiesel-ethanol and biodiesel-methanol blending decreased NO_x emissions compared to pure biodiesel. At the same operating condition of 2500 rpm, the NO emissions of D100, WVB100, SB100, BM100, BME5, BME10, and BME15 were 22.6 ppm, 7.6 ppm, 12.8 ppm, 17.8 ppm, 6.9 ppm, 6.2 ppm, and 5.5 ppm, respectively. Compared to D100, the fuel sample of WVB100, SB100, BM100, BME5, BME10, and BME15 emissions decreased by 66.5%, 43.4%, 21.2%, 69.3%, 72.4%, and 75.8% at the maximum speed of 2500 rpm.

NO_x Emission

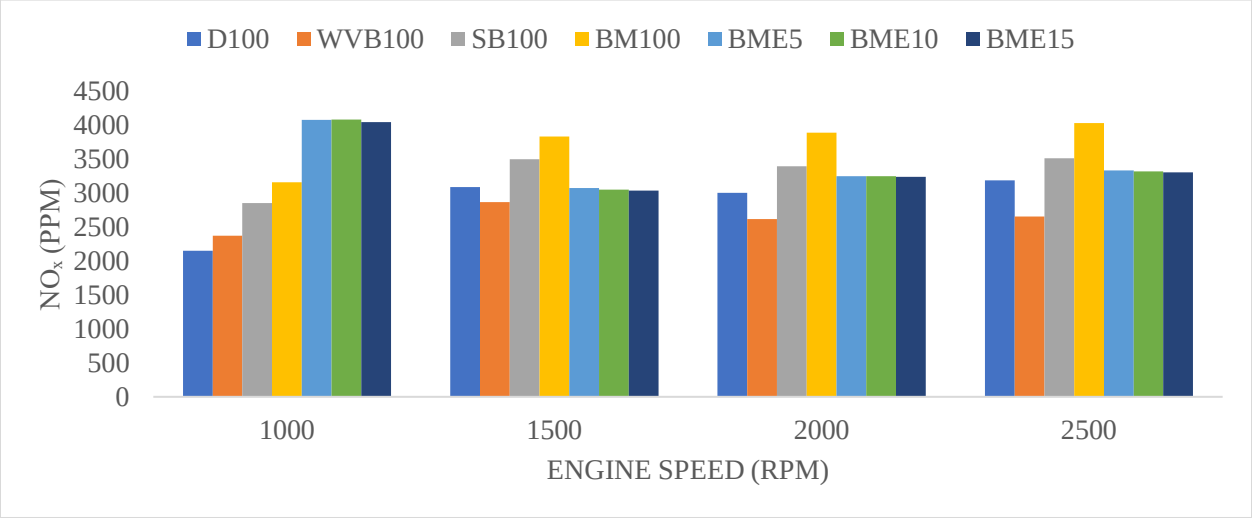

Figure 4.28: Variation of NOx with engine speed of simulated data.

The gas mixture of nitrogen dioxide and nitrogen oxide is the formation of nitrogen oxides (NO_x), which is toxic gas released from the exhaust manifold of the diesel engine, and it badly affects the atmosphere and the public. The formation of NO_x happens at a maximum reaction temperature between nitrogen and oxygen gas (Swarna et al., 2021). The specific NO_x emission was computed using equation (3.33). The variations of NO_x emissions with respect to an engine speed of D100,

WVB100, SB100, BM100, BME5, BME10, and BME15 are presented in Figure 4.28. The predicted results of Diesel-RK showed that the fuel sample of WVB100 attained the lowest NO_x emission compared to D100, SB100, BM100, BME5, BME10, and BME15 at the maximum speed of 2500 rpm. The possible explanation might be due to the presence of native oxygen content in chemical formation (Ilkılıç et al., 2011). However, D100 attained the lowest NO_x emission compared to all testing fuel samples at the minimum speed of 1000 rpm. This decrease might be due to high in-cylinder temperature, the presence of inherent oxygen molecules, better thermodynamic efficiency, and higher heating value (Ashok et al., 2017, Ramesh et al., 2019). At the maximum speed of 2500 rpm, the addition of ethanol to hybrid biodiesel attained lower NO_x emission compared to BM100, and SB100. This might be due to the cooling effect resulting to low NO_x emissions (Babu and Anand, 2017). Another reason might be the higher latent heat of evaporation of alcohol, which represents its transformation from liquid to vapour, and that had been known to mitigate the formation of NO_x; hence the observed decrease in NO_x (Yesilyurt et al., 2020). The addition of ethanol to hybrid biodiesel improves the oxygen concentration resulting in poor combustion situations at the lower temperature of the combustion chamber. The compatible results conducted by Anand et al. (2011), Venkata Subbaiah and Raja Gopal (2011) ascertained that the biodiesel from karanja oil-methanol blends and biodiesel from rice bran-ethanol blends decreased compared to pure diesel fuel. At the maximum speed of 2500 rpm, the NO_x emissions predicted values of D100, WVB100, SB100, BM100, BME5, BME10, and BME15 were found to be 3192 ppm, 2656.5 ppm, 3515.4 ppm, 4035.6 ppm, 3339.6 ppm, 3325.7 ppm, and 3310 ppm, respectively. At the same operating conditions, compared to D100, the fuel samples of SB100, BM100, BME5, BME10, and BME15 were increased by 10.1%, 26.4%, 4.6%, 4.2%, and 3.7%, whereas WVB100 decreased by 16.8%.

PM Emission

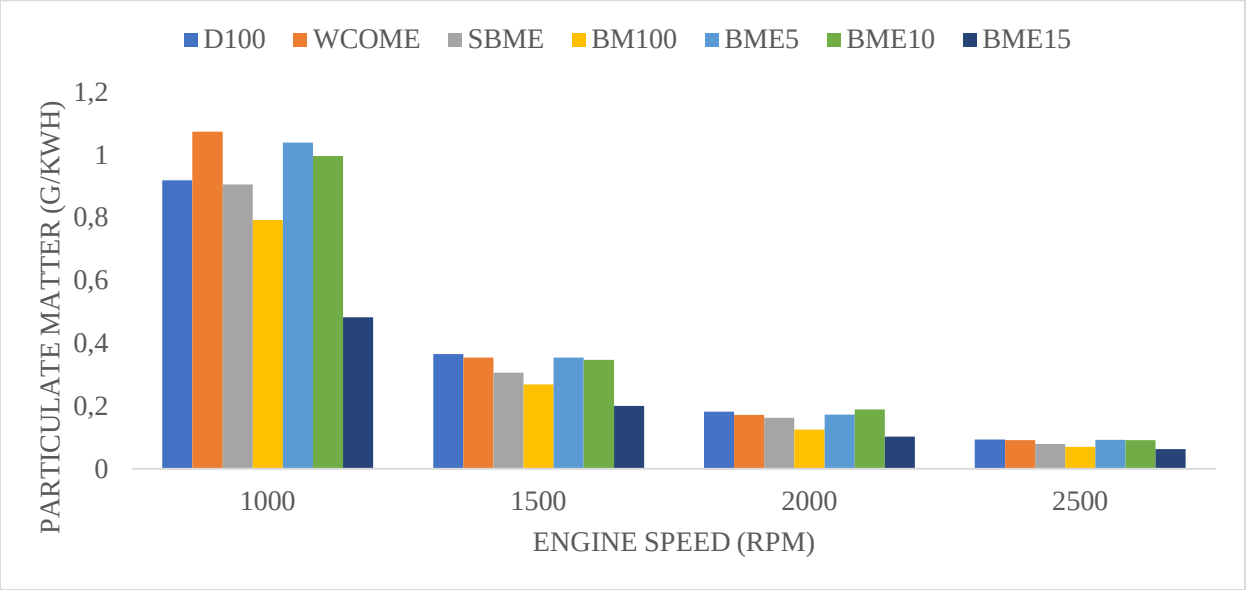

Figure 4.29: Variation of particulate matter with an engine speed of simulated data.

The variations of the PM with respect to an engine speed of D100, WVB100, SB100, BM100, BME5, BME10, and BME15 were presented in Figure 4.29. The particulate matter emission was evaluated using equation (3.37), by Alkidas (1984), as a function of the Bosch smoke number. It can be noted from the figure that the PM emissions decrease with the increase of engine speed. The prediction results from Diesel-RK showed that the PM emissions of D100 attained the highest value of 0.0936 g/kWh while WVB100, SB100, BM100, BME5, BME10, and BME15 attained the minimum values of 0.0918 g/kWh, 0.0787 g/kWh, 0.0697 g/kWh, 0.0925 g/kWh, 0.0917 g/kWh, and 0.0625 g/kWh, respectively. The PM of WVB100, SB100, BM100, BME5, BME10, and BME15 decreased by 2.0%, 16.0%, 25.6%, 1.2%, 2.0%, and 33.2% compared to D100 at the maximum speed. This decrease might be due to high oxygen content, low cetane number, low viscosity, and density leading to better atomization (Shudo et al., 2007). At maximum speed, high combustion temperature weakens the cooling effect, leading to the lowest PM emissions of BME15 compared to other fuels (Wei et al., 2018). The application of ethanol lowers the carbon chain length of the biodiesel mixture leading to decrease PM emissions (McEnally and Pfefferle, 2011). Ghadikolaei (2016) experimentally compared diesel fuel with ethanol blends in a diesel engine and learned that ethanol decreased emissions in all cases. Zhu et al. (2010b) noted that

when the diesel engine is powered with ethanol blends, several factors could contribute to the reduction of PM emission. Firstly, compared with pure biodiesel, the ethanol blends contain high oxygen, which could enhance the combustion process and decrease PM emission. Secondly, the alcohol blends could reduce the cetane number of the fuel and hence increase the ignition delay period and more fuel might burn in the premixed mode, resulting in lower PM emission. Thirdly, alcohol blends could reduce the viscosity and density of the base fuel, leading to better atomization and hence lower PM emission.

Bosch Smoke Emission

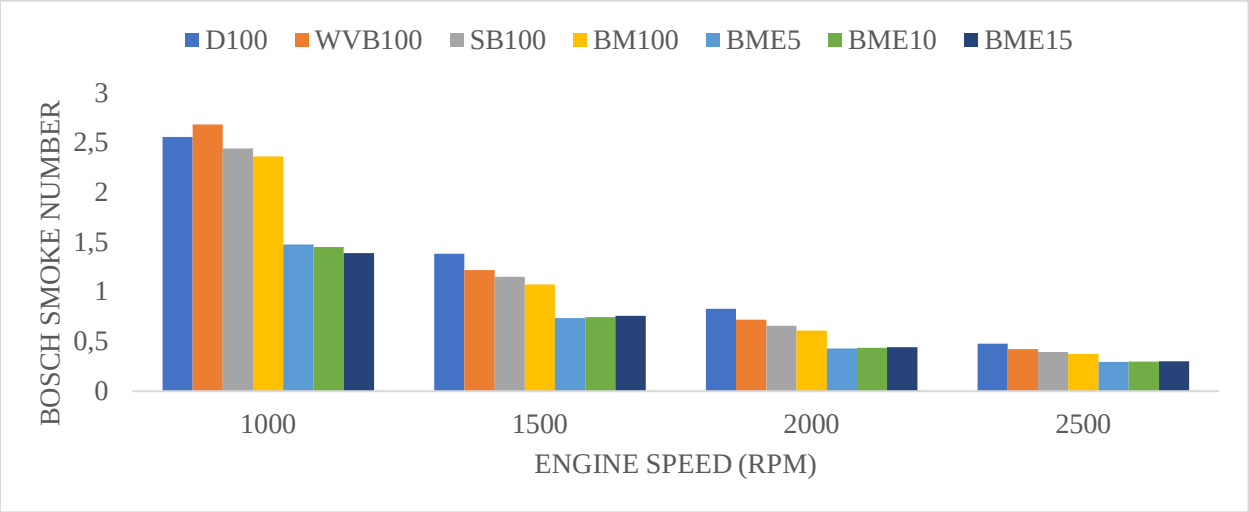

Figure 4.30: Variation of Bosch smoke number with an engine speed of simulated data.

The variations of smoke emissions with engine speeds of D100, WVB100, SB100, BM100, BME5, BME10, and BME15 are shown in Figure 4.30. The Bosch smoke number was evaluated from the Hartridge smoke equation (3.36). The results showed that D100 attained the maximum value of 0.478% whereas WVB100, SB100, BM100, BME5, BME10, and BME15 attained 0.422%, 0.394%, 0.373%, 0.293%, 0.297% and 0.302% at the maximum speed of 2500 rpm. The smoke emissions of WVB100, SB100, BM100, BME5, BME10, and BME15 decreased by 11.7%, 17.7%, 21.9%, 38.7%, 37.9% and 36.9% compared to D100 at the maximum speed of 2500 rpm. This decrease might be due to the excessive volume of oxygen molecules present in the chemical structure of fuel, which assists to complete combustion in the cylinder (Yesilyurt et al., 2020). In addition, hybrid biodiesel-ethanol blends attained the lowest smoke emissions compared to all

tested fuel samples. The possible decrease might be due to the higher latent heat of evaporation and the low cetane number of ethanol. Ilkılıç et al. (2011) reported that the smoke emission emitted by the diesel engine powered by diesel and safflower biodiesel blends decreased compared to standard diesel. Kumar et al. (2016) reported that the smoke emission from diesel engines could be controlled by the addition of alcohol in the fuel blends. Studies conducted by Ashok et al. (2019) stated that the smoke emission for biodiesel-diesel-alcohol blends attained lower emissions compared to pure diesel and biodiesel due to the presence of inherent oxygen content hence decreasing smoke emissions.

4.3 Summary of Experimental and Prediction Studies

Summary of Experimental Studies

This section focused on the experimental equipment required for biodiesel characterization, characteristics of the test engine, specifications, and measuring equipment. The Pignat pilot plant schematic and its description of working were presented. The titration process and the production of biodiesel were presented. Fuel blends preparations and measurements of D100, WVB100, SB100, BM100, BME5, BME10, and BME15 were presented. The experimental setup, operation procedures, and application of X-Tract extreme software have been discussed in detail. Measurement of combustion, performance, and emission characteristics of the engine has been discussed.

The properties of WVB100, SB100, and BM100 fuels have greatly increased the density, viscosity, heating value, and flash point. The biodiesel mixture-ethanol blends decreased the density, viscosity, heating value, and flash point. The D100 decreased density, viscosity, and flash point compared to all biodiesel blended fuel samples. Furthermore, all other tested fuels decreased heating value compared to D100 fuel.

The ICP of the diesel engine fuelled with D100 was higher compared to other tested fuels due to higher heating value, low density, low viscosity, and better fuel atomization. The heat release rate

of D100 was higher compared to other tested fuels at the maximum speed of 2500 rpm due to higher heating values.

The BT of D100 was higher compared to WVB100, SB100, BM100, BME5, BME10, and BME15. The BT of BME15 had the minimum value compared to all testing fuel samples at maximum speed due to low heating value. The D100 attained higher BP compared to other tested fuels due to higher heating values. The BM100 exhibited higher BP compared to WVB100, SB100, BME5, BME10, and BME15. The D100 attained lower BSFC compared to WVB100, SB100, BM100, BME5, BME10, and BME15. The BTE of BM100 attained maximum value compared to WVB100, SB100, BM100, BME5, BME10, and BME15 at the maximum speed of 2500. The BMEP of D100 attained the maximum value of D100 at all engine speeds compared to other tested fuels due to the high heating value.

The fuel sample of D100 emits high CO emissions compared to WVB100, SB100, BM100, BME5, BME10, and BME15 at the minimum and maximum speeds. The BME5, BME10, and BME15 emit the lowest NO emissions compared to all other tested fuels at all engine speeds caused by the higher latent heat of evaporation of ethanol. The HC emissions of all other tested fuels decreased compared to D100 at the minimum and maximum speeds due to the high oxygen content of ethanol and the high cetane number of biodiesels. The CO_2 emissions of SB100, BM100, BME5, BME10, and BME15 fuels decrease at the maximum speed while WVB100 increase compared to D100. A possible reason for this decrease is due to the high oxygen content in the biodiesel blends. The fuel samples of BME5, BME10, and BME15 produced low smoke emissions compared to D100, WVB100, SB100, and BM100 at the maximum speed conditions. The possible decrease of the smoke emissions from BME5, BME10, and BME15 might be due to higher latent heat of evaporation and low cetane number of ethanol.

Summary of Prediction Studies

The application process of Diesel-RK simulation software to assess the combustion, performance, and exhaust gas emissions of the diesel engine fuelled with various fuel samples has been shown. The various underlying equations used in the simulation have been presented.

The combustion parameters such as ICP, HRR, ICT, ignition delay, spray tip penetration, the start of combustion, combustion duration, and frictional mean effective pressure has been computed using Diesel-RK software as the simulation tool. Performance parameters such as BP, BSFC, BT, BTE, BMEP, and emission characteristics such as CO_2, PM, $NO_{x,}$ and Bosch smoke number have also been evaluated using the same software (Diesel-RK).

The peak in-cylinder pressure of WVB100, SB100, BM100, BME5, BME10, and BME15 decreased compared to D100 at the maximum speed due to higher latent heat of vaporization, the lower cetane number postponed the starting point of combustion for the blended fuels. The heat release rate of D100 was higher compared to WVB100, SB100, BM100, BME5, BME10, and BME15 at the maximum speed of 2500 rpm due to high energy content, which led to better combustion. The in-cylinder temperature of D100 was higher compared to other tested fuel samples at the maximum speed due to improved fuel atomization and lower viscosity. The hybrid biodiesel-ethanol blends (BME5, BME10, and BME15) attained longer ignition delays compared to D100, WVB100, SB100, and BM100 due to the low cetane number of ethanol, which is far lower than that of diesel and biodiesel. The spray tip penetration of individual biodiesels and biodiesel mixture attained maximum values compared to hybrid biodiesel-ethanol blends due to higher viscosity and surface tension, which makes biodiesel harder to break up into small droplets.

The start of combustion for hybrid biodiesel-ethanol blends decreased compared to other tested fuels due to low cetane number and higher latent heat of evaporation. The hybrid biodiesel-ethanol blends attained short combustion duration compared to D100, WVB100, SB100, and BM100 due to the higher oxygen content of ethanol, which promotes the combustion process leading to quick combustion. The frictional mean effective pressure fuel samples of WVB100, SB100, BME5, BME10, and BME15 were lower compared to D100 at the maximum speed due to lower heating values.

Diesel-RK simulation for D100 attained the maximum value of brake power and brake torque compared to other tested fuels due to higher heating values. The brake-specific fuel consumption of hybrid biodiesel-ethanol blends increased compared to other tested fuels due to the higher amount of fuel consumed to produce the required energy. The brake thermal efficiency of BME15

increased compared to individual biodiesels (WVB100 and SB100) due to higher oxygen content, higher flame speed, and improved fuel properties, which may lead to a higher burning rate of alcohol blend. The brake mean effective pressure of WVB100, SB100, BM100, BME5, BME10, and BME15 decreased compared to D100 due to low heating value and high oxygen content of alcohol.

The Diesel-RK simulation for CO_2 emissions of BME5, BME10, and BME15 attained the minimum values compared to D100, WVB100, SB100, and BM100 at all engine speeds due to the high oxygen content of ethanol. The NO emission of BME5, BME10, and BME15 was decreased compared to BM100 at the maximum speed of 2500 rpm due to higher latent heat of vaporization. The NO_x emission of WVB100 achieved the lowest value compared to D100, SB100, BM100, BME5, BME10, and BME15 due to the presence of native oxygen content in the chemical formation. The particulate matter emissions of WVB100, SB100, BM100, BME5, BME10, and BME15 decreased compared to that from D100 at the maximum speed of 2500 rpm due to higher volatility and low cetane number of ethanol. The Bosch smoke number emission of D100 was higher compared to WVB100, SB100, BM100, BME5, BME10, and BME15 at the maximum speed of 2500 rpm. Hybrid biodiesel-ethanol blends attained the lowest smoke emissions compared to all tested fuels due to the higher latent heat of evaporation and low cetane number of ethanol.

CHAPTER FIVE

5.0 Validation of numerical with experimental results

An alternative fuel used by diesel engines is always evaluated based on performance, combustion, and emission characteristics. As such, various parameters on the performance, combustion, and exhaust gas emissions of diesel engines have been evaluated both experimentally and numerically in this study.

5.1 Comparison of Numerical and Experimental Results

The predicted results attained using Diesel-RK were validated with experimental results conducted under the same working conditions. The parameters considered during the validation include BP, BSFC, BT, BTE, and BMEP for performance; HRR, ICP for combustion, and CO_2, NO, NO_x, and smoke number for emissions. This is due to the limitations of the Diesel-RK software, which lacked the capacity to analyse all the parameters from the experiment.

5.1.1 Heat Release Rate

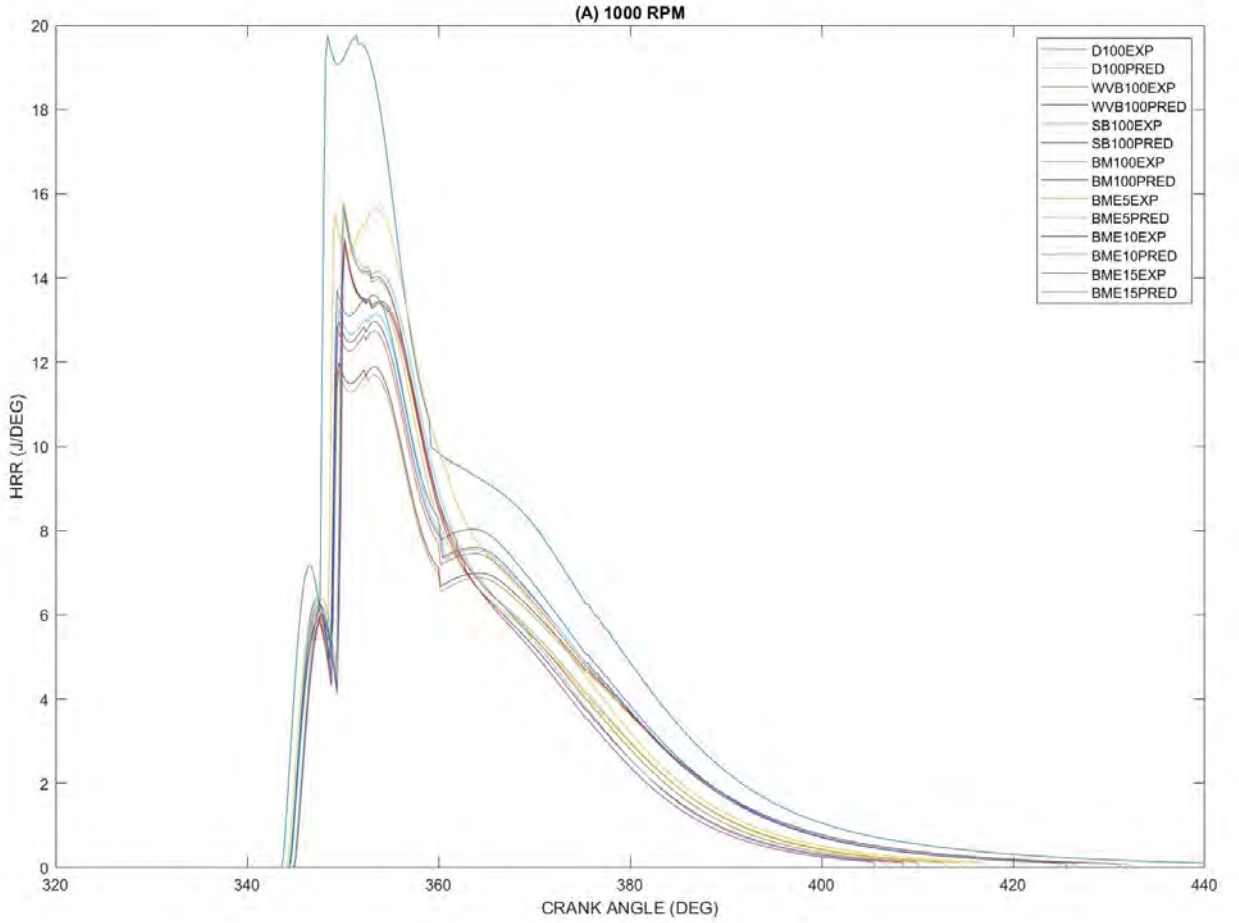

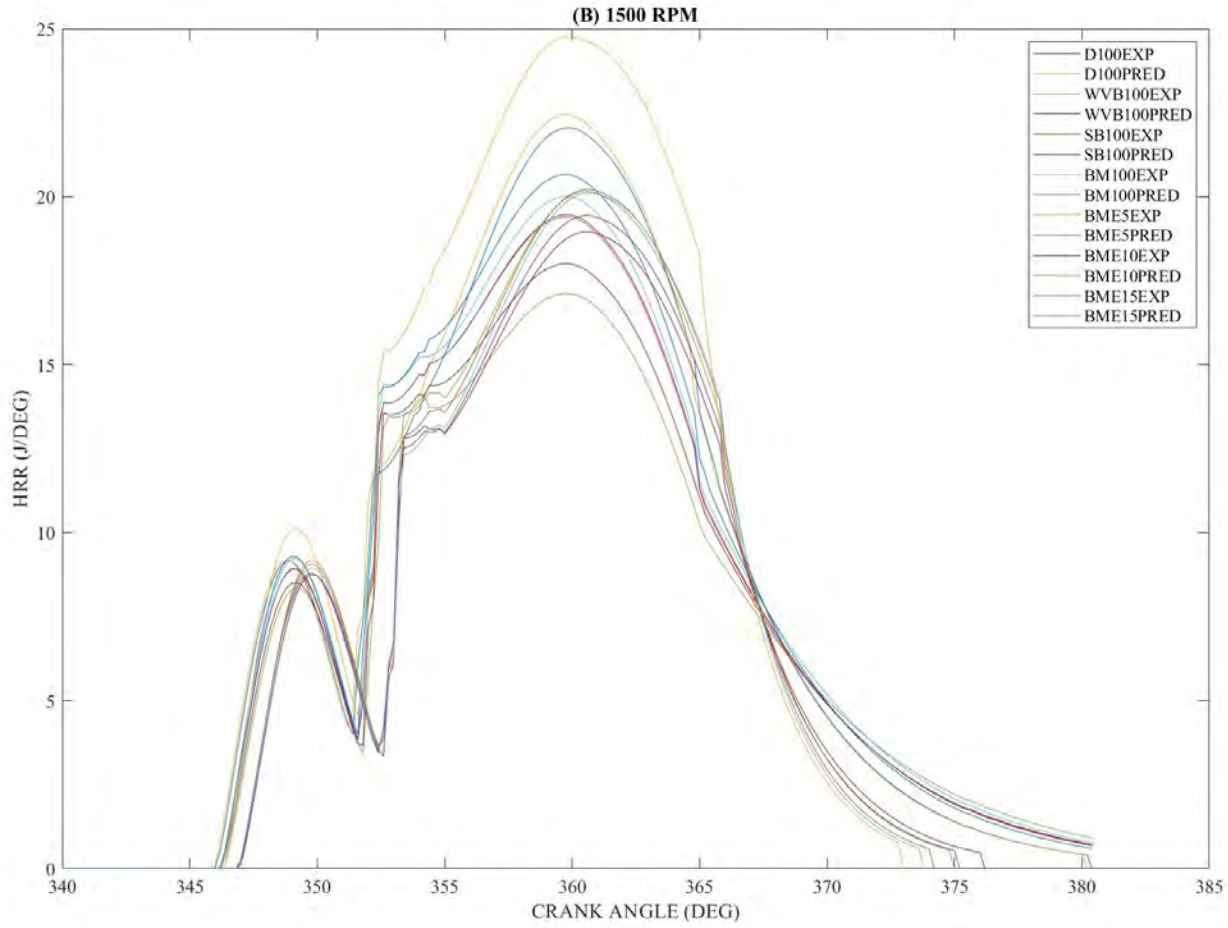
(B) 1500 RPM
HRR (J/DEG)
CRANK ANGLE (DEG)
D100EXP
D100PRED
WVB100EXP
WVB100PRED
SB100EXP
SB100PRED
BM100EXP
BM100PRED
BME5EXP
BME5PRED
BME10EXP
BME10PRED
BME15EXP
BME15PRED
0
5
10
15
20
25
340
345
350
355
360
365
370
375
380
385

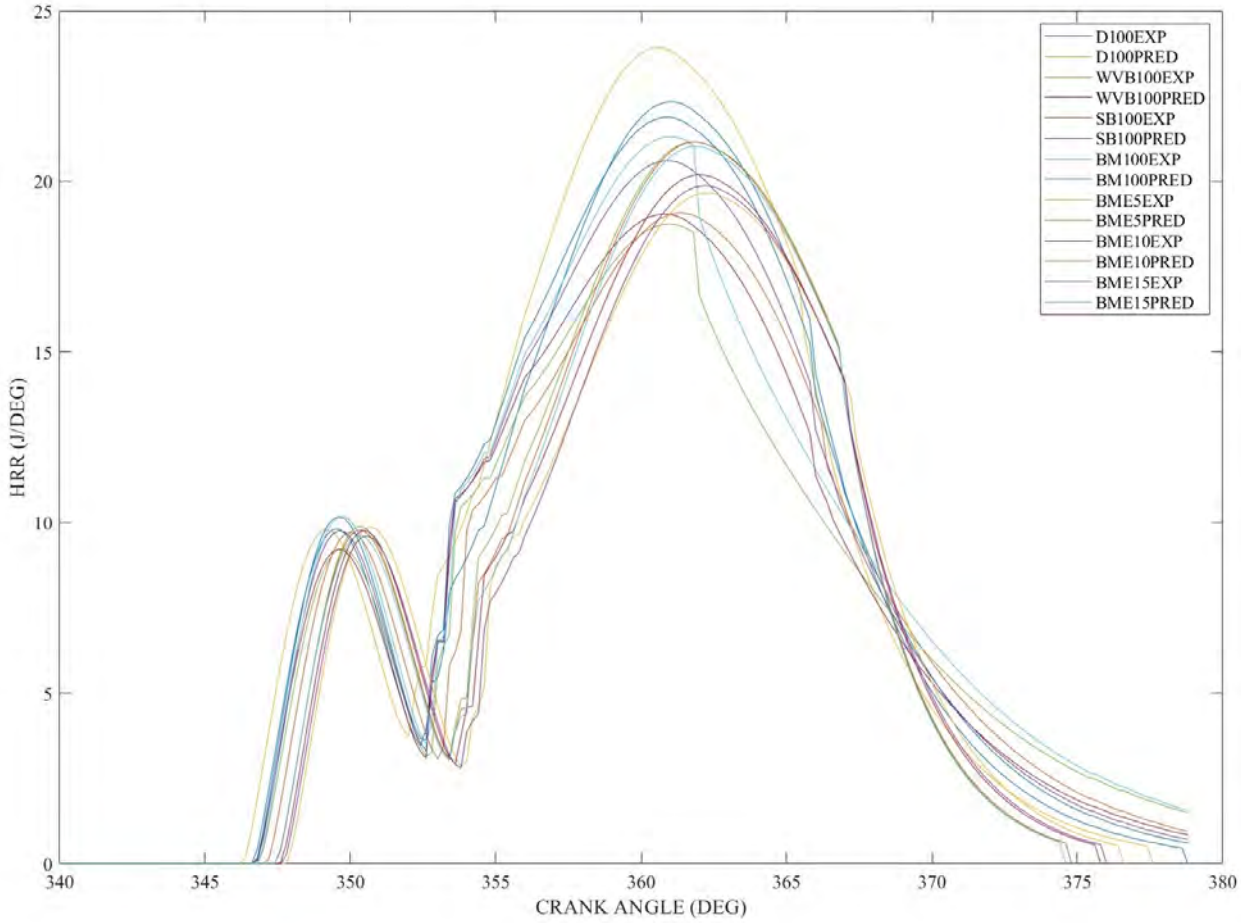
D100EXP
D100PRED
WVB100EXP
WVB100PRED
SB100EXP
SB100PRED
BM100EXP
BM100PRED
BME5EXP
BME5PRED
BME10EXP
BME10PRED
BME15EXP
BME15PRED
HRR (J/DEG)
CRANK ANGLE (DEG)
0
5
10
15
20
25
340
345
350
355
360
365
370
375
380

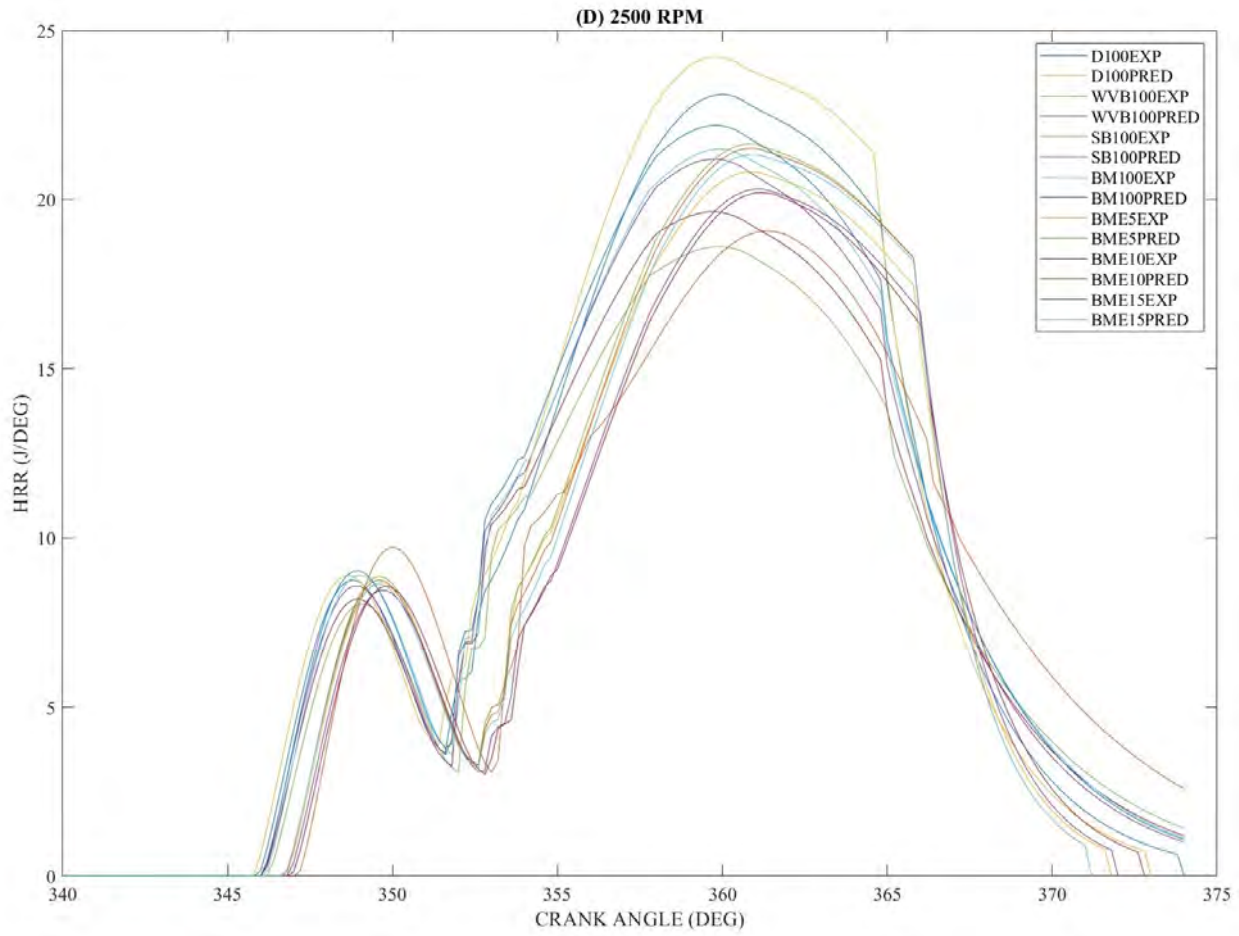

Figure 5.1: Comparison of the heat release rate of Diesel-RK prediction and experimental data.

The heat release rate helps to distinguish the point where the combustion starts, the amount of fuel burned in the premixed stage, and variances in fuel burning rates. The experimental data were compared with prediction data attained from Diesel-RK software as presented in Figure 5.1. In both cases, D100 attained the highest values of heat release at all engine speeds due to high energy content leading to better combustion (Yesilyurt et al., 2020). At 1000 rpm, the percentage error among the measured and predicted was recorded at a range of 0.9% for SB100 and 20.8% for D100. At 1500 rpm, the percentage error among measured and predicted was recorded at a range of 1.7% for D100 and 18.6% for BME5. At 2000 rpm, the percentage error among measured and predicted was recorded at a range of 1.6% for WVB100 and 10.8% for SB100. At 2500 rpm, the percentage error among measured and predicted was recorded at a range of 3.2% for BM100 and 11.9% for SB100. Furthermore, both cases followed a similar pattern of the curve for heat release

rate. The simulation results for Diesel-RK seemed to have predicted maximum values compared to experimental values from the minimum to maximum speed.

5.1.2 In-Cylinder Pressure

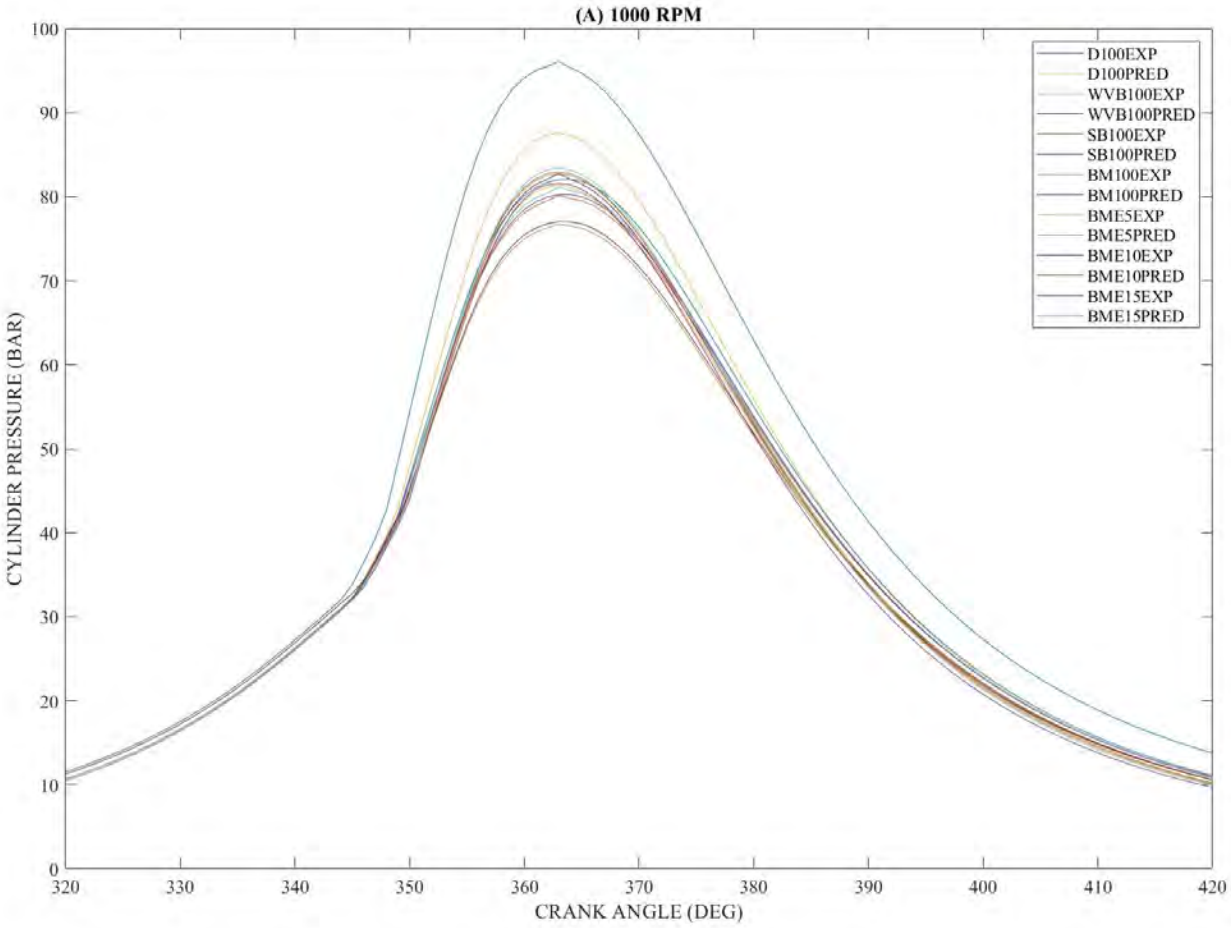

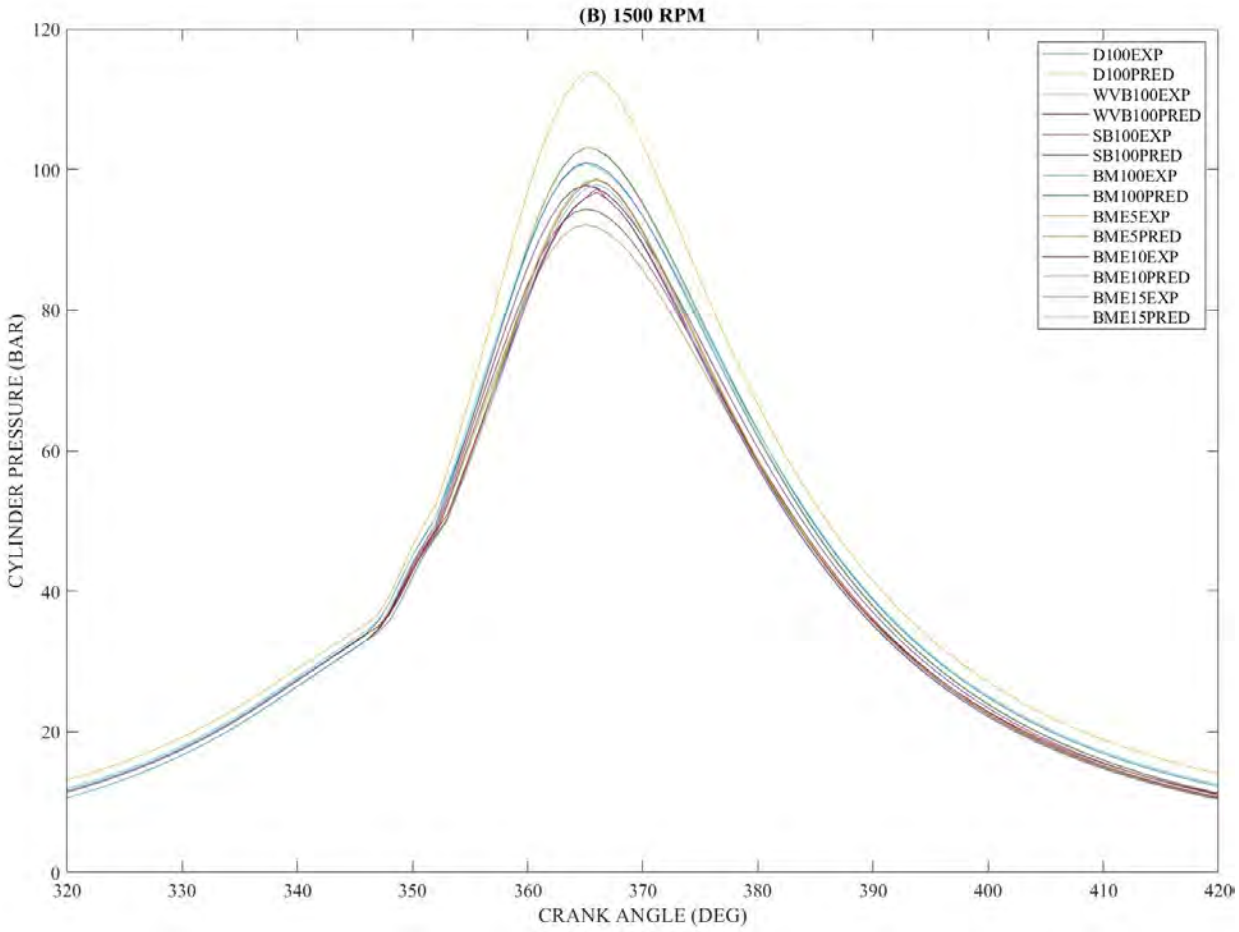
(B) 1500 RPM
D100EXP
D100PRED
WVB100EXP
WVB100PRED
SB100EXP
SB100PRED
BM100EXP
BM100PRED
BME5EXP
BME5PRED
BME10EXP
BME10PRED
BME15EXP
BME15PRED
CYLINDER PRESSURE (BAR)
CRANK ANGLE (DEG)
0
20
40
60
80
100
120
320
330
340
350
360
370
380
390
400
410
420

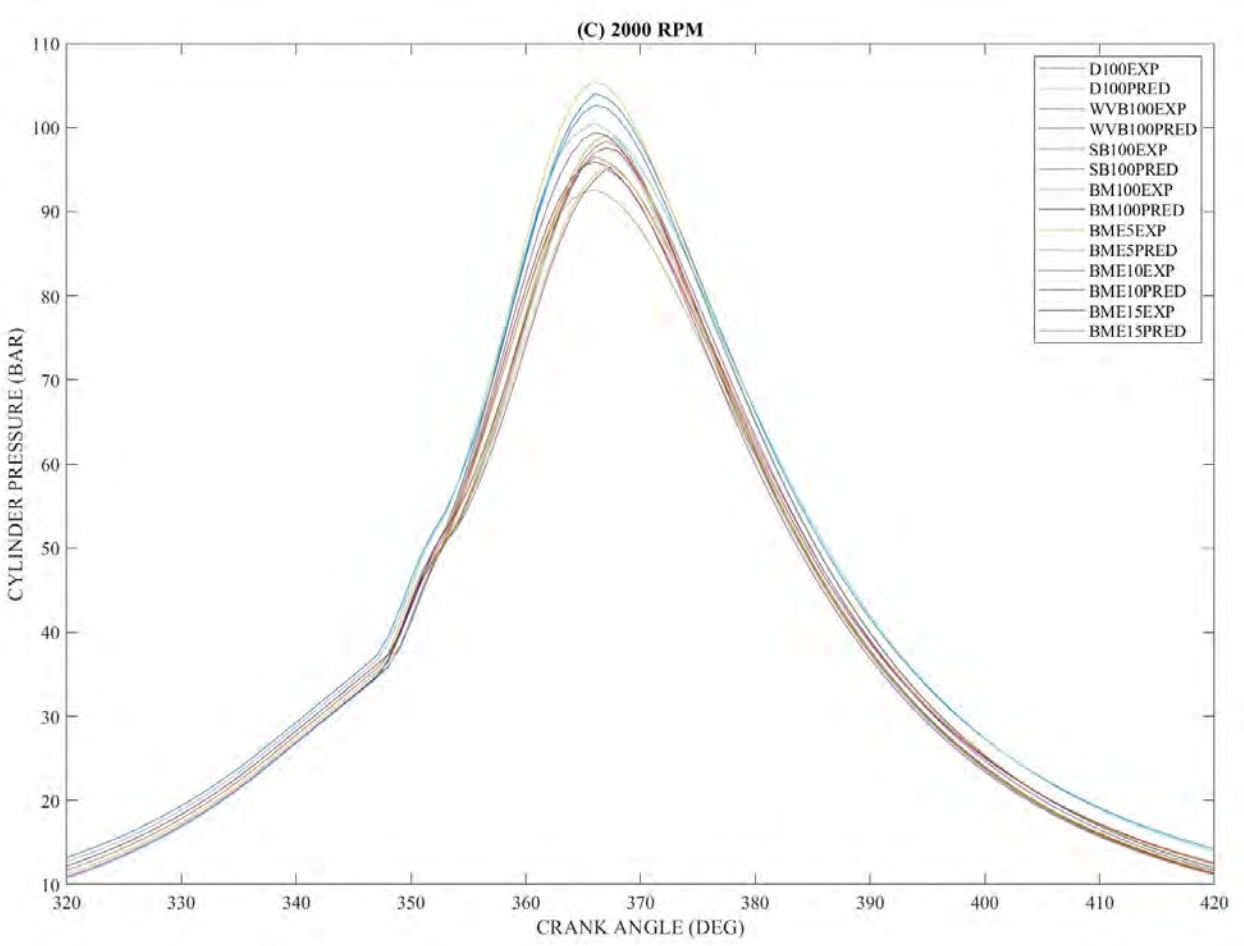
(C) 2000 RPM
CYLINDER PRESSURE (BAR)
CRANK ANGLE (DEG)
D100EXP
D100PRED
WVB100EXP
WVB100PRED
SB100EXP
SB100PRED
BM100EXP
BM100PRED
BME5EXP
BME5PRED
BME10EXP
BME10PRED
BME15EXP
BME15PRED

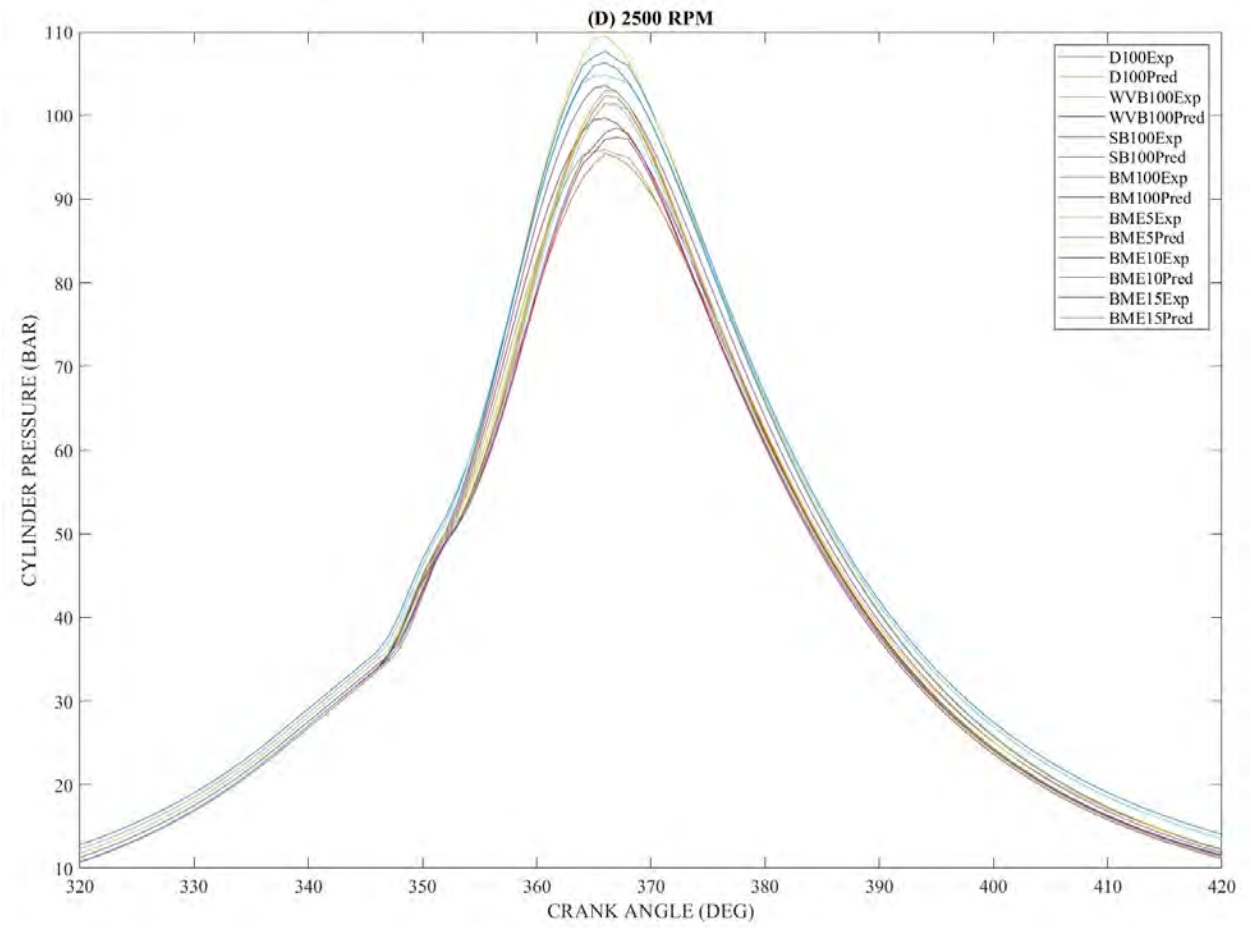

Figure 5.2: Comparison of in-cylinder pressure of Diesel-RK prediction and experimental data.

Figure 5.2 shows the variation of in-cylinder pressure for D100, WVB100, SB100, BM100, BME5, BME10, and BME15 with different crank angles. The experimental and prediction data of in-cylinder pressure with various crank angles for D100, WVB100, SB100, BM100, BME5, BME10, and BME15 shows that D100 attained the maximum cylinder pressure of 107.67 bar and 109.5 bar at a maximum speed of 2500 rpm. The prediction and experimental data for in-cylinder pressure are close to each other. Comparable reports were also emphasized by Kaplan et al. (2006) and by Enweremadu et al. (2022), and the slight discrepancy between the experimental and predicted values can be assigned to marginal losses in the pumping and friction. At 1000 rpm, the minimum and maximum percentage error among measured and predicted was recorded at a range of 0.17% for SB100 and 8.9% for D100. At 1500 rpm, the percentage error among measured and predicted was recorded at 0.02% for D100 and 13.4% for BME5. At 2000 rpm, the percentage

error among measured and predicted was recorded at a range of 0.9% for BME10 and 3.9% for SB100. At 2500 rpm, the percentage error among measured and predicted was recorded at a range of 1.4% for BM100 and 7.9% for SB100. Furthermore, at 2500 rpm, Diesel-RK predicted the maximum data compared to those achieved from the experimental data. It can be found from the graph that the experimental and predicted values match well as most of the data are within the 10% error. Overall, the Diesel-RK software appears to predict higher values than the experimental values. The in-cylinder pressure graphs for the predicted and experimental followed a similar pattern of pressure profile.

5.1.3 Brake Power

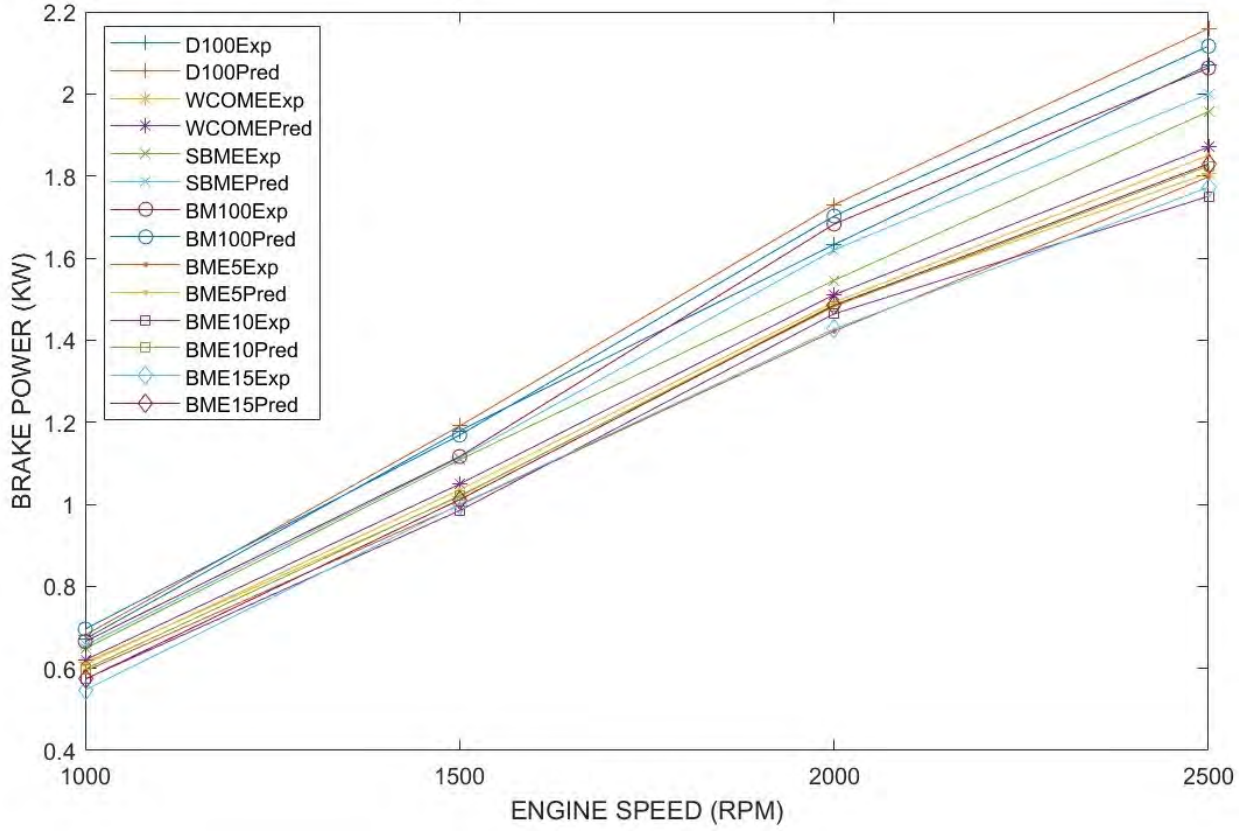

Figure 5.3: Comparison of brake power of Diesel-RK prediction and experimental data.

Figure 5.3 presents the variation for brake power of D100, WVB100, SB100, BM100, BME5, BME10, and BME15 from different speeds. The BP graph shows similar trends both from experimental data and prediction data. Furthermore, the prediction results attained the maximum values compared with experimental results. This might be caused by the engine used to perform

the tests, which had a reduced power output over the years (Enweremadu et al., 2022). The graph showed that the experimental and prediction data for D100 attained the maximum values compared to all testing fuel samples at all engine speeds. This can be attributed to the low heating value, low cetane number, and higher latent heat of evaporation among the individual biodiesels, hybrid biodiesel, and ethanol blends (Can et al., 2004, Maki and Shahad, 2020). At 1000 rpm, the percentage error measured and predicted was recorded at a range of 1.0% for WVB100 and 4.6% for BME15. At 1500 rpm, the percentage error measured and predicted was recorded at 0.5% for SB100 and 4.5% for BM100. At 2000 rpm, the percentage error among measured and predicted was recorded at a range of 1.2% for BM100 and 5.9% for D100. At 2500 rpm, the percentage error among measured and predicted was recorded at a range of 2.2% for SB100 and 4.1% for D100. The graph also shows that the experimental and prediction percentage error match well as much of the data are within the range of 5% error. This shows that the prediction tool can be used to evaluate the engine characteristics fuelled with various fuel blends.

5.1.4 Brake-Specific Fuel Consumption

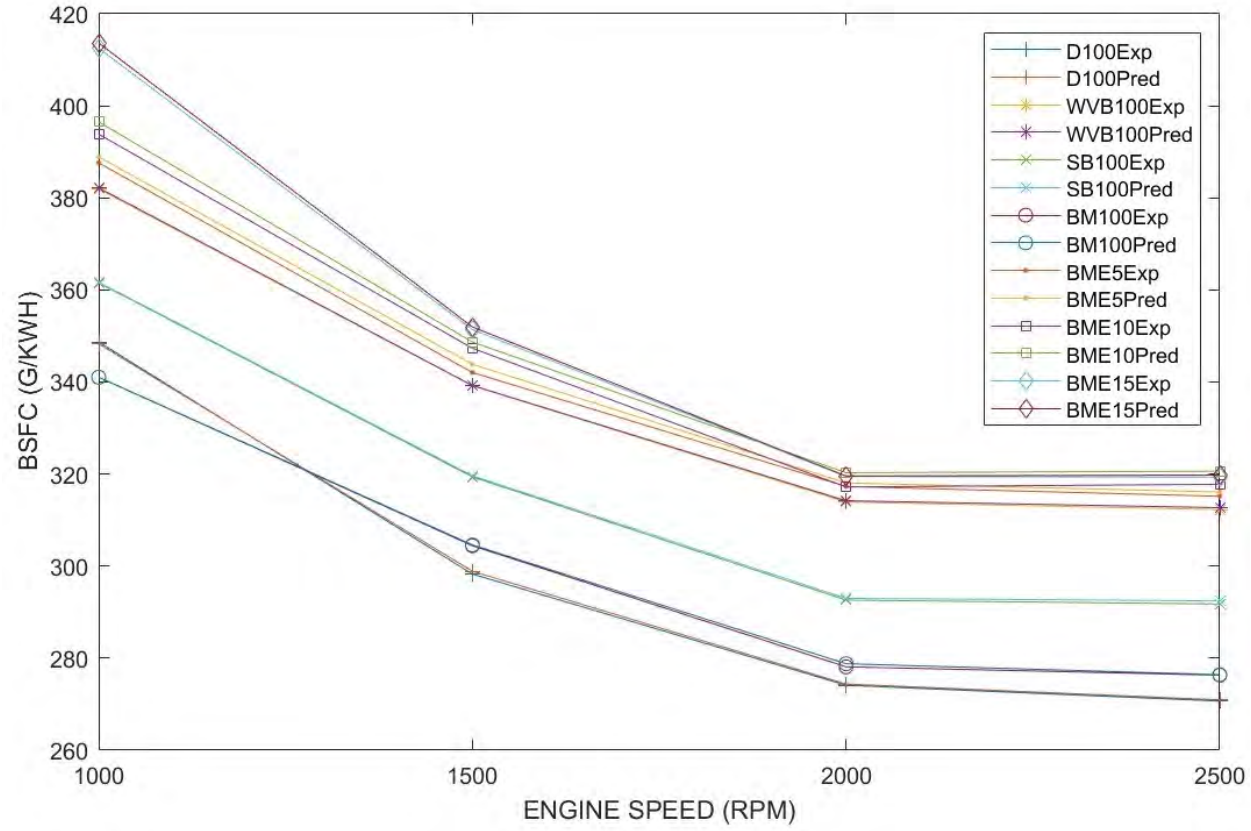

Figure 5.4: Comparison of brake-specific fuel consumption of Diesel-RK prediction and experimental data.

The brake-specific fuel consumption is a vital aspect for evaluating the performance of the engine fuelled with alternative fuel. Figure 5.4 illustrates the experimental and prediction for BSFC of the diesel engine fuelled with D100, WVB100, SB100, BM100, BME5, BME10, and BME15. The experimental and prediction data showed that the individual biodiesels, hybrid biodiesel, and its ethanol blends increased BSFC compared to standard diesel. At 1000 rpm, the percentage error among measured and predicted was recorded at a range of 0.01% for BM100 and 0.7% for BME10. At 1500 rpm, the percentage error among measured and predicted was recorded at a range of 0.02% for WVB100 and 0.5% for BME5. At 2000 rpm, the percentage error among measured and predicted was recorded at a range of 0.04% for BME15 and 1.0% for BME10. At 2500 rpm, percentage error among measured and predicted was recorded at a range of 0.04% for BM100 and 0.9% for BME10. The graph also shows that the experimental and prediction percentage error match well as all data are within the range of 5% error. This shows that the prediction tool can be applied to assess the engine characteristics fuelled with D100, WVB100, SB100, BM100, BME5, BME15, and BME15 at different speeds.

5.1.5 Brake Torque

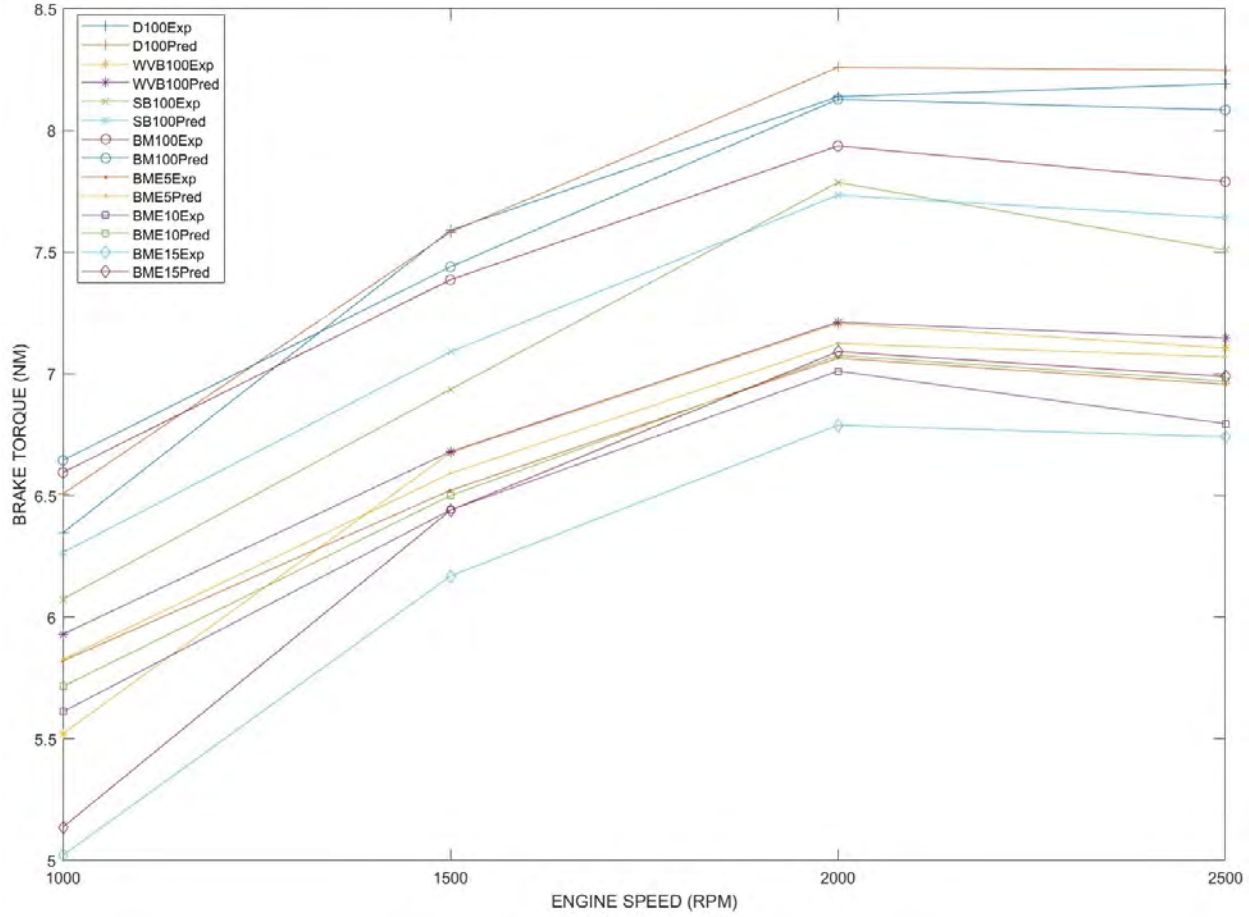

Figure 5.5: Comparison of brake torque of Diesel-RK prediction and experimental data.

Figure 5.5 presents the variation for brake torque of D100, WVB100, SB100, BM100, BME5, BME10, and BME15 fuels from different speeds. The graph shows similar trends for brake torque attained from the experimental data and prediction data from Diesel-RK software. The experimental and prediction data of D100 attained maximum BT compared to all testing fuel samples. This can be attributed to the low heating value, low cetane number, and higher viscosity among the individual biodiesels, hybrid biodiesel, and ethanol blends (Kandasamy et al., 2019, Ramuhaheli et al., 2022). At 1000 rpm, the percentage error among measured and predicted was recorded at a range of 0.1% for BME5 and 6.9% for WVB100. At 1500 rpm, the percentage error between measured and predicted was recorded at 0.07% for WVB100 and 4.2% for BME15. At 2000 rpm, the percentage error among measured and predicted was recorded at a range of 0.08% for WVB100 and 4.3% for BME15. At 2500 rpm, percentage error among measured and predicted

was recorded at a range of 0.6% for WVB100 and 3.6% for BM100. At the maximum speed condition, the data obtained by the prediction for Diesel-RK software were marginally higher compared to those attained from the data analysis of experimental results. The figure shows that most experimental and prediction percentage errors match well as all data are within the range of 5% error.

5.1.6 Brake Thermal Efficiency

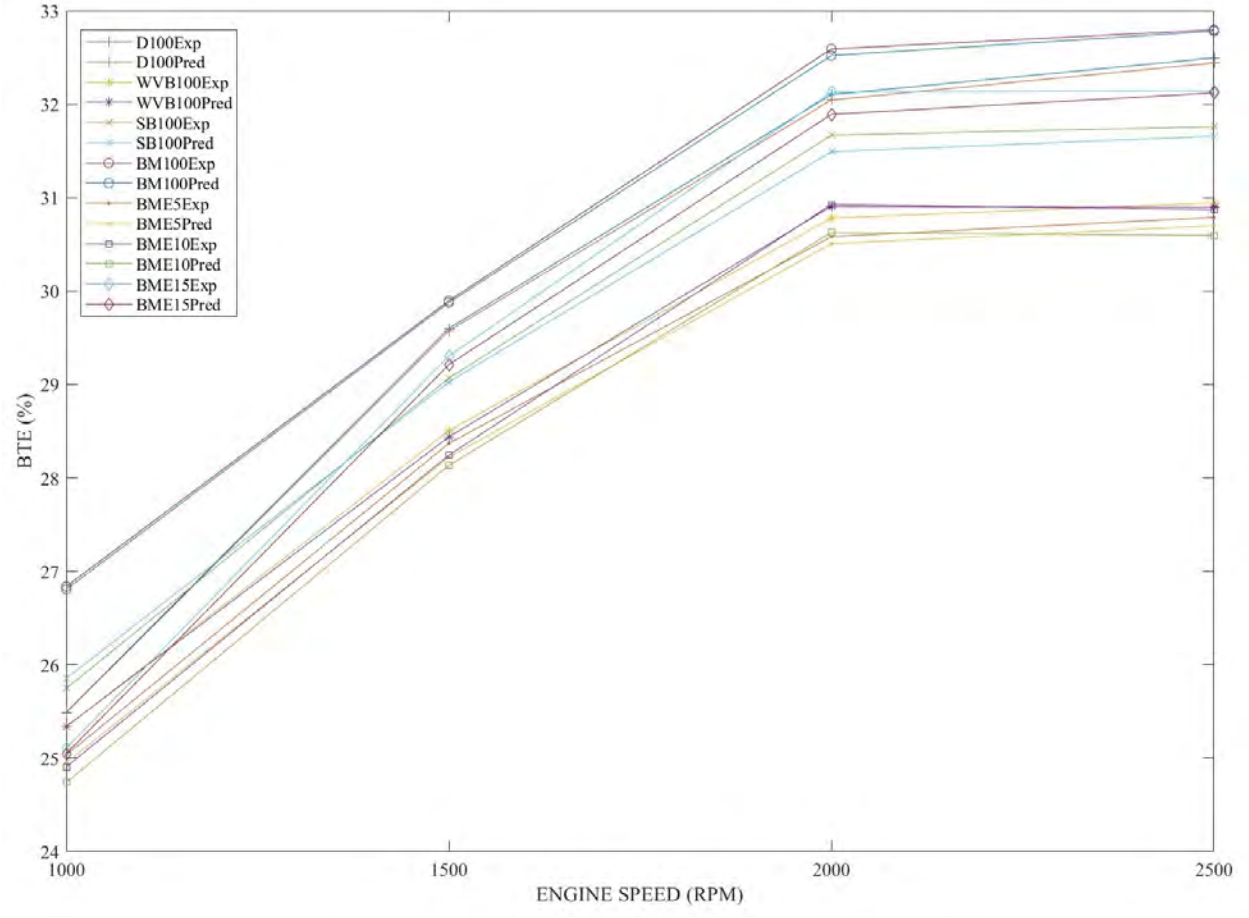

Figure 5.6: Comparison of brake thermal efficiency of Diesel-RK prediction and experimental data.

The variation for brake thermal efficiency of D100, WVB100, SB100, BM100, BME5, BME10, and BME15 at different engine speeds are shown in Figure 5.6. The experimental and prediction data showed that all the test fuels increase with an increase in engine speed (Dhamodaran et al., 2017. At 1000 rpm, the percentage error among measured and predicted was recorded at a range

of 0.01% for WVB100 and 0.7% for BME10. At 1500 rpm, the percentage error among measured and predicted was recorded at a range of 0.07% for BM100 and 0.5% for BME5. At 2000 rpm, the percentage error among measured and predicted was recorded at a range of 0.2% for D100 and 0.9% for BME10. At 2500 rpm, the percentage error among measured and predicted was recorded at a range of 0.04% for BM100 and 0.9% for BME10. At all engine speeds, the majority of the Diesel-RK predicted lower values compared to those achieved from the experimental data. Overall, the experimental and predicted values match well as most of the data are within 5% error.

5.1.7 Brake Mean Effective Pressure

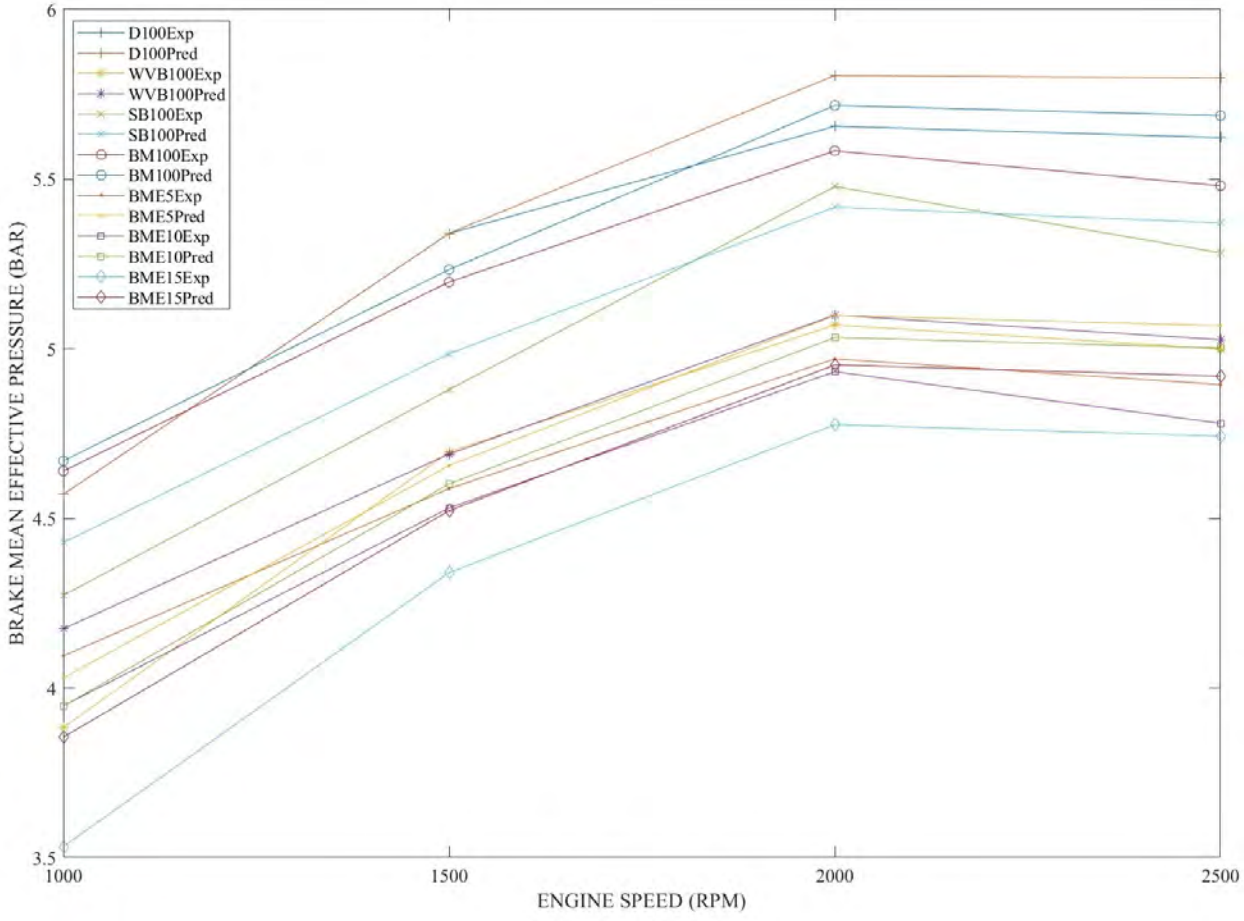

Figure 5.7: Comparison of brake mean effective pressure of Diesel-RK prediction and experimental data.

Figure 5.7 illustrates the experimental and prediction for BMEP of the diesel engine fuelled with D100, WVB100, SB100, BM100, BME5, BME10, and BME15 at various speeds. The results

show that among the biodiesel fuels, the experimental and prediction value of BM100 exhibited the highest BMEP value while BME15 had the lowest. Both experimental and predictive, D100 attained the maximum value within all the tested fuels at all engine speeds. Similar kind of results were stated by (Rajak et al., 2021). At 1000 rpm, the percentage error among measured and predicted was recorded at a range of 0.0% for D100 and 8.4% for BME15. At 1500 rpm, the percentage error measured and predicted was recorded at 0.01% for D100 and 4.0% for BME15. At 2000 rpm, the percentage error among measured and predicted was recorded at a range of 0.6% for WVB100 and 3.6% for BME15. At 2500 rpm, the percentage error among measured and predicted was recorded at a range of 0.5% for WVB100 and 4.4% for BME10. It may be seen from the graph that the experimental and predicted values match well as most of the data are within the range of 5% error. The prediction tool could be used to assess the engine characteristics fuelled with different fuel blends at different speeds. Nonetheless, both the predicted and experimental followed a similar trend for BMEP with engine speed.

5.1.8 CO_2 Emissions

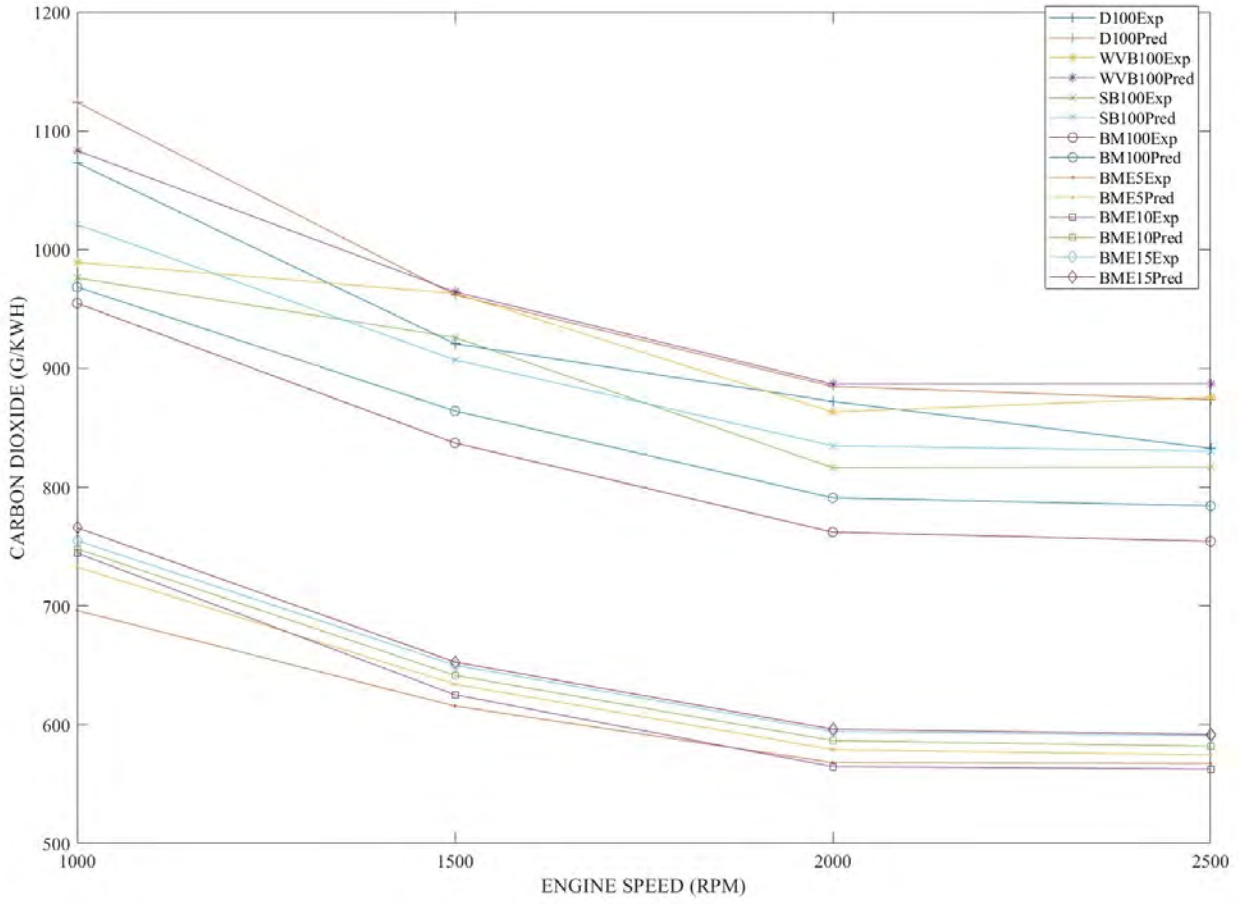

Figure 5.8: Comparison of CO_2 emissions of Diesel-RK prediction and experimental data.

Figure 5.8 shows the variation for CO_2 emission of D100, WVB100, SB100, BM100, BME5, BME10, and BME15 from different speeds. The results show that Diesel-RK prediction values were slightly higher than experimental results at the minimum speed and maximum speed. At 1000 rpm, the percentage error between measured and predicted was recorded at a range of 0.5% for BME10 and 8.7% for WVB100. At 1500 rpm, the percentage error between measured and predicted was recorded at a range of 0.1% for WVB100 and 4.2% for D100. At 2000 rpm, the percentage error between measured and predicted was recorded at a range of 0.3% for BME15 and 3.7% for BME10. At 2500 rpm, the percentage error between measured and predicted was recorded at a range of 0.2% for BME15 and 4.7% for D100. In addition, the experimental and predicted values match well as most of the data are within the range of 5% error. This shows that

the prediction tool can be used to evaluate the emission characteristics of different fuel blends at different speeds of the engine.

5.1.9 NO Emissions

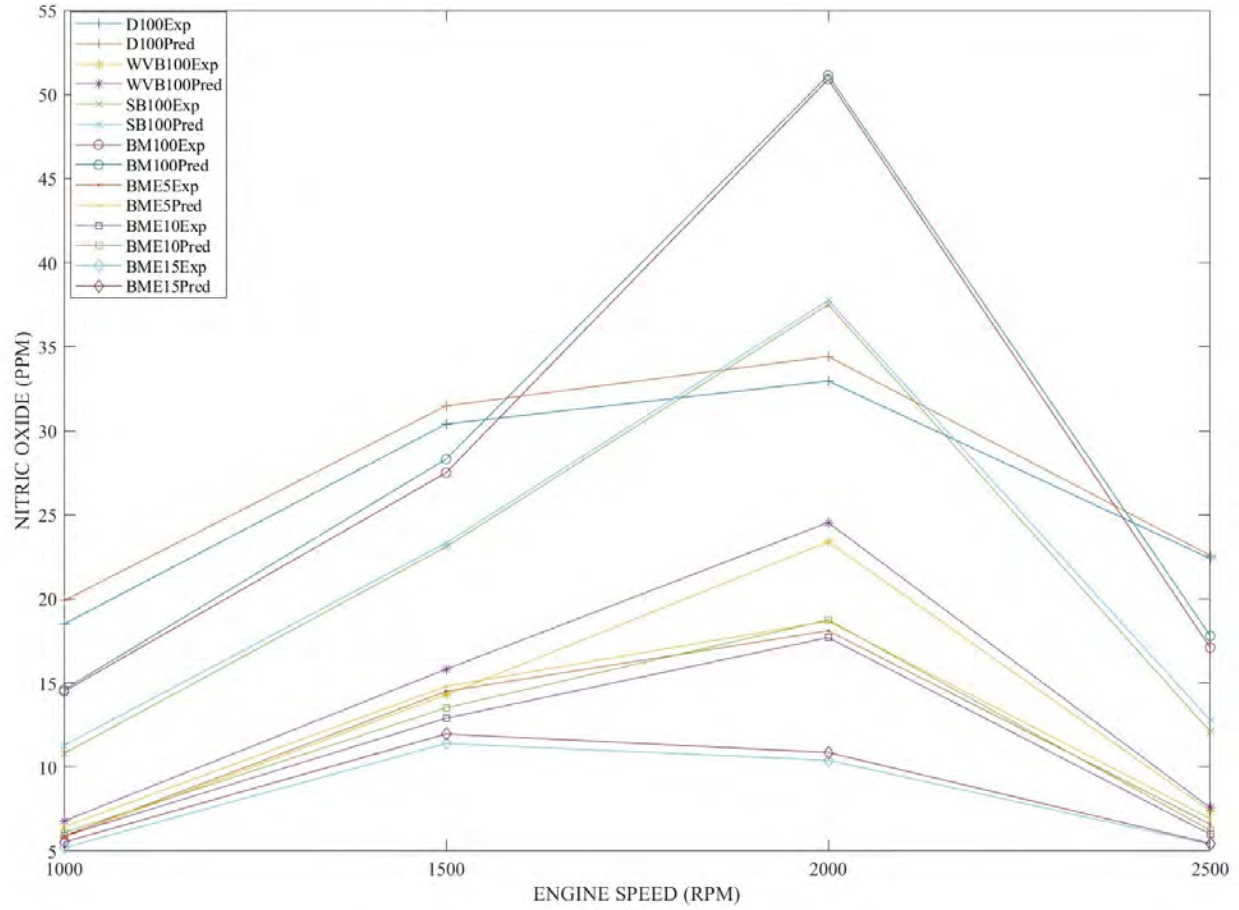

Figure 5.9: Comparison of NO emissions of Diesel-RK prediction and experimental data.

Figure 5.9 shows the variation of NO emission for D100, WVB100, SB100, BM100, BME5, BME10, and BME15 from different speeds. The results show that, at the maximum engine speed, the experimental and prediction data of Diesel-RK for BME15 attained the lowest value compared to all tested fuel samples. This is consistent with earlier findings for biodiesel-ethanol blends in the literature (Yilmaz and Sanchez, 2012; Venkata and Raja, 2011). The experimental and predicted values of all hybrid biodiesel-ethanol blends decrease NO emissions compared to biodiesel mixture, individual biodiesels, and standard diesel fuel at the minimum and maximum speed. At 1000 rpm, the percentage error between measured and predicted was recorded at a range

of 0.7% for BM100 and 14.5% for WVB100. At 1500 rpm, the percentage error between measured and predicted was recorded at 0.9% for SB100 and 9.6% for WVB100. At 2000 rpm, the percentage error between measured and predicted was recorded at a range of 0.5% for BM100 and 5.6% for BME10. At 2500 rpm, the percentage error between measured and predicted was recorded at a range of 0.8% for D100 and 5.3% for SB100. The simulated values show a similar pattern with the experimental values although the simulation shows slightly higher emissions compared to experimental data.

5.1.10 Bosch Smoke Number Emissions

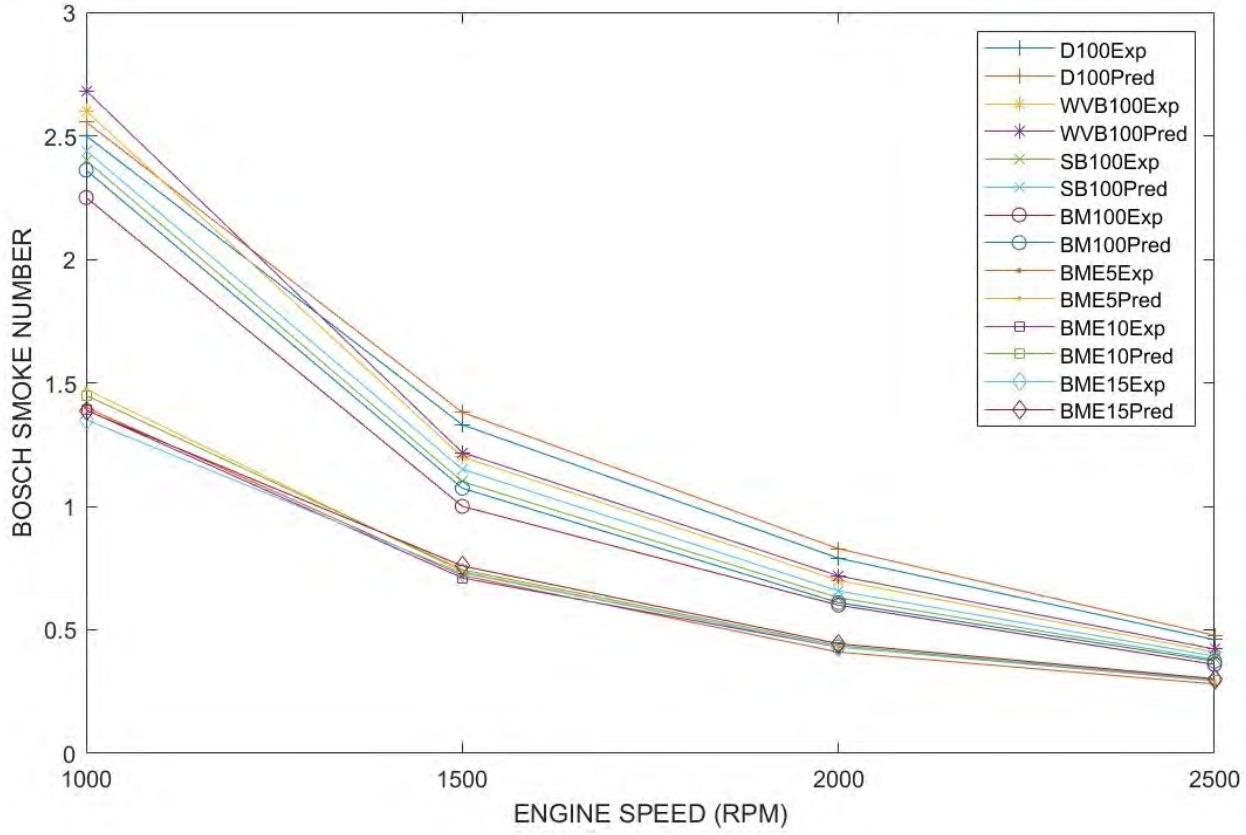

Figure 5.10: Comparison of Bosch smoke number emissions of Diesel-RK prediction and experimental data.

Figure 5.10 graphically presents the variation of Bosch smoke number emissions of a diesel engine fuelled with D100, WVB100, SB100, BM100, BME5, BME10, and BME15 from different speeds. It was noted from the figure that the predicted values of all fuel samples at the minimum and maximum speed attained higher values compared to experimental values. At 1000 rpm, the

percentage error between measured and predicted was recorded at a range of 1.6% for SB100 and 5.0% for BME5. At 1500 rpm, the percentage error between measured and predicted was recorded at 1.5% for WVB100 and 7.3% for BM100. At 2000 rpm, the percentage error between measured and predicted was recorded at a range of 1.5% for BME10 and 4.7% for BME5. At 2500 rpm, the percentage error between measured and predicted was recorded at a range of 0.7% for D100 and 4.1% for SB100. It is apparent from the graph that the experimental and predicted values match well as most of the data are within the range of 5% error.

5.2 Summary of Chapter Five

In general, there were differences between in values from simulation and experiments reaching up to 7% in some cases. In most cases, there will always be differences between simulation and experimental results. The experimental results are based on real time systems, provide much accurate results compared to simulation results. Obtaining the results from the experimental set up that will equal simulation results is always a challenge. The difference is there due to the errors occurred from external disturbances, instrument, human errors, procedural errors, equipment manufacturing errors, etc. On the other hand, the software used may have presumptions that are not properly defined. Simulations and experiments are complementary not competitive approaches and validations may not always bring their values to be the same. If the simulation results are assumed to be exact and based on theoretical concepts, and seem better than the experimental results, one possible way to resolve the difference is to modify the experimental conditions and experiment again.

The combustion, performance, and emission characteristics of individual biodiesels, hybrid biodiesel (biodiesel-biodiesel), and hybrid biodiesel-ethanol blends (biodiesel-biodiesel-ethanol) were assessed both experimentally and numerically. No major variations were detected among the engine parameters of D100, WVB100, SB100, BM100, BME5, BME10, and BME15. The combustion parameters (HRR and ICP) are close to each other due to their comparable properties. The Diesel-RK simulation model prediction data are higher compared to experimental data for HRR, ICP, BP, BT, BSFC, BMEP, and all emission characteristics. All performance, combustion, and exhaust gas emissions graphs for experimental and prediction followed a similar pattern.

CHAPTER SIX

6.0 General discussions and future perspective

6.1 Introduction

This chapter presents an abridged yet holistic discussion on combustion, performance, and emission characteristics of a diesel engine fuelled with biodiesel mixture and alcohol blends relative to the stated objectives of this thesis, conclusions reached, and recommendations for further studies.

6.2 General Discussion

The results of the characterization, combustion, performance, and exhaust gas emissions of the diesel engine were shown in Chapter 3. The properties of the fuel such as density, viscosity, flash point, and heating value for diesel, individual biodiesels, biodiesel mixture, and ethanol blends were measured. However, the fuel samples of WVB100, SB100, and BM100 greatly increased the density, viscosity, flash point, and heating value while the ethanol blends fuel significantly decreased the density, viscosity, flash point, and heating value. The D100 attained the lowest viscosity, density, and flash point compared to all testing fuel samples although the heating value attained the maximum value compared to other testing fuels.

The experimental performance of the diesel engine powered by WVB100, SB100, BM100, BME5, BME10, and BME15 was used and compared with standard diesel. It was identified that D100 attained the maximum brake power and brake torque compared to other tested fuels at the minimum and maximum speeds due to higher heating value. However, it was observed that the brake power of the biodiesel mixture was marginally close to standard diesel due to comparable heating values. The brake specific fuel consumption of all testing fuels was increased compared to standard diesel at the maximum speed of 2500 rpm and this increase of hybrid biodiesel-ethanol blends was due to low heating values and high volume of fuel consumed to generate the amount of power. The brake thermal efficiency of BM100 attained the highest value compared to WVB100, SB100, BME5, BME10, and BME15 at the maximum speed. This may be attributed to

better atomization during injection and the reduction in friction loss associated with higher lubricity. The brake mean effective pressure of D100 attained the maximum values compared to WVB100, SB100, BM100, BME5, BME10, and BME15 at all engine speeds due to the higher heating value of diesel fuel.

The experimental combustion results of ICP for D100 attained the highest value compared to WVB100, SB100, BM100, BME5, BME10, and BME15 at all engine speeds. This was due to higher heating value, low density, low viscosity, and better fuel atomization. However, BM100 attained the maximum value of ICP compared to individual biodiesels and biodiesel mixture-ethanol blends due to the higher calorific value of the biodiesel mixture. The hybrid biodiesel-ethanol blends exhibited higher in-cylinder pressure compared to individual biodiesels (WVB100 and SB100). This improvement is due to the higher oxygen content of ethanol to hybrid biodiesel, which promotes the combustion process. The heat release rate of D100 attained the maximum value compared to other tested fuels at all engine speeds. This was due to higher heating value and short ignition delay with improved fuel atomization due to lower viscosity. The HRR of hybrid biodiesel-ethanol blends was higher compared to individual biodiesel (WVB100 and SB100) at the minimum and maximum speed. This follows from the long ignition delay and higher oxygen content of ethanol.

The experimental emission of CO emitted by D100 was higher compared to WVB100, SB100, BM100, BME5, BME10, and BME15 at the minimum and maximum speed due to higher heating values, which increased combustion chamber temperature. The fuel samples of BME5, BME10, and BME15 attained lower NO emissions compared to all other fuels tested. This could be due to the cooling effect of ethanol blend associated with its lower heating value and higher latent heat of evaporation leading to the decrease of combustion temperature. The hydrocarbon emissions of D100 attained the maximum value compared to all tested fuels due to the A/F mixture, and low oxygen content at the maximum speed. The CO_2 emission of hybrid biodiesel and ethanol blends decreased emissions compared to WVB100, SB100, and BM100 at the maximum speed due to the high oxygen content of ethanol blends. Bosch smoke number emission of D100 attained maximum value compared to WVB100, SB100, BM100, BME5, BME10, and BME15 at the minimum and maximum engine speeds due to the high amount of oxygen molecules present in the chemical

structure that assist to complete combustion within the cylinder. Fuel samples of BME5, BME10, and BME15 attained the lowest Bosch smoke number compared to all testing fuels due to higher latent heat of evaporation and low cetane amount of ethanol.

The application of Diesel-RK simulation to evaluate the engine parameters and emission characteristics was shown in Chapter 4. The in-cylinder pressure for Diesel-RK simulation of D100 attained a higher value compared to WVB100, SB100, BM100, BME5, BME10, and BME15 at the maximum speed of 2500 rpm. The decrease in other tested fuels was due to low temperature, higher latent heat of evaporation, and lower heating value. The heat release rate of BME10 and BME15 attained the maximum value compared to WVB100, SB100, BM100, and BME5 at the minimum speed of 1000 rpm. The higher latent heat of vaporization, auto-ignition temperature, and low cetane number of ethanol delayed the initiation of combustion and produced more fuel-air mixtures during ignition delay and promoted the premixed combustion process. The heat release rate of D100 attained the maximum value compared to other tested fuels at the maximum engine speed due to high energy content, which led to better combustion. The in-cylinder temperature of D100 attained the maximum value compared to WVB100, SB100, BM100, BME5, BME10, and BME15 at all engine speeds due to improved fuel atomization and lower viscosity. At the maximum speed of 2500 rpm, the fuel samples of BME5, BME10, and BME15 attained the longer ignition delay compared to D100, WVB100, SB100, and BM100 due to low cetane number of ethanol, which is far lower than that of diesel and biodiesel. The spray tip penetration of individual biodiesels and biodiesel mixture attained higher values compared to diesel and hybrid biodiesel-ethanol blends. The reason for higher spray tip penetration for biodiesel might be due to higher viscosity and surface tension, which makes biodiesel harder to break up into small droplets compared to other blended fuels. The start of combustion for BME5, BME10, and BME15 attained lower values compared to WVB100, SB100, BM100, and D100 at the maximum speed, and this decrease was due to low cetane number of ethanol. The Diesel-RK prediction for combustion duration of BME5, BME10, and BME15 attained short combustion duration compared to D100, WVB100, SB100, and BM100 at the maximum speed due to the enhancement of the premixed combustion process where more fuel is burned in premixed mode.

The Diesel-RK simulation performance for brake power and brake torque of D100 attained the maximum values compared to WVB100, SB100, BM100, BME5, BME10, and BME15 at the maximum speed due to higher heating values. The simulation for brake specific fuel consumption of WVB100, SB100, BM100, BME5, BME10, and BME15 increased compared to D100 at the maximum speed due to lower heating value. However, the BSFC of BME5, BME10, and BME15 increased compared to WVB100, SB100, BM100, and D100 throughout the entire speed due to the high amount of fuel consumed to produce the required energy. The simulation for brake thermal efficiency of BM100 attained the maximum value compared to WVB100, SB100, BME5, BME10, BME15, and D100 at the maximum speed due to combustion improvement on account of increased oxygen content. The Diesel-RK simulation of D100 attained the maximum value for brake mean effective pressure compared to WVB100, SB100, BM100, BME5, BME10, and BME15 due to the higher heating value.

The Diesel-RK simulation for CO_2 emissions of SB100, BM100, BME5, BME10, and BME15 decreased compared to D100 due to high oxygen content whereas WVB100 increased. The decreased CO2 emission from biodiesel mixture-ethanol blends follows from the high oxygen content of ethanol. The simulation for particulate matter emissions of WVB100, SB100, BM100, BME5, BME10, and BME15 decreased compared to D100 at the maximum speed due to higher volatility and low cetane number of ethanol. The Diesel-RK simulation for NO_x of WVB100 attained the lowest value compared to D100, SB100, BM100, BME5, BME10, and BME15 at the maximum speed of 2500 rpm due to the presence of native oxygen content on the chemical structure. However, hybrid biodiesel-ethanol blends attained lower NO_x emissions compared to BM100, and SB100 due to the high latent heat of vaporization. The Bosch smoke number emissions of BME5, BME10, and BME15 decreased compared to WVB100, SB100, BM100, and D100 at the maximum speed due to higher latent heat of evaporation and low cetane of ethanol.

The validation of experimental and prediction for diesel engines fuelled with various fuels is identified in Chapter 5. The in-cylinder pressure percentage error measured and predicted was recorded at a range of 1.4% for BM100 and 7.9% for SB100 at the maximum speed. The experimental and predicted values of in-cylinder pressure match well as most of the data were within the 10% error. The Diesel-RK software seems to predict higher values compared to

experimental values. The heat release rate percentage error measured and predicted was recorded at a range of 3.2% for BM100 and 11.9% for SB100 at the maximum speed. However, both cases followed a similar pattern of the curve for heat release rate. The simulation results for Diesel-RK seemed to have predicted maximum values for heat release rate compared to experimental values from minimum to maximum speed.

The brake torque percentage error measured and predicted was recorded at a range of 0.6% for WVB100 and 3.6% for BM100 at the maximum speed. At the same operating condition, the data obtained by the prediction for Diesel-RK software were marginally higher compared to those attained from the data analysis of experimental results. The brake power percentage error measured and predicted was recorded at a range of 2.2% for SB100 and 4.1% for D100 at the maximum speed condition. Those results give the impression that experimental and prediction percentage error match well as most of the data are within the range of 5% error. This shows that the prediction tool can be used to assess the engine characteristics fuelled with various fuel blends. The brake specific fuel consumption percentage error among measured and predicted was recorded at a range of 0.04% for BM100 and 0.9% for BME10 at the maximum speed condition. The experimental and prediction percentage error match well as all data are within the range of 5% error. The brake thermal efficiency percentage error measured and predicted was recorded at a range of 0.04% for BM100 and 0.9% for BME10 at the maximum speed. At all engine speeds, the majority of the Diesel-RK predicted lower values compared to those achieved from the experimental data. The brake mean effective pressure percentage error among measured and predicted was recorded at a range of 0.5% for WVB100 and 4.4% for BME10 at the maximum speed. The experimental and predicted values match well as most of the data are within the range of 5% error.

The CO_2 emission percentage error between measured and predicted was recorded at a range of 0.2% for BME15 and 4.7% for D100 at the maximum speed. The NO emission percentage error between measured and predicted was recorded at a range of 0.8% for D100 and 5.3% for SB100 at the maximum speed. The Bosch smoke number emission percentage error between measured and predicted was recorded at a range of 0.7% for D100 and 4.1% for SB100 at the maximum speed condition. It can be seen from the results that the experimental and predicted values of CO_2, NO, and smoke emissions match well, as most of the data were within the range of 5% error. The

prediction tool can be used to assess the emission characteristics of the diesel engine fuelled with different fuel blends at different speeds.

6.3 Conclusions

Based on the set objectives of this study, the following conclusions are made:

- In the fuel samples for individual biodiesels, hybrid biodiesel increased fuel properties such as density, viscosity, and flash point, whereas pure diesel and hybrid biodiesel-ethanol blends decreased the properties.
- The brake torque, brake power, and brake mean effective pressure of pure diesel attained the maximum values compared to individual biodiesels, hybrid biodiesel (biodiesel-biodiesel), and hybrid biodiesel-ethanol (biodiesel-biodiesel-ethanol) blends while the brake specific fuel consumption of all fuel blends was increased compared to pure diesel.
- The heat release rate and in-cylinder pressure of pure diesel attained the maximum values compared to other tested fuel samples.
- The CO, HC, NO, and smoke emissions of pure diesel experimentally attained the maximum values compared to other fuels tested whereas CO_2 emissions of waste vegetable biodiesel were higher compared to other fuels tested.
- The Diesel-RK simulation for D100 attained the maximum values for heat release rate, in-cylinder pressure, and in-cylinder temperature compared to other fuel tested while biodiesel mixture-ethanol blends had longer ignition period than those periods from individual biodiesels and pure diesel at the maximum speed.
- The Diesel-RK simulation for pure diesel attained the maximum values of BP, BT, and BMEP compared to other fuels tested while pure diesel attained the lowest fuel consumption at the maximum speed of 2500 rpm.
- The Diesel-RK simulation for D100 attained the highest values of particulate matter, nitrogen oxide, and Bosch smoke emissions compared to other fuels tested while CO_2 for WVB100 and NO_x for BM100 attained the maximum values compared to other fuels tested at the maximum speed.

- The Diesel-RK simulation model resulted in higher prediction data compared to experimental data for heat release rate, in-cylinder pressure, brake power, brake torque, and brake specific fuel consumption while all the curves followed similar trends.

6.4 Recommendations for Further Studies

Based on the results of the research study, the following recommendations were made:

(i) The results from this study point to the possibility of future studies involving the use of two to three component blends of biodiesel with ethanol to improve properties. Among the physicochemical properties of fuels, the focus of this study was on viscosity, density, heating value and flash point. Other important fuel properties such as oxidation stability, auto-ignition temperature, oxygen content, acid value, cetane number, etc., would need to be investigated to determine the quality of the hybrid biodiesel and hybrid biodiesel-ethanol fuels.

(ii) Experiments to assess the engine performance were conducted at full load condition at different engine speeds that range from 1000 rpm to 2500 rpm with a 500-rpm interval. This was a short-term engine test. To obtain a robust result on engine performance, a long-term engine test with effect of load variation will be required.

(iii) With the evolution of nanotechnology, a study on how nanoparticles may influence fuel consumption, combustion and emission characteristics of the hybrid biodiesel and hybrid biodiesel-ethanol fuels may have to be carried out.

(iv) The experimental and simulation studies on combustion and emission characteristics were preliminary, future research should investigate detailed modelling involving the development of physical and chemical kinetic models; research on the chemical species of the hybrid biodiesel, their blends with ethanol and how they affect combustion and emission.

APPENDICES

Appendix A: Combustion Simulation Curves

A1: In-Cylinder Pressure Curve

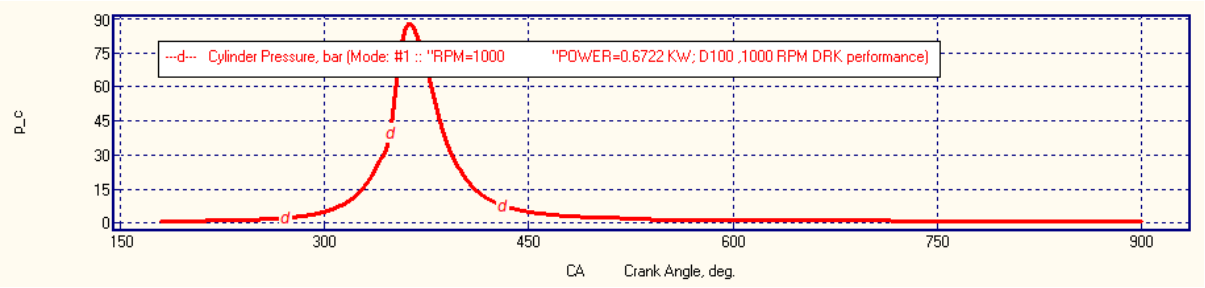

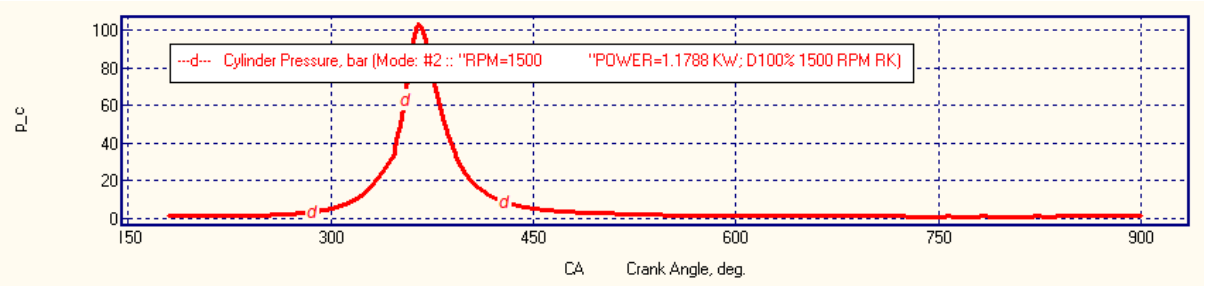

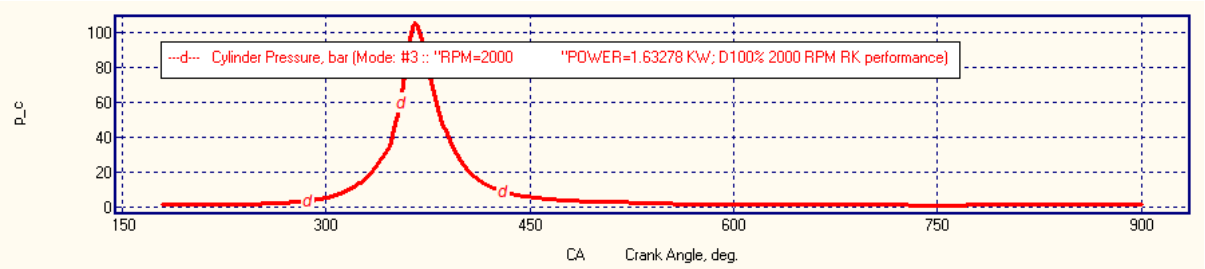

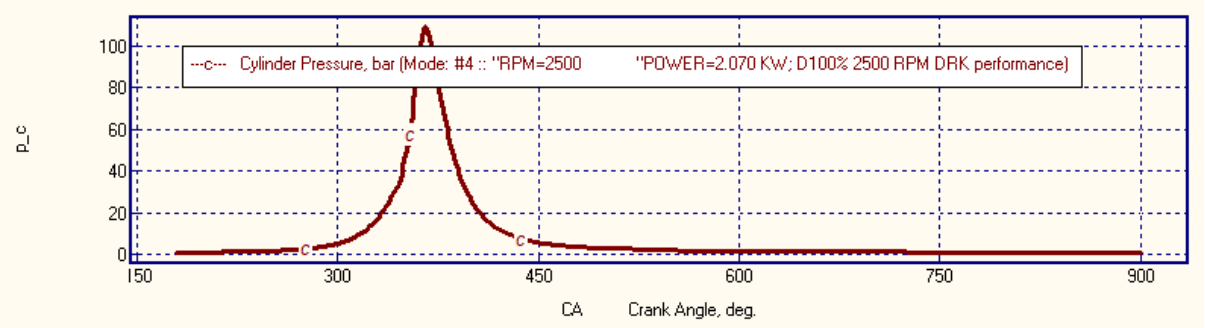

A2: Heat Release Rate Curve

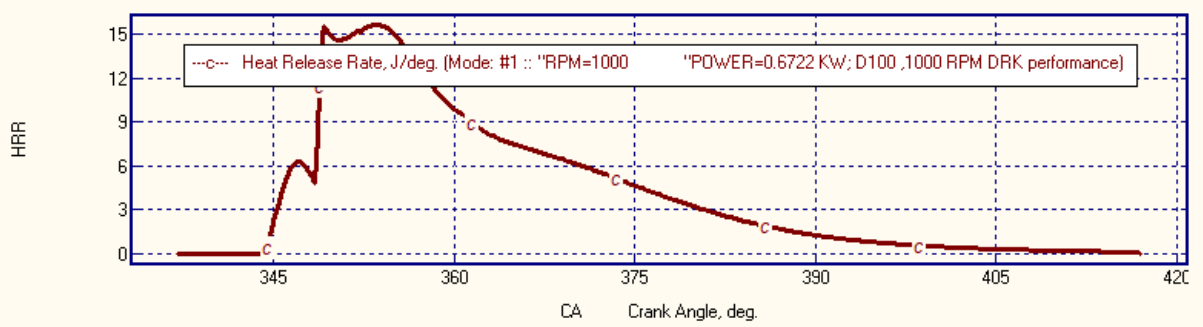

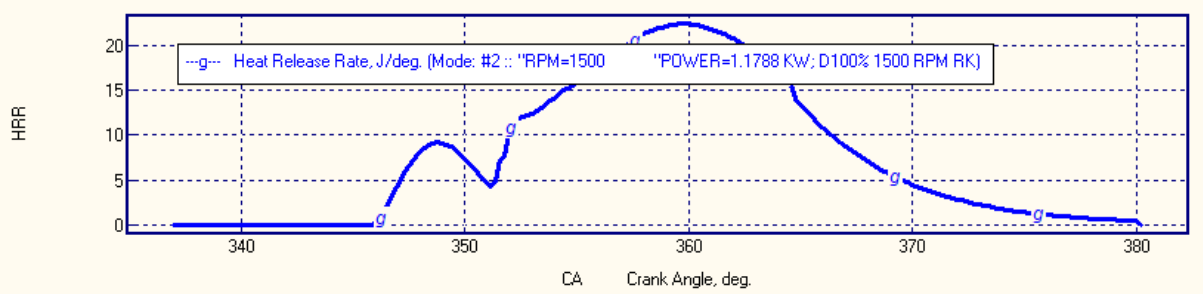

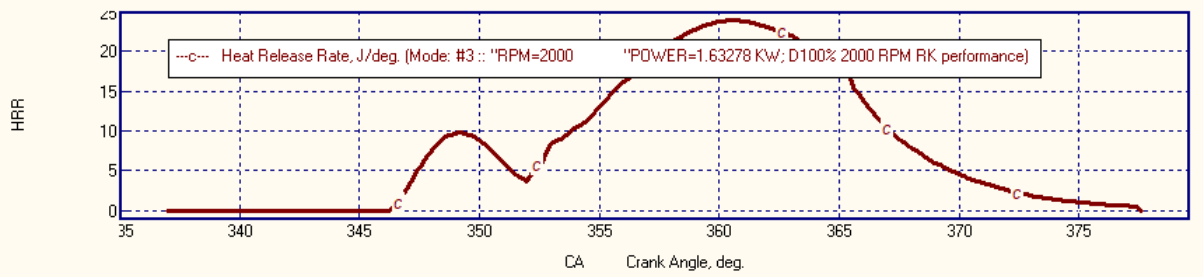

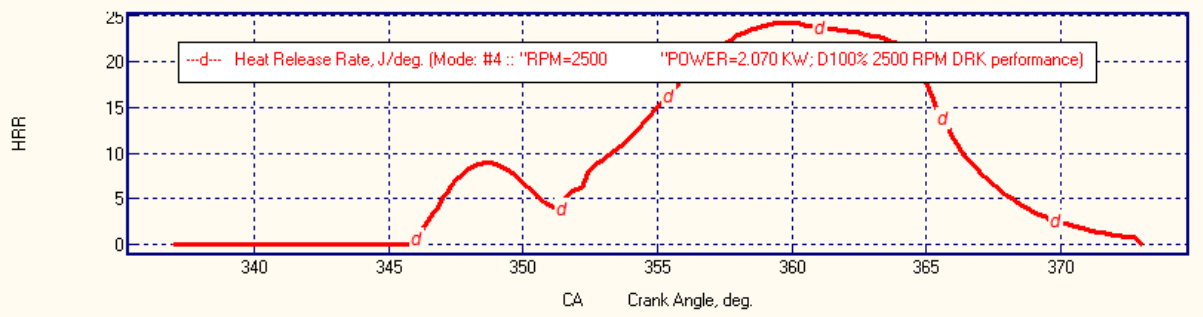

A3: In-Cylinder Temperature Curve

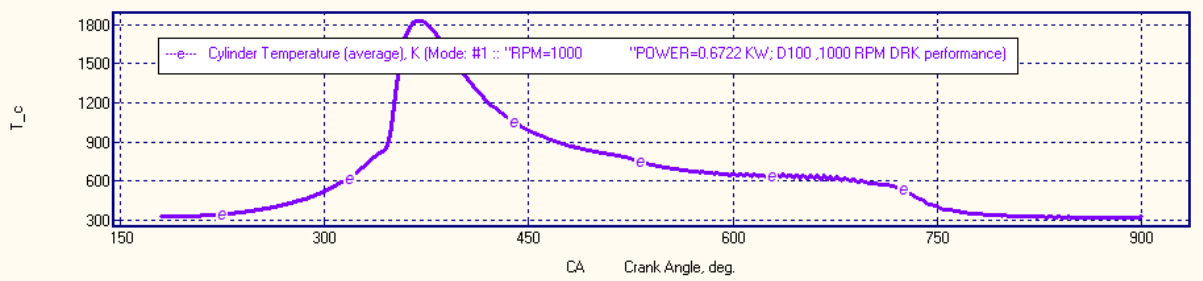

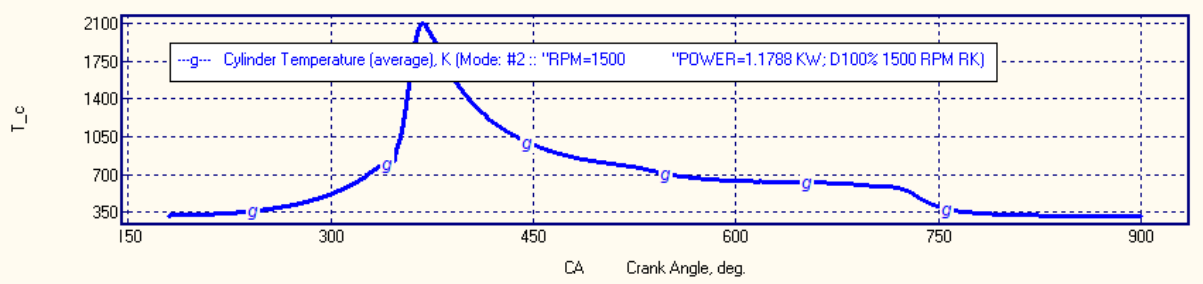

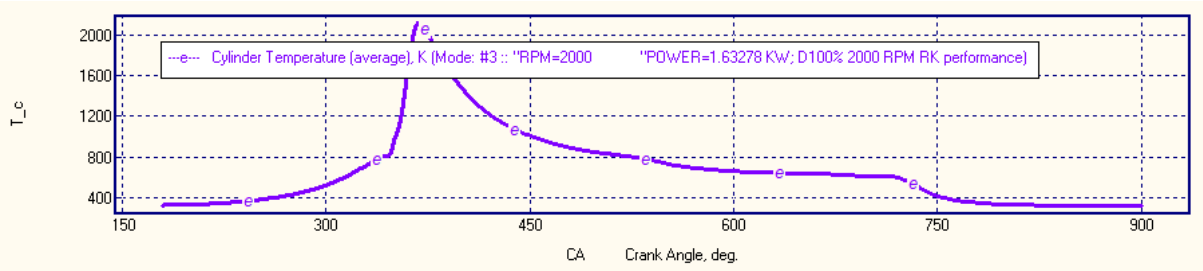

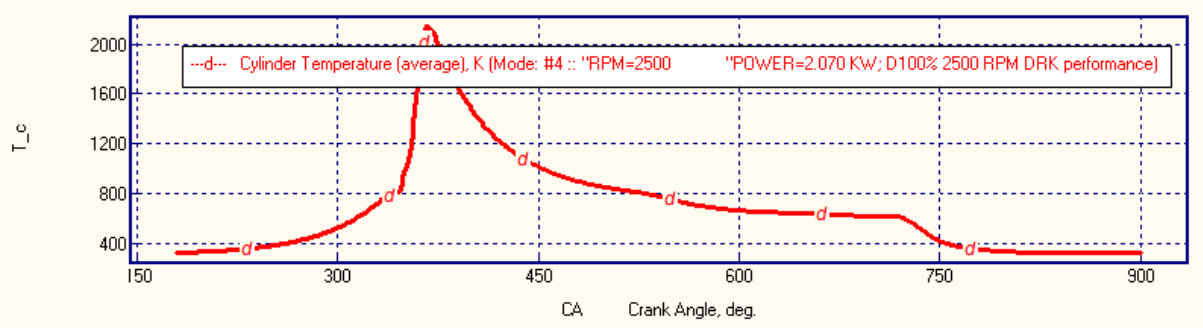

A4: Spray Tip Penetration Curve

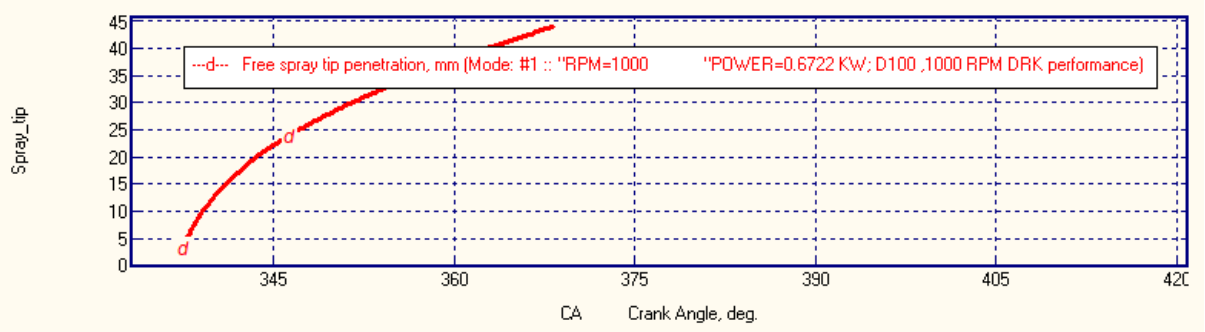

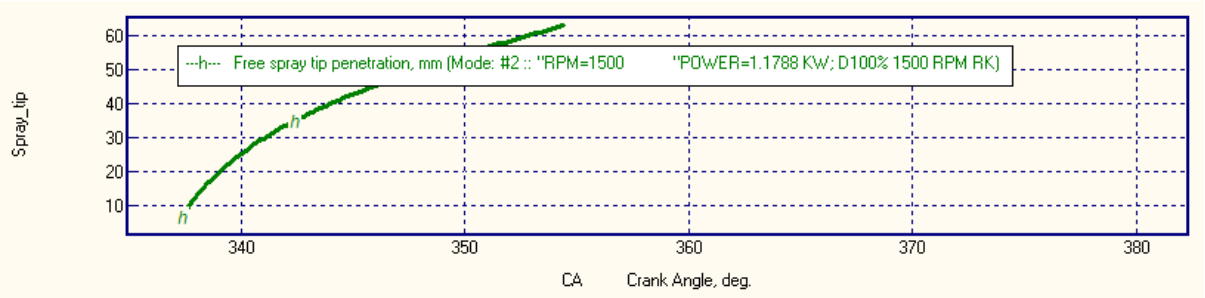

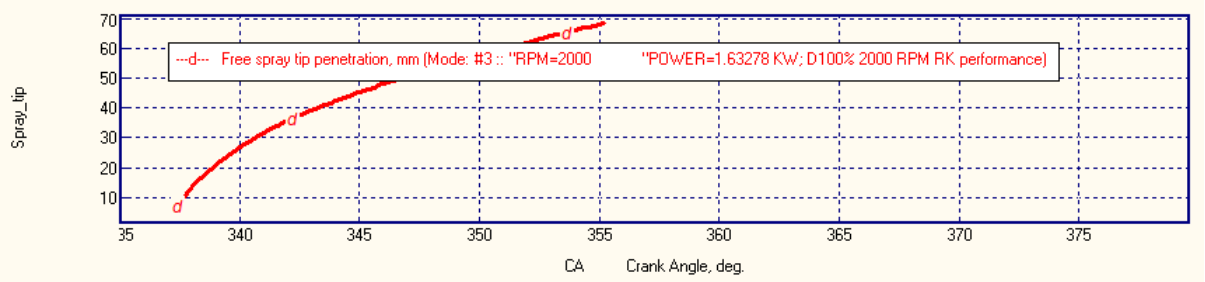

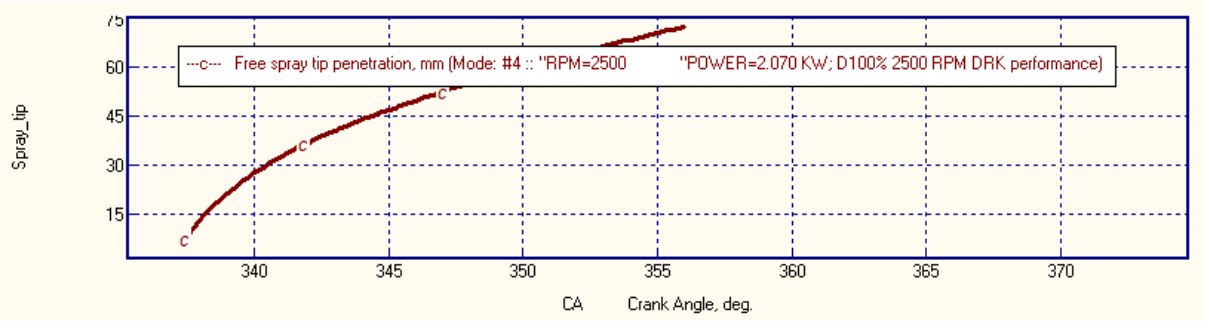

A5: Ignition Delay Period Curve

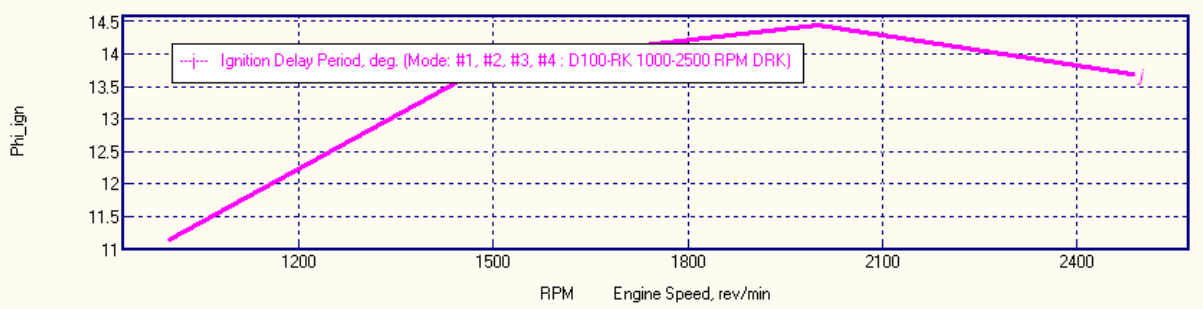

A6: Combustion Duration Curve

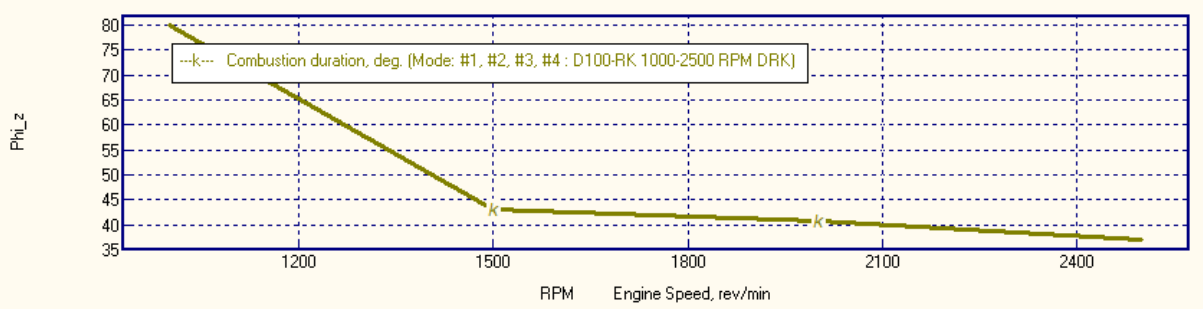

A7: Brake Mean Effective Pressure Curve

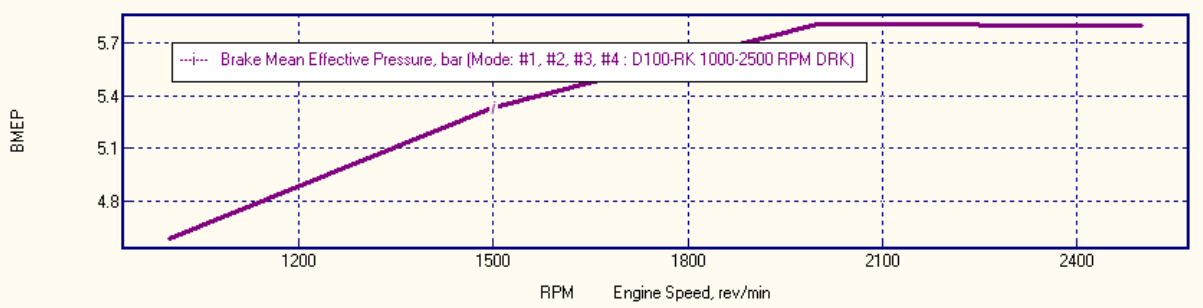

Appendix B: Performance Simulation Curves

B1: Torque Curve

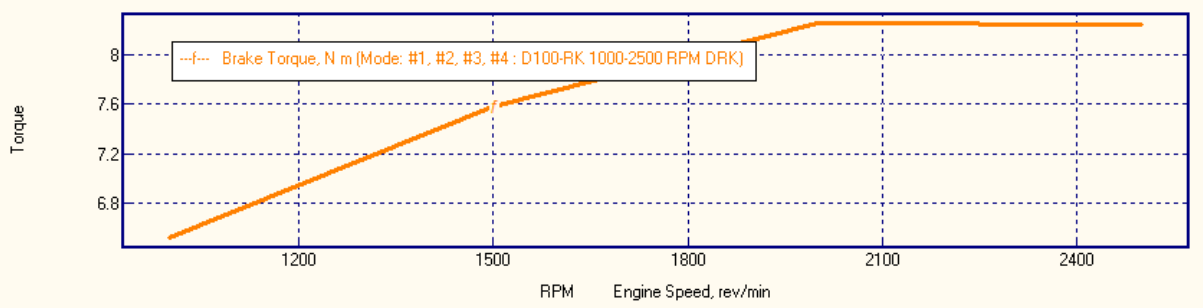

B2: Power Curve

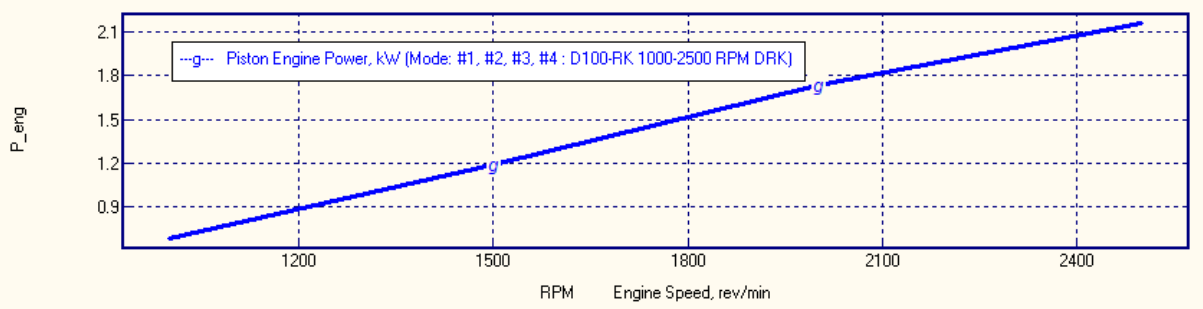

B3: Specific Fuel Consumption Curve

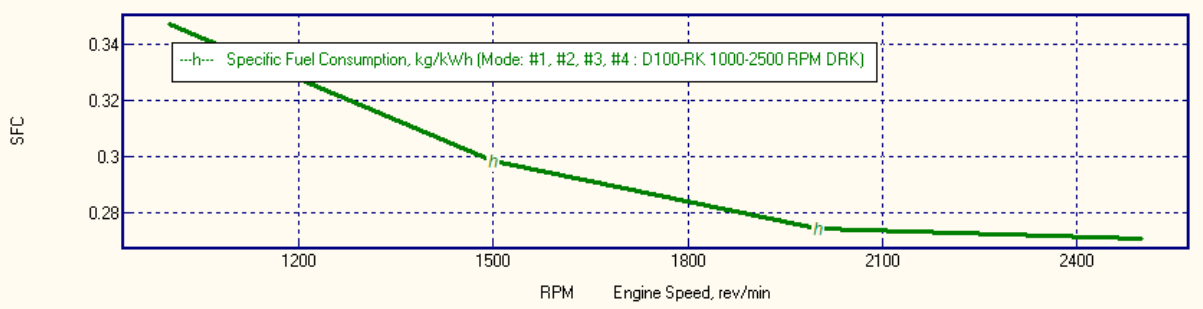

Appendix C: Emissions Simulation Curves

C1: NO_x Curve

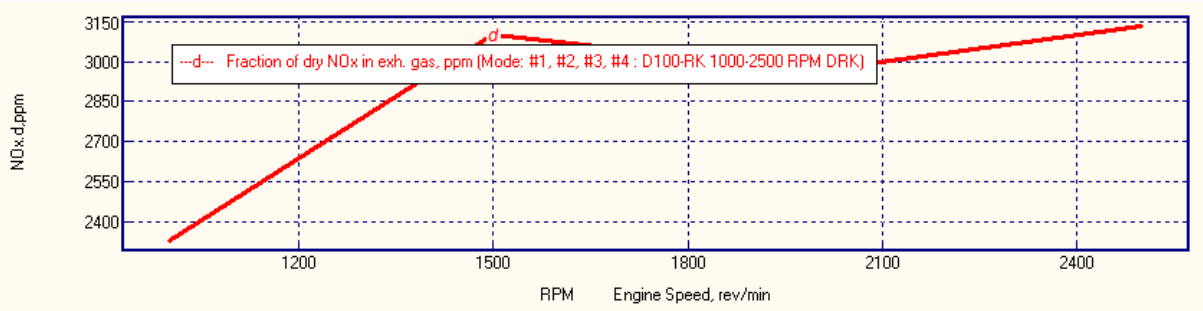

C2: Particulate Matter Curve

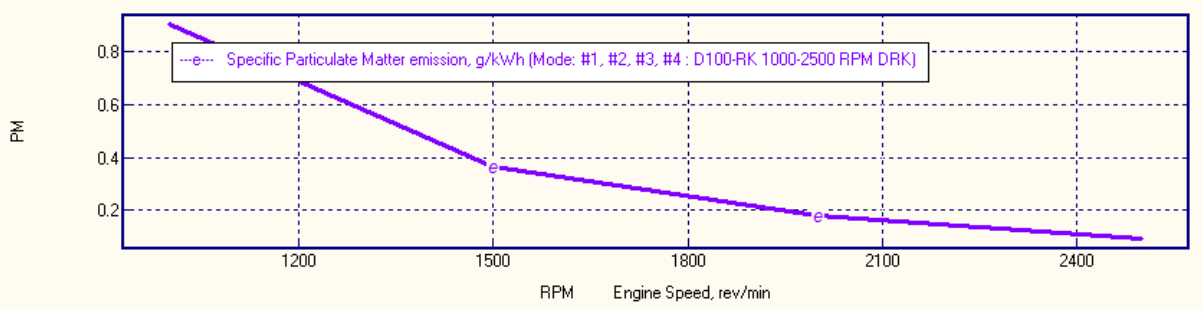

C3: Bosch Smoke Number

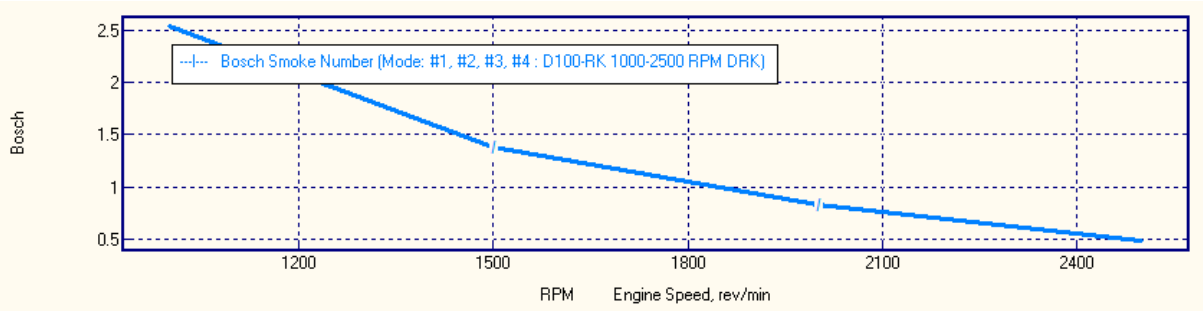

Appendix D: Diesel-RK Software User Interface

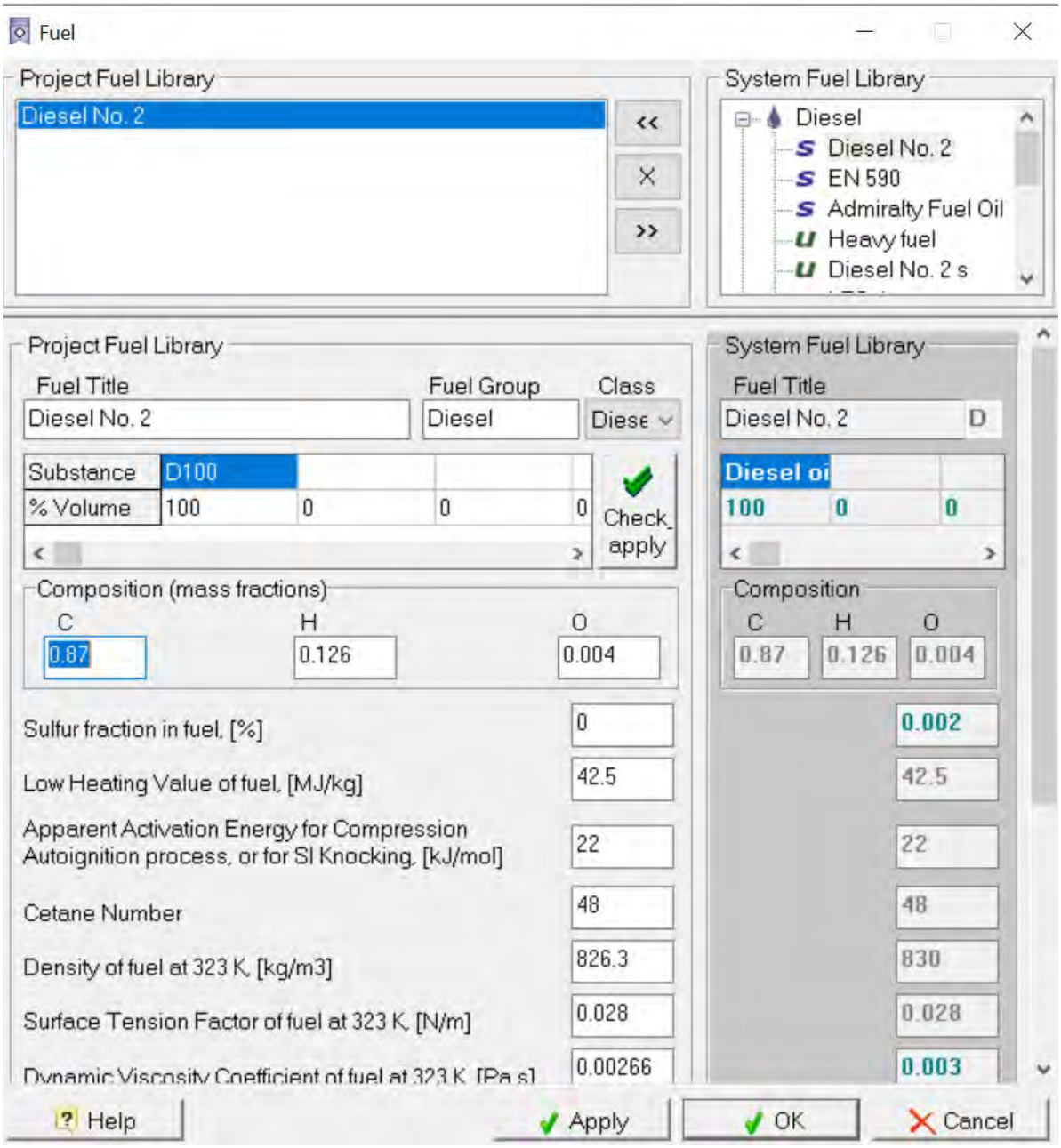

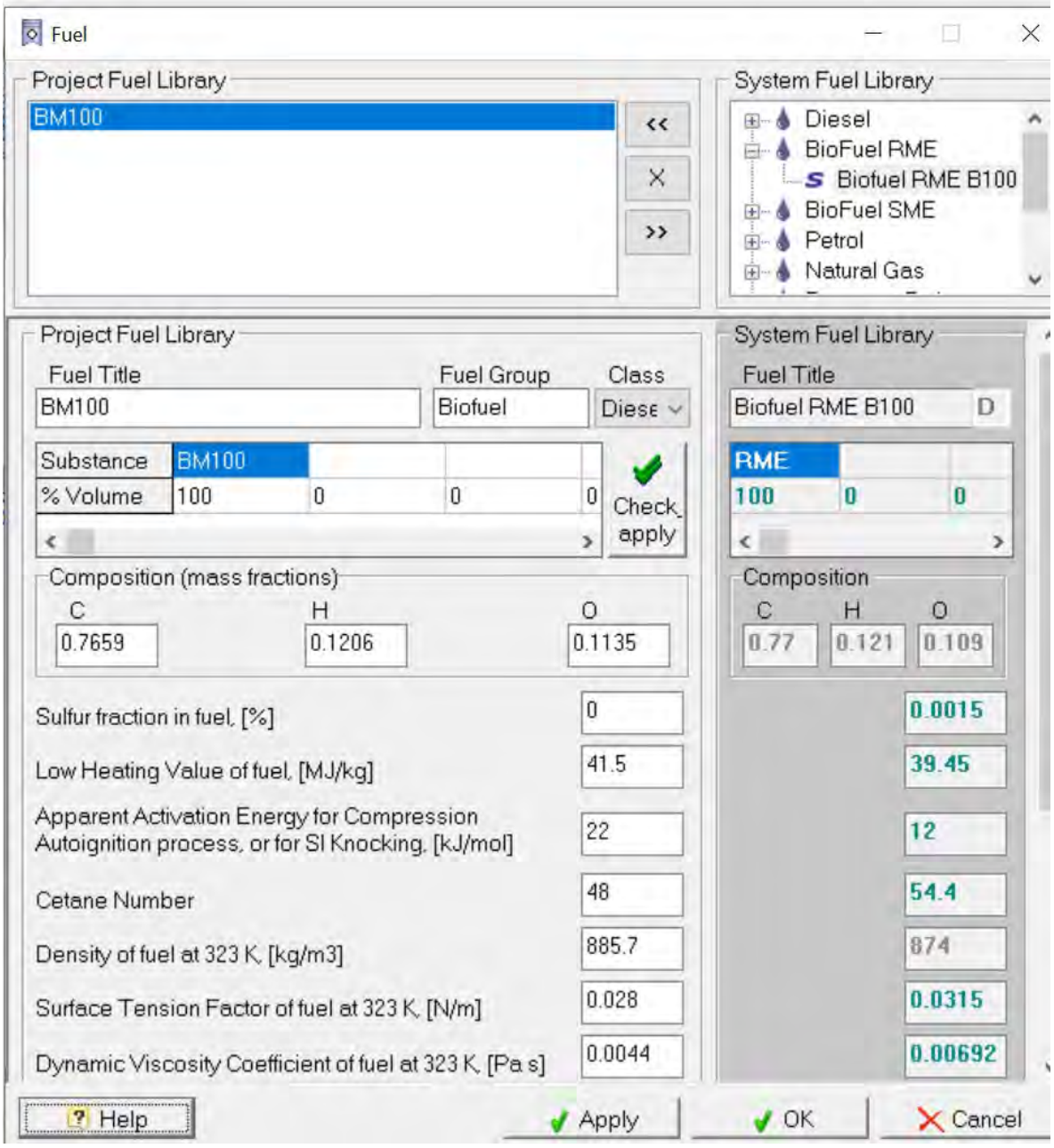
Fuel
Project Fuel Library
BM100
<<
X
>>
System Fuel Library
Diesel
BioFuel RME
Biofuel RME B100
BioFuel SME
Petrol
Natural Gas
Project Fuel Library
Fuel Title
BM100
Fuel Group
Biofuel
Class
Diese
Substance
BM100
% Volume
100
0
0
0
Check, apply
Composition (mass fractions)
C
0.7659
H
0.1206
O
0.1135
Sulfur fraction in fuel, [%]
0
Low Heating Value of fuel, [MJ/kg]
41.5
Apparent Activation Energy for Compression Autoignition process, or for SI Knocking, [kJ/mol]
22
Cetane Number
48
Density of fuel at 323 K, [kg/m3]
885.7
Surface Tension Factor of fuel at 323 K, [N/m]
0.028
Dynamic Viscosity Coefficient of fuel at 323 K, [Pa s]
0.0044
System Fuel Library
Fuel Title
Biofuel RME B100
D
RME
100
0
0
Composition
C
0.77
H
0.121
O
0.109
0.0015
39.45
12
54.4
874
0.0315
0.00692
Help
Apply
OK
Cancel

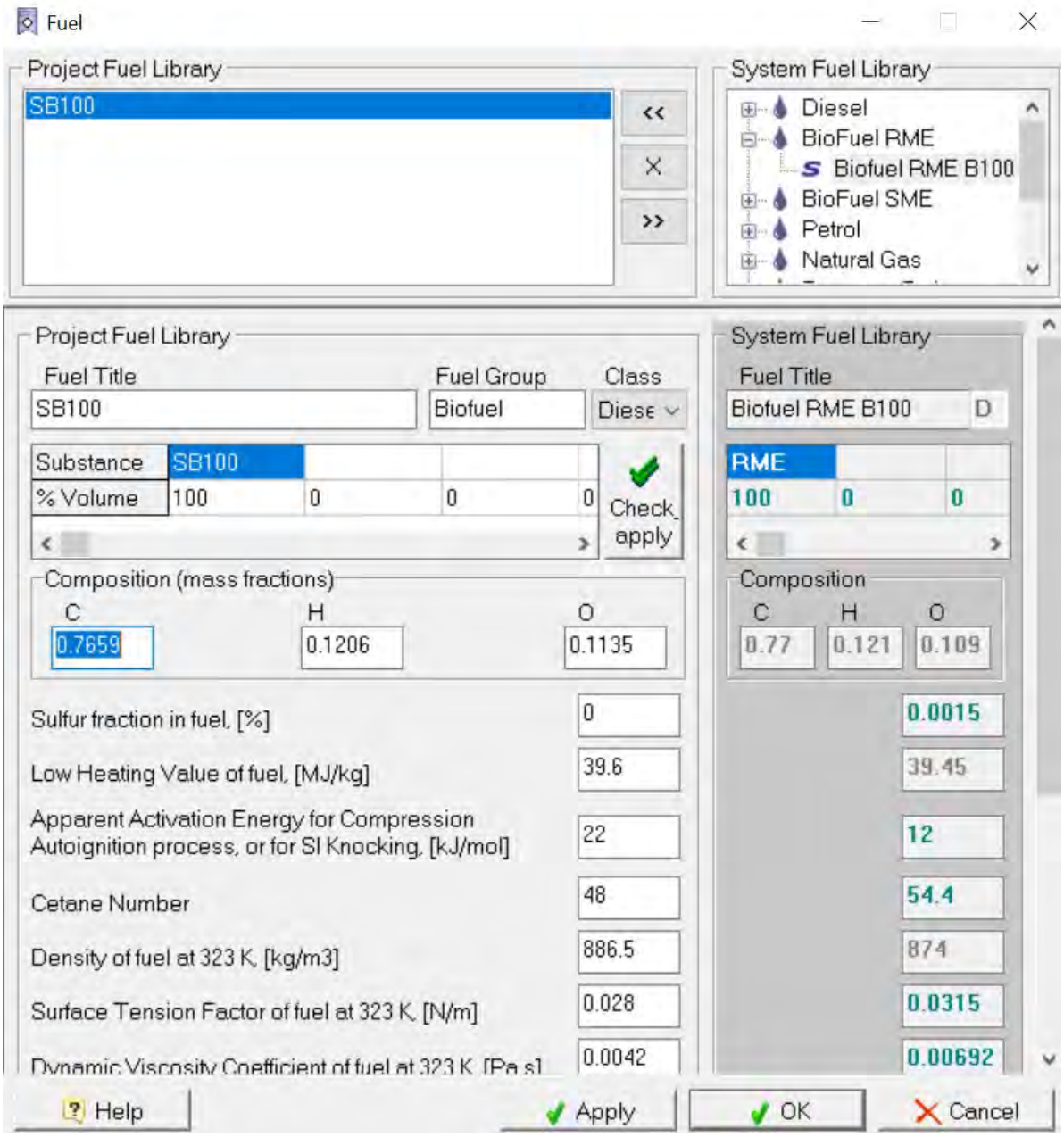
Fuel
Project Fuel Library
SB100
<<
X
>>
System Fuel Library
Diesel
BioFuel RME
Biofuel RME B100
BioFuel SME
Petrol
Natural Gas
Project Fuel Library
Fuel Title
SB100
Fuel Group
Biofuel
Class
Diese
Substance
SB100
% Volume
100
0
0
0
Check, apply
Composition (mass fractions)
C
0.7659
H
0.1206
O
0.1135
Sulfur fraction in fuel, [%]
0
Low Heating Value of fuel, [MJ/kg]
39.6
Apparent Activation Energy for Compression Autoignition process, or for SI Knocking, [kJ/mol]
22
Cetane Number
48
Density of fuel at 323 K, [kg/m3]
886.5
Surface Tension Factor of fuel at 323 K, [N/m]
0.028
Dynamic Viscosity Coefficient of fuel at 323 K, [Pa s]
0.0042
System Fuel Library
Fuel Title
Biofuel RME B100
D
RME
100
0
0
Composition
C
0.77
H
0.121
O
0.109
0.0015
39.45
12
54.4
874
0.0315
0.00692
Help
Apply
OK
Cancel

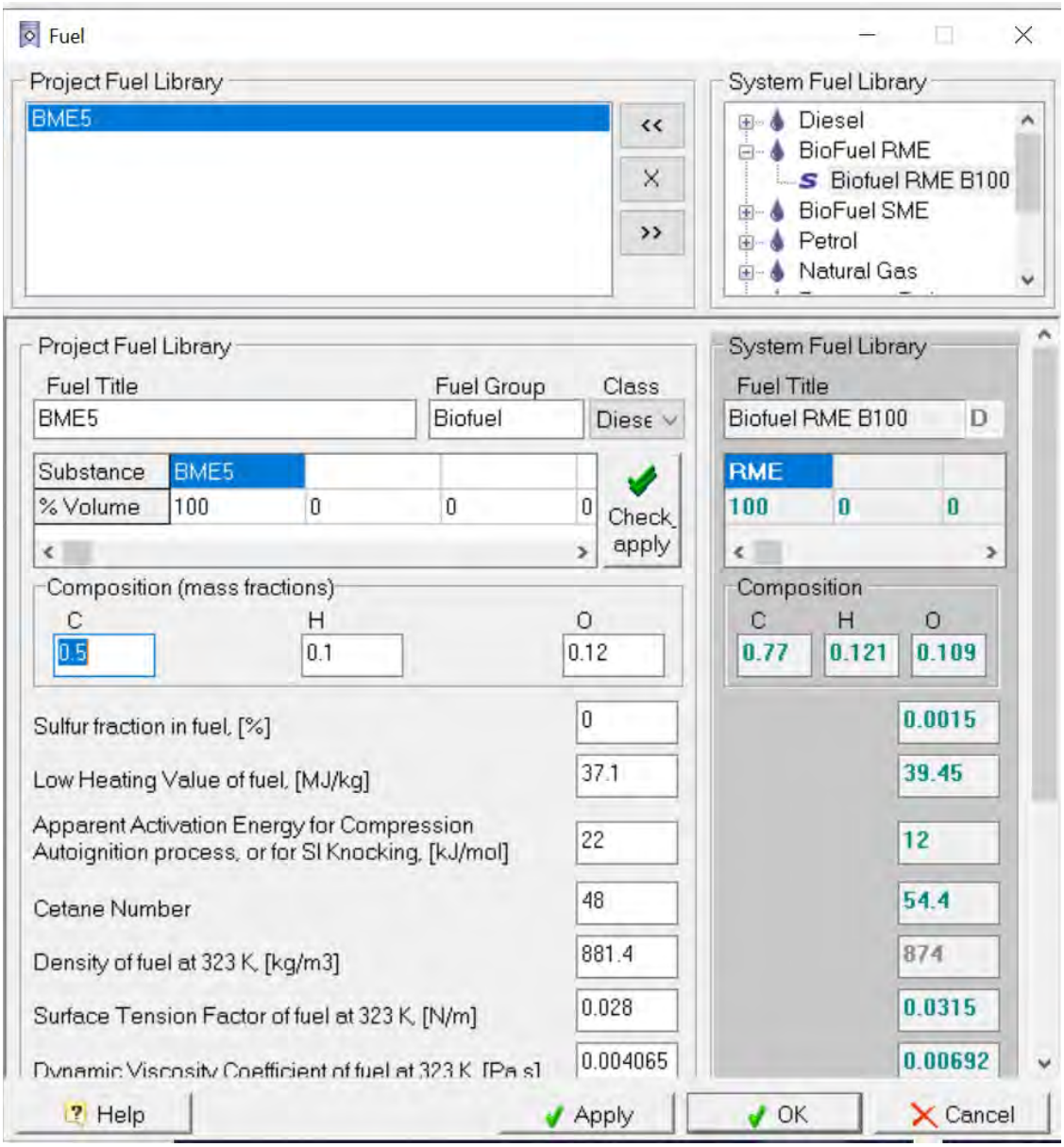
Fuel
Project Fuel Library
BME5
<<
X
>>
System Fuel Library
Diesel
BioFuel RME
Biofuel RME B100
BioFuel SME
Petrol
Natural Gas
Project Fuel Library
Fuel Title
Fuel Group
Class
BME5
Biofuel
Diese
Substance
BME5
% Volume
100
0
0
0
Check, apply
Composition (mass fractions)
C
H
O
0.5
0.1
0.12
Sulfur fraction in fuel, [%]
0
Low Heating Value of fuel, [MJ/kg]
37.1
Apparent Activation Energy for Compression Autoignition process, or for SI Knocking, [kJ/mol]
22
Cetane Number
48
Density of fuel at 323 K, [kg/m3]
881.4
Surface Tension Factor of fuel at 323 K, [N/m]
0.028
Dynamic Viscosity Coefficient of fuel at 323 K, [Pa s]
0.004065
System Fuel Library
Fuel Title
Biofuel RME B100
D
RME
100
0
0
Composition
C
H
O
0.77
0.121
0.109
0.0015
39.45
12
54.4
874
0.0315
0.00692
Help
Apply
OK
Cancel

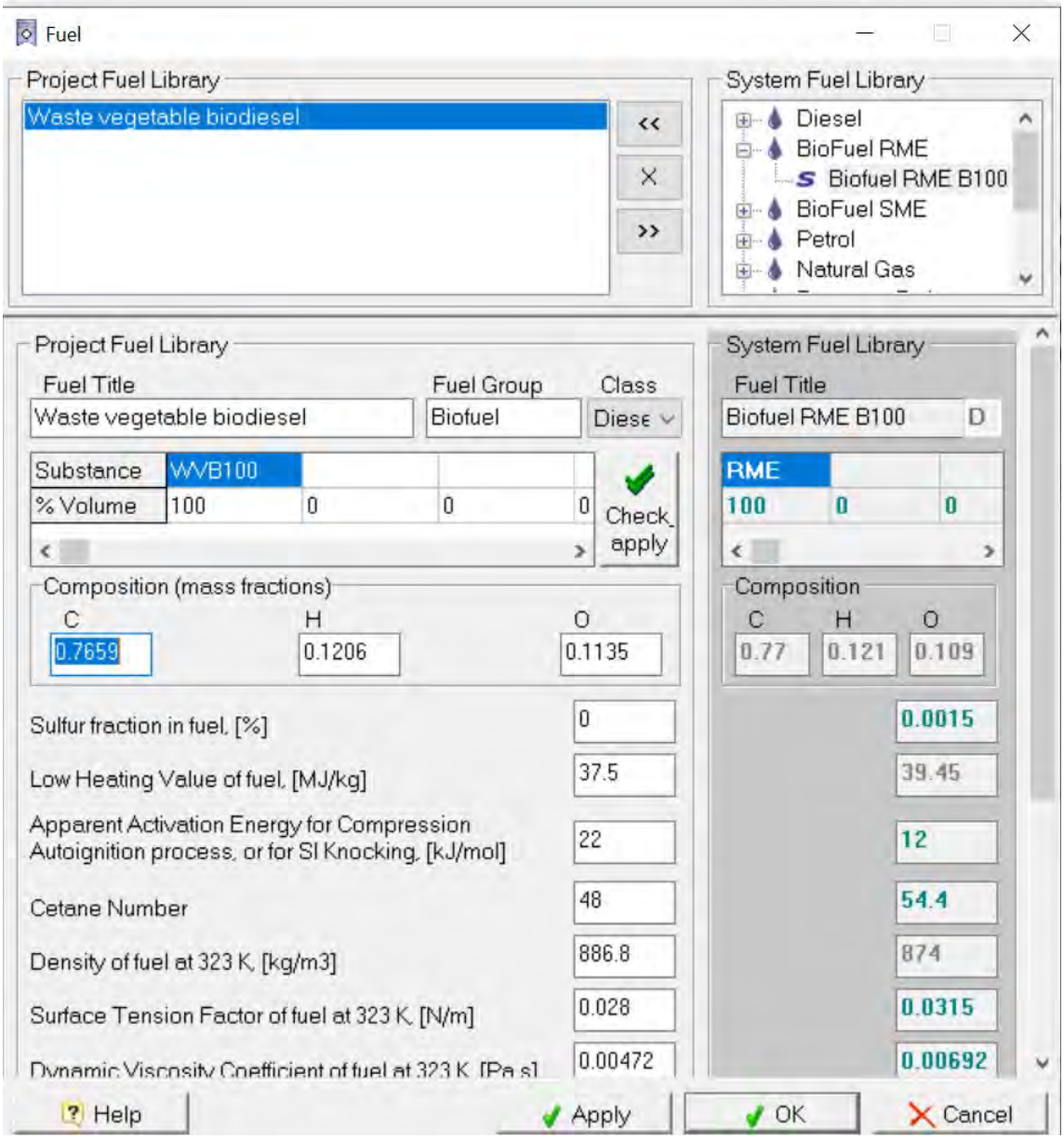
Fuel
Project Fuel Library
Waste vegetable biodiesel
<<
X
>>
System Fuel Library
Diesel
BioFuel RME
Biofuel RME B100
BioFuel SME
Petrol
Natural Gas
Project Fuel Library
Fuel Title
Waste vegetable biodiesel
Fuel Group
Biofuel
Class
Diese
Substance
WVB100
% Volume
100
0
0
0
Check, apply
Composition (mass fractions)
C
0.7659
H
0.1206
O
0.1135
Sulfur fraction in fuel, [%]
0
Low Heating Value of fuel, [MJ/kg]
37.5
Apparent Activation Energy for Compression Autoignition process, or for SI Knocking, [kJ/mol]
22
Cetane Number
48
Density of fuel at 323 K, [kg/m3]
886.8
Surface Tension Factor of fuel at 323 K, [N/m]
0.028
Dynamic Viscosity Coefficient of fuel at 323 K, [Pa s]
0.00472
System Fuel Library
Fuel Title
Biofuel RME B100
D
RME
100
0
0
Composition
C
0.77
H
0.121
O
0.109
0.0015
39.45
12
54.4
874
0.0315
0.00692
Help
Apply
OK
Cancel

References

ABBASZAADEH, A., GHOBADIAN, B., OMIDKHAH, M. R. & NAJAFI, G. 2012. Current biodiesel production technologies: A comparative review. *Energy Conversion and Management,* 63**,** 138-148.

ABBASZADEHMOSAYEBI, G. 2014. *Diesel engine heat release analysis by using newly defined dimensionless parameters.* Brunel University United Kingdom

ACHARYA, N., NANDA, P., PANDA, S. & ACHARYA, S. 2017. Analysis of properties and estimation of optimum blending ratio of blended mahua biodiesel. *Engineering Science and Technology, an International Journal,* 20**,** 511-517.

ADHAM, A. & MABSATE, E. M. 2017. Comparison and optimization of combustion performance and emissions of a single cylinder diesel engine fueled with soy biodiesel-diesel blends. *ARPN Journal of Engineering and Applied Sciences,* 12, 6338-6346.

AKAR, M. A. 2016. Performance and emission characteristics of compression ignition engine operating with false flax biodiesel and butanol blends. *Advances in Mechanical Engineering,* 8**,** 1687814016632677.

AL-DAWODY, M. F. & BHATTI, S. 2011. Effect of soybean oil biofuel blending on the performance and emissions of Diesel engine using diesel-rk software. *International journal of engineering science and technology,* 3**,** 4539-4555.

AL-DAWODY, M. F. & BHATTI, S. 2013. Optimization strategies to reduce the biodiesel NOx effect in diesel engine with experimental verification. *Energy Conversion and Management,* 68**,** 96-104.

AL-DAWODY, M. F. & EDAM, M. S. 2022. Experimental and numerical investigation of adding castor methyl ester and alumina nanoparticles on performance and emissions of a diesel engine. *Fuel,* 307**,** 121784.

AL-DAWODY, M. F. & BHATTI, S. 2014. Experimental and computational investigations for combustion, performance and emission parameters of a diesel engine fueled with soybean biodiesel-diesel blends. *Energy procedia,* 52**,** 421-430.

ALI, O. M., MAMAT, R., ABDULLAH, N. R. & ABDULLAH, A. A. 2016. Analysis of blended fuel properties and engine performance with palm biodiesel–diesel blended fuel. *Renewable Energy,* 86**,** 59-67.

ALI, O. M., YUSAF, T., MAMAT, R., ABDULLAH, N. R. & ABDULLAH, A. A. 2014. Influence of chemical blends on palm oil methyl esters' cold flow properties and fuel characteristics. *Energies,* 7**,** 4364-4380.

ALI, Y., RAZI, M., DE FELICE, F., SABIR, M. & PETRILLO, A. 2019. A VIKOR based approach for assessing the social, environmental and economic effects of "smog" on human health. *Science of the Total Environment,* 650**,** 2897-2905.

ALKIDAS, A. C. 1984. Relationships between smoke measurements and particulate measurements. Society of Automotive Engineers, Inc., Warrendale, PA.

ALPTEKIN, E. 2017. Emission, injection and combustion characteristics of biodiesel and oxygenated fuel blends in a common rail diesel engine. *Energy,* 119**,** 44-52.

ALPTEKIN, E. & CANAKCI, M. 2009. Characterization of the key fuel properties of methyl ester–diesel fuel blends. *Fuel,* 88**,** 75-80.

ALPTEKIN, E., CANAKCI, M., OZSEZEN, A. N., TURKCAN, A. & SANLI, H. 2015. Using waste animal fat based biodiesels–bioethanol–diesel fuel blends in a DI diesel engine. *Fuel,* 157**,** 245-254.

ALSHARIFI, M., ZNAD, H., HENA, S. & ANG, M. 2017. Biodiesel production from canola oil using novel Li/TiO2 as a heterogeneous catalyst prepared via impregnation method. *Renewable Energy,* 114**,** 1077-1089.

AMINI, Z., ILHAM, Z., ONG, H. C., MAZAHERI, H. & CHEN, W.-H. 2017. State of the art and prospective of lipase-catalyzed transesterification reaction for biodiesel production. *Energy Conversion and Management,* 141**,** 339-353.

AMSDEN, A., RAMSHAW, J., O'ROURKE, P. & DUKOWICZ, J. 1985. KIVA: A computer program for two-and three-dimensional fluid flows with chemical reactions and fuel sprays. Los Alamos National Lab., NM (USA).

AN, H., YANG, W. & LI, J. 2015a. Effects of ethanol addition on biodiesel combustion: A modeling study. *Applied energy,* 143**,** 176-188.

AN, H., YANG, W. & LI, J. 2015b. Numerical modeling on a diesel engine fueled by biodiesel–methanol blends. *Energy Conversion and Management,* 93**,** 100-108.

ANAND, K., SHARMA, R. & MEHTA, P. 2010. Experimental investigations on combustion, performance, and emissions characteristics of a neat biodiesel-fuelled, turbocharged, direct

injection diesel engine. *Proceedings of the Institution of Mechanical Engineers, Part D: Journal of Automobile Engineering,* 224**,** 661-679.

ANAND, K., SHARMA, R. & MEHTA, P. S. 2011. Experimental investigations on combustion, performance and emissions characteristics of neat karanji biodiesel and its methanol blend in a diesel engine. *Biomass and bioenergy,* 35**,** 533-541.

ANWAR, M., RASUL, M. G. & ASHWATH, N. 2018. Production optimization and quality assessment of papaya (Carica papaya) biodiesel with response surface methodology. *Energy Conversion and Management,* 156**,** 103-112.

APPAVU, P., MADHAVAN, V. R., VENU, H. & JAYARAMAN, J. 2021. Experimental investigation of an unmodified diesel engine operated with ternary fuel. *Biofuels,* 12**,** 1183-1189.

ARANSIOLA, E. F., OJUMU, T. V., OYEKOLA, O., MADZIMBAMUTO, T. & IKHU-OMOREGBE, D. 2014. A review of current technology for biodiesel production: State of the art. *Biomass and bioenergy,* 61**,** 276-297.

ARUL MOZHI SELVAN, V., ANAND, R. & UDAYAKUMAR, M. 2009. Combustion characteristics of diesohol using biodiesel as an additive in a direct injection compression ignition engine under various compression ratios. *Energy & Fuels,* 23**,** 5413-5422.

ASHOK, B., NANTHAGOPAL, K., DARLA, S., CHYUAN, O. H., RAMESH, A., JACOB, A., SAHIL, G., THIYAGARAJAN, S. & GEO, V. E. 2019. Comparative assessment of hexanol and decanol as oxygenated additives with calophyllum inophyllum biodiesel. *Energy,* 173**,** 494-510.

ASHOK, B., NANTHAGOPAL, K., SUBBARAO, R., JOHNY, A., MOHAN, A. & TAMILARASU, A. 2017. Experimental studies on the effect of metal oxide and antioxidant additives with Calophyllum Inophyllum Methyl ester in compression ignition engine. *Journal of Cleaner Production,* 166**,** 474-484.

ATABANI, A., MAHLIA, T., MASJUKI, H., BADRUDDIN, I. A., YUSSOF, H. W., CHONG, W. & LEE, K. T. 2013a. A comparative evaluation of physical and chemical properties of biodiesel synthesized from edible and non-edible oils and study on the effect of biodiesel blending. *Energy,* 58**,** 296-304.

ATABANI, A., SILITONGA, A., ONG, H., MAHLIA, T., MASJUKI, H., BADRUDDIN, I. A. & FAYAZ, H. 2013b. Non-edible vegetable oils: a critical evaluation of oil extraction, fatty acid compositions, biodiesel production, characteristics, engine performance and emissions production. *Renewable and sustainable energy reviews,* 18**,** 211-245.

ATABANI, A. E., SILITONGA, A. S., BADRUDDIN, I. A., MAHLIA, T., MASJUKI, H. & MEKHILEF, S. 2012. A comprehensive review on biodiesel as an alternative energy resource and its characteristics. *Renewable and sustainable energy reviews,* 16**,** 2070-2093.

ATHAR, M. & ZAIDI, S. 2020. A review of the feedstocks, catalysts, and intensification techniques for sustainable biodiesel production. *Journal of Environmental Chemical Engineering,* 8**,** 104523.

ATMANLI, A. 2016. Comparative analyses of diesel–waste oil biodiesel and propanol, n-butanol or 1-pentanol blends in a diesel engine. *Fuel,* 176**,** 209-215.

ATMANLI, A. & YILMAZ, N. 2020. An experimental assessment on semi-low temperature combustion using waste oil biodiesel/C3-C5 alcohol blends in a diesel engine. *Fuel,* 260**,** 116357.

AWORANTI, O.A., AJANI, A.O. & AGARRY, S.E. 2019. Process parameter estimation of biodiesel production from waste frying oil (vegetable and palm oil) using homogeneous catalyst. *Journal of Food Processing and Technology, 10,* 1-10.

AZÓCAR, L., CIUDAD, G., HEIPIEPER, H. J., MUÑOZ, R. & NAVIA, R. 2010. Improving fatty acid methyl ester production yield in a lipase-catalyzed process using waste frying oils as feedstock. *Journal of bioscience and bioengineering,* 109**,** 609-614.

BABU, D. & ANAND, R. 2017. Effect of biodiesel-diesel-n-pentanol and biodiesel-diesel-n-hexanol blends on diesel engine emission and combustion characteristics. *Energy,* 133**,** 761-776.

BALAT, M. 2011. Potential alternatives to edible oils for biodiesel production–A review of current work. *Energy conversion and management,* 52**,** 1479-1492.

BALAT, M. & BALAT, H. 2010. Progress in biodiesel processing. *Applied energy,* 87**,** 1815-1835.

BARABAS, I., TODORUŢ, A. & BĂLDEAN, D. 2010. Performance and emission characteristics of an CI engine fueled with diesel–biodiesel–bioethanol blends. *Fuel,* 89**,** 3827-3832.

BASHIR, M. A., WU, S., ZHU, J., KROSURI, A., KHAN, M. U. & AKA, R. J. N. 2022. Recent development of advanced processing technologies for biodiesel production: A critical review. *Fuel Processing Technology,* 227**,** 107120.

BERCHMANS, H. J., MORISHITA, K. & TAKARADA, T. 2013. Kinetic study of hydroxide-catalyzed methanolysis of Jatropha curcas–waste food oil mixture for biodiesel production. *Fuel,* 104**,** 46-52.

BHUIYA, M., RASUL, M., KHAN, M., ASHWATH, N. & AZAD, A. 2016. Prospects of 2nd generation biodiesel as a sustainable fuel—Part: 1 selection of feedstocks, oil extraction techniques and conversion technologies. *Renewable and Sustainable Energy Reviews,* 55**,** 1109-1128.

BHURAT, S. S., PANDEY, S., CHINTALA, V. & RANJIT, P. 2019. Experimental study on performance and emissions characteristics of single cylinder diesel engine with ethanol and biodiesel blended fuels with diesel. *Materials Today: Proceedings,* 17**,** 220-226.

BHUSHAN, S., KALRA, A., SIMSEK, H., KUMAR, G. & PRAJAPATI, S. K. 2020. Current trends and prospects in microalgae-based bioenergy production. *Journal of Environmental Chemical Engineering,* 8**,** 104025.

BILGEN, S. 2014. Structure and environmental impact of global energy consumption. *Renewable and Sustainable Energy Reviews,* 38**,** 890-902.

BOOG, J. H. F., SILVEIRA, E. L. C., DE CALAND, L. B. & TUBINO, M. 2011. Determining the residual alcohol in biodiesel through its flash point. *Fuel,* 90**,** 905-907.

BORA, B. J., SAHA, U. K., CHATTERJEE, S. & VEER, V. 2014. Effect of compression ratio on performance, combustion and emission characteristics of a dual fuel diesel engine run on raw biogas. *Energy conversion and management,* 87**,** 1000-1009.

BORGES, M. E. & DÍAZ, L. 2012. Recent developments on heterogeneous catalysts for biodiesel production by oil esterification and transesterification reactions: A review. *Renewable and Sustainable Energy Reviews,* 16**,** 2839-2849.

BRUNT, M. F., RAI, H. & EMTAGE, A. L. 1998. The calculation of heat release energy from engine cylinder pressure data. *SAE transactions***,** 1596-1609.

BUKKARAPU, K. R. & KRISHNASAMY, A. 2021. A critical review on available models to predict engine fuel properties of biodiesel. *Renewable and Sustainable Energy Reviews***,** 111925.

BURRETT, R., CLINI, C., DIXON, R., ECKHART, M., EL-ASHRY, M., GUPTA, D., HADDOUCHE, A., HALES, D., HAMILTON, K., HOUSE, C. & HOSKYNS, U.S.J. 2009. Renewable energy policy network for the 21st century. *REN21 Renewables Global Status Report*.

CAN, Ö., CELIKTEN, I. & USTA, N. 2004. Effects of ethanol addition on performance and emissions of a turbocharged indirect injection diesel engine running at different injection pressures. *Energy conversion and Management,* 45**,** 2429-2440.

CAPUANO, L. 2018. International energy outlook 2018 (IEO2018). *US Energy Information Administration (EIA): Washington, DC, USA,* 2018**,** 21.

CARARETO, N. D., KIMURA, C. Y., OLIVEIRA, E. C., COSTA, M. C. & MEIRELLES, A. J. 2012. Flash points of mixtures containing ethyl esters or ethylic biodiesel and ethanol. *Fuel,* 96**,** 319-326.

CHAI, F., CAO, F., ZHAI, F., CHEN, Y., WANG, X. & SU, Z. 2007. Transesterification of vegetable oil to biodiesel using a heteropolyacid solid catalyst. *Advanced Synthesis & Catalysis,* 349**,** 1057-1065.

CHANGE, I. P. O. C. 2014. IPCC. *Climate change*.

CHEENKACHORN, K. & FUNGTAMMASAN, B. 2009. Biodiesel as an additive for diesohol. *International Journal of Green Energy,* 6**,** 57-72.

CHEENKACHORN, K. & FUNGTAMMASAN, B. 2010. An investigation of diesel-ethanol-biodiesel blends for diesel engine: part 2—emission and engine performance of a light-duty truck. *Energy Sources, Part A: Recovery, Utilization, and Environmental Effects,* 32**,** 894-900.

CHIN, J.-Y., BATTERMAN, S. A., NORTHROP, W. F., BOHAC, S. V. & ASSANIS, D. N. 2012. Gaseous and particulate emissions from diesel engines at idle and under load: comparison of biodiesel blend and ultralow sulfur diesel fuels. *Energy & fuels,* 26**,** 6737-6748.

CHOWDARY, P. K., GANJI, P. R., KUMAR, M. S., KUMAR, C. R. & RAO, S. S. 2016. Numerical analysis of CI engine to control emissions using exhaust gas recirculation and advanced start of injection. *Alexandria Engineering Journal,* 55**,** 1881-1891.

CIHAN, Ö. 2021. Experimental and numerical investigation of the effect of fig seed oil methyl ester biodiesel blends on combustion characteristics and performance in a diesel engine. *Energy Reports,* 7**,** 5846-5856.

CUDDIHY, J. L. 2014. *A user-friendly, two-zone heat release model for predicting spark-ignition engine performance and emissions.* University of Idaho.

DATTA, A. & MANDAL, B. K. 2017. Engine performance, combustion and emission characteristics of a compression ignition engine operating on different biodiesel-alcohol blends. *Energy,* 125**,** 470-483.

DATTA, A. & MANDAL, B. K. 2018. Numerical prediction of the performance, combustion and emission characteristics of a CI engine using different biodiesels. *Clean Technologies and Environmental Policy,* 20**,** 1773-1790.

DE ARAÚJO, C. D. M., DE ANDRADE, C. C., E SILVA, E. D. S. & DUPAS, F. A. 2013. Biodiesel production from used cooking oil: A review. *Renewable and Sustainable Energy Reviews,* 27**,** 445-452.

DE LIMA DA SILVA, N. V., BENEDITO BATISTELLA, C. S., MACIEL FILHO, R. & MACIEL, M. R. W. 2009. Biodiesel production from castor oil: optimization of alkaline ethanolysis. *Energy & Fuels,* 23**,** 5636-5642.

DE OLIVEIRA, F. C. & COELHO, S. T. 2017. History, evolution, and environmental impact of biodiesel in Brazil: A review. *Renewable and Sustainable Energy Reviews,* 75**,** 168-179.

DEMIRBAS, A. 2005. Biodiesel production from vegetable oils via catalytic and non-catalytic supercritical methanol transesterification methods. *Progress in energy and combustion science,* 31**,** 466-487.

DEMIRBAS, A. 2009. Progress and recent trends in biodiesel fuels. *Energy conversion and management,* 50**,** 14-34.

DESANTES, J., GALINDO, J., GUARDIOLA, C. & DOLZ, V. 2010. Air mass flow estimation in turbocharged diesel engines from in-cylinder pressure measurement. *Experimental Thermal and Fluid Science,* 34**,** 37-47.

DEVARAJAN, Y., MUNUSWAMY, D. B. & MAHALINGAM, A. 2019. Investigation on behavior of diesel engine performance, emission, and combustion characteristics using nano-additive in neat biodiesel. *Heat and Mass Transfer,* 55**,** 1641-1650.

DHAMODARAN, G., KRISHNAN, R., POCHAREDDY, Y.K., PYARELAL, H.M., SIVASUBRAMANIAN, H. & GANESHRAM, A.K. 2017. A comparative study of combustion, emission, and performance characteristics of rice-bran-, neem-, and cottonseed-oil biodiesels with varying degree of unsaturation. *Fuel,* 187, 296-305.

DONG, T., GAO, D., MIAO, C., YU, X., DEGAN, C., GARCIA-PÉREZ, M., RASCO, B., SABLANI, S. S. & CHEN, S. 2015. Two-step microalgal biodiesel production using acidic catalyst generated from pyrolysis-derived bio-char. *Energy conversion and management,* 105**,** 1389-1396.

DWIVEDI, G., SHARMA, M., VERMA, P. & KUMAR, P. 2018. Engine performance using waste cooking biodiesel and its blends with kerosene and ethanol. *Materials Today: Proceedings,* 5**,** 22955-22962.

DWIVEDI, G. & SHARMA, M. P. 2015. Investigation and improvement in cold flow properties of Pongamia biodiesel. *Waste and Biomass Valorization,* 6**,** 73-79.

DWIVEDI, G. & SHARMA, M. P. 2016. Investigation of cold flow properties of waste cooking biodiesel. *Journal of Clean Energy Technologies,* 3**,** 205-208.

ECONOMICS, B. E. 2018. BP Energy Outlook. *BP plc: London, UK*.

EDITH, O., JANIUS, R. B. & YUNUS, R. 2012. Factors affecting the cold flow behaviour of biodiesel and methods for improvement—a review. *Pertanika J. Sci. Technol,* 20**,** 1-14.

EMIROĞLU, A. O. & ŞEN, M. 2018. Combustion, performance and exhaust emission characterizations of a diesel engine operating with a ternary blend (alcohol-biodiesel-diesel fuel). *Applied Thermal Engineering,* 133**,** 371-380.

ENDALEW, A. K., KIROS, Y. & ZANZI, R. 2011. Heterogeneous catalysis for biodiesel production from Jatropha curcas oil (JCO). *Energy,* 36**,** 2693-2700.

ENWEREMADU, C., SAMUEL, O. & RUTTO, H. 2022. Experimental Studies and Theoretical Modelling of Diesel Engine Running on Biodiesels from South African Sunflower and Canola Oils. *Environmental and Climate Technologies,* 26**,** 630-647.

ENWEREMADU, C. C., RUTTO, H. L. & PELEOWO, N. 2011. Performance evaluation of a diesel engine fueled with methyl ester of shea butter. *World Academy of Science, Engineering and Technology,* 79**,** 142-146.

FANG, Q., FANG, J., ZHUANG, J. & HUANG, Z. 2013. Effects of ethanol–diesel–biodiesel blends on combustion and emissions in premixed low temperature combustion. *Applied Thermal Engineering,* 54**,** 541-548.

FAZAL, M., HASEEB, A. & MASJUKI, H. 2014. A critical review on the tribological compatibility of automotive materials in palm biodiesel. *Energy Conversion and Management,* 79**,** 180-186.

FAZAL, M., HASEEB, A. & MASJUKI, H. H. 2013. Investigation of friction and wear characteristics of palm biodiesel. *Energy conversion and management,* 67**,** 251-256.

FERNANDO, S. & HANNA, M. 2004. Development of a novel biofuel blend using ethanol− biodiesel− diesel microemulsions: EB-diesel. *Energy & Fuels,* 18**,** 1695-1703.

GAD, M., EL-SHAFAY, A. & HASHISH, H. A. 2021. Assessment of diesel engine performance, emissions and combustion characteristics burning biodiesel blends from jatropha seeds. *Process Safety and Environmental Protection,* 147**,** 518-526.

GALEANO, J. D., MITCHELL, D. A. & KRIEGER, N. 2017. Biodiesel production by solvent-free ethanolysis of palm oil catalyzed by fermented solids containing lipases of Burkholderia contaminans. *Biochemical Engineering Journal,* 127**,** 77-86.

GANESAN, S., SIVASUBRAMANIAN, R., SAJIN, J., SUBBIAH, G. & DEVARAJAN, Y. 2019. Performance and emission study on the effect of oxygenated additive in neat biodiesel fueled diesel engine. *Energy Sources A: Recovery, Utilization and Environmental Effects,* 41**,** 2017-2027.

GANESAN, V. 2000. *Computer simulation of Compression-Ignition engine processes*, Universities press.

GATOWSKI, J., BALLES, E. N., CHUN, K. M., NELSON, F., EKCHIAN, J. & HEYWOOD, J. B. 1984. Heat release analysis of engine pressure data. *SAE transactions***,** 961-977.

GAUTAM, P. S., VISHNOI, P. K. & GUPTA, V. 2022. A single zone thermodynamic simulation model for predicting the combustion and performance characteristics of a CI engine and its validation using statistical analysis. *Fuel,* 315**,** 123285.

GENG, L., BI, L., LI, Q., CHEN, H. & XIE, Y. 2021. Experimental study on spray characteristics, combustion stability, and emission performance of a CRDI diesel engine operated with biodiesel–ethanol blends. *Energy Reports,* 7**,** 904-915.

GEO, V. E., SONTHALIA, A., NAGARAJAN, G. & NAGALINGAM, B. 2017. Studies on performance, combustion and emission of a single cylinder diesel engine fuelled with rubber seed oil and its biodiesel along with ethanol as injected fuel. *Fuel*, 209**,** 733-741.

GHADIKOLAEI, M. A. 2016. Effect of alcohol blend and fumigation on regulated and unregulated emissions of IC engines—A review. *Renewable and Sustainable Energy Reviews*, 57**,** 1440-1495.

GHAZALI, W. N. M. W., MAMAT, R., MASJUKI, H. H. & NAJAFI, G. 2015. Effects of biodiesel from different feedstocks on engine performance and emissions: A review. *Renewable and Sustainable Energy Reviews,* 51**,** 585-602.

GHOBADIAN, B., YUSAF, T., NAJAFI, G. & KHATAMIFAR, M. 2009. Diesterol: an environment-friendly IC engine fuel. *Renewable Energy,* 34**,** 335-342.

GOLIMOWSKI, W., PASYNIUK, P. & BERGER, W. 2013. Common rail diesel tractor engine performance running on pure plant oil. *Fuel,* 103**,** 227-231.

GRYGLEWICZ, S., MUSZYŃSKI, M. & NOWICKI, J. 2013. Enzymatic synthesis of rapeseed oil-based lubricants. *Industrial crops and products,* 45**,** 25-29.

GUARIEIRO, L. L. N., DE ALMEIDA GUERREIRO, E. T., DOS SANTOS AMPARO, K. K., MANERA, V. B., REGIS, A. C. D., SANTOS, A. G., FERREIRA, V. P., LEÃO, D. J., TORRES, E. A. & DE ANDRADE, J. B. 2014. Assessment of the use of oxygenated fuels on emissions and performance of a diesel engine. *Microchemical Journal,* 117**,** 94-99.

GUARIEIRO, L. L. N., DE SOUZA, A. F., TORRES, E. A. & DE ANDRADE, J. B. 2009. Emission profile of 18 carbonyl compounds, CO, CO2, and NOx emitted by a diesel engine fuelled with diesel and ternary blends containing diesel, ethanol and biodiesel or vegetable oils. *Atmospheric Environment,* 43**,** 2754-2761.

HAMZE, H., AKIA, M. & YAZDANI, F. 2015. Optimization of biodiesel production from the waste cooking oil using response surface methodology. *Process Safety and Environmental Protection,* 94**,** 1-10.

HANAKI, K. & PORTUGAL-PEREIRA, J. 2018. The effect of biofuel production on greenhouse gas emission reductions. *Biofuels and Sustainability.* Springer, Tokyo.

HASSAN, M. H. & KALAM, M. A. 2013. An overview of biofuel as a renewable energy source: development and challenges. *Procedia Engineering,* 56**,** 39-53.

HEIDARI-MALENI, A., GUNDOSHMIAN, T. M., JAHANBAKHSHI, A. & GHOBADIAN, B. 2020. Performance improvement and exhaust emissions reduction in diesel engine through the use of graphene quantum dot (GQD) nanoparticles and ethanol-biodiesel blends. *Fuel,* 267**,** 117116.

HELWANI, Z., OTHMAN, M., AZIZ, N., FERNANDO, W. & KIM, J. 2009. Technologies for production of biodiesel focusing on green catalytic techniques: a review. *Fuel Processing Technology,* 90**,** 1502-1514.

HEYWOOD, J. 1988. *Internal combustion engine fundamentals,* McGraw-Hill Book Co. *New York.*

HEYWOOD, J. 2017. *The two-stroke cycle engine: its development, operation, and design*, Routledge, New York.

HEYWOOD, J. B. 2018. *Internal combustion engine fundamentals,* 2nd Edition, McGraw-Hill Education, New York.

HOANG, A. T. & PHAM, M. T. 2018. Influences of heating temperatures on physical properties, spray characteristics of bio-oils and fuel supply system of a conventional diesel engine. *Int. J. Adv. Sci. Eng. Inf. Technol,* 8**,** 2231-2240.

HOEKMAN, S. K., BROCH, A., ROBBINS, C., CENICEROS, E. & NATARAJAN, M. 2012. Review of biodiesel composition, properties, and specifications. *Renewable and sustainable energy reviews,* 16**,** 143-169.

HULWAN, D. B. & JOSHI, S. V. 2011. Performance, emission and combustion characteristic of a multicylinder DI diesel engine running on diesel–ethanol–biodiesel blends of high ethanol content. *Applied Energy,* 88**,** 5042-5055.

HÜRDOĞAN, E., OZALP, C., KARA, O. & OZCANLI, M. 2017. Experimental investigation on performance and emission characteristics of waste tire pyrolysis oil–diesel blends in a diesel engine. *International journal of hydrogen energy,* 42**,** 23373-23378.

ILKıLıÇ, C., AYDıN, S., BEHCET, R. & AYDIN, H. 2011. Biodiesel from safflower oil and its application in a diesel engine. *Fuel processing technology,* 92**,** 356-362.

ISLAM, M. A., RAHMAN, M. M., HEIMANN, K., NABI, M. N., RISTOVSKI, Z. D., DOWELL, A., THOMAS, G., FENG, B., VON ALVENSLEBEN, N. & BROWN, R. J. 2015. Combustion analysis of microalgae methyl ester in a common rail direct injection diesel engine. *Fuel,* 143**,** 351-360.

JACOBSON, K., GOPINATH, R., MEHER, L. C. & DALAI, A. K. 2008. Solid acid catalyzed biodiesel production from waste cooking oil. *Applied Catalysis B: Environmental,* 85**,** 86-91.

JAIN, S. & SHARMA, M. 2010. Prospects of biodiesel from Jatropha in India: a review. *Renewable and Sustainable Energy Reviews,* 14**,** 763-771.

JAYED, M., MASJUKI, H. H., SAIDUR, R., KALAM, M. & JAHIRUL, M. I. 2009. Environmental aspects and challenges of oilseed produced biodiesel in Southeast Asia. *Renewable and Sustainable Energy Reviews,* 13**,** 2452-2462.

JEON, J., LEE, J. T., KWON, S. I. & PARK, S. 2016. Combustion performance, flame, and soot characteristics of gasoline–diesel pre-blended fuel in an optical compression-ignition engine. *Energy Conversion and Management,* 116**,** 174-183.

JHA, S., FERNANDO, S., COLUMBUS, E. & WILLCUTT, H. 2009. A comparative study of exhaust emissions using diesel-biodiesel-ethanol blends in new and used engines. *Transactions of the ASABE,* 52**,** 375-381.

KANDASAMY, S. K., SELVARAJ, A. S. & RAJAGOPAL, T. K. R. 2019. Experimental investigations of ethanol blended biodiesel fuel on automotive diesel engine performance, emission and durability characteristics. *Renewable Energy,* 141**,** 411-419.

KANNAN, G. 2013. Effect of injection pressures and timings on the performance emission and combustion characteristics of a direct injection diesel engine using biodiesel-diesel-ethanol blend. SAE Technical Paper.

KAPLAN, C., ARSLAN, R. & SÜRMEN, A. 2006. Performance characteristics of sunflower methyl esters as biodiesel. *Energy Sources,* 28**,** 751-755.

KARABEKTAS, M., ERGEN, G. & HOSOZ, M. 2014. The effects of using diethylether as additive on the performance and emissions of a diesel engine fuelled with CNG. *Fuel,* 115**,** 855-860.

KARMAKAR, B., SAMANTA, S. & HALDER, G. 2020. Delonix regia heterogeneous catalyzed two-step biodiesel production from Pongamia pinnata oil using methanol and 2-propanol. *Journal of Cleaner Production,* 255**,** 120313.

KARMEE, S. K. & CHADHA, A. 2005. Preparation of biodiesel from crude oil of Pongamia pinnata. *Bioresource technology,* 96**,** 1425-1429.

KATHIRVEL, S., LAYEK, A. & MUTHURAMAN, S. 2016. Exploration of waste cooking oil methyl esters (WCOME) as fuel in compression ignition engines: a critical review. *Engineering Science and Technology, an International Journal*, *19*,1018-1026.

KATRAŠNIK, T. 2016. Innovative 0D transient momentum based spray model for real-time simulations of CI engines. *Energy,* 112**,** 494-508.

KAUR, M., MALHOTRA, R. & ALI, A. 2018. Tungsten supported Ti/SiO2 nanoflowers as reusable heterogeneous catalyst for biodiesel production. *Renewable Energy,* 116**,** 109-119.

KAVITHA, K. R., BEEMKUMAR, N. & RAJASEKAR, R. 2019. Experimental investigation of diesel engine performance fuelled with the blends of Jatropha curcas, ethanol, and diesel. *Environmental Science and Pollution Research,* 26**,** 8633-8639.

KHAN, S., SIDDIQUE, R., SAJJAD, W., NABI, G., HAYAT, K. M., DUAN, P. & YAO, L. 2017. Biodiesel production from algae to overcome the energy crisis. *HAYATI Journal of Biosciences*, 24**,** 163-167.

KHOOBBAKHT, G., KARIMI, M. & KHEIRALIPOUR, K. 2019. Effects of biodiesel-ethanol-diesel blends on the performance indicators of a diesel engine: A study by response surface modeling. *Applied Thermal Engineering,* 148**,** 1385-1394.

KIBAZOHI, O. & SANGWAN, R. S. 2011. Vegetable oil production potential from Jatropha curcas, Croton megalocarpus, Aleurites moluccana, Moringa oleifera and Pachira glabra:

assessment of renewable energy resources for bio-energy production in Africa. *Biomass and Bioenergy,* 35**,** 1352-1356.

KORKUT, I. & BAYRAMOGLU, M. 2018. Selection of catalyst and reaction conditions for ultrasound assisted biodiesel production from canola oil. *Renewable energy,* 116**,** 543-551.

KÖSE, Ö., TÜTER, M. & AKSOY, H. A. 2002. Immobilized *Candida antarctica* lipase-catalyzed alcoholysis of cotton seed oil in a solvent-free medium. *Bioresource technology,* 83, 125-129.

KOUZU, M., KASUNO, T., TAJIKA, M., SUGIMOTO, Y., YAMANAKA, S. & HIDAKA, J. 2008. Calcium oxide as a solid base catalyst for transesterification of soybean oil and its application to biodiesel production. *Fuel,* 87**,** 2798-2806.

KRISHNAMOORTHI, M. & MALAYALAMURTHI, R. 2017. Experimental investigation on performance, emission behavior and exergy analysis of a variable compression ratio engine fueled with diesel-aegle marmelos oil-diethyl ether blends. *Energy,* 128**,** 312-328.

KRISHNAMOORTHI, M., MALAYALAMURTHI, R. & SHAMEER, P. M. 2018. RSM based optimization of performance and emission characteristics of DI compression ignition engine fuelled with diesel/aegle marmelos oil/diethyl ether blends at varying compression ratio, injection pressure and injection timing. *Fuel,* 221**,** 283-297.

KULESHOV, A. 2005. Model for predicting air-fuel mixing, combustion and emissions in DI diesel engines over whole operating range. SAE Technical Paper.

KULESHOV, A. 2006. Use of multi-zone DI diesel spray combustion model for simulation and optimization of performance and emissions of engines with multiple injection. *SAE paper***,** 1385.

KULESHOV, A. 2007. Multi-zone DI diesel spray combustion model and its application for matching the injector design with piston bowl shape. *SAE Technical Papers,* 2007.

KULESHOV, A. 2009. Multi-zone DI diesel spray combustion model for thermodynamic simulation of engine with PCCI and high EGR level. *SAE International Journal of Engines,* 2**,** 1811-1834.

KULESHOV, A. & GREKHOV, L. 2013. Multidimensional optimization of DI diesel engine process using multi-zone fuel spray combustion model and detailed chemistry NOx formation model. *SAE Technical Paper***,** 01-0882.

KULESHOV, A., KOZLOV, A. & MAHKAMOV, K. 2010. Self-ignition delay prediction in PCCI direct injection diesel engines using multi-zone spray combustion model and detailed chemistry. SAE Technical Paper.

KULESHOV, A. & MAHKAMOV, K. 2008. Multi-zone diesel fuel spray combustion model for the simulation of a diesel engine running on biofuel. *Proceedings of the Institution of Mechanical Engineers, Part A: Journal of Power and Energy,* 222**,** 309-321.

KUMAR, A. & SHARMA, S. 2011. Potential non-edible oil resources as biodiesel feedstock: an Indian perspective. *Renewable and Sustainable Energy Reviews,* 15**,** 1791-1800.

KUMAR, B. R., SARAVANAN, S., RANA, D. & NAGENDRAN, A. 2016. A comparative analysis on combustion and emissions of some next generation higher-alcohol/diesel blends in a direct-injection diesel engine. *Energy Conversion and Management,* 119**,** 246-256.

KUSZEWSKI, H. 2019. Experimental investigation of the autoignition properties of ethanol–biodiesel fuel blends. *Fuel,* 235**,** 1301-1308.

KWANCHAREON, P., LUENGNARUEMITCHAI, A. & JAI-IN, S. 2007. Solubility of a diesel–biodiesel–ethanol blend, its fuel properties, and its emission characteristics from diesel engine. *Fuel,* 86**,** 1053-1061.

LAPPI, H. & ALÉN, R. 2011. Pyrolysis of vegetable oil soaps—palm, olive, rapeseed and castor oils. *Journal of Analytical and Applied Pyrolysis,* 91**,** 154-158.

LAPUERTA, M., ARMAS, O. & GARCIA-CONTRERAS, R. 2007. Stability of diesel–bioethanol blends for use in diesel engines. *Fuel,* 86**,** 1351-1357.

LAPUERTA, M., GARCÍA-CONTRERAS, R., CAMPOS-FERNÁNDEZ, J. & DORADO, M. P. 2010. Stability, lubricity, viscosity, and cold-flow properties of alcohol− diesel blends. *Energy & fuels,* 24**,** 4497-4502.

LAPUERTA, M., HERNÁNDEZ, J. J., FERNÁNDEZ-RODRÍGUEZ, D. & COVA-BONILLO, A. 2017. Autoignition of blends of n-butanol and ethanol with diesel or biodiesel fuels in a constant-volume combustion chamber. *Energy,* 118**,** 613-621.

LEI, T., WANG, Z., CHANG, X., LIN, L., YAN, X., SUN, Y., SHI, X., HE, X. & ZHU, J. 2016. Performance and emission characteristics of a diesel engine running on optimized ethyl levulinate–biodiesel–diesel blends. *Energy,* 95**,** 29-40.

LEUNG, D. & GUO, Y. 2006. Transesterification of neat and used frying oil: optimization for biodiesel production. *Fuel processing technology,* 87**,** 883-890.

LEUNG, D. Y., WU, X. & LEUNG, M. 2010. A review on biodiesel production using catalyzed transesterification. *Applied energy,* 87**,** 1083-1095.

LI, L., DU, W., LIU, D., WANG, L. & LI, Z. 2006. Lipase-catalyzed transesterification of rapeseed oils for biodiesel production with a novel organic solvent as the reaction medium. *Journal of Molecular Catalysis B: Enzymatic,* 43**,** 58-62.

LI, L., WANG, J., WANG, Z. & XIAO, J. 2015. Combustion and emission characteristics of diesel engine fueled with diesel/biodiesel/pentanol fuel blends. *Fuel,* 156**,** 211-218.

LIAQUAT, A., MASJUKI, H., KALAM, M., FAZAL, M., KHAN, A. F., FAYAZ, H. & VARMAN, M. 2013. Impact of palm biodiesel blend on injector deposit formation. *Applied energy,* 111**,** 882-893.

LIM, S. & TEONG, L. K. 2010. Recent trends, opportunities and challenges of biodiesel in Malaysia: an overview. *Renewable and Sustainable Energy Reviews,* 14**,** 938-954.

LIU, H., JIAQIANG, E., DENG, Y., XIE, C. & ZHU, H. 2016. Experimental study on pyrolysis characteristics of the tobacco stem based on microwave heating method. *Applied Thermal Engineering,* 106**,** 473-479.

LIU, H., LEE, C.-F., HUO, M. & YAO, M. 2011. Comparison of ethanol and butanol as additives in soybean biodiesel using a constant volume combustion chamber. *Energy & fuels,* 25**,** 1837-1846.

LIU, H., MA, X., LI, B., CHEN, L., WANG, Z. & WANG, J. 2017. Combustion and emission characteristics of a direct injection diesel engine fueled with biodiesel and PODE/biodiesel fuel blends. *Fuel,* 209**,** 62-68.

LIU, X., HE, H., WANG, Y., ZHU, S. & PIAO, X. 2008. Transesterification of soybean oil to biodiesel using CaO as a solid base catalyst. *Fuel,* 87**,** 216-221.

MA, F. & HANNA, M. A. 1999. Biodiesel production: a review. *Bioresource technology,* 70**,** 1-15.

MADIWALE, S., KARTHIKEYAN, A. & BHOJWANI, V. 2018. Properties investigation and performance analysis of a diesel engine fuelled with Jatropha, Soybean, Palm and Cottonseed biodiesel using Ethanol as an additive. *Materials Today: Proceedings,* 5**,** 657-664.

MAGHBOULI, A., YANG, W., AN, H., LI, J., CHOU, S. K. & CHUA, K. J. 2013. An advanced combustion model coupled with detailed chemical reaction mechanism for DI diesel engine simulation. *Applied energy,* 111**,** 758-770.

MAHER, K. & BRESSLER, D. 2007. Pyrolysis of triglyceride materials for the production of renewable fuels and chemicals. *Bioresource technology,* 98**,** 2351-2368.

MAHMUDUL, H., HAGOS, F., MAMAT, R., ADAM, A. A., ISHAK, W. & ALENEZI, R. 2017. Production, characterization and performance of biodiesel as an alternative fuel in diesel engines–A review. *Renewable and Sustainable Energy Reviews,* 72**,** 497-509.

MAKI, D. F. & SHAHAD, H. A. 2020. An experimental investigation on thermal performance and exhaust gas emission of CI engine fueled by diesel-ethanol blended with waste oil biodiesel as co-solvent. *Test Engineering and Management,* 83, 12781-12793.s

MARINKOVIĆ, D. M., STANKOVIĆ, M. V., VELIČKOVIĆ, A. V., AVRAMOVIĆ, J. M., MILADINOVIĆ, M. R., STAMENKOVIĆ, O. O., VELJKOVIĆ, V. B. & JOVANOVIĆ, D. M. 2016. Calcium oxide as a promising heterogeneous catalyst for biodiesel production: Current state and perspectives. *Renewable and sustainable energy reviews,* 56**,** 1387-1408.

MARTIN, M. & PRITHVIRAJ, D. 2011. Performance of pre-heated cottonseed oil and diesel fuel blends in a compression ignition engine. *JJMIE,* 5**,** 235-240.

MASJUKI, H. & MOFIJUR, M. 2010. Biofuel engine: a new challenge. *Malaysia: University of Malaya*.

MAT YASIN, M. H., MAMAT, R., YUSOP, A. F., RAHIM, R., AZIZ, A. & SHAH, L. A. 2013. Fuel physical characteristics of biodiesel blend fuels with alcohol as additives. *Procedia Engineering,* 53**,** 701-706.

MAURYA, R. K., MAURYA & LUBY 2019. *Reciprocating engine combustion diagnostics*, Springer.

MCENALLY, C. S. & PFEFFERLE, L. D. 2011. Sooting tendencies of oxygenated hydrocarbons in laboratory-scale flames. *Environmental science & technology,* 45**,** 2498-2503.

MEHER, L. C., SAGAR, D. V. & NAIK, S. 2006. Technical aspects of biodiesel production by transesterification—a review. *Renewable and sustainable energy reviews,* 10**,** 248-268.

MICIC, R. 2020. Storing, distribution and blending of biodiesel. *Agricultural Engineering International: CIGR Journal,* 22**,** 105-111.

MIHAELA, P., JOSEF, R., MONICA, N. & RUDOLF, Z. 2013. Perspectives of safflower oil as biodiesel source for South Eastern Europe (comparative study: Safflower, soybean and rapeseed). *Fuel,* 111**,** 114-119.

MOFIJUR, M., MASJUKI, H., KALAM, M., ATABANI, A., SHAHABUDDIN, M., PALASH, S. & HAZRAT, M. 2013. Effect of biodiesel from various feedstocks on combustion

characteristics, engine durability and materials compatibility: A review. *Renewable and Sustainable Energy Reviews,* 28**,** 441-455.

MONIRUL, I., MASJUKI, H., KALAM, M., ZULKIFLI, N., RASHEDUL, H., RASHED, M., IMDADUL, H. & MOSAROF, M. 2015. A comprehensive review on biodiesel cold flow properties and oxidation stability along with their improvement processes. *RSC advances,* 5**,** 86631-86655.

NANTHAGOPAL, K., ASHOK, B., SARAVANAN, B., PATHY, M. R., SAHIL, G., RAMESH, A., NABI, M. N. & RASUL, M. G. 2019. Study on decanol and Calophyllum Inophyllum biodiesel as ternary blends in CI engine. *Fuel,* 239**,** 862-873.

NOOROLLAHI, Y., AZADBAKHT, M. & GHOBADIAN, B. 2018. The effect of different diesterol (diesel–biodiesel–ethanol) blends on small air-cooled diesel engine performance and its exhaust gases. *Energy,* 142**,** 196-200.

NOUR, M., ATTIA, A. M. & NADA, S. A. 2019. Combustion, performance and emission analysis of diesel engine fuelled by higher alcohols (butanol, octanol and heptanol)/diesel blends. *Energy conversion and management,* 185**,** 313-329.

OGUNKUNLE, O. & AHMED, N. A. 2019a. Response surface analysis for optimisation of reaction parameters of biodiesel production from alcoholysis of Parinari polyandra seed oil. *International Journal of Sustainable Energy,* 38**,** 630-648.

OGUNKUNLE, O. & AHMED, N. A. 2019b. A review of global current scenario of biodiesel adoption and combustion in vehicular diesel engines. *Energy Reports,* 5**,** 1560-1579.

OLIVARES, R. D. C., RIVERA, S. S. & MC LEOD, J. E. N. 2015. Database for accidents and incidents in the fuel ethanol industry. *Journal of Loss Prevention in the Process Industries,* 38**,** 276-297.

PAN, S., ZHANG, G., SUN, Y. & CHAKRABORTY, P. 2009. Accumulating characteristics of platinum group elements (PGE) in urban environments, China. *Science of the Total Environment,* 407**,** 4248-4252.

PARISH, E. S., KLINE, K. L., DALE, V. H., EFROYMSON, R. A., MCBRIDE, A. C., JOHNSON, T. L., HILLIARD, M. R. & BIELICKI, J. M. 2013. Comparing scales of environmental effects from gasoline and ethanol production. *Environmental Management,* 51**,** 307-338.

PARK, S. H., CHA, J. & LEE, C. S. 2012. Impact of biodiesel in bioethanol blended diesel on the engine performance and emissions characteristics in compression ignition engine. *Applied Energy,* 99**,** 334-343.

PARK, S. H., KIM, S. H. & LEE, C. S. 2009. Mixing stability and spray behavior characteristics of diesel− ethanol− methyl ester blended fuels in a common-rail diesel injection system. *Energy & Fuels,* 23**,** 5228-5235.

PARLAK, A., KARABAS, H., AYHAN, V., YASAR, H., SOYHAN, H. S. & OZSERT, I. 2009. Comparison of the variables affecting the yield of tobacco seed oil methyl ester for KOH and NaOH catalysts. *Energy & Fuels,* 23**,** 1818-1824.

PAUL, A., PANUA, R. & DEBROY, D. 2017. An experimental study of combustion, performance, exergy and emission characteristics of a CI engine fueled by Diesel-ethanol-biodiesel blends. *Energy,* 141**,** 839-852.

PENG, B.-X., SHU, Q., WANG, J.-F., WANG, G.-R., WANG, D.-Z. & HAN, M.-H. 2008. Biodiesel production from waste oil feedstocks by solid acid catalysis. *Process Safety and Environmental Protection,* 86**,** 441-447.

PETERS, J., RAND, M. & ZIEMKE, M. 1982. Investigation of soybean oil as a diesel fuel extender. *ASAE Tech. Pap.;(United States),* 82.

PETRANOVIĆ, Z., BEŠENIĆ, T., VUJANOVIĆ, M. & DUIĆ, N. 2017. Modelling pollutant emissions in diesel engines, influence of biofuel on pollutant formation. *Journal of environmental management,* 203**,** 1038-1046.

PETRANOVIĆ, Z., VUJANOVIĆ, M. & DUIĆ, N. 2015. Towards a more sustainable transport sector by numerically simulating fuel spray and pollutant formation in diesel engines. *Journal of cleaner production,* 88**,** 272-279.

PINZI, S., LÓPEZ, I., LEIVA-CANDIA, D., REDEL-MACIAS, M. D., HERREROS, J., CUBERO-ATIENZA, A. & DORADO, M. P. 2018. Castor oil enhanced effect on fuel ethanol-diesel fuel blend properties. *Applied Energy,* 224**,** 409-416.

PRADELLE, F., BRAGA, S. L., DE AGUIAR MARTINS, A. R. F., TURKOVICS, F. & PRADELLE, R. N. C. 2019. Experimental assessment of some key physicochemical properties of diesel-biodiesel-ethanol (DBE) blends for use in compression ignition engines. *Fuel,* 248**,** 241-253.

PRBAKARAN, B. & VISWANATHAN, D. 2018. Experimental investigation of effects of addition of ethanol to bio-diesel on performance, combustion and emission characteristics in CI engine. *Alexandria engineering journal,* 57**,** 383-389.

PULKRABEK, W. W. 2004. *Engineering fundamentals of the internal combustion engine,* 2nd Edition, Pearson Prentice Hall, New Jersey.

QI, D., CHEN, H., GENG, L., BIAN, Y. Z. & REN, X. C. 2010. Performance and combustion characteristics of biodiesel–diesel–methanol blend fuelled engine. *Applied Energy,* 87**,** 1679-1686.

QIAN, J., YUN, Z. & SHI, H. 2010. Cogeneration of biodiesel and nontoxic cottonseed meal from cottonseed processed by two-phase solvent extraction. *Energy Conversion and Management,* 51**,** 2750-2756.

RAJAK, U., NASHINE, P., CHAURASIYA, P. K., VERMA, T. N., PATEL, D. K. & DWIVEDI, G. 2021. Experimental & predicative analysis of engine characteristics of various biodiesels. *Fuel,* 285**,** 119097.

RAJAK, U., NASHINE, P., SINGH, T. S. & VERMA, T. N. 2018a. Numerical investigation of performance, combustion and emission characteristics of various biofuels. *Energy Conversion and Management,* 156**,** 235-252.

RAJAK, U., NASHINE, P. & VERMA, T. 2018b. Comparative assessment of the emission characteristics of first, second and third generation biodiesels as fuel in a diesel engine. *Journal of Thermal Engineering,* 6**,** 211-225.

RAJAK, U. & VERMA, T. N. 2019. A comparative analysis of engine characteristics from various biodiesels: Numerical study. *Energy Conversion and Management,* 180**,** 904-923.

RAJAK, U. & VERMA, T. N. 2020. Influence of combustion and emission characteristics on a compression ignition engine from a different generation of biodiesel. *Engineering Science and Technology, an International Journal,* 23**,** 10-20.

RAMESH, A., ASHOK, B., NANTHAGOPAL, K., PATHY, M. R., TAMBARE, A., MALI, P., PHUKE, P., PATIL, S. & SUBBARAO, R. 2019. Influence of hexanol as additive with Calophyllum Inophyllum biodiesel for CI engine applications. *Fuel,* 249**,** 472-485.

RAMÍREZ, A., AGGARWAL, S., SOM, S., RUTTER, T. & LONGMAN, D. 2014. Effects of blending a heavy alcohol (C20H40O with diesel in a heavy-duty compression-ignition engine. *Fuel,* 136**,** 89-102.

RAMUHAHELI, S., VEEREDHI, V. & ENWEREMADU, C. 2022. The Performance and Emission Characteristics Assessment of Hybrid Biodiesel/Ethanol Blends in a Diesel Engine. *Rigas Tehniskas Universitates Zinatniskie Raksti*, 26, 670-683.

RAMUHAHELI, S., VASUDEVARAO, V. & ENWEREMADU, C. 2023. Experimental assessment of performance and emission characteristics of a diesel engine fueled with hybrid biodiesel and its blends with ethanol. In *AIP Conference Proceedings*, 2643, 050042.

RANDAZZO, M. L. & SODRÉ, J. R. 2011a. Cold start and fuel consumption of a vehicle fuelled with blends of diesel oil–soybean biodiesel–ethanol. *Fuel,* 90**,** 3291-3294.

RANDAZZO, M. L. & SODRÉ, J. R. 2011b. Exhaust emissions from a diesel powered vehicle fuelled by soybean biodiesel blends (B3–B20) with ethanol as an additive (B20E2–B20E5). *Fuel,* 90**,** 98-103.

RANGANATHAN, S. V., NARASIMHAN, S. L. & MUTHUKUMAR, K. 2008. An overview of enzymatic production of biodiesel. *Bioresource technology,* 99**,** 3975-3981.

RASHEDUL, H., MASJUKI, H., KALAM, M., ASHRAFUL, A., RAHMAN, S. A. & SHAHIR, S. 2014. The effect of additives on properties, performance and emission of biodiesel fuelled compression ignition engine. *Energy Conversion and Management,* 88**,** 348-364.

RASHID, U., ANWAR, F., ANSARI, T. M., ARIF, M. & AHMAD, M. 2009a. Optimization of alkaline transesterification of rice bran oil for biodiesel production using response surface methodology. *Journal of Chemical Technology & Biotechnology,* 84**,** 1364-1370.

RASHID, U., ANWAR, F. & KNOTHE, G. 2009b. Evaluation of biodiesel obtained from cottonseed oil. *Fuel Processing Technology,* 90**,** 1157-1163.

RASHID, U., ANWAR, F., MOSER, B. R. & ASHRAF, S. 2008. Production of sunflower oil methyl esters by optimized alkali-catalyzed methanolysis. *Biomass and bioenergy,* 32**,** 1202-1205.

RATHORE, V., NEWALKAR, B. L. & BADONI, R. 2016. Processing of vegetable oil for biofuel production through conventional and non-conventional routes. *Energy for Sustainable Development,* 31**,** 24-49.

REHAM, S., MASJUKI, H. H., KALAM, M., SHANCITA, I., FATTAH, I. R. & RUHUL, A. 2015. Study on stability, fuel properties, engine combustion, performance and emission characteristics of biofuel emulsion. *Renewable and Sustainable Energy Reviews,* 52**,** 1566-1579.

REYERO, I., ARZAMENDI, G. & GANDÍA, L. M. 2014. Heterogenization of the biodiesel synthesis catalysis: CaO and novel calcium compounds as transesterification catalysts. *Chemical Engineering Research and Design,* 92**,** 1519-1530.

RICO, J. & SAUER, I. 2015. A review of Brazilian biodiesel experiences. *Renewable and Sustainable Energy Reviews,* 45**,** 513-529.

SADAF, S., IQBAL, J., ULLAH, I., BHATTI, H. N., NOUREN, S., NISAR, J. & IQBAL, M. 2018. Biodiesel production from waste cooking oil: an efficient technique to convert waste into biodiesel. *Sustainable cities and society,* 41**,** 220-226.

SALAM, S. & VERMA, T. N. 2019. Appending empirical modelling to numerical solution for behaviour characterisation of microalgae biodiesel. *Energy conversion and management,* 180**,** 496-510.

SANJID, A., MASJUKI, H., KALAM, M., RAHMAN, S. A., ABEDIN, M. & PALASH, S. 2014. Production of palm and jatropha based biodiesel and investigation of palm-jatropha combined blend properties, performance, exhaust emission and noise in an unmodified diesel engine. *Journal of cleaner production,* 65**,** 295-303.

SHAHID, E. M. & JAMAL, Y. 2011. Production of biodiesel: a technical review. *Renewable and Sustainable Energy Reviews,* 15**,** 4732-4745.

SHAHIR, S., MASJUKI, H., KALAM, M., IMRAN, A., FATTAH, I. R. & SANJID, A. 2014. Feasibility of diesel–biodiesel–ethanol/bioethanol blend as existing CI engine fuel: An assessment of properties, material compatibility, safety and combustion. *Renewable and Sustainable Energy Reviews,* 32**,** 379-395.

SHAO, P., MENG, X., HE, J. & SUN, P. 2008. Analysis of immobilized Candida rugosa lipase catalyzed preparation of biodiesel from rapeseed soapstock. *food and bioproducts processing,* 86**,** 283-289.

SHARMA, T. K., RAO, G. A. P. & MURTHY, K. M. 2015. Effective reduction of in-cylinder peak pressures in Homogeneous Charge Compression Ignition Engine–A computational study. *Alexandria Engineering Journal,* 54**,** 373-382.

SHARMA, Y. & SINGH, B. 2009. Development of biodiesel: current scenario. *Renewable and sustainable energy reviews,* 13**,** 1646-1651.

SHARMA, Y., SINGH, B. & KORSTAD, J. 2010. Application of an efficient nonconventional heterogeneous catalyst for biodiesel synthesis from Pongamia pinnata oil. *Energy & Fuels,* 24**,** 3223-3231.

SHIRNESHAN, A., BAGHERZADEH, S. A., NAJAFI, G., MAMAT, R. & MAZLAN, M. 2021. Optimization and investigation the effects of using biodiesel-ethanol blends on the performance and emission characteristics of a diesel engine by genetic algorithm. *Fuel,* 289**,** 119753.

SHUDO, T., HIRAGA, K. & OGAWA, H. 2007. Mechanisms in reducing smoke and NOx from BDF combustion by ethanol blending and EGR. SAE Technical Paper.

SIA, C. B., KANSEDO, J., TAN, Y. H. & LEE, K. T. 2020. Evaluation on biodiesel cold flow properties, oxidative stability and enhancement strategies: A review. *Biocatalysis and Agricultural Biotechnology,* 24**,** 101514.

SIERRA-CANTOR, J. F. & GUERRERO-FAJARDO, C. A. 2017. Methods for improving the cold flow properties of biodiesel with high saturated fatty acids content: A review. *Renewable and Sustainable Energy Reviews,* 72**,** 774-790.

SILITONGA, A., ATABANI, A., MAHLIA, T., MASJUKI, H., BADRUDDIN, I. A. & MEKHILEF, S. 2011. A review on prospect of Jatropha curcas for biodiesel in Indonesia. *Renewable and Sustainable Energy Reviews,* 15**,** 3733-3756.

SILITONGA, A., MASJUKI, H., MAHLIA, T., ONG, H., ATABANI, A. & CHONG, W. 2013a. A global comparative review of biodiesel production from jatropha curcas using different homogeneous acid and alkaline catalysts: Study of physical and chemical properties. *Renewable and Sustainable Energy Reviews,* 24**,** 514-533.

SILITONGA, A., MASJUKI, H., MAHLIA, T., ONG, H., CHONG, W. & BOOSROH, M. 2013b. Overview properties of biodiesel diesel blends from edible and non-edible feedstock. *Renewable and Sustainable Energy Reviews,* 22**,** 346-360.

SILITONGA, A., ONG, H. C., MAHLIA, T., MASJUKI, H. & CHONG, W. 2014. Biodiesel conversion from high FFA crude jatropha curcas, calophyllum inophyllum and ceiba pentandra oil. *Energy procedia,* 61**,** 480-483.

SINGH, T. S., VERMA, T. N., NASHINE, P. & SHIJAGURUMAYUM, C. 2018. BS-III diesel vehicles in Imphal, India: an emission perspective. *Air Pollution and Control.* Springer.

SIVA, R., MUNUSWAMY, D. B. & DEVARAJAN, Y. 2019. Emission and performance study emulsified orange peel oil biodiesel in an aspirated research engine. *Petroleum Science,* 16**,** 180-186.

SIVALAKSHMI, S. & BALUSAMY, T. 2012. Influence of ethanol addition on a diesel engine fuelled with neem oil methyl ester. *International journal of green energy,* 9**,** 218-228.

SONI, D. K. & GUPTA, R. 2016. Numerical investigation of emission reduction techniques applied on methanol blended diesel engine. *Alexandria Engineering Journal,* 55**,** 1867-1879.

SRIVASTAVA, A. & PRASAD, R. 2000. Triglycerides-based diesel fuels. *Renewable and sustainable energy reviews,* 4**,** 111-133.

SUBHEDAR, P. B. & GOGATE, P. R. 2016. Ultrasound assisted intensification of biodiesel production using enzymatic interesterification. *Ultrasonics sonochemistry,* 29**,** 67-75.

SUBRAMANIAM, D., MURUGESAN, A., AVINASH, A. & KUMARAVEL, A. 2013. Bio-diesel production and its engine characteristics—An expatiate view. *Renewable and sustainable energy reviews,* 22**,** 361-370.

SUDESHKUMAR, P. M. & DEVARADJANE, G. 2011. Development of a simulation model for compression ignition engine running with ignition improved blend. *Thermal Science,* 15**,** 1131-1144.

SWARNA, S., SWAMY, M., DIVAKARA, T., KRISHNAMURTHY, K. & SHASHIDHAR, S. 2021. Experimental assessment of ternary fuel blends of diesel, hybrid biodiesel and alcohol in naturally aspirated CI engine. *International Journal of Environmental Science and Technology***,** 1-32.

SWARNA, S., SWAMY, M., DIVAKARA, T., KRISHNAMURTHY, K. & SHASHIDHAR, S. 2022. Experimental assessment of ternary fuel blends of diesel, hybrid biodiesel and alcohol in naturally aspirated CI engine. *International Journal of Environmental Science and Technology,* 19**,** 8523-8554.

SYAFIUDDIN, A., CHONG, J. H., YUNIARTO, A. & HADIBARATA, T. 2020. The current scenario and challenges of biodiesel production in Asian countries: A review. *Bioresource Technology Reports,* 12**,** 100608.

TAHER, H., NASHEF, E., ANVAR, N. & AL-ZUHAIR, S. 2017. Enzymatic production of biodiesel from waste oil in ionic liquid medium. *Biofuels., 10, 463-472.*

TANTIRUNGROTECHAI, J., THEPWATEE, S. & YOOSUK, B. 2013. Biodiesel synthesis over Sr/MgO solid base catalyst. *Fuel,* 106**,** 279-284.

TAPANES, N. C. O., ARANDA, D. A. G., DE MESQUITA CARNEIRO, J. W. & ANTUNES, O. A. C. 2008. Transesterification of Jatropha curcas oil glycerides: theoretical and experimental studies of biodiesel reaction. *Fuel,* 87**,** 2286-2295.

THAKKAR, K., KACHHWAHA, S.S., KODGIRE, P. & SRINIVASAN, S. 2021. Combustion investigation of ternary blend mixture of biodiesel/n-butanol/diesel: CI engine performance and emission control. *Renewable and Sustainable Energy Reviews*, *137*, 110468

THIYAGARAJAN, S., SONTHALIA, A., GEO, V. E., PRAKASH, T., KARTHICKEYAN, V., ASHOK, B., NANTHAGOPAL, K. & DHINESH, B. 2020. Effect of manifold injection of methanol/n-pentanol in safflower biodiesel fuelled CI engine. *Fuel,* 261**,** 116378.

THOR, M., ANDERSSON, I. & MCKELVEY, T. 2009. Parameterized diesel engine heat release modeling for combustion phasing analysis. SAE Technical Paper.

TSE, H. 2016. Combustion and emissions of a diesel engine fueled with diesel-biodiesel-ethanol blends and supplemented with intake CO2 charge dilution. *Developments in Combustion Technology.* Intech Open London.

TUTAK, W., JAMROZIK, A., PYRC, M. & SOBIEPAŃSKI, M. 2017. A comparative study of co-combustion process of diesel-ethanol and biodiesel-ethanol blends in the direct injection diesel engine. *Applied Thermal Engineering,* 117**,** 155-163.

UPRETY, B. K., CHAIWONG, W., EWELIKE, C. & RAKSHIT, S. K. 2016. Biodiesel production using heterogeneous catalysts including wood ash and the importance of enhancing byproduct glycerol purity. *Energy Conversion and Management,* 115**,** 191-199.

VENKANNA, B. & VENKATARAMANA REDDY, C. 2012. Direct injection diesel engine performance, emission, and combustion characteristics using diesel fuel, nonedible honne oil methyl ester, and blends with diesel fuel. *International journal of energy research,* 36**,** 1247-1261.

VENKATA SUBBAIAH, G. & RAJA GOPAL, K. 2011. An experimental investigation on the performance and emission characteristics of a diesel engine fuelled with rice bran biodiesel and ethanol blends. *International Journal of Green Energy,* 8**,** 197-208.

VENKATRAMAN, M. & DEVARADJANE, G. 2011. Simulation studies of a CI engine for better performance and emission using diesel-diesel biodiesel blends. *International Journal on Design and Manufacturing Technologies,* 5.

VERMA, P. & SHARMA, M. 2016. Review of process parameters for biodiesel production from different feedstocks. *Renewable and sustainable energy reviews,* 62**,** 1063-1071.

VERMA, P., SHARMA, M. & DWIVEDI, G. 2015. Operational and environmental impact of biodiesel on engine performance. *International Journal of Renewable Energy Research,* 5**,** 961-970.

VERMA, P., SHARMA, M. & DWIVEDI, G. 2016. Evaluation and enhancement of cold flow properties of palm oil and its biodiesel. *Energy Reports,* 2**,** 8-13.

VUJANOVIĆ, M., PETRANOVIĆ, Z., EDELBAUER, W. & DUIĆ, N. 2016. Modelling spray and combustion processes in diesel engine by using the coupled Eulerian–Eulerian and Eulerian–Lagrangian method. *Energy conversion and management,* 125**,** 15-25.

WANCURA, J. H., ROSSET, D. V., TRES, M. V., OLIVEIRA, J. V., MAZUTTI, M. A. & JAHN, S. L. 2018. Production of biodiesel catalyzed by lipase from Thermomyces lanuginosus in its soluble form. *The Canadian Journal of Chemical Engineering,* 96**,** 2361-2368.

WANG, J.-X., CHEN, K.-T., WEN, B.-Z., LIAO, Y.-H. B. & CHEN, C.-C. 2012. Transesterification of soybean oil to biodiesel using cement as a solid base catalyst. *Journal of the Taiwan Institute of Chemical Engineers,* 43**,** 215-219.

WEI, L., CHEUNG, C. & NING, Z. 2018. Effects of biodiesel-ethanol and biodiesel-butanol blends on the combustion, performance and emissions of a diesel engine. *Energy,* 155**,** 957-970.

WOSCHNI, G. 1967. A universally applicable equation for the instantaneous heat transfer coefficient in the internal combustion engine. SAE Technical paper.

XIAO-RAN, L., SHI-HAI, X., XIAO, L. & PENG, W. 2015. Study of combustion characteristics of oxygenated fuels under oxygen deficient condition. *Petroleum Processing and Petrochemicals,* 46**,** 67.

XIAO, H., GUO, F., WANG, R., YANG, X., LI, S. & RUAN, J. 2020. Combustion performance and emission characteristics of diesel engine fueled with iso-butanol/biodiesel blends. *Fuel,* 268**,** 117387.

YAMIN, J. A. 2022. Analysis of Internal Combustion Engine Performance Using Design of Experiment. *Tehnički vjesnik,* 29**,** 483-496.

YAN, S., DIMAGGIO, C., MOHAN, S., KIM, M., SALLEY, S. O. & NG, K. 2010. Advancements in heterogeneous catalysis for biodiesel synthesis. *Topics in Catalysis,* 53**,** 721-736.

YESILYURT, M. K. 2020. A detailed investigation on the performance, combustion, and exhaust emission characteristics of a diesel engine running on the blend of diesel fuel, biodiesel and 1-heptanol (C7 alcohol) as a next-generation higher alcohol. *Fuel,* 275**,** 117893.

YESILYURT, M. K., AYDIN, M., YILBASI, Z. & ARSLAN, M. 2020. Investigation on the structural effects of the addition of alcohols having various chain lengths into the vegetable oil-biodiesel-diesel fuel blends: An attempt for improving the performance, combustion, and exhaust emission characteristics of a compression ignition engine. *Fuel,* 269**,** 117455.

YESILYURT, M. K., ERYILMAZ, T. & ARSLAN, M. 2018. A comparative analysis of the engine performance, exhaust emissions and combustion behaviors of a compression ignition engine fuelled with biodiesel/diesel/1-butanol (C4 alcohol) and biodiesel/diesel/n-pentanol (C5 alcohol) fuel blends. *Energy,* 165**,** 1332-1351.

YILMAZ, N. & SANCHEZ, T. M. 2012. Analysis of operating a diesel engine on biodiesel-ethanol and biodiesel-methanol blends. *Energy,* 46**,** 126-129.

YILMAZ, N., VIGIL, F. M., BENALIL, K., DAVIS, S. M. & CALVA, A. 2014a. Effect of biodiesel–butanol fuel blends on emissions and performance characteristics of a diesel engine. *Fuel,* 135**,** 46-50.

YILMAZ, N., VIGIL, F. M., DONALDSON, A. B. & DARABSEH, T. 2014b. Investigation of CI engine emissions in biodiesel–ethanol–diesel blends as a function of ethanol concentration. *Fuel,* 115**,** 790-793.

YUVARAJAN, D. & RAMANAN, M. V. 2016. Experimental analysis on neat mustard oil methyl ester subjected to ultrasonication and microwave irradiation in four stroke single cylinder diesel engine. *Journal of Mechanical Science and Technology,* 30**,** 437-446.

ZHAN, C., FENG, Z., ZHANG, M., TANG, C. & HUANG, Z. 2018. Experimental investigation on effect of ethanol and di-ethyl ether addition on the spray characteristics of diesel/biodiesel blends under high injection pressure. *Fuel,* 218**,** 1-11.

ZHAO, K., CAO, X., DI, Q., WANG, M., CAO, H., DENG, L., LIU, J., WANG, F. & TAN, T. 2017. Synthesis, characterization and optimization of a two-step immobilized lipase. *Renewable energy,* 103**,** 383-387.

ZHENG, Z., WANG, X., ZHONG, X., HU, B., LIU, H. & YAO, M. 2016. Experimental study on the combustion and emissions fueling biodiesel/n-butanol, biodiesel/ethanol and biodiesel/2, 5-dimethylfuran on a diesel engine. *Energy,* 115**,** 539-549.

ZHOU, D., YANG, W., AN, H., LI, J. & SHU, C. 2015. A numerical study on RCCI engine fueled by biodiesel/methanol. *Energy Conversion and Management,* 89**,** 798-807.

ZHU, L., CHEUNG, C., ZHANG, W. & HUANG, Z. 2010a. Emissions characteristics of a diesel engine operating on biodiesel and biodiesel blended with ethanol and methanol. *Science of the Total Environment,* 408**,** 914-921.

ZHU, L., CHEUNG, C., ZHANG, W. & HUANG, Z. 2011a. Combustion, performance and emission characteristics of a DI diesel engine fueled with ethanol–biodiesel blends. *Fuel,* 90**,** 1743-1750.

ZHU, L., CHEUNG, C. S., ZHANG, W. & HUANG, Z. 2010b. Emissions characteristics of a diesel engine operating on biodiesel and biodiesel blended with ethanol and methanol. *Science of the Total Environment,* 408**,** 914-921.

ZHU, L., CHEUNG, C. S., ZHANG, W. & HUANG, Z. 2011b. Combustion, performance and emission characteristics of a DI diesel engine fueled with ethanol–biodiesel blends. *Fuel,* 90**,** 1743-1750.

ZÖLDY, M. 2011. Ethanol–biodiesel–diesel blends as a diesel extender option on compression ignition engines. *Transport,* 26**,** 303-309.